Turbulent flame development in a high-pressure combustion vessel.

By:

Matthew P Ormsby

B.Eng. , M.Sc (Eng)

Submitted in accordance with the requirements for the degree of

Doctor of Philosophy

School of Mechanical Engineering

The University of Leeds

March 2005

The candidate confirms that the work submitted is his own and that appropriate credit has been given where reference has been made to the work of others

For me...who else

Abstract

The objective of this work was to extend the range of turbulent burning velocities presented in the literature by performing new measurements at elevated pressures over a range of turbulent velocities, u' (r.m.s. deviation from the mean velocity). The influence of equivalence ratio was investigated for a fixed $u' = 2$ m/s at 0.5 MPa for methane, a 70 % methane/ 30 % hydrogen mixture, methanol, iso-octane and a gasoline (Shell dutch-pura). The mixtures were varied from the lean ignition limit to rich limit up to a maximum equivalence ratio of 2. Further measurements were performed with iso-octane and the effect of r.m.s. turbulent velocity ($u' = 0.5$, 1, 2, 4, 6 m/s), pressure ($P = 0.1$, 0.5, 1 MPa) and equivalence ratio ($\phi = 0.8$, 1.0 , 1.2 and 1.4) were investigated, to produce a database.

Turbulent flames were centrally ignited in isotropic turbulence in the Leeds fan stirred bomb. Flame progress was monitored using high-speed schlieren photography and pressure measurements. The turbulent burning velocity based on the production of burned mass, u_{tr}, was obtained from both techniques. The burning velocities obtained from schlieren imaging and pressure measurements were in good agreement. The turbulent flames continually accelerated throughout the time that they were monitored. This was the result of turbulent flame development, with the range of turbulent scales wrinkling the flame surface increasing as the flames grew. It was shown that flame development occurred primarily as a result of the kernel radius, rather than the time from ignition.

For each turbulent condition, corresponding spherically expanding laminar flames were ignited and imaged with schlieren photography. The measurements were processed to give the stretch free laminar burning velocity and also the Markstein number, a measure of the influence of stretch on the burning velocity. The peak laminar burning velocity was found to be in the range $1 > \phi > 1.2$ depending on the fuel. At 0.5 MPa a number of the flames were observed to become cellular, in some cases this occurred from ignition, this has been linked to negative Markstein numbers which were observed with lean methane and rich iso-octane – air mixtures.

The peak in the turbulent burning velocity with equivalence ratio varied considerably with the different fuels, and did not correspond to that for the laminar burning velocity. In the case of methane and the 70 % methane/ 30 % hydrogen mixture the peak turbulent burning velocity was lean of stoichiometric. In contrast, for iso-octane and the gasoline, the peak in u_{tr} was beyond $\phi = 1.3$. It was concluded that the shift in the peak could be explained by comparison with the measured Markstein numbers.

In the iso-octane database, pressure was not observed to have a significant influence on the turbulent burning velocity for some conditions, however, when fuel rich higher pressure gave an increase in u_{tr}. Turndown of u_{tr} (the burning velocity does not increase as with the turbulent velocity) was observed at high turbulence velocities, although this depended on the equivalence ratio. The measurements were then compared with existing turbulent burning velocity expressions and correlations. In general these expressions were found not to predict the effect of equivalence ratio well.

Acknowledgments

I wish to greatly thank my supervisors Dr R. Woolley and Prof. C.G.W. Sheppard for their endless dedication through the four-year period of research and during the preparation of this thesis.

I thank the School of Mechanical Engineering for funding the first three years of this study and Jaguar cars for funding my final year.

My thanks are also due to all of the staff in the Thermodynamics Laboratory and the other research students along the way.

PUBLICATIONS

The work in the thesis has given rise to two publications.

- The influence of fuel air ratio on the turbulent burning velocity of iso-octane air flames. Presented by the author at the Fourth International Seminar: Fire and Explosions Hazard, Derry, Belfast (2003). Published in the Seminar Proceedings.

- The variation of turbulent burning rate of methane, methanol and iso-octane air mixtures with equivalence ratio at elevated pressure. Accepted for publication in Combustion Science and Technology.

Table of Contents

Nomenclature

a	radius of vessel,
d	flame diameter
f_s	fan speed
k	wave number
K	Karlovitz stretch factor
$\bar{k}_\eta$	dimensionless wave number
L	integral length scale
L_b	burned gas Markstein length
L_c, L_s, L_{cr}, L_{sr}	Markstein lengths
Le	Lewis number
M_{ac}, M_{as}, M_{acr}, M_{asr}	Markstein numbers,
P	pressure
P_i	initial pressure
P_e	final pressure
R_λ	Reynolds number for Taylor scale
r_i	radius of gas where no unburned mixture remains
r_b	gas radius accounting for expansion
R_a, R_j, R_m, R_t, R_ξ	reference flame radii
Re	Reynolds number
R_{sch}	schlieren flame radius
r_u	cold flame radius
S	flame speed factor
S_n	stretched flame speed
S_s	unstretched flame speed
S_u	burning velocity
t	time from ignition

T_i	initial temperature
T_u	unburned gas temperature
U	u_t / u'
u'	r.m.s turbulent velocity
u'_k	effective r.m.s turbulent velocity
u_l	unstretched laminar burning velocity
u_n	stretched laminar burning velocity
$u_{nr,p}$, $u_{tr,p}$	burning velocity from pressure records
u_t	turbulent burning velocity
u_{te}	turbulent burning velocity (entrainment)
u_{tr}	turbulent burning velocity (production of burned mass)
v_g	gas velocity ahead of the flame

Greek Symbols

α	flame stretch rate
α_c	stretch rate due to flame curvature
α_s	stretch rate due to flame strain
δ_l	(inner) laminar flame thickness
ϕ	equivalence ratio
γ	ratio of specific heats
η	Kolmogorov scale
λ	Taylor turbulent length scale
ρ_b	burned gas density
ρ_u	unburned gas density
τ	integral time scale
ν	kinematic viscosity

List of Tables

List of Figures

Chapter 1 Introduction

1.1 General Introduction

Throughout the world, combustion of fossil fuels still provides more than 80% of the energy consumed. The world demand for energy is rising, other environmental energy sources are slowly becoming available however it is most likely that fossil fuel combustion will continue to provide the majority share. Hydrogen is currently being politically marketed as the future energy, but currently there is no viable technological or economical source of producing hydrogen in the required quantity. Until the advent of nuclear fusion combustion of fossil fuels remain the only realistic means to provide for world energy demand. The 'energy problem' is of growing concern, the forecasts of crude oil and natural gas production all predict a fall in supply over the next generation, the problem is compounded by the fact that demand is expected to grow. As the availability of crude oil and natural gas diminishes society will have to make the best use of the available supply. Particularly, transport vehicles from cars to aeroplanes, which are dependent upon energy dense gasoline, will have to become much more efficient if modern day family car and world travel are to continue being available to all.

Demands for improvements in heat engine and turbine design in terms of both improving efficiency and reductions in other pollutants requires an improved fundamental understanding of combustion e.g. reburn technologies and gasoline direct injection in engines. However, our comprehension of combustion is still far from complete. In a pre-mixed flame the simultaneous occurrence of chemical reaction and transport of mass, momentum and energy makes analyses of these problems difficult. Practical flames are nearly all turbulent which further complicates combustion research. Of primary importance is the 'burning rate' which directly affects the heat release and pressure development in energy conversion systems, it is often expressed as a burning velocity.

In this work a recently developed experimental technique has been used to measure the turbulent burning velocity based on the rate of production of burned mass, u_{tr}, over an extensive range of conditions. Laminar flames have also been studied over the same range of conditions.

1.2 Philosophy of current work

The main source of turbulent burning data is the 1992 Leeds correlation by Bradley *et al.* (1992) which contains 1650 measurements of u_t. With the realisation of the importance of proper definition of the u_t and with the developments in measuring accurate values of u_t, there has been cause to re-investigate turbulent burning velocities (Gillespie *et al.*, 2000).

In this current study a newly developed technique has been utilised. The method uses a single flame kernel ignited centrally filmed using high-speed schlieren photography, which has been supported by laser sheet measurements performed by Bradley *et al.* (2003). The new method allows for direct measurement of u_{tr} from a schlieren flame speed.

The 1992 correlation contained measurements mainly at atmospheric pressure and temperature with no experimental data above 0.2 MPa and less than 3% measured above 100°C, furthermore the majority of data was at stoichiometry. The 1992 correlation does not include data at the elevated temperatures and pressures experienced in real energy conversion systems where operating flame conditions can exceed 6MPa, 1000 K, turbulent r.m.s velocities of 20 m/s and any equivalence ratio within the flammability range. It was therefore decided to perform new measurements over the full range of conditions that were experimentally practical; the base pressure was chosen as 0.5 MPa and experiments were performed over the range 0.1 MPa to 1.0 MPa. It was also decided to probe the effect of equivalence ratio over the ignition range, fuels were chosen to determine any effect of the Lewis number / Markstein number. The turbulent r.m.s velocity was studied up to a maximum u' of 6 m/s. Within the time frame of this work it was felt impossible to extent this project to studying the effect of temperature.

The overall aim of this work was to move towards generating a new turbulent burning velocity correlation.

1.3 Laminar Flames

The understanding of laminar combustion is a pre-requisite to the understanding of turbulent flames as it has become widely accepted that under certain conditions a turbulent flame can be treated as an array of laminar flamelets (Bradley, 1992). The one dimensional unstretched laminar burning velocity is an intrinsic property of a combustible fuel-air mixture. It is defined as, 'the velocity, relative to and normal to the flame front, with which the unburned gas moves into the front and is transformed in to products under laminar flow conditions', (Heywood 1998). The unstretched laminar burning velocity, u_l, is a physico-chemical parameter dependent only on mixture composition, pressure and temperature. Shown in Fig. 1.1 are the reported values of the laminar burning velocity for atmospheric, 298 K, methane-air flames from years 1915 to 2000, reproduced from Bradley (2000). It was only towards the end of the 20th century that there was convergence towards an 'accurate' value with the better understanding of flame stretch. Flame stretch occurs in flame sheets due to transverse velocity components and flame curvature, both of which stretch the flame. The rate of stretch has been found to alter the burning velocity; Aung *et al.* (1995), Bradley *et al.* (1998). Experimentally a perfectly one dimensional unstretched laminar flame can not be achieved, due to this and inadequate account taken of key variables that affect measurements of u_l there has been historically great variation in measured values. The effect of flame stretch and the accurate measurement of the laminar burning velocity in covered in more detail in Chapter 3.3.

'The flame front of a flame does not represent a discontinuity between unburned and burned gas' Gillespie *et al.* (2000). Shown in Fig. 1.2 is an illustration of the structure of a pre-mixed methane-air flame (Peters 2000). The structure of a laminar flame is made of several zones, firstly the preheat zone, followed by the many reaction zones and the oxidation layer. The actual distance between completely unburned and burned gas is difficult to quantify because the reaction to burned gas occurs gradually. The laminar flame thickness, δ_l, is defined as a characteristic length rather than an actual, various definitions have been suggested. In the current work hydrodynamic length is used throughout, $\delta_l = \nu/u_l$; where ν is the

mixtures kinematic viscosity. The flame thickness is an important parameter as its size determines to what extent turbulence may interact with a flame.

Another topic of laminar flames worthy of discussion here is flame instability. Law *et al.* (1997) described the development of flame instabilities in the form of cells and ridges of characteristic sizes over the flame surface as 'perhaps one of the most beautiful and fascinating phenomena in flame dynamics'. In this study cellular flames were observed at many conditions (see flame images of Chapter 4), however, here the mechanisms behind flame instability is not an area of interest, often these effects were a hindrance to gaining accurate data from the laminar flames.

1.4 Turbulent flames

It is possible to define a u_t 'based on the entrainment of fresh unburned gas into the flame (u_{te}) or on the mass rate of burning necessary to produce the actual rate of heat release (u_{tr})' Gillespie *et al.* (2000). Problems in measuring u_t arise due to the number of variables; fuel, equivalence ratio, temperature, pressure, ignition method, r.m.s turbulence velocity, length scale, and flow field. There have been many studies but due to the number of variables, different possible u_t definitions and the difficulty of measurement there remains considerable debate on the effect one variable may have. In the reported data it is not always clear which definition of u_t has been used, turbulence parameters have not always been properly measured.

1.5 Regimes in Premixed Turbulent combustion

Turbulent flames found in practical applications cover a wide range of conditions. Regime diagrams have been proposed by Borghi (1985), Peters (1986), Abdel-Gayed and Bradley (1989) and Poinsot *et al.* (1990). Dimensional analysis reveals several regimes of premixed combustion modes when thought of in terms of two dimensionless numbers, the ratios of;

1. the root mean square velocity fluctuation of the turbulent flow (u') to the laminar burning velocity (u_l),
2. the turbulent integral length scale (L) to laminar flame thickness (δ_l).

The integral length scale is one of the many length scales defined to characterise turbulence; it physically represents the mean size of the largest eddies in a turbulent flow. Other scales include the Taylor microscale, λ, which is an intermediate length scale, and the Kolmogorov microscale, η, which is the smallest scale where eddies are small enough to interfere with flame reaction thickness.

Figure 1.3 shows the suggested regimes of Peters (2000), in this figure the laminar burning velocity has been given the notation s_l. In this diagram different regime transitions are associated with lines corresponding to values of more dimensionless numbers. The Reynolds number is defined as,

$$\mathrm{Re} = \frac{u' L}{u_l \delta_l} \qquad 1.1$$

Turbulent flame stretch is quantified by the Karlovitz stretch factor, K (Ka).

$$K = \frac{u' \delta_l}{u_l \lambda} \qquad 1.2$$

K can be thought of as the ratio of chemical to eddy lifetimes. A second Karlovitz number is also defined which is relevant to the laminar flame thickness (Peters,2000).

$$K_\delta = \delta_l^{\,2} K \qquad 1.3$$

The lines drawn by $Re = 1$ and $K = 1$ represent the boundaries between different regimes of premixed turbulent combustion. Also the lines $u'/u_l = 1$ and K_δ which further subdivide the plot. The regimes of premixed combustion are identified as:

1. Laminar flame regime, characterised by $Re < 1$,
2. Wrinkled flamelet regime, characterised by $Re > 1$, $K < 1$ and $u' < u_l$
3. Corrugated flamelet regime, characterised $Re > 1$, $K < 1$ and $u' > u_l$,
4. Thin reaction zone, characterised $Re > 1$, $K > 1$ and $K_\delta > 1$,
5. Broken reaction zone, characterised by $Re > 1$, $K > 1$ and $K_\delta < 1$.

The regimes of interest in the current work are 'corrugated flamelets' and 'thin reaction zones'. In both cases the turbulent flame can be treated as an array of 'laminar flamelets' burning at (nominally) u_l. In the corrugated flamelet regime the entire reactive-diffusive flame structure, which includes preheat and oxidation layers is smaller than η. This allows the entire flame structure to exist within eddies of the Kolmogorov scale, the flame structure is therefore unperturbed by turbulent fluctuations and remains quasi-steady (Peters, 2000). In this regime the larger eddies existing in the flow wrinkle the flame surface.

In the thin reaction zone Kolmogorov scales become small enough to enter into the flame structure and can bodily transport hence manipulate the pre-heat zone, however these small eddies are still larger than the inner laminar flame thickness, δ_l.

Stated simply in the corrugated flamelet regime the time taken by a turbulent eddy to rotate is less than the time the flame front takes to pass through that area of space. Within the 'thin reaction zone' the turbulent eddies rotate at a faster rate and have time to disrupt the preheat zone ahead of the flame.

1.6 Building on the Leeds 1992 correlation.

In the Leeds correlation (1992) the data was shown non-dimensionally in terms of u_t/u_l and u'_k/u_l, where u'_k is the effective r.m.s turbulent velocity influencing the flame. The ratio of u_t/u_l represents the increase in the burning velocity due to turbulence, the ratio u'_k/u_l is a flame 'wrinkling factor'. The effect that flame stretch has upon a flame is related by using the Lewis number, defined by;

$$Le = {D_T}/{D_{ij}} = \frac{thermal}{mass} \; diffusion \qquad 1.4$$

Where the diffusion coefficient of the deficient the reactant (into nitrogen) is known. Bradley *et al.* (1992) found that the best correlation to the experimental data was found when using the product of $K\,Le$.

This correlation contains the majority of u_t data captured to 1992 but little is data at elevated pressure or over a wide range of equivalence ratio. This correlation was described as a correlation of u_{te} by Gillespie *et al.* (2000). Abdel-Gayed *et al.*

(1987) identified the second definition of u_{tr}, a true burning rate based on the conversion rate to burned products.

Since 1992 our understanding of premixed combustion has developed in a number of ways;

- The importance of flame stretch in laminar flames has lead to a huge improvement in the reproducibility of laminar burning velocity measurements.
- The importance of the careful definition of the turbulent burning velocity has been realised.
- The effect of elevated pressure on premixed combustion has become increasingly questioned.

1.7 Scope of the thesis

This thesis reports an experimental study of turbulent burning velocities over a range of pressures, fuel types, equivalence ratio and turbulence levels (660 experiments). Schlieren photography has primarily been used, simultaneous pressure recordings have also been taken throughout. Laminar burning velocities were also found for each condition.

The experimental techniques used are reported in Chapter 2, in Chapter 3 the measurement of laminar and turbulent burning velocities are discussed. Chapter 4 presents a substantial number of new laminar burning velocities and associated measured markstein lengths, these values make interesting comparisons with the turbulent experiments.

Chapter 5 discusses the trends found in turbulent experiments and suggests a methodology for correlating the turbulent measurements. Chapter 6 investigates the effect of equivalence ratio on the turbulent burning velocity, experiments here were performed to the ignition limits (both rich and lean) of five fuels ranging from reference fuels to a commercial gasoline. In Chapter 7 a new experimental database of iso-octane air mixtures has been collected, pressures ranged from atmospheric pressure to 1 MPa, using a limited number of equivalence ratios but over a wide

range of r.m.s turbulence levels. This new database and the results of Chapter 6 have been compared with several existing turbulent burning velocity correlations.

Conclusions from the current work and suggestions for further research are presented in Chapter 8.

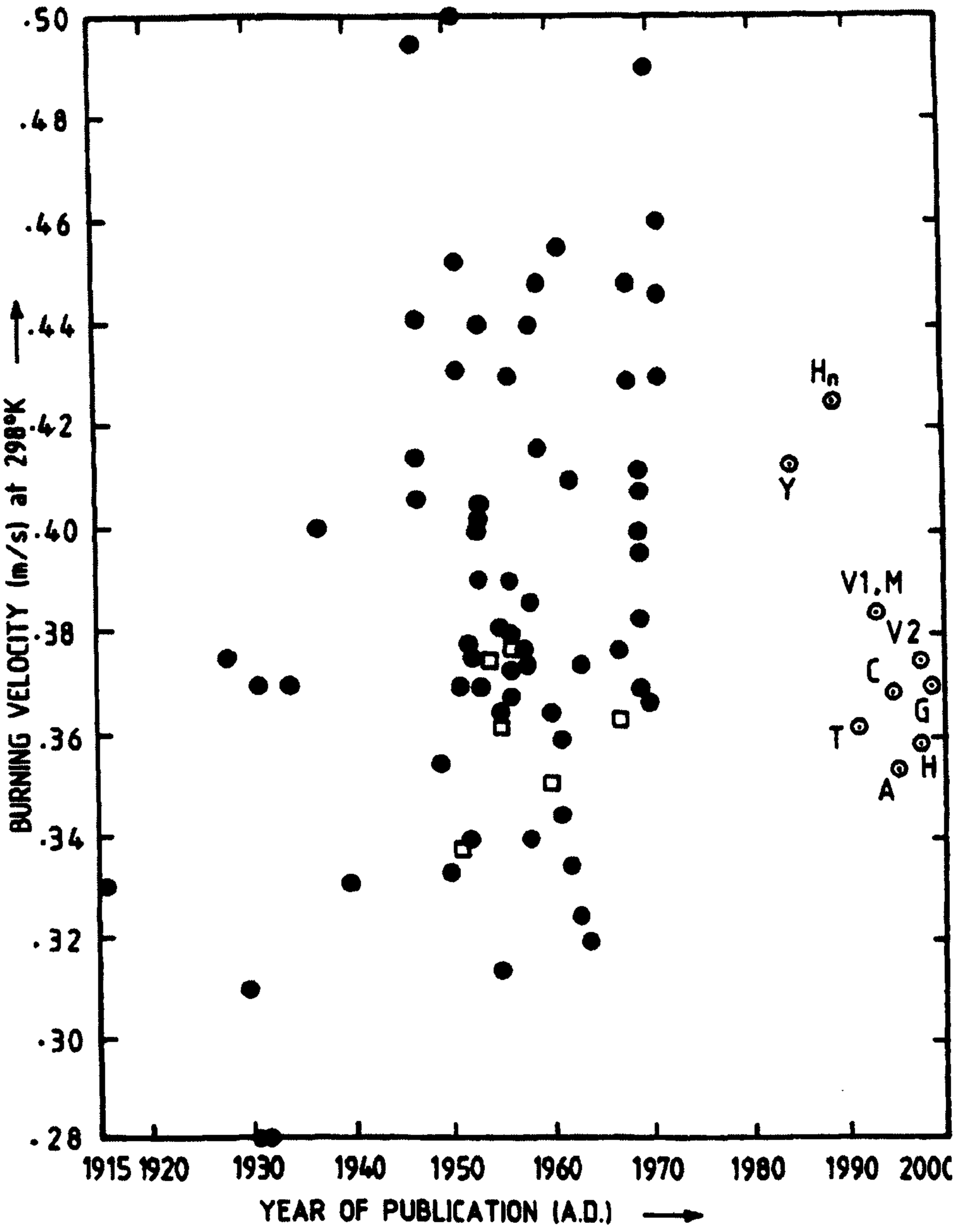

Figure 1.1. Maximum measured burning velocities of methane-air mixtures (initial ambient conditions – 0.1 MPa) since 1915. For key to data before 1972 see Andrews and Bradley, 1972. Square symbol indicates open-tube method. Reference for later data are: A Aunge *et al.* (1995), C Clarke *et al.* (1995), G Gu *et al.* (2000) ,H Hassan *et al.* (1998), Hn Haniff *et al.* (1989), M Van Maaren *et al.* (1994), T Taylor (1991), V1 Vagelopoulos *et al.* (1994), V2 Vagelopoulos *et al.* (1998), Y Yamaoka and Tsuji. (1984). Source: Bradley (2000).

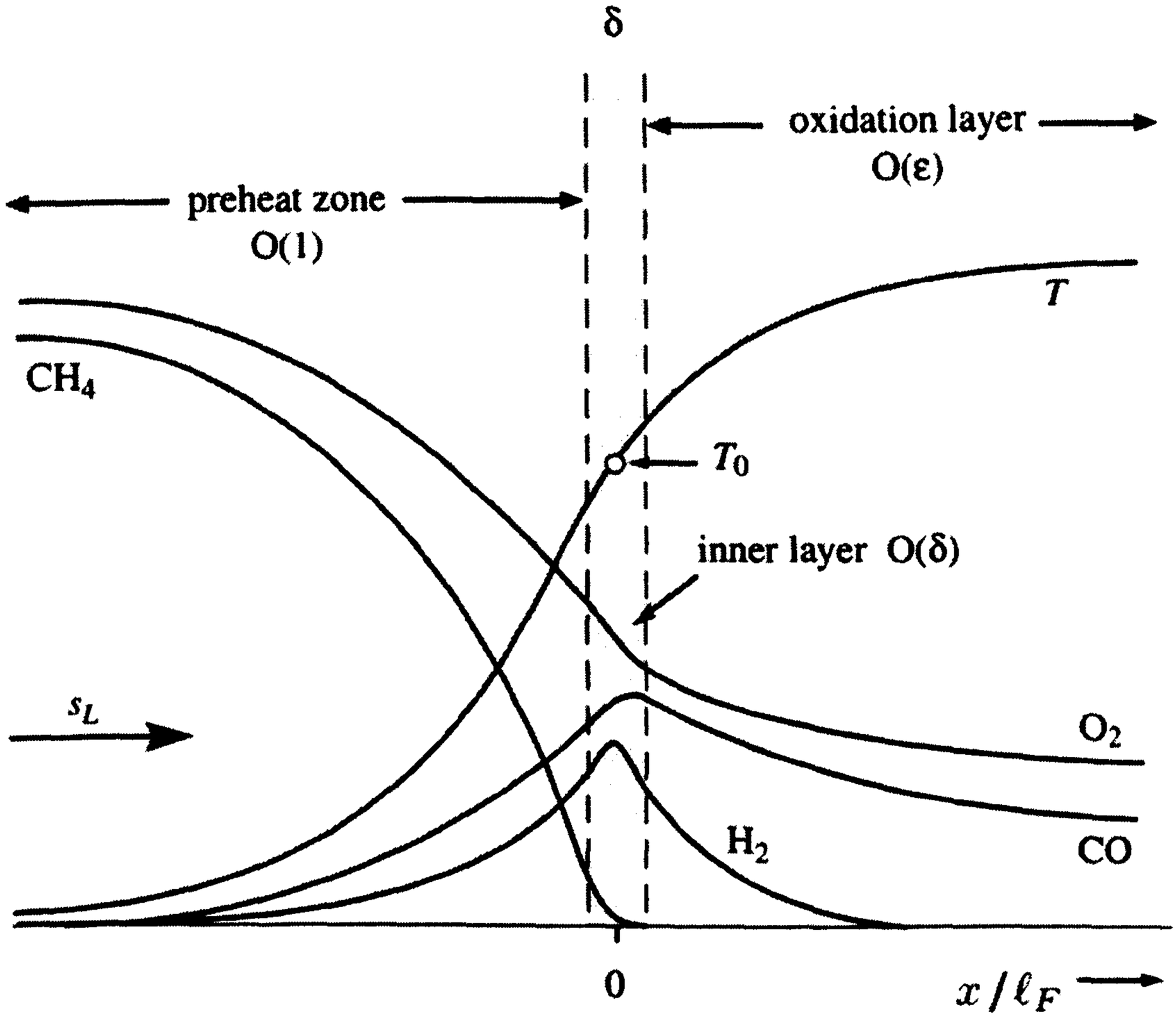

Figure 1.2 Schematic illustration of the sturcture of a pre-mixed methane-air flame.
(reproduced from Peters 2000)

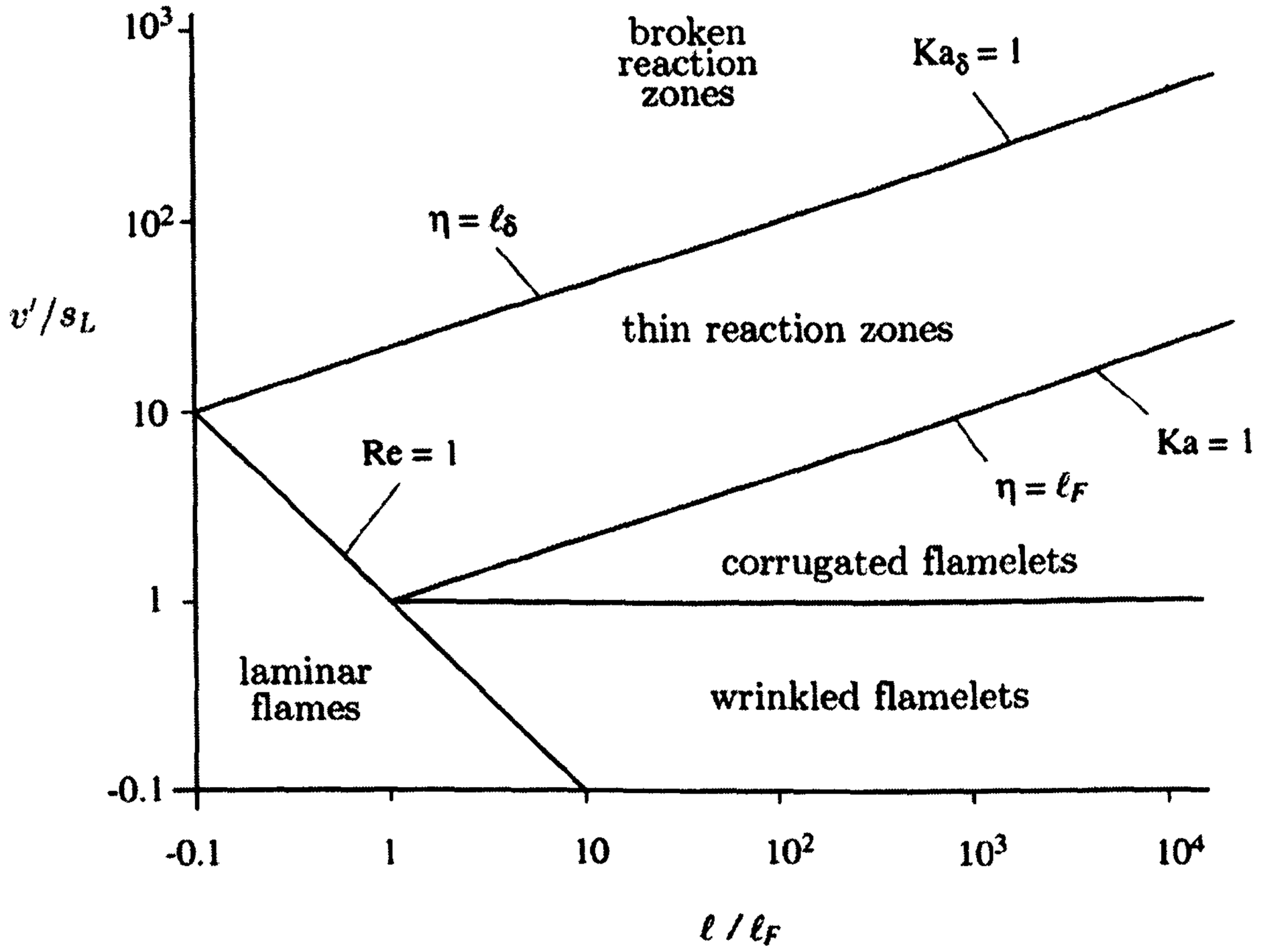

Figure 1.3 Regimes for pre-mixed turbulent combustion. (reproduced from Peters (2000))

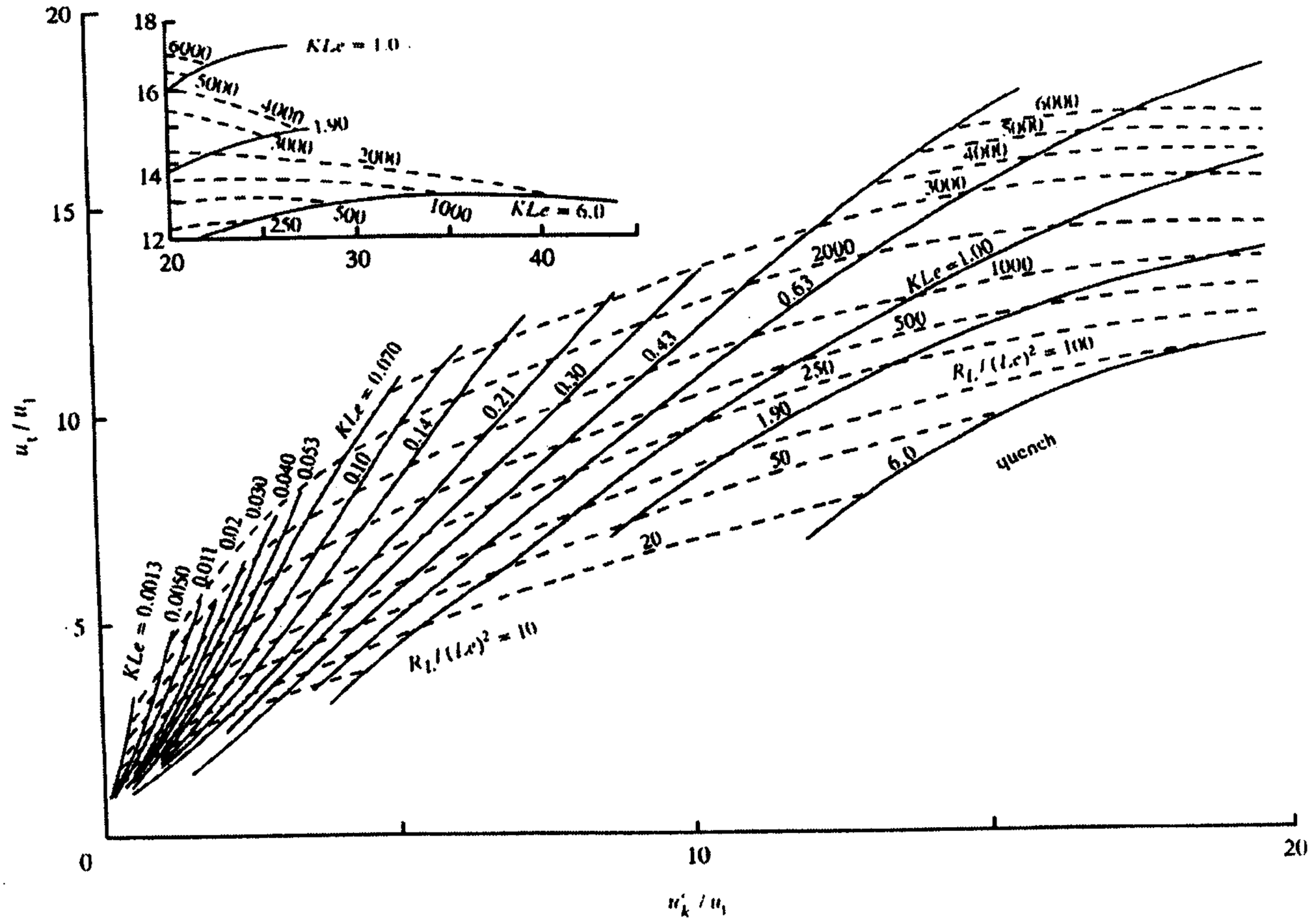

Figure 1.4 Correlation of turbulent burning velocity by Bradley *et al.* (1992)

Chapter 2 Experimental Apparatus and Techniques

2.1 Introduction.

Deflagrations were studied for methane, methanol, iso-octane, binary mixtures of methane and hydrogen and a commercially available gasoline (Dutch Pura) supplied by Shell Global Solutions. Fuel-air mixtures were ignited centrally and the expanding flame propagation was studied by schlieren photography using high-speed digital cameras and simultaneous pressure recordings. Both laminar and turbulent flames have been studied for a range of pressures and fuel-air ratios. Iso-octane experiments have been performed over an extended range to build a new database for a range of unstudied conditions. At a fixed turbulence of $u' = 2$ m/s, pressure of 0.5 MPa and 360 K all of the fuels studied were tested over their ignition range up to a maximum equivalence ratio of 2. The turbulence induced by the fans in the vessel has previously been studied with LDV (Bradley *et al.*, 1996a). Apparatus common to these techniques are reported, brief descriptions have been given where detailed information exists in the literature.

2.2 The combustion vessel

Experiments were performed in a stainless steel vessel (Fig.2.1) of inner diameter 380 mm, initial mixtures could be made up to temperatures of 600 K and pressures of 1.5 MPa. Three pairs of orthogonal quartz windows of diameter 150 mm and thickness 100 mm were mounted in the vessel, providing excellent optical access for photographic and laser sheet techniques.

Turbulence was generated in the bomb by four identical eight bladed fans in a tetrahedron configuration. The fans were directly coupled to electric motors with separate speed controllers. Each fan was separately adjustable between 3.3 to 167 Hz (200 to 10,000 r.p.m.) and controlled by solid state variable frequency converter

units. The individual fans were kept within ±5% of each other to attain the required turbulence intensity.

Previous workers found a central region of uniform isotropic turbulence where the r.m.s turbulence velocity, u', was found to be represented by

$$u'\,(\text{m/s}) = 0.00119\, f_s\,(\text{rpm}) \qquad (2.1)$$

where f_s is the fan speed (Bradley *et al.*, 1996a). This correlation was found valid for all operating pressures, temperatures and mixture viscosity. The integral length scale L was found by two-point correlation to be 20 mm and was independent of all operating variables, Nwagwe *et al.* (2000).

The initial mixture temperature was measured using a 1.5 mm diameter K type stainless steel thermocouple that was situated near the vessel inner surface. The mixture temperature was displayed on a CAL320 PID temperature controller, the unit also controlled the vessel heater during mixture preparation. The entire vessel was preheated by a 2 kW heater situated within the vessel. When the operating temperature was reached the controller unit switched the heater on and off to maintain the desired temperature. The external surfaces of the vessel were insulated to minimise heat losses. An external piezoresistive pressure transducer (Druck) was employed to measure the internal pressure during mixture preparation and initial pressure, this transducer was situated outside the vessel and was isolated just prior to ignition as its maximum working pressure was 1.5 MPa.

2.3 Mixture preparation

Mixtures were prepared in the vessel. After every experiment pressurised laboratory air was flushed through the vessel for a minimum of 3 minutes. The bomb was then evacuated twice to 0.02 MPa (absolute) and then filled to atmospheric pressure with dry cylinder air provided by BOC and finally evacuated to 0.01 MPa. This operation ensured there was less than 0.5 % residual products from the previous experiment. After the final evacuation the vacuum line was sealed and the main exhaust valve closed. The vessel was then filled to around half an

atmosphere with dry cylinder air to allow mixing of incoming fuel and to have enough gas in the chamber for an accurate temperature reading.

Gaseous fuel mixtures were prepared using partial pressures. Liquid fuels were injected into the vessel with a "Gas Tight" syringe through a needle valve. Two syringes were available a 10 cm^3 and a 50 cm^3 which were used depending on the volume of fuel required. Fuels were injected into the vessel under the partial vacuum (circa 0.05 MPa) after the purging of the vessel, dry cylinder air was then added to the desired pressure. Dry cylinder air was used to remove any effect of day to day atmospheric humidity variation. The fans were run during preparation to ensure full mixing and to maintain heat transfer around the vessel from the heater.

The heating control of the vessel was found to be limited with the PID controller being able to maintain the vessel temperature to within a range of approximately +/-5 ^{0}C. To avoid possible variation in the mixture stoichiometry, the bomb temperature was maintained at 20 ^{0}C above the ignition temperature. When attaining the ignition pressure the vessel heater was switched off causing the vessel and mixture to cool. During this process the pressure in the vessel would slowly (of the order of 1-2 min) reduce and dry cylinder air was added to maintain the desired pressure, the pressure repeatability was within +/- 0.001 MPa. It was found that there was no leakage from the vessel during this period, turning the heater back on resulted in returning to the original pressure and temperature. This process ensured that the ignition temperature reading was consistently 360 K throughout all of the deflagrations, its is possible that this value is not truly representative of the entire bomb temperature, but by allowing this cooling process the ignition temperature was consistent. Applying this method gave a large improvement in experimental repeatability, reducing the variations in pressure and temperature which would manifest in a shift in mixture equivalence ratio. When adding gaseous fuels into the "overheated" bomb is was necessary to account for the partial pressure difference between the fuel addition temperature and the ignition temperature.

For laminar studies the fans were switched off when the mixture was prepared, 60 seconds were then timed before ignition. In turbulent tests the fans were

maintained at the desired ignition turbulence intensity throughout mixture preparation and firing.

2.4 Ignition systems

Ignition was initiated from an in house built stainless steel/ceramic sparkplug with gap of 0.5 mm mounted in the centre of the vessel. A Lucas 12 V transistorised automotive ignition coil system was connected to the spark electrode assembly. The ignition circuit was earthed via the spark plug holder and the main body of the vessel. Average spark energy was measured by Bradley *et al*. (1996a) to be 23 mJ. For fuel lean conditions (only iso-octane database experiments, Chapter 7) close to mixture flammability limits, a high-powered spark producing 300-400 mJ ignition system was used, described by Atzler (1999).

2.5 Transient pressure recording

The pressure rise during the explosion was measured by a piezoelectric dynamic pressure transducer Kistler 701 which was flush mounted on the inner wall of the vessel. The charge from the transducer was converted to a voltage (0-10 V) by a Kistler 5007 charge amplifier. An analogue to digital converter (ADC) Microlink4000 digitised the voltages from the charge amplifier, which were then stored on a PC. The charge amplifier sensitivity was fixed for all experiments at 0.1 bar/volt allowing the first 0.1 MPa rise in pressure to be digitised. The Microlink 4000 ADC had a limited 10 bit resolution, (10^2 bit over 10 volts with a sensitivity of 0.1 bar/volt gave the smallest measurable increment of 9.77×10^{-3} volts and 9.77×10^{-4} bar). Due to this limitation only the initial stages of combustion were recorded before the flame reached the fans (100 mm from spark gap). It was necessary to supply a +0.2 V offset as a slight negative voltage was outputted from the Kistler 5007 charge amplifier. Sampling was performed at 20 kHz for all experiments.

Ignition was triggered from a "make" in a safe area of the laboratory protected by a steel reinforced wall. The trigger signal was split into three by a trigger box sending a "break" to the camera controller, a "make" to the Lucas electronic ignition

amplifier and a "TTL" signal to the ADC comparator started the collection of pressure data.

2.6 Digital schlieren photography

A total of three high-speed digital cameras were used through the current study. The experimental schlieren set up which collected the iso-octane database slightly differed from that used in the later work.

The iso-octane database (discussed in Chapter 7) turbulent optical experimental set up was as follows (shown in Fig.2.2). A 20 mV He-Ne laser was used as a schlieren light source, expanded by a microscope objective 40/:65/160 onto a plane concave lens diameter 47 mm and a focus of –50 mm. This over expanded the beam so using only the bright centre of the lasers' gausian profile reducing the light distribution over the bomb window. An iris was placed after this lens to remove stray light. A 150 mm plane convex lens with a focus of 1000 mm was used to normally adjust (make parallel) the light prior to entering the bomb. A 150 mm plane convex lens with focus of 500 mm focused the light to a pinhole (diameter of less than 1 mm). The pinhole blocked off some of the incident light allowing the refraction of light due the changes in density to be clearly visualised. Light from the pinhole was projected onto a glass diffuse screen. A Kodak Ektapro 4540mx (NDOS) imager was positioned at the end of the Schlieren system. A Nikon AF micro 60 mm aperture 1.8 mm was attached to the camera focusing the image from the diffuse screen onto the camera chip (256x256 pixels with 256 grey scale). The digital camera framed at 4500 frames per second storing each image in TIFF format to the camera controller and via a SCSI link to a personal computer after each explosion.

Later turbulent work (effect of equivalence ratio discussed in Chapter6) was performed using the Photosonics Phantom 4 (CMOS) camera (shown in and Fig. 2.3). Which allowed 3700 frames per second to be captured (256x256 pixels with 256 grey scale). The He-Ne laser was replace with a 20 W tungsten element lamp which provided a significant improvement in image quality due to its flat beam profile compared to the gausian laser beam. A convex lens with was positioned at

its focal length (50 mm) from the tungsten element, an iris was place at the upstream focal length of the convex lens providing a single point light source. This light was then focused into normal adjustment using the 150 mm plane convex lens with a focus of 1000 mm, the 150 mm plane convex lens with focus of 500 mm focused the light to a pinhole (diameter of less than 1mm). The light from the final pinhole was focused directly onto the camera chip avoiding the need for the diffuse screen. A PC using a Firewire connection controlled the camera, image sequences were saved in a manufacturer specific "*.cin" format which was converted to a string of tiff images within the Photosonics software.

The third camera the Photosonics Phantom 9 (CMOS) was used for the turbulent dutch-pura turbulent testing (effect of equivalence ratio discussed in Chapter6). This camera captured was used at (512x512 pixels with 256 grey scale) 3700 frames per second. The schlieren optics remained the same as used with the Phantom 4 camera.

All laminar work was captured at 1000 frames a second at (512x512 pixels with 256 grey scale) using the Phantom 4 camera and experimental set-up.

2.7 Data processing

2.7.1 Schlieren images collected using the Kodak Ektapro 4540mx

Shown in Fig. 2.4 is an example image captured when using the Kodak Ektapro 4540mx, it was taken immediately prior to ignition. The light level across the bomb was gausian with the beam noticeably off centre. Diffraction patterns generated in the optic system were visible. The marks on the window are small chips and dirt build up.

2.7.1.2 Optical image distortion (Ektapro 4540mx)

The spatial resolution (mm^2/pixel) was found to vary over the bomb window (only found when using Kodak Ektapro 4540mx). The laser light entering the bomb not being in normally adjusted caused this. Transparent calibration sheets one with concentric circles increasing in 1cm diameters and the second a 1cm grid were place

just in front of the bomb window and the camera triggered. The captured images showed a clear distortion with radius, fortunately the distortion was found to be one-dimensional with radius (Fig. 2.5). The graph Fig. 2.6 of measured radius against real radius shows the distortion increasing with the distance from the spark (found using a fixed scalefactor of 0.6399). A function was found relating radial pixel distance and spatial resolution, the function related the scalefactor (real length (mm) to image length (pixel lengths)) to distance from the spark plug in pixel lengths.

$$Scalefactor = (-0.0006 \times radius\ in\ pixel\ lengths) + 0.6399 \qquad (2.2)$$

2.7.1.3 Image quality (Ektapro 4540mx)

Attempts were made to batch process the operation of finding the flame edge, to produce a binary image file using Adobe PhotoShop 6.0 filters. Small flames showed a clearly defined edge. Unfortunately for flames larger than 5 cm radius the edge degraded. The gausian profile of the laser beam profile caused the schlieren signal to weaken radially from the centre, background grey scale values were 256 (white) at the spark plug to circa 40 approaching the bomb widow. As flames passed through the weaker schlieren area a proportion of pixels either side of the flame front had equal values due to the relatively poor grey scale resolution of the camera. This caused a thresholding method to be ineffective.

2.7.1.4 Image processing (Ektapro 4540mx)

The use of the digital camera has aided the time consuming processing of turbulent flames compared with traditional wet filming. The camera stored 4500 (256x256pixel) images per second in Tiff format. All image processing was performed using Adobe PhotoShop 6.0 which allowed "actions" to be programmed which then could be run as a batch on all images in a directory. Ignition was recognised as the first frame containing burnt material visible on the schlieren imaging. To find burning velocities from the flame image required the flame area to be found for each frame of the explosion. The first stage was to equalise the images, this was done in a batch operation (Fig. 2.7 (a) and (b)). The "equalise" command redistributes the brightness values of the pixels in an image to distribute the intermediate pixel values evenly throughout the greyscale.

2.7.1.4 Hand tracing (Ektapro 4540mx)

The flame edge was then traced by hand using the lasso tool in conjunction with an action, which filled the selected flame area white, and the outer area black (Fig.2.7 (c) and (d)). Tracing images by hand was very time consuming, tedious and had inaccuracies. The individual error of each frame decreased with flame area, early frames had an area of as little as 5 pixels, the inclusion of one extra pixel results in a 20 % error. These initial kernels were also subject to spark effects and flow distortion cause by the spark plug itself.

This error in tracing individual frames was reduced as in the final burning velocity calculation the rate of change of flame area was found by using the "least squares" method to calculate the gradient of a straight line over a number of intervals. Repeated hand processing of the same explosion resulted typically 1 % variation in the burning velocity (at 30mm radius) between processing attempts.

2.7.1.5 Calculation of Flame area (Ektapro 4540mx)

The flame areas were found by reading the binary image files into a Fortran program "Edge7.exe". The input to the program was a script file containing the variables; spark gap co-ordinates in pixels, number of files to be processed and the file names. The program stored edge co-ordinates and then by integration totalled the pixel y co-ordinates around the binary flame edge when moving clockwise and subtracted when anti-clockwise.

"Edge7.exe" had to be altered to account for the optical distortion, The program outputted a list of areas (mm^2) and radii (mm) in a small text file. A "edge" file was also outputted for each image listing the edge co-ordinates in mm from the spark plug. The radius was that of a circle with the same area, this spherical assumption was necessary, its error should not be disregarded.

2.7.2 Schlieren images collected using Photosonics Phantom 4 and 9.

The image quality (grey scale distribution) was vastly improved due to the flat beam produced by the tungsten element Fig. 2.8. Care was taken using the transparent sheets during the optical set-up to ensure there was no optical distortion with all later work. True batch processing was now achieved within Adobe PhotoShop 6.0 by simply subtracting the background (pre-explosion) image from the subsequent images and then applying a threshold. This gave a binary image for each frame, the area taken up by the spark plug did then have to be draw in manually. This process was tedious it was however necessary to carry out by hand. The first several frames had to be hand traced (approximately to a flame radius of 2mm) due to the spark plug. Flame areas were calculated using a later edition of Edge7.exe named Edgesingle.exe. This later program simply counted the number of white pixels in the image and calculated radii based on a spherical assumption.

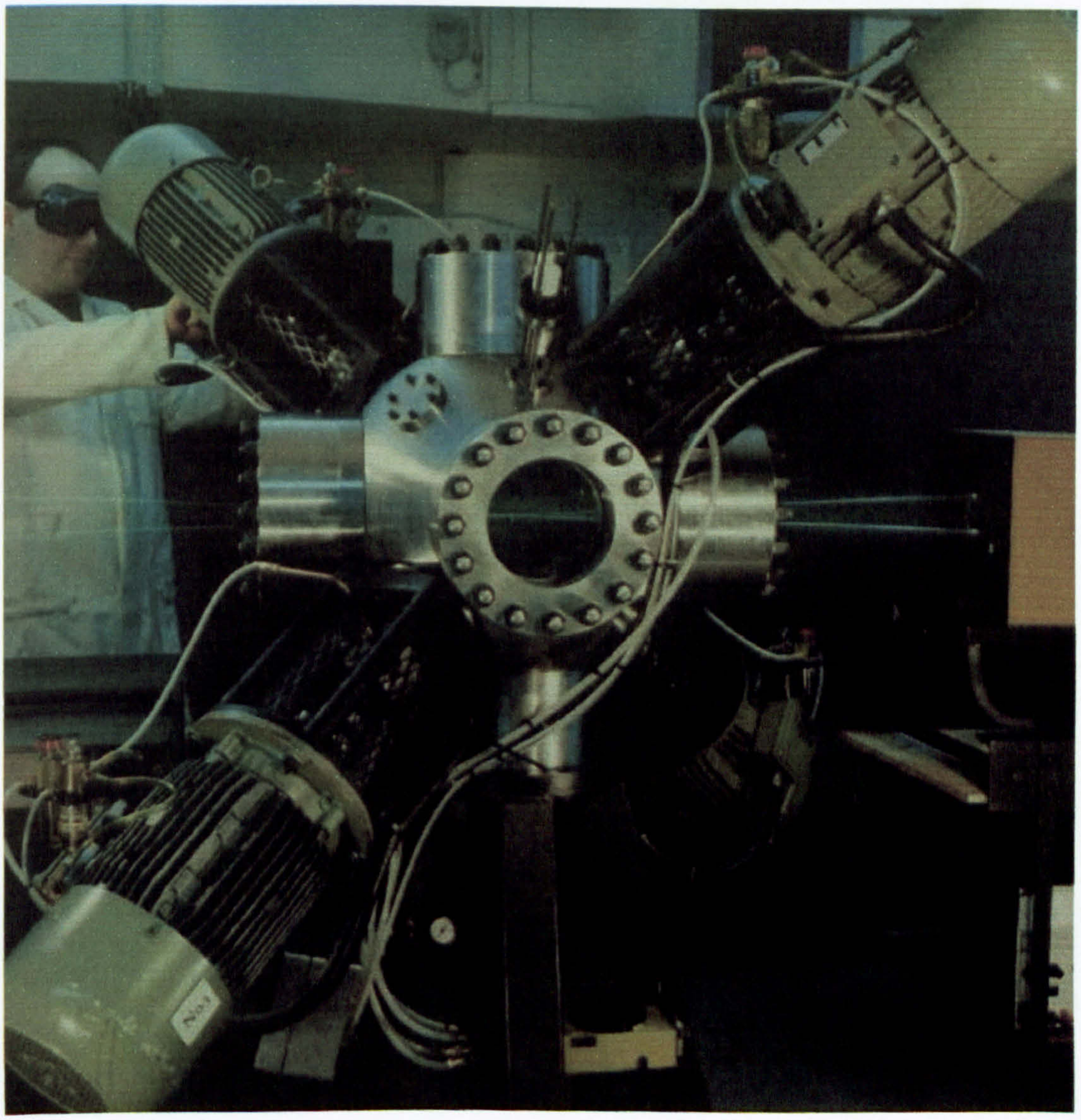

Figure 2.1 The fan-stirred Combustion vessel.

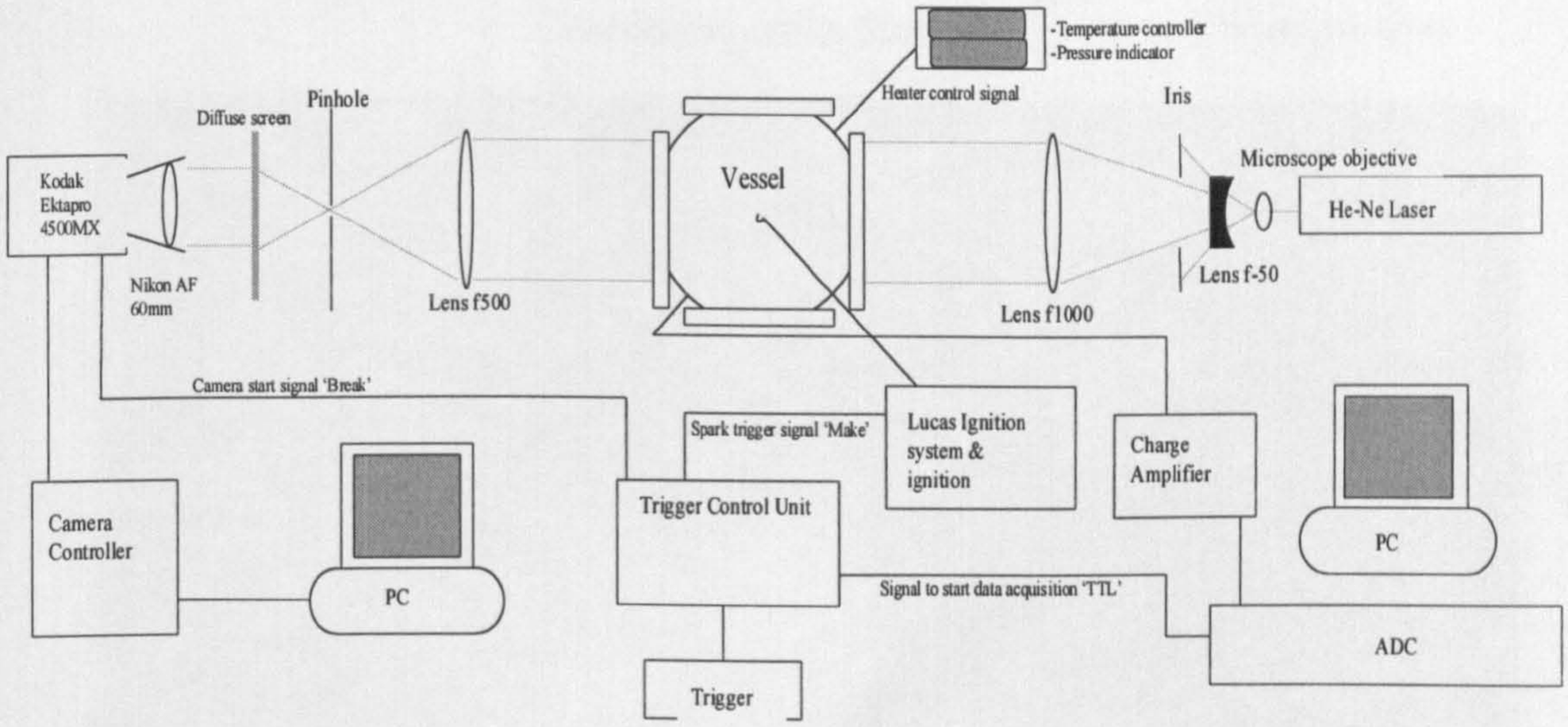

Figure 2.2 Optical set-up for schlieren photographic studies of turbulent flames with the Kodak Ektapro 4540mx.

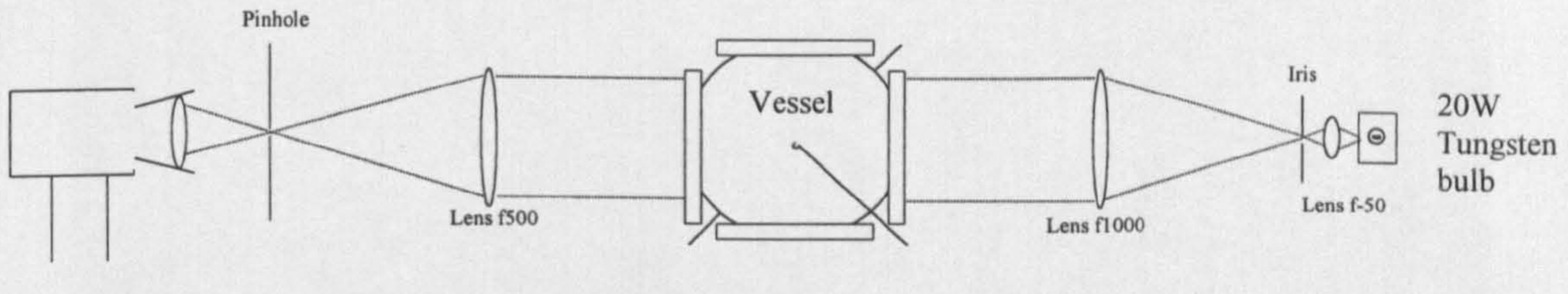

Figure 2.3 Optical set-up for schlieren photographic studies of turbulent and laminar flames with the Phantom digital cameras.

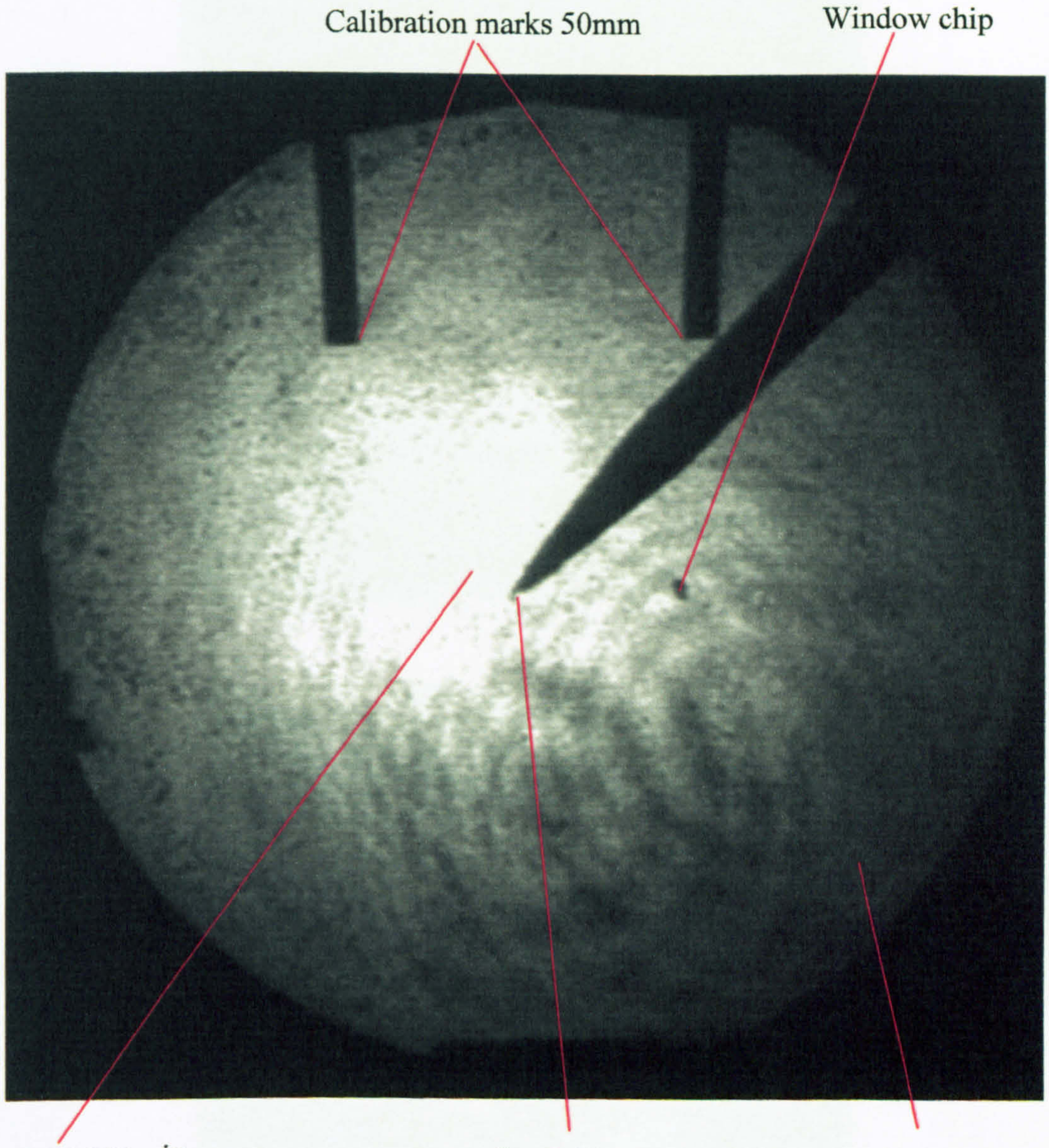

Figure 2.4 Example schlieren image gained from the Kodak Ektapro 4540mx schlieren configuration.

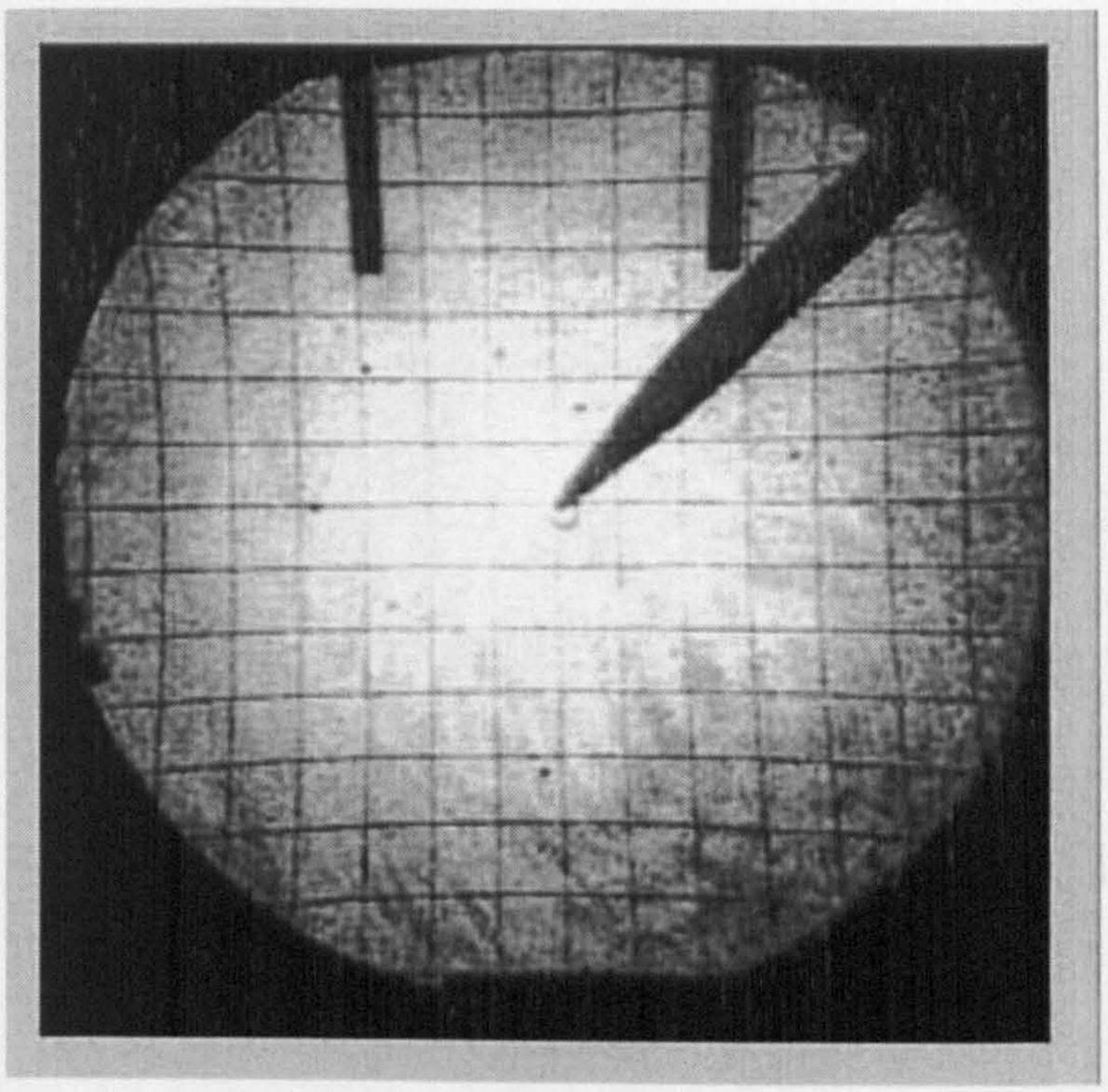

(a)

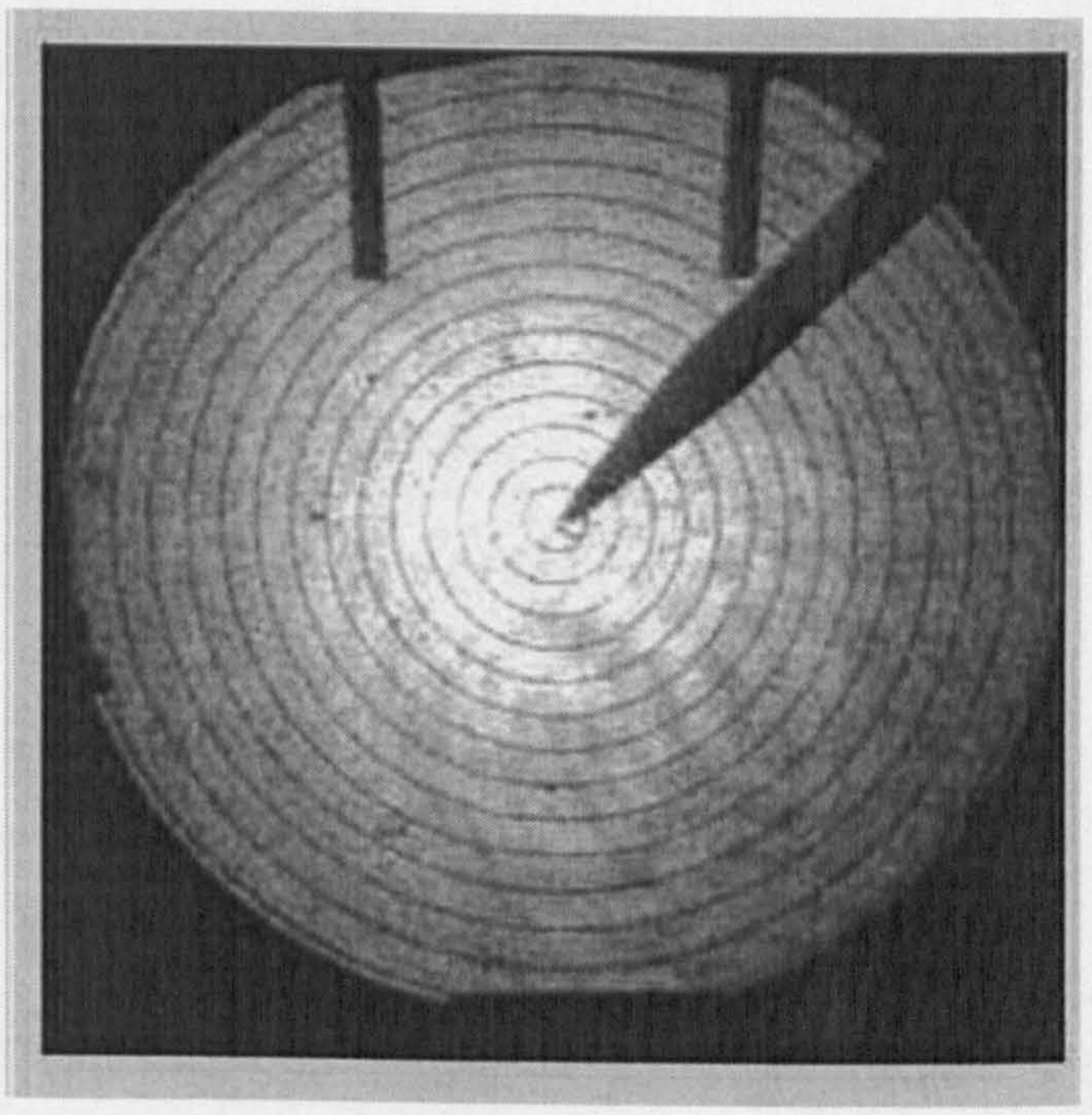

(b)

Figure 2.5 Image distortion with the Kodak Ektapro 4540mx schlieren configuration

(a) 1cm Squares, (b) Concentric circles of increasing radius of 1cm

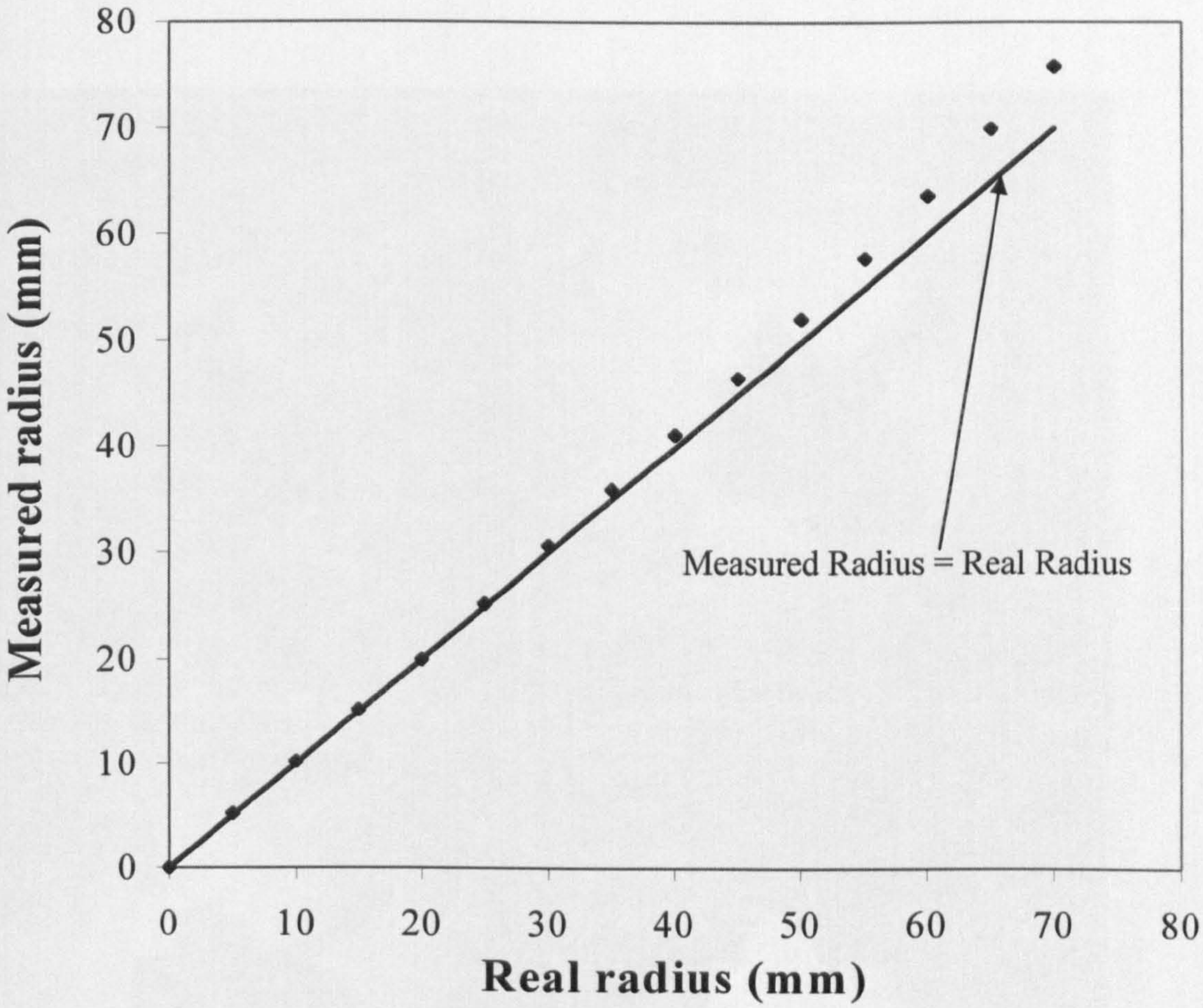

Figure 2.6 Measured radius against the known real radius.

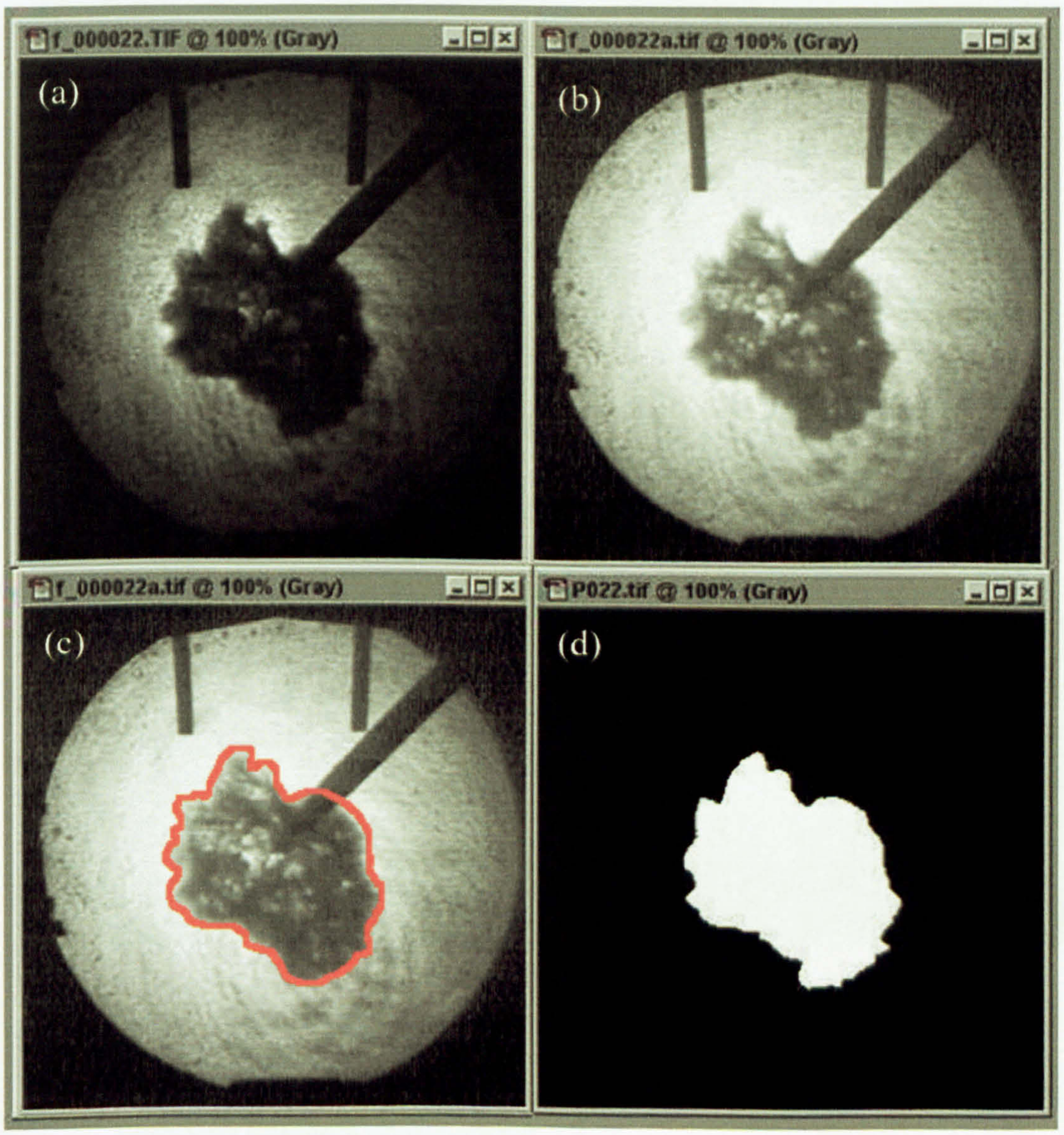

Figure 2.7 Image processing (a) original image, (b) "equalised" image, (c) hand traced selected flame area, (d) binary image)

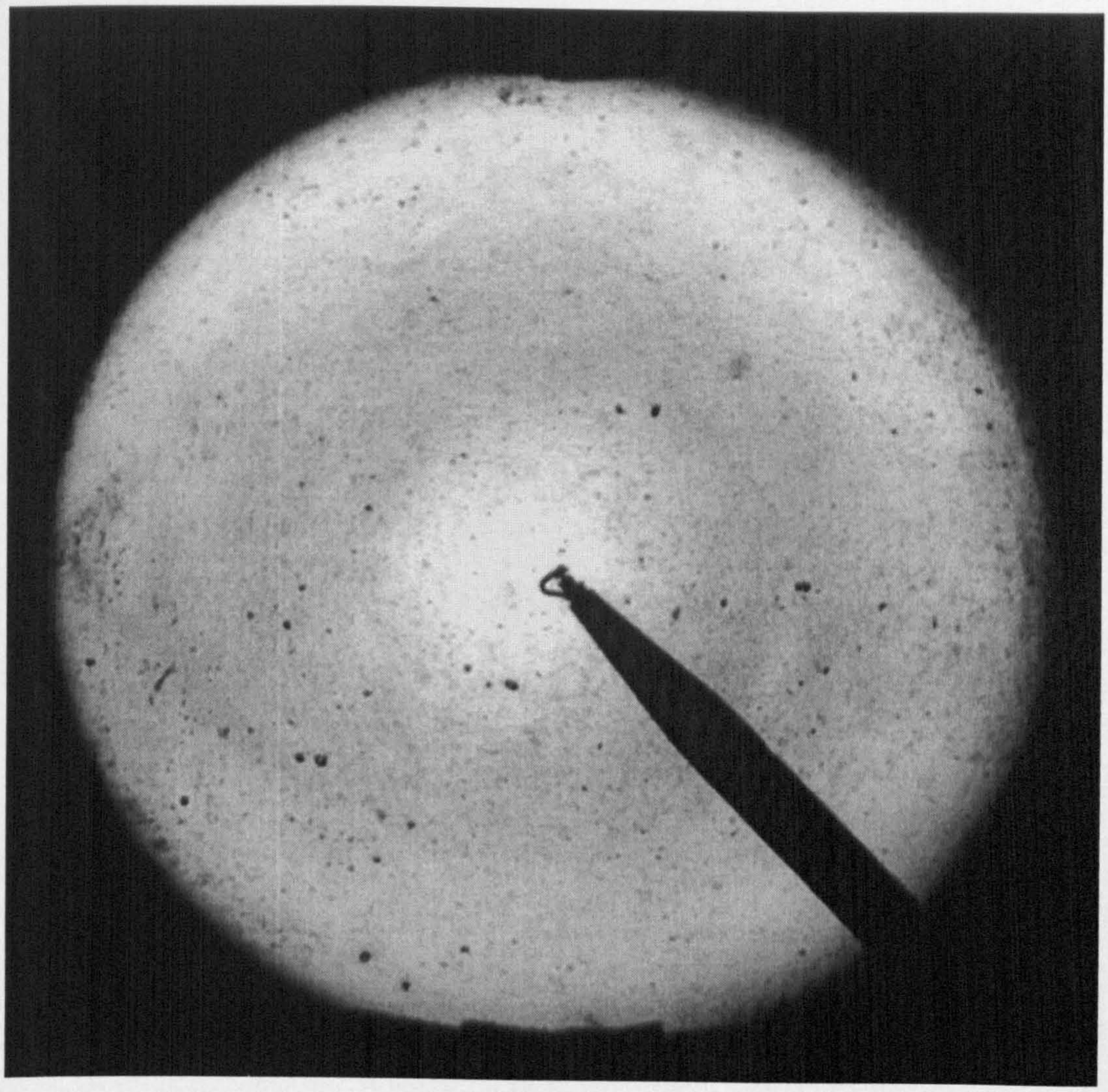

Figure 2.8 Example schlieren image gained from the Phantom 4 camera and improved schlieren configuration.

Chapter 3 Measurement of Laminar & Turbulent Burning Velocity & Markstein Length.

3.1 Introduction

In this study, spherically expanding flames have been investigated over a range of initial pressures, equivalence ratios, fuel types and turbulence intensities ranging from laminar to a u' of 6 m/s. Whilst the present study is focused on turbulent burning rates, laminar flames have also been measured at each condition to obtain the laminar burning velocity and related Markstein values, which each influence the turbulent burning velocity.

Simultaneous digital schlieren photography and pressure recordings were taken. Pressure based burning velocities were obtained for comparison with the expanded optically derived turbulent burning method. The collection of pressure records furthered the optical study of developing flames beyond the vessel window.

Measurement of the laminar burning velocity has developed over recent decades mainly as a result of the increased understanding of flame stretch. There are many previous workers who have completed experimental studies at well-defined stretch rates over a variety of conditions. (Taylor 1991, Ali 1995, Aung *et al.*1995, Bradley *et al.* 1996, Bradley *et al.* 1998, Aung *et al.* 1997)

Spherically expanding flames are well suited for laminar burning velocity measurement, as their flame stretch is uniform and unambiguously defined (Bradley *et al.* 1996, Dixon-Lewis 1990). The flames grow in the experimental vessel without geometric or flow constraints and reach the periphery of the optically viewed area without any significant increase in pressure. Within this pre-pressure period flame speed is observed directly from measurements of flame radius with schlieren photography. Calculation of the rate of change in area readily yields the stretch rate at any given flame radius allowing the unstretched laminar burning velocity and associated Markstein length to be found. Optical observation of the

flame allows the onset of cellularity to be noted where the flame can not longer be treated as a true laminar flame.

Turbulent flames are similarly recorded with digital schlieren photography and grow within the field of view during a pre-pressure period. Determination of turbulent burning rates is complicated by areas existing behind the flame front which are still burning. The schlieren image masks these unburnt areas behind the flame front. Previous to this work a simultaneous study of schlieren and sheet imaging was completed (Bradley *et al.* 2003), which determined the volume occupied by burnt gas within the schlieren image. A method of finding the turbulent burning velocity from the schlieren recording was shown (discussed in 3.4). This current work utilises these findings to gain defined turbulent burning velocities within a well-characterised flow.

3.2 Developing laminar flames

Laminar burning velocities and Markstein lengths were found from digital schlieren photography. Shown in Fig. 3.1 is an example explosion of stoichiometric methane-air at an initial pressure of 0.5 MPa and 360 K. The spark plug and spark kernel shape initially distorted the flame kernel, however laminar flames soon gain a spherical shape (Kono *et al.*, 1989). The flame was originally smooth, it grew cracks formed on the flame surface, which then cross cracked accompanied by the formation of dimples. A critical point is reached when 'small scale cellular cracking' quickly covers the whole flame surface. The flame speed then accelerates rapidly as stretch decreases. The radius at this critical point normalised by the laminar flame thickness is termed the critical Peclet number, Pe_{cl}. The laminar burning velocity by definition can only be determined from smooth stable flames or the earlier stable parts of a cellular flame. At conditions where the laminar flame had no stable area to find an accurate u_l an approximate value was found by restricting the processing to the very early stages where the cellularties effects were minimised, but there was significant spark influence. These estimated u_l's although not fully accurate, they are a "best guess" whose values prove useful.

3.3 Measurement of Laminar Burning velocity and Markstein lengths

The calculation of flame speed, S_n, first requires that r_u, the cold flame front radius (defined as the isotherm that is 5 K above the temperature of the reactants) is found. Bradley *et al.*, (2000) have shown this to be related to the schlieren flame front radius r_{sch}, by;

$$r_u = r_{sch} + 1.95\delta_l\left(\frac{\rho_u}{\rho_b}\right)^{0.5} \qquad 3.1$$

Here ρ_u and ρ_b are the densities of the unburned and burned gas, δ_l is the laminar flame thickness given by $\delta_l = \nu/u_l$ where ν is the kinematic viscosity of the unburned mixture and u_l is the laminar burning velocity. Values of gas densities and kinematic viscosity were calculated using the Gaseq equilibrium program (Morley, C., 2001). The calculation of r_u requires u_l to be first estimated using r_{sch} and then Eq. 3.1 is adopted to give r_u. Values derived (for the example flame Fig 3.1) of r_u are shown in Fig 3.2. The stretched flame speeds, S_n, can now be evaluated from;

$$S_n = \frac{dr_u}{dt} \qquad 3.2$$

Measured flame speeds at different flame radii for the example flame are shown in Fig 3.3. The total stretch rate , α, acting on the flame is defined as (Clavin, 1985);

$$\alpha = \frac{1}{A}\frac{dA}{dt} = \frac{2}{r_u}\frac{dr_u}{dt} = \frac{2}{r_u}S_n \qquad 3.3$$

Where A is the flame area. The relationship between flame speed and the total stretch has been shown to be (Clavin, 1985);

$$S_s - S_n = L_b\alpha \qquad 3.4$$

This is a linear equation the gradient of which is defined as the Markstein length, L_b, the constant S_s is the unstretched flame speed at which $\alpha = 0$, shown in Fig. 3.4. The unstretched laminar burning velocity is then deduced using (Bradley *et al.*,1996);

$$u_l = S_s\frac{\rho_b}{\rho_u} \qquad 3.5$$

Eq. 3.5 is valid only at a flame at zero stretch. The stretched burning velocity, u_n, can be found from;

$$u_n = S\left[S_n \frac{\rho_b}{\rho_u}\right] \qquad 3.6$$

Here S is a generalised function depending on the flame radius and density ratio, which accounts for the effects of flame thickness on the mean density of the burned gases. The function S has been computed for methane-air and propane-air flames (Bradley *et al.* 1996, Gu 1998) at 0.1 MPa and 300 K over a range of equivalence ratios.

$$S = 1 + 1.2\left[\frac{\delta_l}{r_u}\left(\frac{\rho_u}{\rho_b}\right)^{2.2}\right] - 0.15\left[\frac{\delta_l}{r_u}\left(\frac{\rho_u}{\rho_b}\right)^{2.2}\right]^2 \qquad 3.7$$

This expression was used by Gu *et al.* (2000) who state that; "although it has not been validated at alternative temperatures and pressures, it is unlikely that its use will results in serious errors because it predicts the appropriate trends in flame thickness for variations in pressure and temperature." Importantly it must be noted that the use of S plays no role in determining u_l or L_b.

Bradley *et al.*, (1996) presented a second definition of the stretched burning velocity, u_{nr}, based on the rate of production of burned gas which differs from u_n (based on the entrainment velocity of unburned mixture into the flame front). In a non-planar flame with finite flame thickness the mass of unburned gas entrained into the flame front, $\dot{m}_e$, differs from the rate of formation of product, $\dot{m}_r$. At small radii the effect of the flame thickness is important, but as the flames grow both u_n and u_{nr} tend towards u_l. Bradley *et al.* (1996) show that u_n and u_{nr} are related by;

$$u_{nr} = \frac{\rho_b}{\rho_u - \rho_b}(S_s - u_n) \qquad 3.8$$

Figure 3.5 shows the measured stretched laminar-burning velocities against stretch for the example stoichiometric methane-air mixture. The difference between u_n and u_{nr} can clearly be seen, in this case the rate of mixture entrainment u_n, increased with

stretch, the rate of u_{nr} reduced with stretch. Importantly u_n and u_{nr} do both converge on u_l.

In a spherically expanding flame in the pre-pressure period there are two contributions to stretch, firstly from curvature given by;

$$\alpha_c = \frac{2u_n}{r_u} \qquad 3.9$$

Secondly from flow field aerodynamic strain;

$$\alpha_s = \frac{2v_g}{r_u} \qquad 3.10$$

Where v_g is the gas velocity ahead of the flame front caused by the expansion of the burned gasses. These two stretch mechanisms combined with the two definitions of stretched burning velocity give the variation in burning velocity as;

$$u_l - u_n = L_c\alpha_c + L_s\alpha_s \qquad 3.11$$

Where L_c and L_s are Markstein lengths associated with curvature and flow strain.

$$u_l - u_{nr} = L_{cr}\alpha_c + L_{sr}\alpha_s \qquad 3.12$$

Where L_{cr} and L_{sr} are Markstein lengths for curvature and flow strain respectively for u_{nr}. The total stretch is given by $\alpha = \alpha_s + \alpha_c$, however, as v_g is generally much larger than u_n, α_c can to a first approximation be neglected from Eq. 3.11 and 3.12 (Gillespie *et al.* 2000).

$$u_l - u_n \cong L_s\alpha_s \qquad 3.13$$

$$u_l - u_{nr} \cong L_{sr}\alpha_s \qquad 3.14$$

Markstein numbers (Markstein, G. H., 1951) were also further derived where;

$$Ma_{sr} = \frac{L_{sr}}{\delta_l} \qquad 3.15$$

3.4 Burned gas distribution in premixed turbulent flames

Prior to this work Bradley *et al.* (2003) completed an investigation within the experimental vessel. The research aimed to quantify the amount of unburned mixture present behind the schlieren flame front, by simultaneously using cine

schlieren photography and laser sheet imaging (utilising Mie scattering). The scattering from tobacco smoke was imaged from a sheet situated close to the spark plug. In this sheet the burned and unburned zones were unambiguously visualised. Bradley *et al.* (2003) used the following assumptions;

1. Mean radii can be defined that range from a root radius, R_r, within a sphere of which radius all the gas is burned and a tip radius, R_t, outside a sphere of which radius all the gas is unburned.
2. The structure of the turbulence field is isotropic at any given radius.
3. Effects of reaction zone and laser sheet thickness are neglected and the two-dimensional image reveals the boundary between solely unburned and burned gas.
4. The unburned and burned gas densities are those of the initial cold reactants and adiabatically burned products ρ_u and ρ_b respectively.

3.4.1 Reference radii

The turbulent burning velocity depends on the reference flame surface chosen. In the case of a laminar flame, the chosen surface may be the boundary of either completely burned or unburned gas, or a location somewhere between the two. The mass burning rate in any flame might be expressed as the consumption of cold reactants or the production of hot products, these are not identical in explosion flames as the mass of preheating and reacting gasses are changing. Whichever reference is taken the final values can differ from one another.

The turbulent case is further complicated by the relatively thick flame brush, this results in a number of ways that the average flame radius may be defined. The choice of reference flame radius greatly effects the turbulent burning velocity. Figure 3.6 shows a suggested depiction of a turbulent flame. The root radius, R_r, within which all gas is burned, R_t is the tip radius beyond which all gas is unburned and R_j a general radius. R_j can be defined in a number of ways. The three principal definitions considered (Bradley *et al.*, 2002);

1. R_j is equal to radius R_v where the volume of unburned gas inside a sphere of this radius is equal to the volume of burned outside it.
2. R_j is equal to radius R_m where the mass of unburned gas inside a sphere of this radius is equal to the mass of the burned gas outside it
3. R_j is equal to radius R_a where the area of unburned gas on the flame image inside the circumference with this radius is equal to that of burned gas outside it.

The temporal variations in these definitions of reference radii were evaluated from the 2D sheet images, schlieren imaging produces a mean radius which produced a "mean" radius obtained from the 2D projected area of the 3D flame. This schlieren radius lied somewhere between R_a and R_t, the uncertainty was caused by the blurring effect of the overlapping series of 2D images, the "mountain range silhouette" effect. A further radius R_ξ was defined to represent this;

$$R_\xi = R_a + \xi(R_t - R_a) \qquad 3.16$$

Figure 3.7 shows the variations in reference radii from laser sheet imaging with time for a range of conditions. All radii increase with time, though the rates differ, the diversion of growth rates is due to the increasing flame brush thickness. The schlieren radius usually lied between R_t and R_v being closer to R_v, Fig 3.7 (c) however shows an example where the flame did not remain in the centre of the vessel (where the laser sheet was positioned) but was convected, in this case R_{sch} was initially the largest radius. The ability of schlieren imaging to view through the whole isotropic region of the vessel has clear advantages over 2D sheet.

The experimental finding that R_{sch} was usually close to R_v provided a useful practical method of measuring R_v from schlieren imaging, using the linear relationship $R_v = (\frac{1}{1.11})R_{sch} - 2.1$ which was proven over the range of $2\text{ mm} \leq R_v \geq 40$ mm.

Figure 3.8 shows the relationship between u_{tr} (R_v) found over all conditions from the laser sheet images and schlieren derived turbulent burning velocity, $\frac{\rho_b}{\rho_u}\frac{dR_{sch}}{dt}$. Where the density ratio, ρ_b/ρ_u, accounts for the expansion of gasses behind

the flame front. The values display some scatter from the line of best fit but the extent of scatter was found to be not a function of initial condition but due to shot to shot variation. The best linear correlation was found to be;

$$u_{tr}(R_v) = \left(\frac{1}{1.11}\frac{\rho_b}{\rho_u}\right)\frac{dR_{sch}}{dt} \qquad 3.17$$

The correlation was found over a number of experimental conditions, the maximum ratio of u'/u_l was 10.71. In this current work experiments were performed at higher turbulence intensities beyond the proven range of Eq. 3.17. In the iso-octane database (Chapter 7) the tests where $u' > 3$ m/s exceed the proven range.

3.5 Turbulent burning velocity derived from high-speed digital photography.

Turbulent burning velocities, u_{tr}, have been found from digital schlieren photography. The measurement of u_{tr} is relatively simplified by invoking Eq. 3.17, which relates u_{tr} to $\frac{dR_{sch}}{dt}$. The (1/1.11) constant adjusts the schlieren flame radius to R_v (where the rate of production of burned mass is equivalent to consumption). The schlieren radius R_{sch} is readily available from the turbulent developing schlieren imaged flame shown in Fig 3.9, the flame speed is then found by differentiating against time typically over 5 captured frames. Values of ρ_b/ρ_u were found using the Gaseq equilibrium program (Morley, C. 2001).

3.6 Pressure measurements to support optically derived values.

Pressure recordings were taken simultaneously with the digital schlieren photography. Lewis and Von Elbe derived a method of relating the pressure rise in a closed combustion vessel to the rate of production of reacted gas and further to a burning velocity on a mass based approach. The flame assumptions are;

1. There are no heat losses to the walls of the vessel.
2. All flames propagate spherically toward the walls of the spherical vessel.

3. Unburned gases are compressed isentropically.

4. The pressure is equalised throughout the vessel.

Lewis and Von Elbe showed; a flame radius, r_i, can be assumed as;

$$\frac{r_i}{a} = \left(\frac{P - P_i}{P_e - P_i}\right)^{1/3} \qquad 3.18$$

Where, a, is the radius of vessel, P_i and P_e are the initial and final pressure respectively. P is the pressure rise recorded throughout the combustion process. The flame radius, r_i, is an assumed flame radius behind which there is no expansion of hot gasses. A second radius, r_b, is formed which accounts for gas expansion.

$$\frac{r_b}{a} = \left[1 - \frac{P_i}{P}\frac{T_u}{T_i}\frac{P_e - P}{P_e - P_i}\right]^{1/3} \qquad 3.19$$

Temperature of unburned gas, T_u, (assumes adiabatic compression), T_i, the initial gas temperature.

$$T_u = T_i(P/P_i)^{(\gamma_u - 1)/\gamma_u} \qquad 3.20$$

The flame speeds can now be found from a time pressure record by potting r_b values against time and determining the slopes of dr_b/dt. The burning velocity can be found from;

$$s_u = \frac{dr_i}{dt}\left(\frac{r_i}{r_b}\right)^2\left(\frac{P_i}{P}\right)^{1/\gamma_u} \qquad 3.21$$

Where, s_u, is the burning velocity based on the production of hot products. This method can only be applied to the observation of the pressure rise in the early stages of the process where the volume of burned gas is small. In the calculation of P_e the final pressure from thermodynamic data, it is necessary to use average specific heats, as compression of gas changes the unburned gas mixture properties. The calculated P_e is not the true final pressure in the vessel but represents an extrapolated value from the initial stages. Calculations of final pressure and γ were found using the Gaseq equilibrium program (Morley, C. 2001).

Al-Shahrany (2002) has shown Lewis and Von Elbe pressure analysis to compliment schlieren based burning velocities for a range of laminar cases at 0.5

MPa for $\phi = 0.8$, 1 and 1.2. This methodology has been extended to experiments performed in turbulence.

The notation s_u has previously been use to describe laminar burning velocities derived from pressure records, the current notation used will be $u_{nr,p}$ for experiments performed in a laminar field and $u_{tr,p}$ to describe turbulent burning velocities found from the pressure rise during an explosion. K. Saeed and C. R. Stone (2004) completed an experimental study of laminar methanol flames in an explosion bomb, the approach suggested by Lewis and Von Elbe was compared with a more advanced multizone model. The percentage difference between the models was shown to be no more than 1 % at 0.1 MPa of pressure rise (as used in this study). The single zone approach used here is therefore justified.

Shown in Fig 3.10 are the measured schlieren radii for a turbulent methane-air flame where u' = 2 m/s at 0.5 MPa and 360 K. Also shown in this image is the recorded pressure rise shown against time from ignition. There was an initial sudden rise in the recorded pressure immediately after ignition, possibly caused by a shock-wave from the spark discharge. The recorded pressure remains near zero until 6 ms (in this case) and then exponentially rises to 0.1 MPa, the maximum pressure rise recorded in all cases.

The vessel window has a diameter of 150 mm, the maximum turbulent flame radius varied depended on the flame shape. In this case flame reached a R_{sch} of 52 mm where there was a pressure rise of 0.02 MPa. Later comparisons of turbulent burning velocities are made at a radius of 30 mm, typically at this radius the pressure rise is circa 0.002 MPa (a 1/50 of an atmosphere).

Figure 3.11 shows the turbulent burning velocity measured by the two techniques from schlieren and pressure. The optically derived result initially has a fall in its value followed by a steady increase in u_{tr}. This increase is caused by turbulent flame development, which is discussed in Chapter 5. The pressure derived value of turbulent burning velocity, $u_{tr,p}$, is initially negative which is an erroneous result, in the very early stages the pressure rise is very small, the restricted digital resolution of the ADC manifests in digital noise in the pressure recording. It is not until there is enough of a pressure rise that this technique becomes applicable. The

pressure-based measurement continues beyond (the vessel window) the optical derived results until in this case a time of 13 ms relating to a pressure rise of just under 0.1 MPa. The turbulence generating fans situated in the vessel are 100 mm from the spark gap, with the fixed amplifier sensitivity of 0.1 bars/volt allows pressure measurement just into the fan blades where the recording ends.

In this case at around 7 ms, the measured values of turbulent burning velocity are in general agreement, this was typical for all experiments in this study.

Time (ms)	0.5 MPa
0	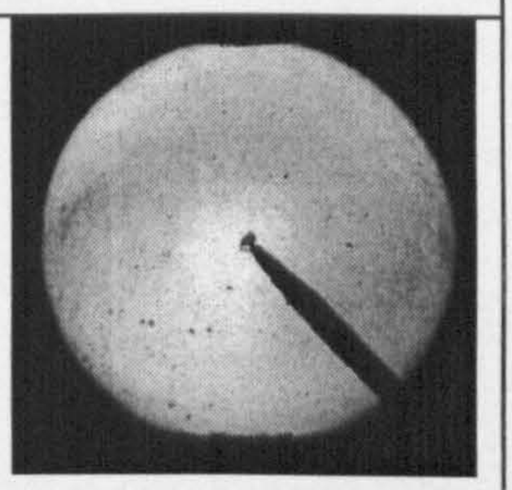
4	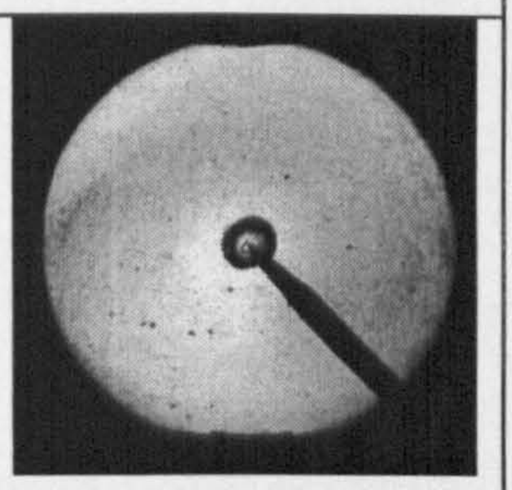
8	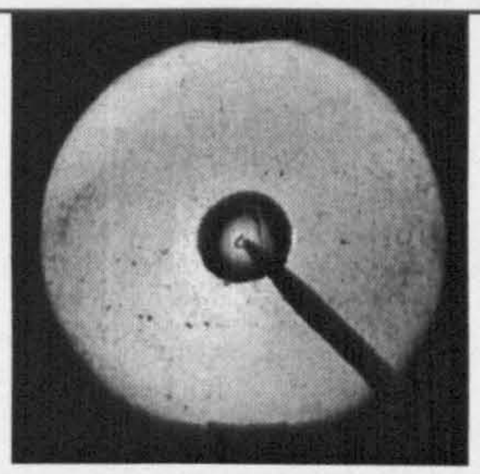
12	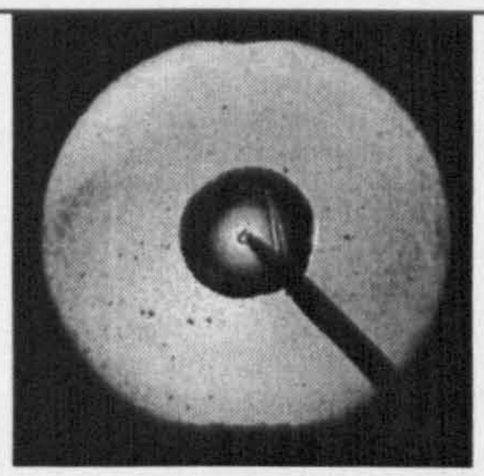
16	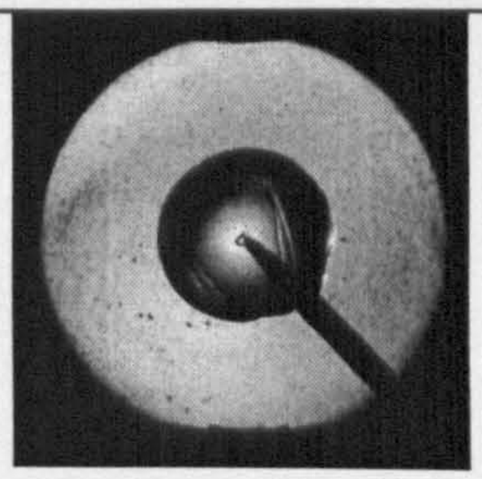

Time (ms)	0.5 MPa
20	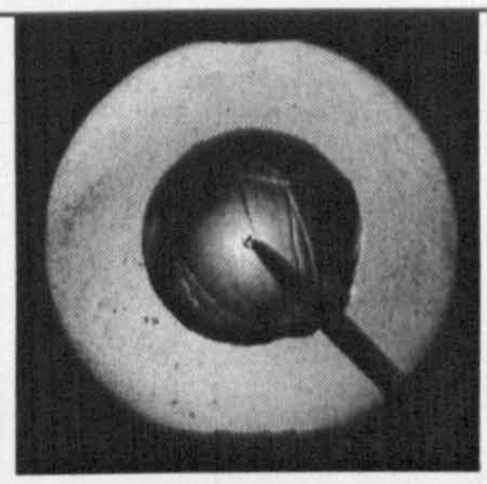
24	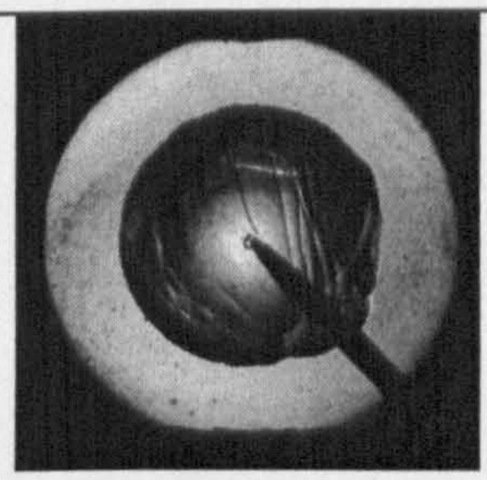
28	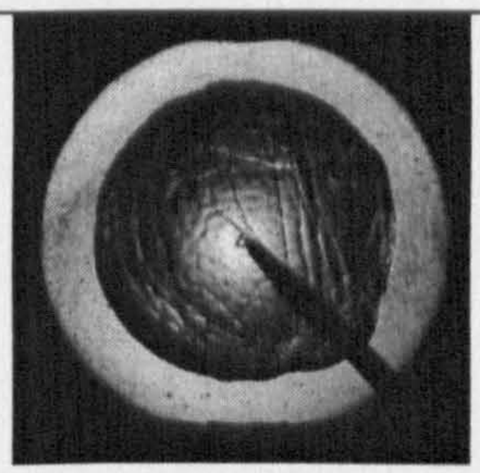
32	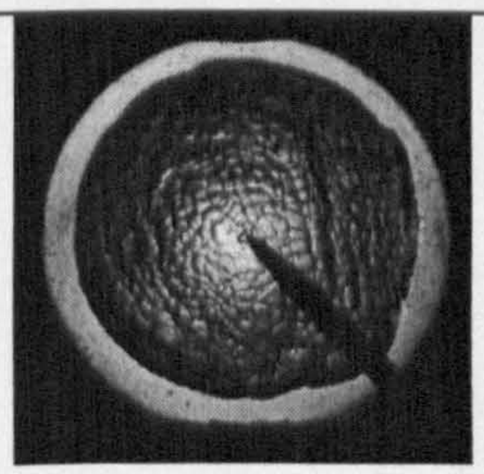

Figure 3.1 Laminar flame propagation of an example stoichiometric methane-air flame at an initial pressure of 0.5 MPa and temperature of 360 K. The developing flame was recorded at 1000 frames per second only every fourth frame is shown.

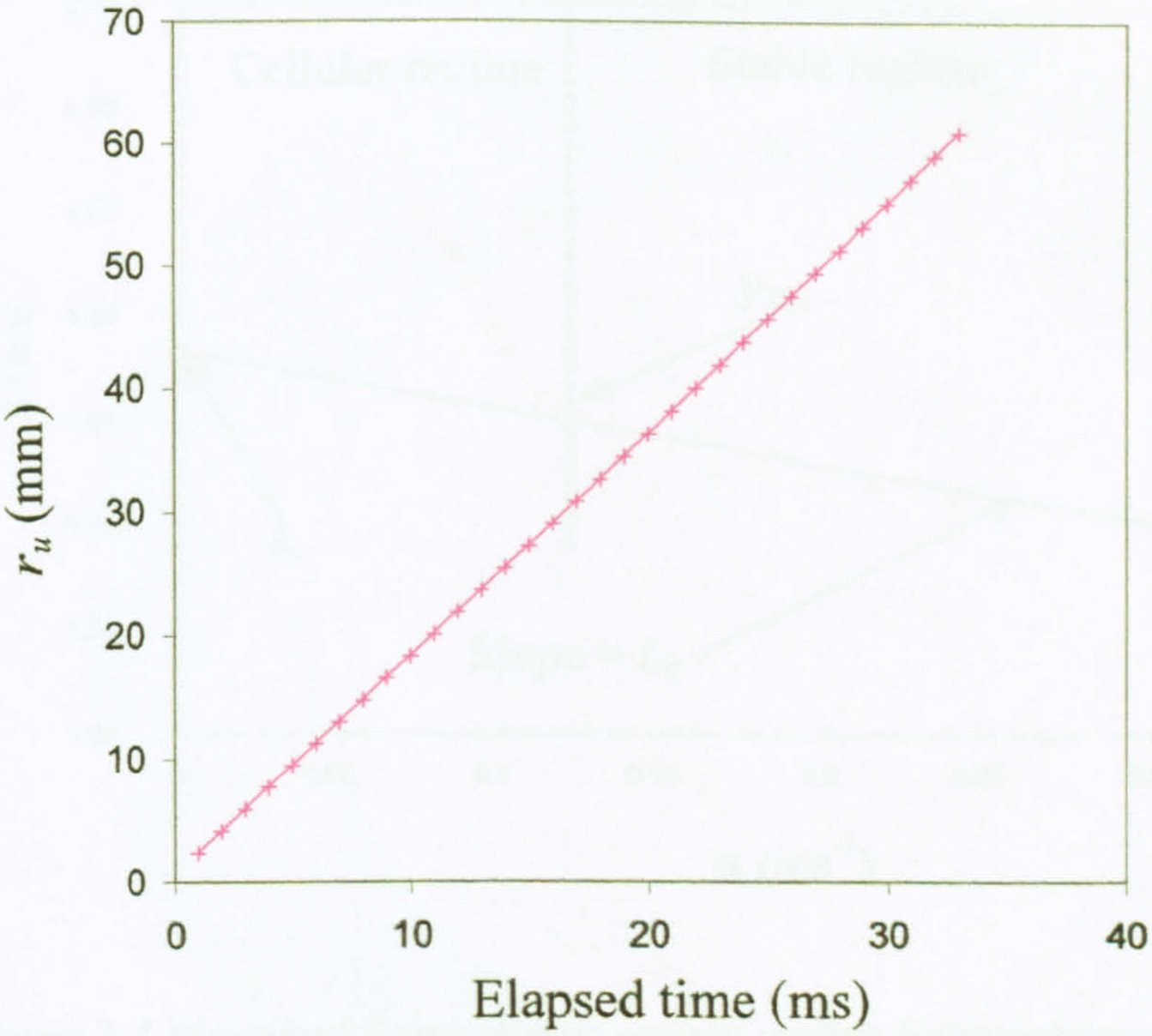

Figure 3.2 Laminar cold front radii r_u for methane-air at initial pressure of 0.5 MPa and temperature of 360 K

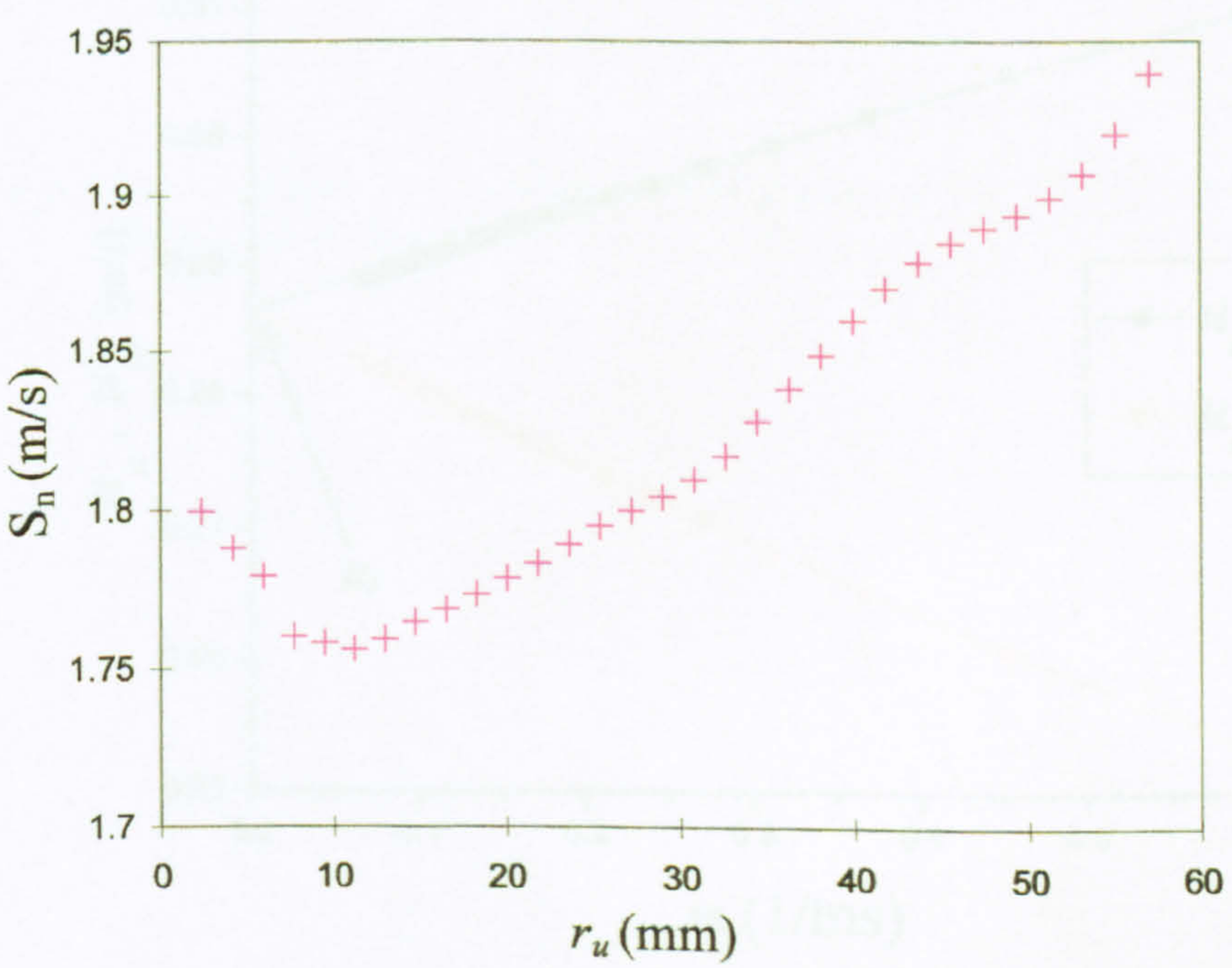

Figure 3.3 Measured flame speeds at different flame radii for stoichiometric methane-air mixtures at initial pressure of 0.5 MPa and temperature of 360 K.

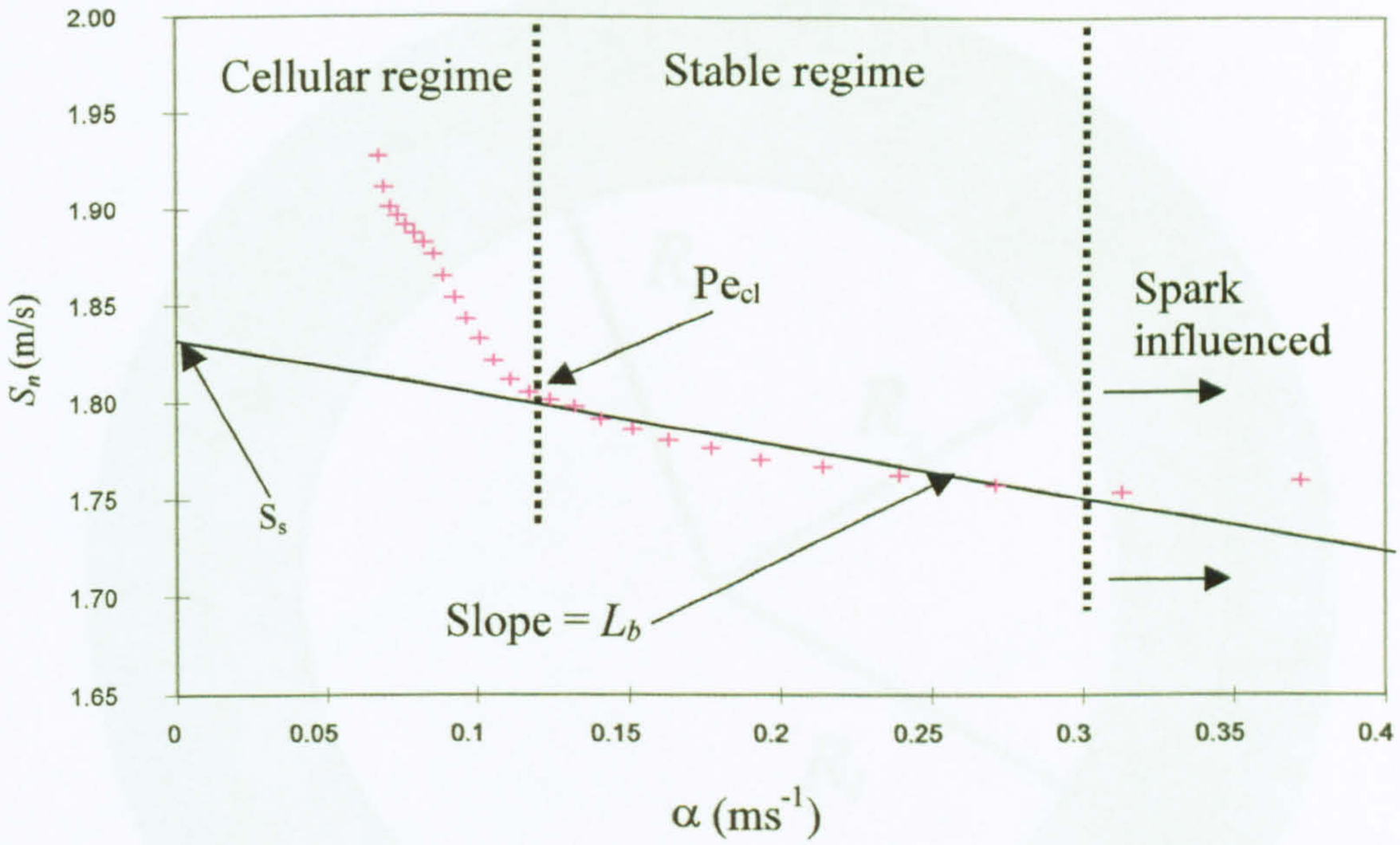

Figure 3.4 Measured flame speeds against stretch for stoichiometric methane-air mixtures at initial pressure of 0.5 MPa and temperature of 360 K.

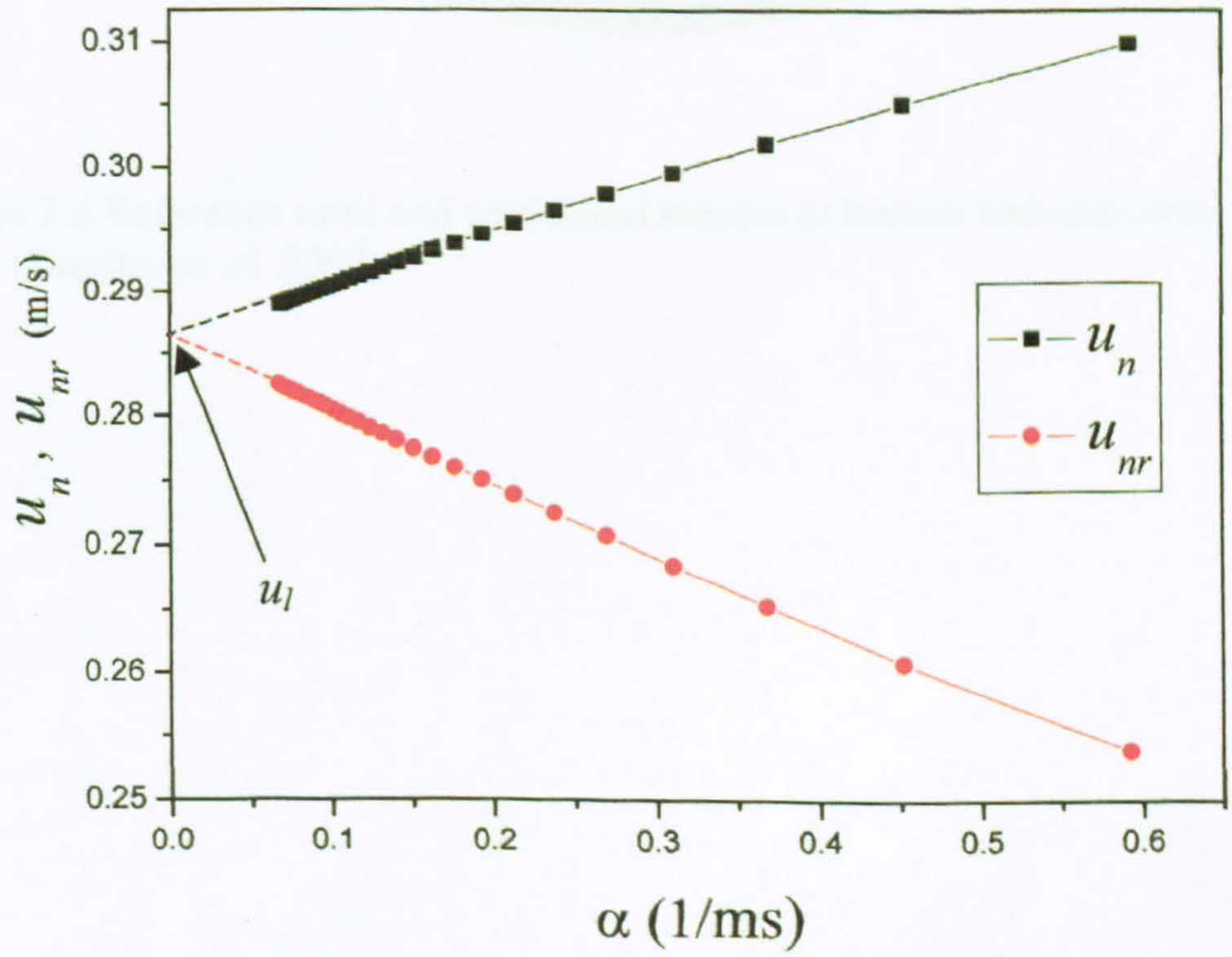

Figure 3.5 Measured stretched laminar-burning velocities against stretch for stoichiometric methane-air mixtures at initial pressure of 0.5 MPa and temperature of 360 K.

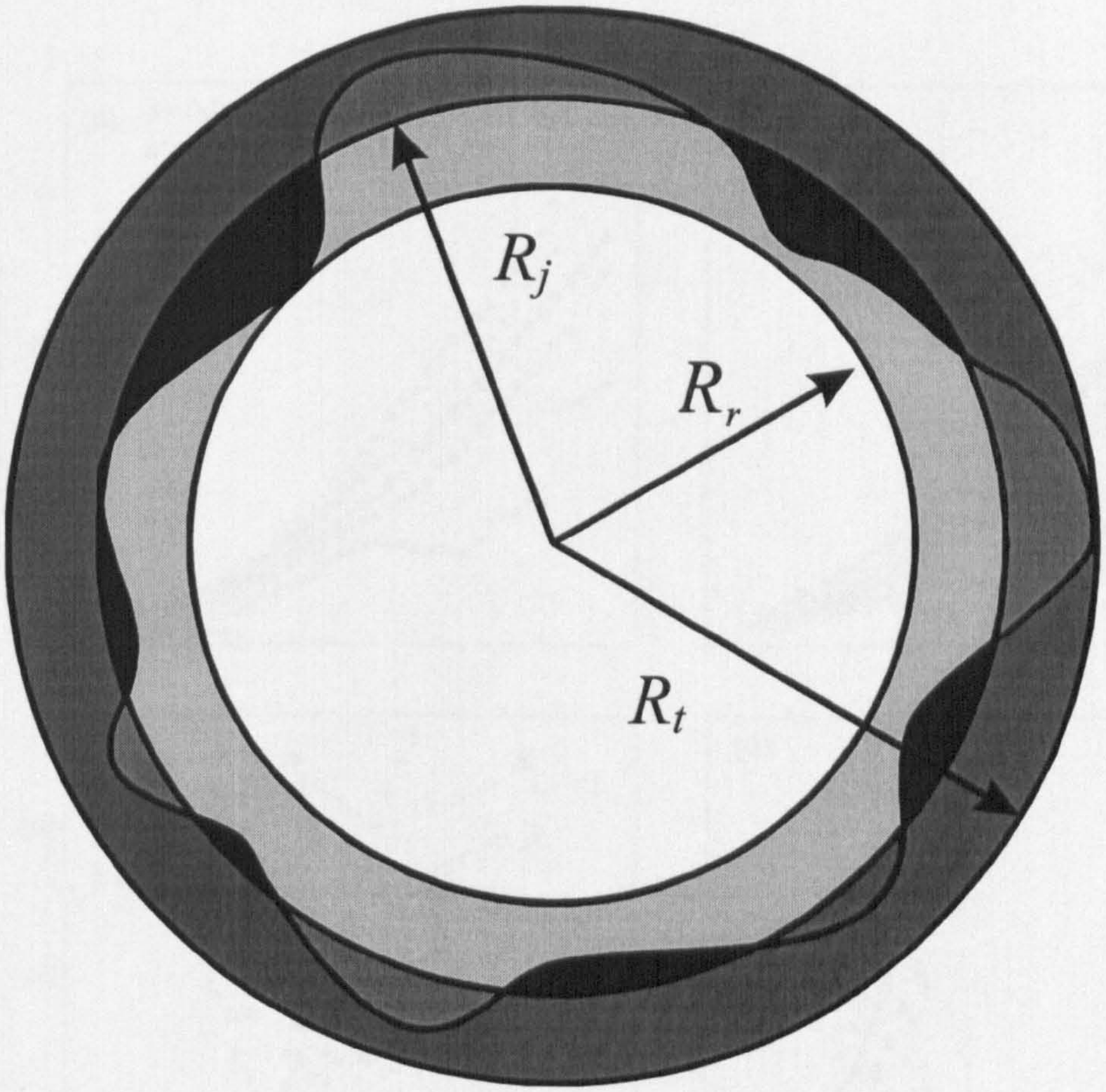

Figure 3.6 Reference radii and associated masses of burned and unburned gas.
(Bradley *et al.* 2002)

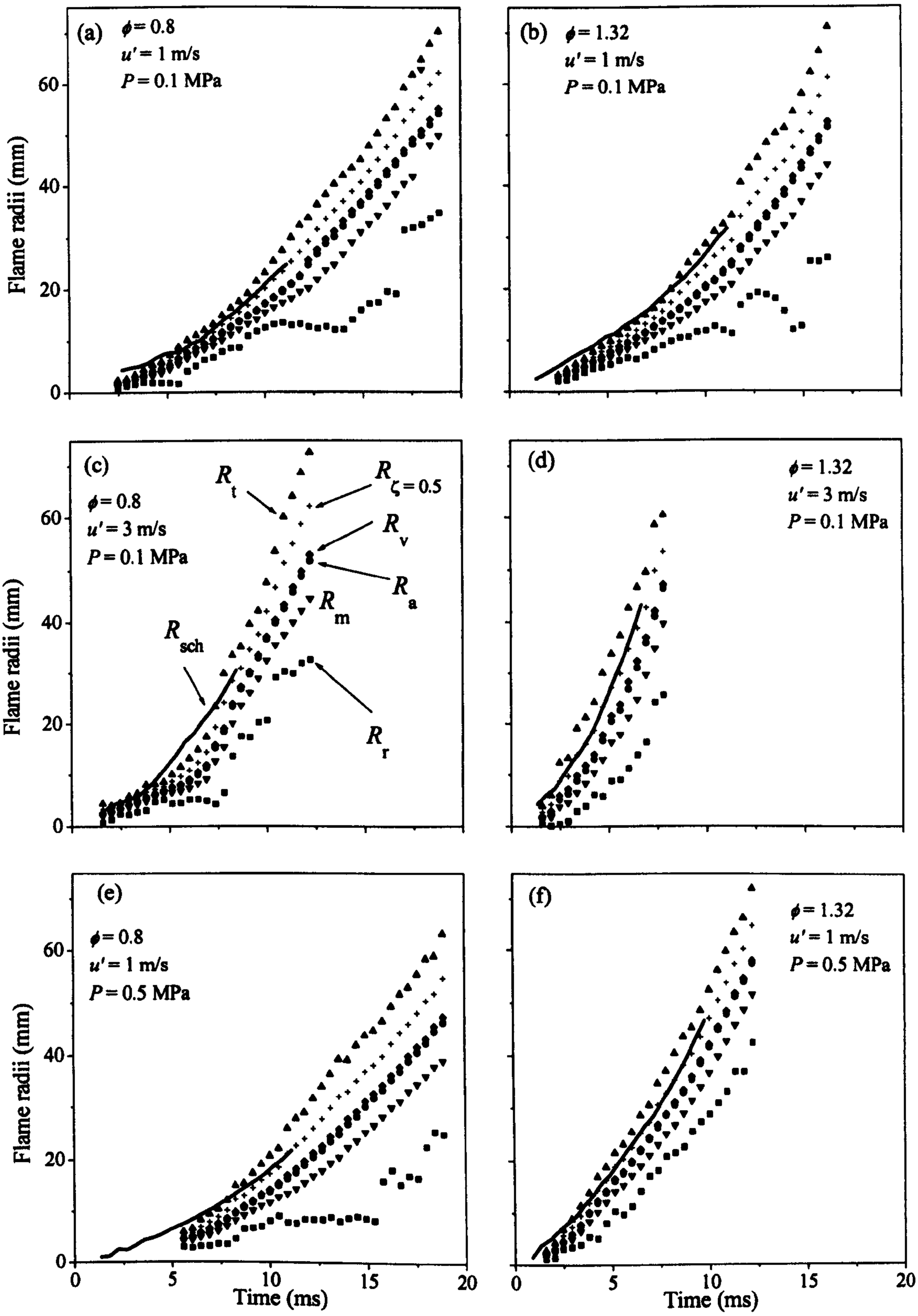

Figure 3.7 Variations of six reference flame radii and schlieren radii (full curves) with elapsed time from ignition for propane air flames. Reproduced from Bradley *et al.* 2002

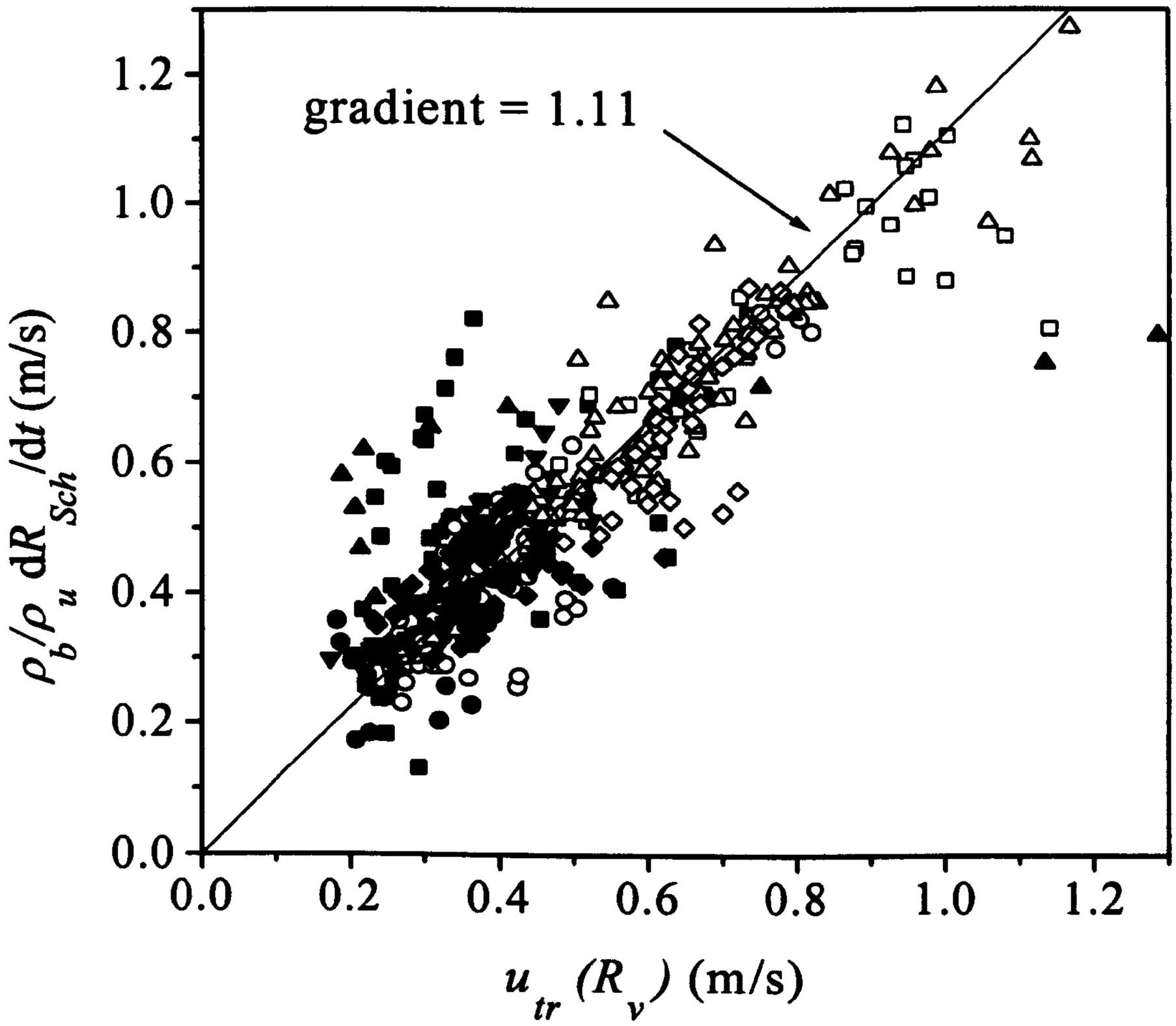

Figure 3.8 Comparison of u_t (R_v) from Mie images with those from schlieren images derived from $\frac{\rho_b}{\rho_u}\frac{dR_{sch}}{dt}$. Closed symbols $\phi = 0.8$, open symbols $\phi = 1.32$ for propane-air mixtures $u' = 1$ to 3 m/s, pressures 0.1 to 0.5 MPa all at 300 K. (Bradley *et al* 2002)

Time (ms)	0.5 MPa
1.6	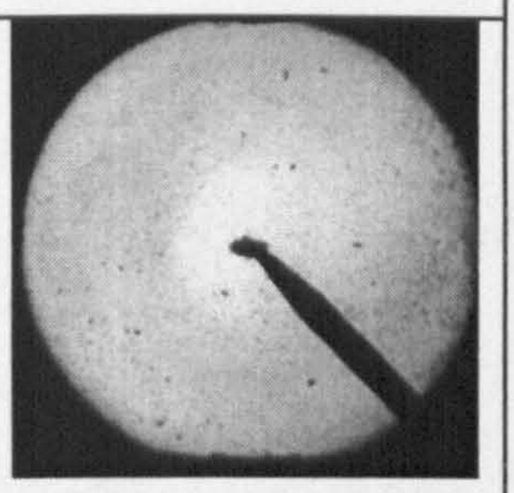
2.4	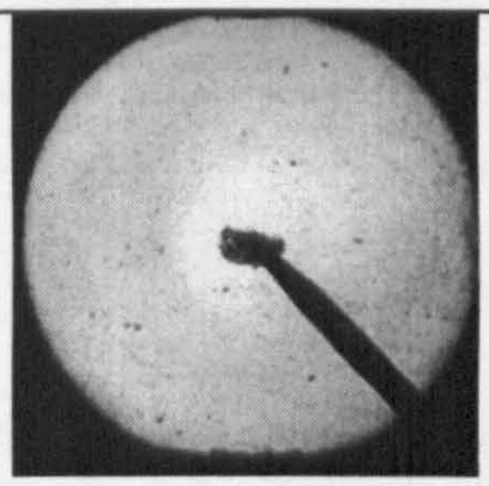
3.2	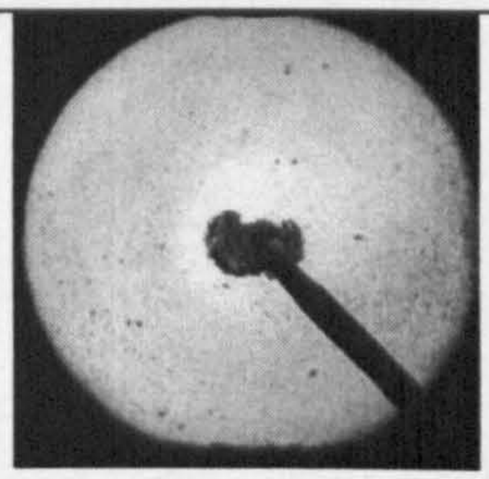
4.0	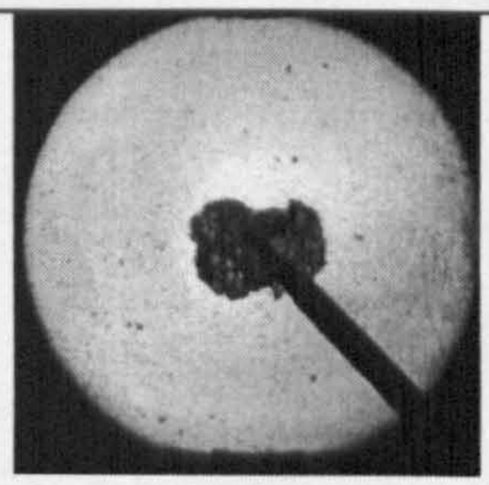
4.8	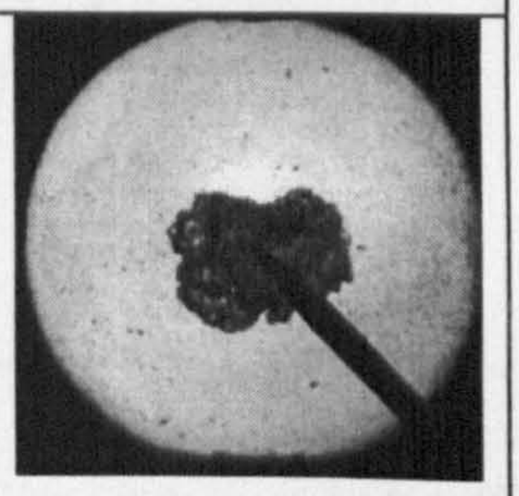

Time (ms)	0.5 MPa
5.6	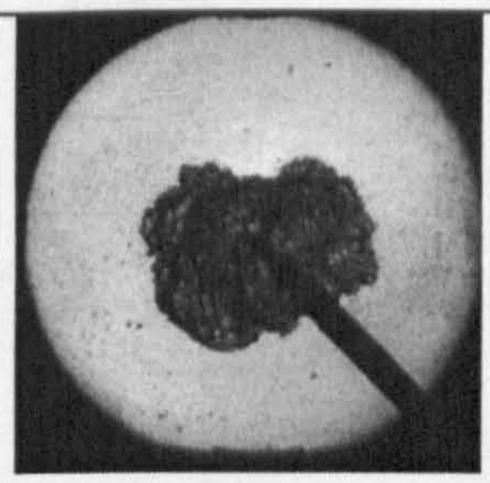
6.4	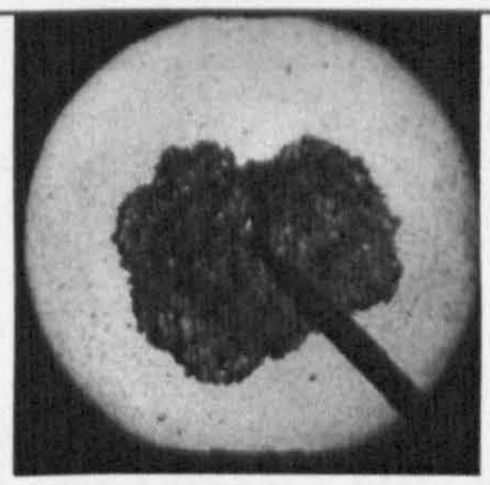
7.2	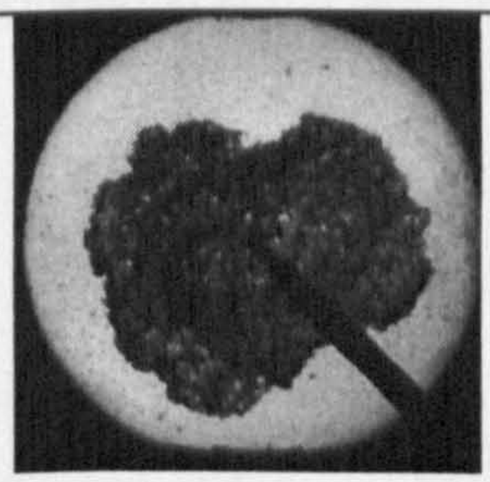
8.0	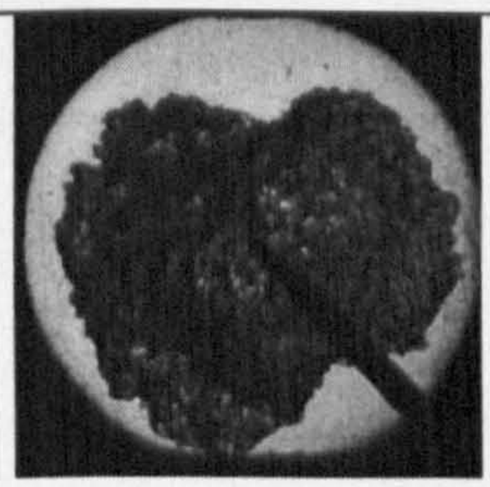

Figure 3.9 Turbulent flame propagation at a $u' = 2$ m/s of a stoichiometric methane-air flame at an initial pressure of 0.5 MPa and temperature of 360 K. This developing flame was recorded at 3700 frames per second only every third frame is shown.

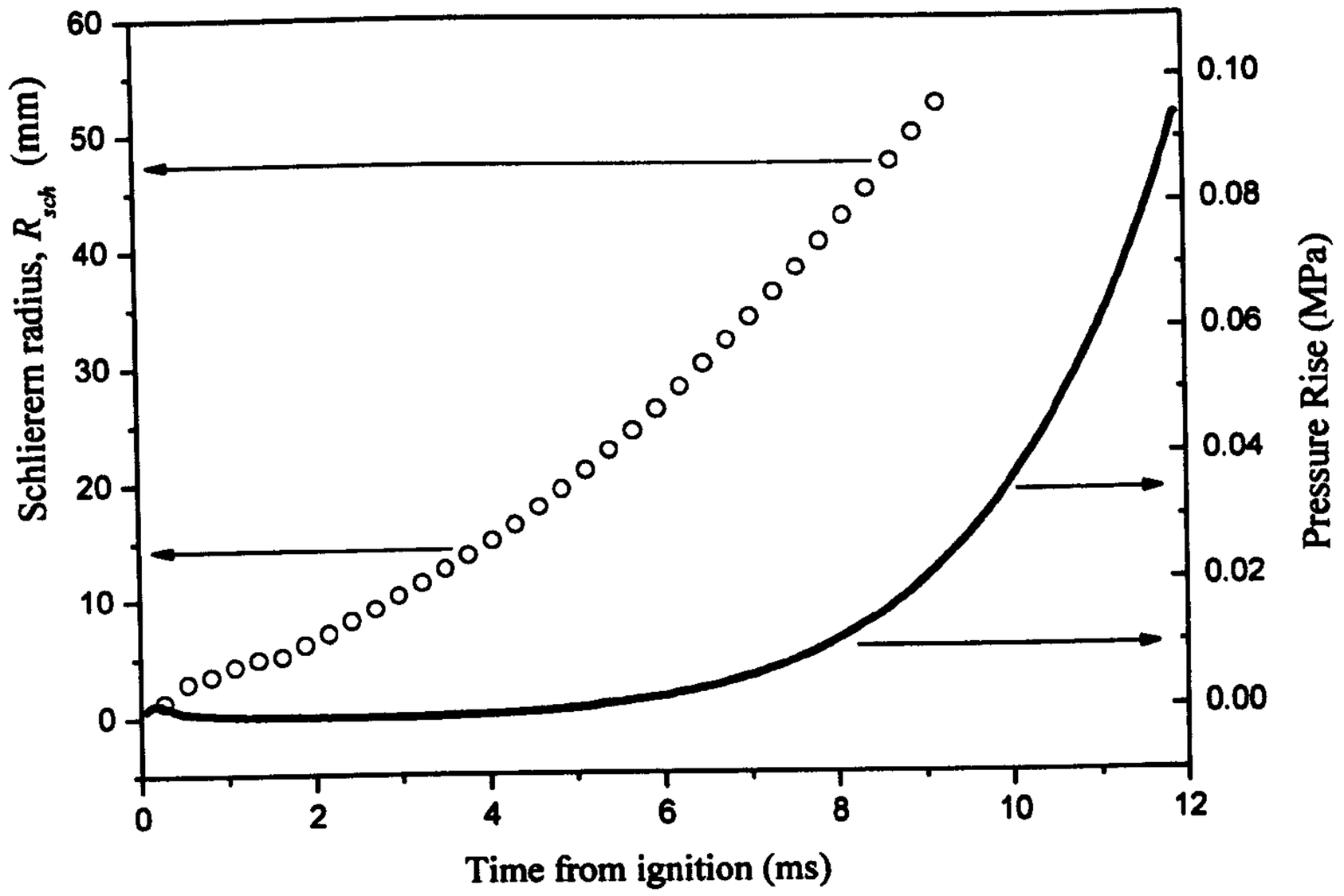

Figure 3.10 Turbulent schlieren radius R_{sch} and measured pressure rise shown against time from ignition. For methane-air u' = 2 m/s, ϕ = 1.0 at 0.5 MPa and 360 K.

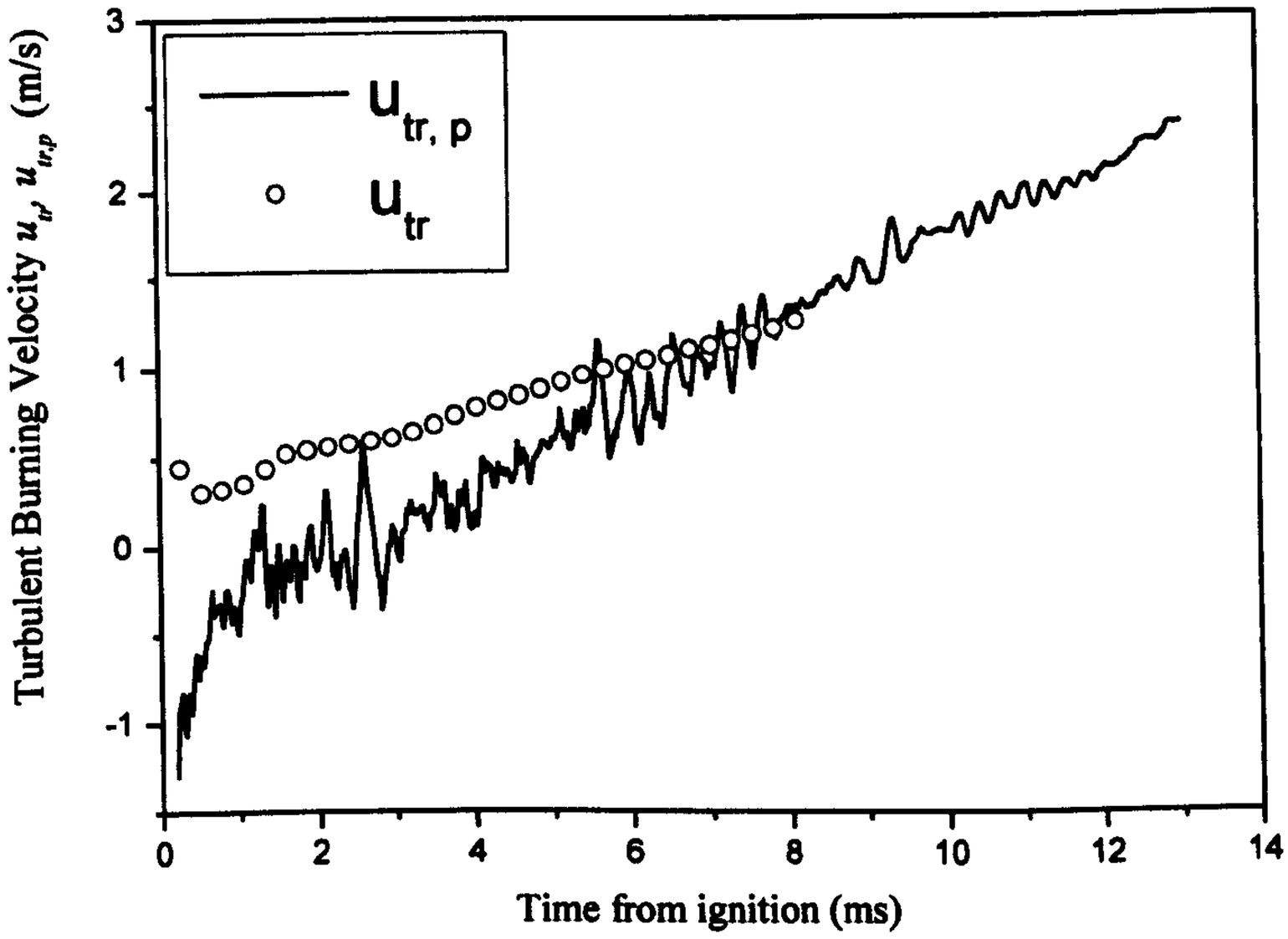

Figure 3.11 Turbulent burning velocity found from schlieren u_{tr} and pressure analysis, $u_{tr,p}$, shown against time from ignition. For methane-air u' = 2 m/s, ϕ = 1.0 at 0.5 MPa and 360 K.

Chapter 4 Results; Laminar burning velocities and Markstein numbers

4.1 Introduction

In this study, spherically expanding laminar flames have been employed to determine the unstretched laminar burning velocity and associated Markstein numbers for a number of fuel air mixtures. This was achieved by the analysis of high speed schlieren images of flames in the spherical combustion bomb, described in Chapter 3. Assuming the turbulent flame front consists of an array of laminar flamelets (Bradley, 1992) the laminar burning velocity provides the underlying burnrate of a turbulent flame (Bradley *et al.*, 1998).

Air and fuel were premixed, the fuels used were; methane, a mixture of methane and hydrogen (30/70), methanol, a commercial gasoline (dutch-pura), and iso-octane. All of the fuels were tested at 360 K and 0.5 MPa over the range of equivalence ratios that could be successfully ignited, up to $\phi = 2$. Iso-octane air deflagrations were also performed at pressures of 0.1 MPa and 1.0 MPa, for equivalence ratios of 0.8, 1.0, 1.2 and 1.4.

Results derived from the laminar flames are presented in this chapter, experimental results are compared where possible with those of other researchers.

4.2 Choice of fuels

All the fuels chosen (with the exception of iso-octane) are automotive fuels. Although methane is burned in the form of natural gas which is typically at least 95% methane with a number of other species e.g. butane, nitrogen. Iso-octane is a commonly adopted representative reference single component gasoline with similar physical and burning properties (Heywood, 1988). In premixed turbulent combustion theory the fuel burning is typically represented by its laminar burning velocity with air at the same conditions (Bradley, 1992). However Bradley *et al.*

(1992) have shown that the Lewis number of the fuel can also have an influence on the turbulent burning velocity. The Lewis number is defined as;

$$Le = {D_T}/{D_{ij}} = \frac{thermal}{mass} \; diffusion \qquad 4.1$$

Where the diffusion coefficient of the deficient reactant into nitrogen is used, (for fuel lean conditions the fuel is the deficient reactant, when fuel rich oxygen is deficient). Shown in Fig. 4.1 are the Lewis numbers with equivalence for the single component fuels studied. The values shown for methane were obtained from a program written by Haq, details are given in Haq (1998). Lewis numbers for iso-octane and methanol were calculated using a program originally written by Hynes (1996). It can be seen that a wide range of Lewis numbers are covered from values less than one for fuel rich iso-octane and methanol to values of almost 3 for lean iso-octane-air. Using the simple definition above it is not possible to determine *Le* for multi-component fuels. There is clearly a step change in *Le* values at $\phi = 1$, (here diffusion coefficients of the fuel and oxygen were averaged) the result of relying on a single diffusion coefficient to characterise the real, much more complicated case of multiple diffusion of radicals and species throughout the flame front. This has resulted in the adoption of Markstein numbers, which can be determined by direct measure of the influence of stretch on the laminar flame.

4.3 Flame growth and changes in structure with pressure and equivalence ratio

Shown in Fig. 4.2 (a) are schlieren images of a spherically expanding laminar flame at $\phi = 1$ and 0.1 MPa. Two longitudinal cracks are evident across the surface, these are thought to be initiated during the ignition process, the result of disturbance from the spark or interaction of the flame with the spark electrodes. Images from Laser Induced Fluorescence (LIF) have shown that the cracks take the form of a "dent" in the flame surface (Haq *et al.*, 2002).

Illustrated in Fig. 4.2 (b) is a similar spherically expanding laminar flame at 0.5 MPa and $\phi = 1.0$. As in the 0.1 MPa case cracks can be seen across the flame from ignition. Between 20 and 28 ms the number of cracks across the flame surface

increases. The cracks are not perfectly longitudinal and distance between the cracks decreases as the flame grows. At 32 ms the flame surface is 'cellular' as small scale mottling covers the whole surface. Figure 4.2 (c) shows the same stoichiometry but for the higher pressure of 1.0 MPa, at this condition the flame becomes cellular earlier (~ 24 ms) and the cell size is smaller.

The number of cracks, or cells, increases as the radius increases. Other studies have shown that there is a critical radius (defined in terms of a Pelect number, *Pe*; where $Pe = r/\delta_l$ and r is the flame radius and δ_l the flame thickness) at which the flame speed suddenly accelerates (Bradley *et al.* 1998). This is associated with the sudden increase in the number of cells observed here, resulting in an increase in the surface area. It should be noted that the schlieren technique simultaneously images both sides of the flame; therefore not all the visible cells will be on the same side of the flame surface.

Shown in Fig. 4.3 (a) are schlieren images of methane-air flames at a radius of approximately 50 mm over a range of equivalence ratios. At $\phi = 0.6$ the flame was so slow it was buoyant, resulting in the distinctive shape with a curved spherical top but flat bottom, this flame did not reach a radius of 50 mm, the final image where the flame meets the edge of the window is shown. The flame surface was smooth with a few cracks. At $\phi = 0.7$ the flames were not significantly buoyant but small scale cracking was evident across the surface. The density of cracking increased reaching a maximum at $\phi = 0.9$ where the flame surface was completely cellular. From $\phi = 1.0$ to 1.3 the flames became increasingly "stable" (less cellular). The stoichiometric flame had large scale cracks with some small scale mottling. At $\phi = 1.1$ there were no small scale cells but a number of large scale cells, some of which were round in contrast to $\phi = 0.7$ where the cells were formed longitudinally. The surface of the $\phi = 1.2$ and 1.3 flames were smooth.

In the case of the methane/hydrogen mixture (Fig. 4.3 (b)) it was possible to ignite $\phi = 0.5$, the leanest mixture tested in this study. These flames were buoyant, with the characteristic curved top and flat bottomed shape, in this case the unburned mixture was drawn upwards through the middle of the flame. The $\phi = 0.6$ mixture was not buoyant but very cellular, with a range of large and small scales existing across the flame surface. The outside schlieren edge was visibly wrinkled with

peaks and valleys visible on the flame surface. The ϕ = 0.7, 0.8 and 0.9 flames appeared similar to the ϕ = 0.6, very cellular. At ϕ = 1.0 although the flame was cellular it appeared to have a more uniform range of cell sizes compared with the leaner flames. As the equivalence ratio became richer the flames appear increasingly stable, the ϕ = 1.1 flame was cracked but not cellular and the ϕ = 1.2 and 1.3 flames were stable, the ϕ = 1.3 flame being slightly buoyant. The methane/hydrogen mixture could also be ignited at ϕ = 1.4 although not shown, the flames were buoyant and smooth.

Comparing the methane and methane/hydrogen flames at lean and stoichiometric equivalence ratios, the methane/hydrogen mixture could be ignited at over an extended range of equivalence ratios (± 0.1) and the flames were more cellular than the methane flame at the same equivalence ratio. However, at rich equivalence ratios the flames for the two fuels appear identical. The addition of hydrogen was more significant (in terms of flame stability) under fuel lean conditions where the fuel was the deficient reactant and there was excess oxygen. However, at rich equivalence ratios where there was excess fuel the addition of hydrogen did not appear to have a significant effect on the appearance of the flames.

Figure 4.4 shows schlieren images of (a) dutch-pura, (b) iso-octane and (c) methanol, again shown at a fixed radius of 50 mm over a range of equivalence ratios. The dutch-pura ϕ = 0.8 flame appeared stable, at ϕ = 0.9 a few longitudinal cracks were seen as with the lean methane flame. At ϕ = 1.0 surface mottling was visible. From ϕ = 1.1 the flames were very cellular, moving richer the schlieren edge was becoming less spherical due to the flame surface becoming a series of peaks and valleys, this was particularly obvious with the ϕ = 1.6 and ϕ = 1.8 flames. The trend of flame stability of the dutch-pura flames contrasts with the methane, with the lean flames stable and becoming increasing cellular moving rich.

Iso-octane is shown in Fig. 4.4 (b) in the central column. The lean ϕ = 0.8 had a number of longitudinal cracks, at ϕ = 0.9 there was surface mottling with an absence of large cells, at ϕ = 1.0 the mottling was reduced and large scale cells were visible. From ϕ = 1.1 the flame surface was heavily cellular with an increase in the amplitude of the "peaks and valley" moving richer, the ϕ = 1.8 flame appeared

almost turbulent in appearance. It was possible to ignite this mixture at $\phi = 2.0$, the richest condition in this study. It must be noted that dutch-pura and methanol may also have ignited at this very rich condition, this however was not attempted as the iso-octane $\phi = 2.0$ experiment left a heavy soot residue in the vessel. This $\phi = 2.0$ iso-octane flame at this condition was close to the ignition limit of this fuel, a buoyant flame ensued with a stable upper-side and heavily cellular underside. It is probable that the stable upper part of this flame was caused by stretch induced by the upward flow of burnt gasses. The trend of flame stability with equivalence ratio compares with dutch-pura, however iso-octane flames were more unstable than for the corresponding equivalence ratio of dutch-pura under fuel lean conditions.

Methanol (Fig. 4.4 the third column) measurements began at $\phi = 0.8$ where a stable flame with no obvious structure was observed. From $\phi = 0.9$ to $\phi = 1.8$ the images appeared very similar with an highly cellular appearance over the experimental range (excluding $\phi = 0.8$).

Shown in Fig. 4.5 is the critical radius at which each flame became unstable, these radii were determined where the flame-speed deviated from the linear response to stretch (this point may be seen on Fig. 3.4 where the beginning of the cellular regime is labelled). Flames that are stable throughout the viewing period are shown. Buoyant flames have been separated to the top of the figure, flame stretch for these flames is ambiguous due to induced vertical flow of the less dense burned gasses. Flames which became unstable early (less than 8 mm radius) have been placed within the "spark effected area". The data plotted in this figure may be seen in the final column of Tables 4.1 to 4.5. The observation of increasing propensity of cellularity for rich or lean equivalence ratios observed in the schlieren images is shown and supported in this figure. A larger critical radius is indicative of a more stable flame. Methane which at its lowest tested equivalence ratio ($\phi = 0.8$) was stable, suddenly becomes unstable approaching stoichiometry, flame stability then increases for fuel rich equivalence ratios. A similar trend exists with the hydrogen enriched methane flames, the critical radius increases with equivalence ratio. Iso-octane and dutch-pura becoming increasingly unstable moving richer, iso-octane has consistently lower values of critical radius than dutch-pura. The lean methanol

flames are more stable than the rich, from stoichiometry upward the value of critical radius was approximately constant, around 20 mm.

Shown in the final column of Table 4.6(a, b, c) is the value of critical radii over a range of pressures for iso-octane $\phi = 0.8$, 1.0, 1.2 and 1.4. At 0.1 MPa all of these conditions were stable during the filmed deflagration. At 0.5 the $\phi = 0.8$ and $\phi = 1.0$ flames were stable, $\phi = 1.2$ and $\phi = 1.4$ reached the critical radius at 20 and 8 mm respectively. At the high pressure of 1.0 MPa the $\phi = 0.8$ flame was again stable, the $\phi = 1.0$ flame became unstable at 29 mm, the $\phi = 1.2$ at 6 mm and the $\phi = 1.4$ flame was unstable from inception. The general trend was that increasing pressure and equivalence ratio (with iso-octane) increased the propensity to cellularity.

For flames which were unstable from inception or became unstable within the area effected by ignition it was impossible to determine true laminar burning velocities and associated markstein numbers. A best guess at the laminar burning velocity was attempted by fitting the linear flame stretch to flame-speed within this spark effected zone. These "best guess" values are likely to be overestimated due to cellularity increasing the flame surface area. These values do prove useful in making qualitative comparisons with the turbulent experiments (Verhelst *et al.*, 2004).

4.4 Influence of stretch on flame-speed

In the present study, premixtures of air with methane, binary methane and hydrogen mixtures, methanol, iso-octane and dutch-pura are ignited centrally which grew spherically. Laminar flame-speed, S_n, was obtained from the measured radius against time. The flame-speed has a dependence on flame radius due to flame stretch, α. From S_n and flame radius corresponding values of α were calculated. From the plot of S_n against α, values of S_s, u_l and various Markstein lengths have been obtained, as discussed in Chapter 3. Flame-speeds against flame stretch can be seen in Fig. 4.6 to Fig. 4.10, tabulated data deduced from these figures can be seen in Tables 4.1to 4.5. Where no data for Markstein numbers are shown the quoted laminar burning velocity must be taken as an estimation. These estimations were

found by fitting flame-speed against stretch over the initial parts of the experiments within the spark-effected area.

Shown in Fig. 4.6 are the variations of S_n with α, for all of the tested conditions of methane from $\phi = 0.6$ to $\phi = 1.3$. A single representative example was chosen from at least two experiments performed at each condition. The fastest flame-speed was observed for $\phi = 1.0$, this equivalence ratio has been plotted on both upper and lower graphs for comparison with the other mixtures. The greatest values for α were attained at the early stages of experimental spherical development, and then dropped as the flame grew.

For the fastest condition of $\phi = 1.0$, values of S_n increases as the effect of α reduced. Here, stretch had an adverse effect on the flame-speed, which is indicative of a positive L_b. The point where the critical radius was reached can clearly be seen in this case occurring at a value of α of 0.11 (1/ms). The $\phi = 0.9$ flame was slower than that of $\phi = 1.0$, the flame-speed reduced with stretch, meaning that stretch positively effects flame-speed at this condition. Moving leaner the flames have reduced flame-speeds and respond positively to stretch. The $\phi = 0.6$ flame was buoyant, no fit with α was made. For richer mixtures than $\phi = 1.0$, shown on the lower graph, the flames became slower, and increasingly they responded adversely with stretch. For $\phi = 1.1$ the flame speed dropped after ignition, the fit of S_n and α performed on the later non-spark influenced part of the flame was linear, both experiments performed at this condition showed the same phenomena. Final values found from this figure maybe seen in Table 4.1.

Flame-speed against stretch for binary methane hydrogen mixtures with air are shown in Fig. 4.7. The fastest condition with this fuel was again at $\phi = 1.0$, the leaner flames responded positively to stretch, the rich responded adversely. It was not possible to accurately fit S_n and α below $\phi = 0.8$ as the flames were cellular, the extreme lean case of $\phi = 0.5$ was buoyant, as was the richest case of $\phi = 1.4$. The $\phi = 1.3$ flame showed a strong 'spark' effect, however a fit was possible. Final values found from this figure maybe seen in Table 4.2.

Shown in Fig. 4.8 are the variations of S_n with α, for all of the tested conditions for dutch-pura from $\phi = 0.8$ to $\phi = 1.8$. The fastest flame-speed was

observed for $\phi = 1.1$, where values of S_n increased as the effect of α reduced. Here stretch had an adverse effect on the flame-speed, indicating a positive L_b. The critical radius was at a value of α of 1.8 1/ms. Moving leaner these flames were stable and so a good fit to linear stretch exists for these deflagrations. The observed flame-speed reduced through $\phi = 1.0$, $\phi = 0.9$ to $\phi = 0.8$, these flames also had a positive L_b. The leanest case $\phi = 0.8$ initially did not conform to a linear response with stretch. This might be due to ignition mechanisms and also a response of stretch caused by flame curvature which has been neglected throughout, as strain effects generally dominate (Gu *et al.* 2000). It is possible that for very slow flames with a positive L_b that the effect of stretch from curvature may initially play a stronger role. Later in flame development of this $\phi = 0.8$ case (> 9 mm) S_n varies with α linearly, it is this part of the deflagration which has been used to determine the derived values of u_l and L_b.

For the rich dutch-pura, the flame-speed of $\phi = 1.2$ was nearly as fast as $\phi = 1.1$, with later values of Sn being quicker than those of $\phi = 1.1$, this was due to a larger increase in flame surface area due to greater cellularity. Initially this flame had a linear response to stretch, the effect of stretch on the flame-speed was positive with flame-speed reducing as stretch fell. The $\phi = 1.3$ and $\phi = 1.4$ flames also initially responded to reducing stretch with an associated fall in S_s. These flames were more unstable than the lean cases. Beyond $\phi = 1.4$ the flame-speeds reduced and the flames became so unstable that is was impossible to gain an accurate fit with S_s and α. Final values found from this figure maybe seen in Table 4.3.

Shown in Fig. 4.9 is the variation in flame-speed against α for iso-octane across the ignition range. The fastest condition was at $\phi = 1.1$, leaner flames were slower responding to stretch adversely, the leanest conditions did not initially respond to stretch linearly. The richer conditions of $\phi = 1.2$ and $\phi = 1.3$ were very close to the fastest equivalence ratio of $\phi = 1.1$. There was a transition in the sign of L_b between $\phi = 1.1$ and 1.2. For $\phi = 1.4$ and above the flame-speeds fell, it was impossible to make a linear fit for these rich cases. The $\phi = 2.0$ flame responded with the opposite gradient to the other rich conditions, although this flame was buoyant. Final values found from this figure maybe seen in Table 4.4.

Methanol flame-speeds against α are shown in Fig. 4.10, here, the fastest equivalence ratio was for $\phi = 1.2$, the flame-speeds reducing with lower equivalence ratio. The lean flames responded adversely to stretch, the richer flames however showed the opposite effect. The flame-speeds on the rich side reduce as with the other fuels, the values however remain relatively high with the intersect of S_n and α being greater than a value of 1 m/s for the $\phi = 1.8$ flame. Final values found from this figure maybe seen in Table 4.6.

Show in Fig. 4.11 (a) are the flame-speeds against α for iso-octane air for pressures 0.1, 0.5 and 1.0 MPa, at a temperature of 360 K, for the equivalence ratios of $\phi = 0.8, \phi = 1.0, \phi = 1.2$ and $\phi = 1.4$. At 0.1 MPa all of the flames are stable throughout the schlieren viewed deflagrations. At high values of stretch when the flames were small the equivalence ratio of $\phi = 1.2$ displayed the fastest flame-speed. When fitted with stretch however it was clear that stretch adversely effects the flame-speed to a lesser extent than at $\phi = 1.0$, the value of S_s at zero stretch was lower than that of $\phi = 1.0$. The fastest value of S_s at 0.1 MPa was therefore at $\phi = 1.0$. The lean case at this pressure initially displayed a non-linear response to stretch, as with $\phi = 0.8$ 0.5 MPa iso-octane experiments.

The 0.5 MPa results on this figure have already been discussed but have been shown on this figure for completeness. The magnitude (gradient) of the effect of flame stretch at 0.5 MPa was lower than at 0.1 MPa. At 1.0 MPa it was impossible to derive true values for the laminar burning velocity and markstein lengths for the rich conditions as the flames were unstable from inception. The stoichiometric flame had the fastest measurable value of S_s. The magnitude of the effect of stretch on the burning velocity was further reduced at 1.0 MPa compared to the 0.1 MPa and 0.5 MPa cases. The stoichiometric value of S_s was the slowest for all pressures. Final values found from this figure maybe seen in Table 4.6.

4.5 Derived Laminar burning velocities and Markstein values

The derived 0.5 MPa laminar burning velocity values for all of the fuels are plotted on Fig. 4.12 against equivalence ratio. The agreement between deflagrations at the same condition was generally very good, the experimental repeatability of the

binary methane-hydrogen mixtures was not as good as the other mixtures due to the increased error of mixing two fuels with air during mixture preparation. Third order polynomial fits have been added to the data over the range where it was possible to gain an accurate measurement of u_l, the conditions beyond the fitted line were either unstable or buoyant.

Methane had its peak burning velocity at $\phi = 1.0$ (28 cm/s), with the burning velocity falling approximately equally on either side, although it was possible to ignite this mixture further into the lean ($\phi = 0.6$) than into the rich ($\phi = 1.3$). The mixtures with methane enriched with (30%) hydrogen behaved differently. The measured peak burning velocity was at $\phi = 1.0$ and had a value of 37 cm/s which was much faster than methane (28 cm/s). The leaner conditions with this fuel were consistently higher than the equivalent methane only measurements. On the rich side ($\phi > 1.1$), there was no measured increase in the laminar burning velocity with the addition of hydrogen. It was possible to ignite this fuel 0.1 of an equivalence ratio further into the lean and rich than methane. The leanest condition with this fuel is $\phi = 0.5$, where the experimentally estimated value for u_l was 3.5 cm/s. As with the earlier observed changes in flame structure the effect of adding hydrogen to methane was more effecting in lean flames, in rich flames where the availability of oxygen is rate depending, addition of hydrogen did not give an increase in u_l.

The values of u_l for the gasoline (dutch-pura) and iso-octane were very similar. The peak burning velocity of the gasoline was achieved at $\phi = 1.1$, having a value of 32 cm/s. The values of u_l fell more quickly moving leaner than moving rich; also it was possible to ignite this mixture much further into the rich side than lean. Iso-octane also had its peak laminar burning velocity at $\phi = 1.1$ (31 cm/s) although similar trends are observed as with the gasoline. The gasoline was slightly faster than iso-octane at the peak by around 1 cm/s, this difference was also measurable moving lean, the richer values were indistinguishable with the current experimental limits.

Methanol had the fastest measured values of u_l, the peak burning velocity was attained at $\phi = 1.2$ and had a value of 40 cm/s.

The experimental variation in L_b with equivalence ratio for all of the 0.5 MPa laminar conditions is shown, where experimentally determinable, in Fig. 4.13. In

general the repeatability in the measured results at each condition was good. In this case linear fits have been added. Iso-octane displays the most positive L_b of all the lean conditions, the L_b of iso-octane reduces moving richer becoming negative for equivalence ratios greater than $\phi = 1.2$. Values of L_b above $\phi = 1.4$ are not shown for this fuel as these flames were cellular either from inception or became unstable within the spark effected zone. For other similar conditions values for L_b have been omitted from this figure. Dutch-pura follows a similar trend to iso-octane, however, the magnitudes of L_b are lower for both rich and lean conditions. L_b becomes negative at the same equivalence ratio as iso-octane.

Methanol is the intermediate case here, the trend is of reducing L_b with as ϕ increases, values of L_b become negative circa $\phi = 1.4$.

Methane has the opposite trend to the heavier fuels, with the lean conditions having negative values of L_b becoming positive around $\phi = 0.9$. The rich methane conditions were strongly positive reaching values equal to the lean iso-octane. Mixtures of methane and hydrogen have lower values of L_b until $\phi = 1.4$ where the linear fits suggest the values were similar. For this fuel L_b becomes positive at a greater equivalence ratio (of circa $\phi = 1.05$) compared to methane. In general both these fuels displayed the same trend of increasing L_b moving richer in contrast with the heavier fuels.

The variation in Ma_{sr} with equivalence ratio is shown in Fig. 4.14. The same general trends of Ma_{sr} with equivalence ratio are seen as with L_b. Gillespie *et al.* (2000) suggested that Ma_{sr} is the most appropriate representative of flame stretch behaviour when considering turbulent flames.

Shown in Fig. 4.15 are the laminar burning velocities plotted against pressure for iso-octane air flames for equivalence ratios of $\phi = 0.8$, $\phi = 1.0$, $\phi = 1.2$ and $\phi = 1.4$ for pressures of 0.1, 0.5 and 1.0 MPa. At atmospheric 0.1 MPa the fastest equivalence ratio was at stoichiometry with a value of about 51 cm/s. The equivalence ratio $\phi = 1.2$ (44 cm/s) had the next highest value closely followed by $\phi = 0.8$ with an average value of 44.5 cm/s although there was a discrepancy between the two measurements of 3 cm/s. At $\phi = 1.4$ the value u_l was still relatively high at 30.5 cm/s.

Moving to 0.5 MPa there was a distinct fall in the value of laminar burning velocities. The fastest stoichiometry at this pressure was at $\phi = 1.1$, as shown earlier on Fig. 4.11, here on Fig. 4.15 the values of $\phi = 1.0$ and $\phi = 1.2$ are equal have mean value of 30.5 cm/s. The mean value at $\phi = 1.4$ (24 cm/s) is greater than that at $\phi = 0.8$ (20 cm/s). At the higher pressure of 1.0 MPa there was a further fall in the laminar burning velocities, the same trend as at 0.5 MPa was repeated with mean values being; $\phi = 0.8 = 16$ cm/s, $\phi = 1.0 = 24.5$ cm/s, $\phi = 1.2 = 25.5$ cm/s, $\phi = 1.4 = 21.5$ cm/s.

Shown in Fig. 4.16 are the experimental variations in L_b with ϕ for iso-octane air mixtures over the range of experimental pressures from atmospheric to 1.0 MPa. The repeatability of the results at each condition is fair. It is clear that moving from lean to rich the L_b reduces. At 0.1 MPa L_b values are consistently higher than the 0.5 MPa and 1.0 MPa flames. To a first approximation values of L_b at 0.5MPa are a factor of 5 times lower than 0.1 MPa, the 1.0 MPa values of L_b are half that of 0.5 MPa and a factor of ten times lower than the 0.1 MPa flames.

Figure 4.17 shows the variation in Ma_{sr} with equivalence ratio. The same general trends of Ma_{sr} with equivalence ratio are seen as with L_b.

4.6 Comparisons with other workers

The current measurements of laminar burning velocity have been compared with the empirical correlation from Bradley *et al.* (1998) and with the power law presented by Metghalchi and Keck (1982);

Bradley *et al.* 1988 reported;

$$u_l = 0.48\left(\frac{T_u}{358}\right)^{1.01}(P)^{-0.282}\, m/s \quad (\phi = 1.0) \qquad 4.2$$

$$u_l = 0.40\left(\frac{T_u}{358}\right)^{1.07}(P)^{-0.348}\, m/s\, (\phi = 0.8) \qquad 4.3$$

where P is measured in bar.

Metghalchi and Keck (1982) reported;

$$u_l = u_{l,0}\left(\frac{T_u}{T_0}\right)^{\alpha}\left(\frac{p}{p_0}\right)^{\beta} \qquad 4.4$$

where $T_0 = 298$ K and $p_0 = 0.1$ MPa,

$$\alpha = 2.18 - 0.8(\phi - 1) \qquad 4.5$$

$$\beta = -0.16 + 0.22(\phi - 1) \qquad 4.6$$

$$u_{l,0} = B_m + B_\phi(\phi - \phi_m)^2 \qquad 4.7$$

Where α and β are constants for a given fuel and ϕ_m is the equivalence ratio at which $u_{l,0}$ is a maximum with a value of B_m. For iso-octane $\phi_m = 1.13$, $B_m = 26.3$ and $B_\phi = -84.7$, for methanol $\phi_m = 1.11$, $B_m = 36.9$ and $B_\phi = -140.5$. (Metghalchi and Keck, 1982).

Shown in Fig. 4.18 are laminar burning velocity plotted against equivalence ratio for 0.1, 0.5 and 1.0 MPa. Both correlations predict a fall in u_l with an increase in pressure. This is confirmed with the current study. The agreement between the current study and those of Bradley *et al.* (1998) is generally good, for all pressures with a maximum discrepancy of 10 % (at $\phi = 0.8$, 0.5 MPa.) between the mean of the two flames in the current study and the predicted value of Bradley *et al.* (1998).

Atmospheric pressure measurements were far lower than those predicted by Metghalchi and Keck. At 0.5 MPa the values from the two correlations and results from the current study are in general agreement with the current study being very close to the predicted value from Metghalchi and Keck. At the higher pressure of 1.0 MPa the $\phi = 0.8$ and 1.0 measurements from the current study agree with those of Metghalchi and Keck (1982) and Bradley *et al.* (1998). The 1.0 MPa rich values from this current study are lower than those predicted by Metghalchi and Keck. Flames at this high-pressure rich condition became unstable within the spark effected regime, as earlier noted these two results are estimated.

Shown in Fig. 4.19 is a comparison of the results from the current study with values predicted by Eq.4.4 Metghalchi and Keck (1982) for iso-octane and methanol at 0.5 MPa, 360 K over the range of equivalence ratios tested. Third order polynomial fits have been made to both the current results and the results from Eq. 4.4. Iso-octane values compare remarkably well from $\phi = 0.8$ to 1.4, in this work it

was only possible to accurately determine values for u_l up to $\phi = 1.4$. Rich iso-octane u_l values have been plotted on this diagram as they are later used for comparison with turbulent values. These rich experimental values are consistently higher than those predicted by Metghalchi and Keck (1982).

In this study it was possible to gain true stretch free laminar burning velocities for methanol at 0.5 MPa, as they remained stable to an adequate radii. Metghalchi and Keck (1982) predict faster values of u_l from $\phi = 0.5$ to 1.3 than found in this study. The peak burning velocity predicted by Eq. 4.4 was 0.1 of an equivalence ratio interval leaner than experimentally found where the peak equivalence ratio was found at $\phi = 1.21$ and was 3 cm/s slower than the predicted peak burning velocity. Richer than $\phi = 1.3$ the values from this study are substantially greater e.g. $\phi = 1.6$ Eq.4.4 predicts $u_l = 4$ cm/s but $u_l = 26.5$ cm/s was measured.

ϕ	u_l (m/s)	s_s (m/s)	ρ_u/ρ_b	L_b (mm)	M_{as}	M_{ac}	M_{asr}	M_{acr}	Critical Radius (mm)
0.6	0.056	0.26	4.75						buoyant
0.6	0.056	0.27	4.75						buoyant
0.7	0.128	0.67	5.23	-0.26	-6.28	-3.78	-0.28	-0.87	>65
0.7	0.124	0.65	5.23	-0.19	-5.88	-3.38	0.12	-0.47	>65
0.8	0.198	1.12	5.68	-0.51	-9.34	-6.42	-2.86	-3.49	27
0.8	0.201	1.14	5.68	-0.21	-7.05	-4.12	-0.56	-1.19	24
0.9	0.259	1.57	6.09	-0.18	-7.53	-4.15	-0.59	-1.26	28
0.9	0.265	1.61	6.09	-0.06	-6.40	-3.02	0.54	-0.13	26
1	0.286	1.83	6.40	0.27	-3.42	0.35	3.87	3.17	31
1	0.281	1.80	6.40	0.21	-4.03	-0.26	3.26	2.56	36
1.1	0.264	1.69	6.41	0.41	-2.30	1.50	5.01	4.31	47
1.1	0.263	1.68	6.41	0.45	-1.97	1.84	5.35	4.64	50
1.2	0.214	1.34	6.29	0.33	-3.48	0.21	3.70	3.00	>65
1.2	0.212	1.33	6.29	0.36	-3.33	0.37	3.86	3.16	>65
1.3	0.130	0.80	6.16	0.91	-1.62	2.13	5.48	4.75	>65
1.3	0.129	0.79	6.16	0.87	-1.84	1.89	5.25	4.53	>65

Table 4.1 Experimental results for methane-air mixtures at an initial pressure of 0.5 MPa and temperature of 360 K.

ϕ	u_l (m/s)	s_s (m/s)	ρ_u/ρ_b	L_b (mm)	M_{as}	M_{ac}	M_{asr}	M_{acr}	Critical Radius (mm)
0.5	0.033	0.14	4.25						<4
0.5	0.036	0.15	4.25						<4
0.6	0.119	0.56	4.75						<4
0.6	0.124	0.59	4.75						<4
0.7	0.174	0.91	5.22						4
0.7	0.189	0.98	5.22						4
0.8	0.275	1.55	5.65	-0.57	-11.52	-8.67	-5.09	-5.70	8
0.8	0.298	1.68	5.65	-0.45	-10.64	-7.79	-4.20	-4.82	8
0.9	0.353	2.13	6.04	-0.39	-10.92	-7.62	-4.04	-4.70	10
0.9	0.340	2.05	6.04	-0.17	-7.93	-4.63	-1.06	-1.71	10
1	0.377	2.39	6.34	0.02	-5.80	-2.13	1.42	0.73	15
1	0.367	2.32	6.34	-0.15	-7.96	-4.29	-0.74	-1.43	15
1.1	0.336	2.13	6.35	0.09	-5.07	-1.37	2.17	1.48	17
1.1	0.328	2.09	6.35	0.14	-4.44	-0.74	2.80	2.10	17
1.2	0.215	1.34	6.24	0.29	-3.79	-0.16	3.33	2.64	>65
1.2	0.194	1.21	6.24	0.37	-3.42	0.24	3.71	3.02	>65
1.3	0.106	0.65	6.11	0.55	-3.85	0.13	3.29	2.51	>65
1.3	0.115	0.71	6.11	0.56	-3.60	0.30	3.51	2.75	>65
1.4	0.095	0.57	5.99	0.91	-2.68	1.27	4.38	3.59	>65
1.4	0.084	0.50	5.99	1.28	-2.07	2.23	5.17	4.31	>65

Table 4.2 Experimental results for binary mixtures of 30%H_2+70%CH_4-air mixtures at an initial pressure of 0.5 MPa and temperature of 360 K.

ϕ	u_l (m/s)	s_s (m/s)	ρ_u/ρ_b	L_b (mm)	M_{as}	M_{ac}	M_{asr}	M_{acr}	Critical Radius (mm)
0.8	0.216	1.33	6.15	0.64	-0.36	3.18	6.67	5.98	>65
0.8	0.214	1.32	6.15	0.50	-1.59	1.94	5.44	4.75	>65
0.9	0.264	1.75	6.64	0.43	-2.26	1.85	5.32	4.59	>65
0.9	0.259	1.72	6.64	0.35	-3.08	1.05	4.50	3.77	>65
1	0.310	2.17	7.01	0.36	-2.94	1.68	5.08	4.31	42
1	0.306	2.14	7.01	0.32	-3.42	1.20	4.59	3.83	44
1.1	0.322	2.30	7.12	0.20	-4.72	0.05	3.42	2.64	26
1.1	0.320	2.28	7.12	0.17	-5.09	-0.32	3.05	2.27	26
1.2	0.313	2.21	7.07	-0.02	-7.20	-2.51	0.88	0.10	19
1.2	0.313	2.21	7.07	0.02	-6.72	-2.03	1.36	0.59	20
1.3	0.281	1.96	6.98	-0.07	-7.49	-2.92	0.48	-0.28	13
1.3	0.284	1.98	6.98	0.04	-6.47	-1.90	1.50	0.74	13
1.4	0.247	1.70	6.88	-0.15	-8.11	-3.66	-0.24	-1.00	10
1.4	0.237	1.63	6.88	-0.31	-9.46	-5.01	-1.59	-2.35	10
1.5	0.193	1.31	6.78						8
1.5	0.188	1.28	6.78						8
1.6	0.146	0.98	6.68						4
1.6	0.142	0.95	6.68						4
1.8	0.082	0.53	6.46						<4
1.8	0.074	0.48	6.46						<4

Table 4.3 Experimental results for dutch-pura–air mixtures at an initial pressure of 0.5 MPa and temperature of 360 K.

ϕ	u_l (m/s)	s_s (m/s)	ρ_u/ρ_b	L_b (mm)	M_{as}	M_{ac}	M_{asr}	M_{acr}	Critical Radius (mm)
0.8	0.199	1.22	6.11	0.87	0.79	4.53	7.84	7.11	>65
0.8	0.203	1.24	6.11	0.89	1.09	4.86	8.15	7.41	>65
0.9	0.261	1.72	6.59	0.76	0.81	4.86	8.32	7.60	>65
0.9	0.264	1.74	6.59	0.60	-0.62	3.42	6.89	6.17	>65
1	0.298	2.07	6.95	0.51	-1.60	3.40	6.44	5.60	>65
1	0.298	2.07	6.95	0.53	-1.39	3.52	6.63	5.80	>65
1.1	0.303	2.14	7.05	0.33	-3.56	1.20	4.51	3.72	20
1.1	0.311	2.19	7.05	0.47	-1.99	2.77	6.09	5.30	20
1.2	0.299	2.09	6.99	-0.10	-8.20	-2.02	0.15	-0.88	19
1.2	0.308	2.15	6.99	0.08	-6.08	-1.09	1.99	1.16	18
1.3	0.290	2.00	6.90	-0.07	-7.45	-2.90	0.45	-0.32	11
1.4	0.252	1.71	6.80	-0.05	-7.11	-2.66	0.68	-0.09	8
1.4	0.226	1.53	6.80	-0.35	-9.47	-5.00	-1.67	-2.44	8
1.5	0.200	1.34	6.70						4
1.6	0.142	0.94	6.60						<4
1.6	0.160	1.06	6.60						<4
1.8	0.063	0.40	6.39						<4
1.8	0.082	0.52	6.39						<4
2	0.047	0.29	6.16						buoyant
2	0.054	0.33	6.16						buoyant

Table 4.4 Experimental results for iso-octane-air mixtures at an initial pressure of 0.5 MPa and temperature of 360 K.

ϕ	u_l (m/s)	s_s (m/s)	ρ_u/ρ_b	L_b (mm)	M_{as}	M_{ac}	M_{asr}	M_{acr}	Critical Radius (mm)
0.7	0.142	0.79	5.59	0.30	-3.40	-0.51	3.00	2.37	>65
0.7	0.143	0.80	5.59	0.37	-2.94	-0.02	3.47	2.83	>65
0.8	0.215	1.30	6.05	0.26	-3.48	-0.11	3.42	2.76	52
0.8	0.217	1.31	6.05	0.21	-3.88	-0.51	3.03	2.36	49
0.9	0.283	1.83	6.47	0.22	-3.81	0.05	3.57	2.86	30
0.9	0.287	1.86	6.47	0.22	-3.74	0.11	3.63	2.93	30
1	0.349	2.37	6.79	0.13	-5.09	0.08	2.85	1.96	23
1	0.348	2.36	6.79	0.08	-5.61	-1.06	2.19	1.40	23
1.1	0.391	2.68	6.86	0.08	-5.57	-1.18	2.26	1.51	18
1.1	0.390	2.68	6.86	0.08	-5.50	-1.12	2.32	1.57	18
1.2	0.411	2.79	6.79	0.03	-6.15	-1.87	1.60	0.86	16
1.2	0.405	2.75	6.79	-0.03	-7.00	-2.71	0.75	0.01	16
1.4	0.369	2.45	6.63	-0.05	-7.13	-3.06	0.43	-0.29	19
1.4	0.372	2.46	6.63	-0.05	-7.13	-3.06	0.43	-0.30	19
1.6	0.268	1.73	6.46	-0.10	-7.36	-3.51	0.01	-0.70	19
1.6	0.263	1.70	6.46	-0.18	-8.22	-4.36	-0.85	-1.55	20
1.8	0.176	1.11	6.30	-0.23	-7.81	-4.10	-0.62	-1.32	22
1.8	0.178	1.12	6.30	-0.12	-6.99	-3.29	0.20	-0.50	25

Table 4.5 Experimental results for methanol-air mixtures at an initial pressure of 0.5 MPa and temperature of 360 K.

(a) 0.1 MPa

ϕ	u_l (m/s)	s_s (m/s)	ρ_u/ρ_b	L_b (mm)	M_{as}	M_{ac}	M_{asr}	M_{acr}	Critical Radius (mm)
0.8	0.439	2.67	6.09	3.97	7.65	11.53	14.73	13.97	>65
0.8	0.413	2.51	6.09	4.01	6.98	10.78	14.03	13.29	>65
1	0.511	3.50	6.84	3.25	4.85	9.68	12.77	11.94	>65
1	0.503	3.44	6.84	3.04	3.93	8.79	11.86	11.02	>65
1.2	0.444	3.09	6.96	0.92	-4.08	1.00	4.00	3.14	>65
1.2	0.441	3.07	6.96	0.95	-4.07	1.29	4.08	3.18	>65
1.4	0.307	2.08	6.80	-0.14	-7.10	-1.99	0.86	-0.02	>65
1.4	0.304	2.07	6.80	-0.13	-7.10	-1.90	0.89	-0.01	>65

(b) 0.5 MPa

ϕ	u_l (m/s)	s_s (m/s)	ρ_u/ρ_b	L_b (mm)	M_{as}	M_{ac}	M_{asr}	M_{acr}	Critical Radius (mm)
0.8	0.199	1.22	6.11	0.87	0.79	4.53	7.84	7.11	>65
0.8	0.203	1.24	6.11	0.89	1.09	4.86	8.15	7.41	>65
1	0.298	2.07	6.95	0.51	-1.60	3.40	6.44	5.60	>65
1	0.298	2.07	6.95	0.53	-1.39	3.52	6.63	5.80	>65
1.2	0.299	2.09	6.99	-0.10	-8.20	-2.02	0.15	-0.88	20
1.2	0.308	2.15	6.99	0.08	-6.08	-1.09	1.99	1.16	20
1.4	0.252	1.71	6.80	-0.05	-7.11	-2.66	0.68	-0.09	8
1.4	0.226	1.53	6.80	-0.35	-9.47	-5.00	-1.67	-2.44	8

(c) 1.0 MPa

ϕ	u_l (m/s)	s_s (m/s)	ρ_u/ρ_b	L_b (mm)	M_{as}	M_{ac}	M_{asr}	M_{acr}	Critical Radius (mm)
0.8	0.159	0.98	6.12	0.54	0.76	4.30	7.76	7.07	>65
0.8	0.164	1.01	6.12	0.45	-0.10	3.42	6.89	6.21	>65
1	0.246	1.72	6.99	0.23	-2.98	1.63	5.01	4.24	28
1	0.245	1.71	6.99	0.21	-3.29	1.31	4.70	3.93	29
1.2	0.244	1.71	7.00						6
1.2	0.244	1.71	7.00						6
1.4	0.212	1.44	6.81						<4
1.4	0.216	1.47	6.81						<4

Table 4.6 Experimental results for iso-octane-air mixtures at an initial pressure of; (a) 0.1 MPa, (b) 0.5 MPa and (c) 1.0 MPa at 360 K

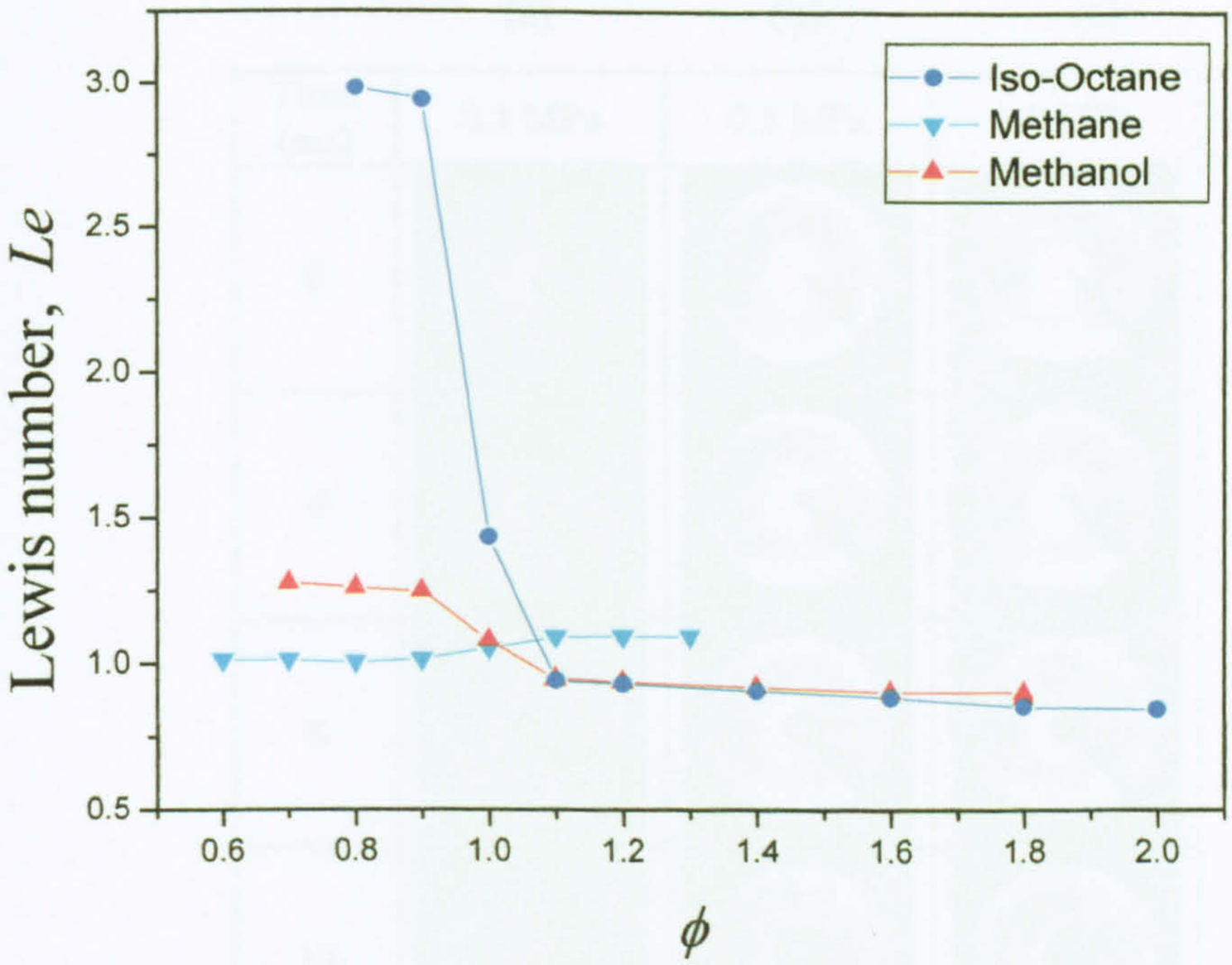

Figure 4.1 Calculated Lewis numbers at 0.5 MPa 360 K for methane, methanol and iso-octane.

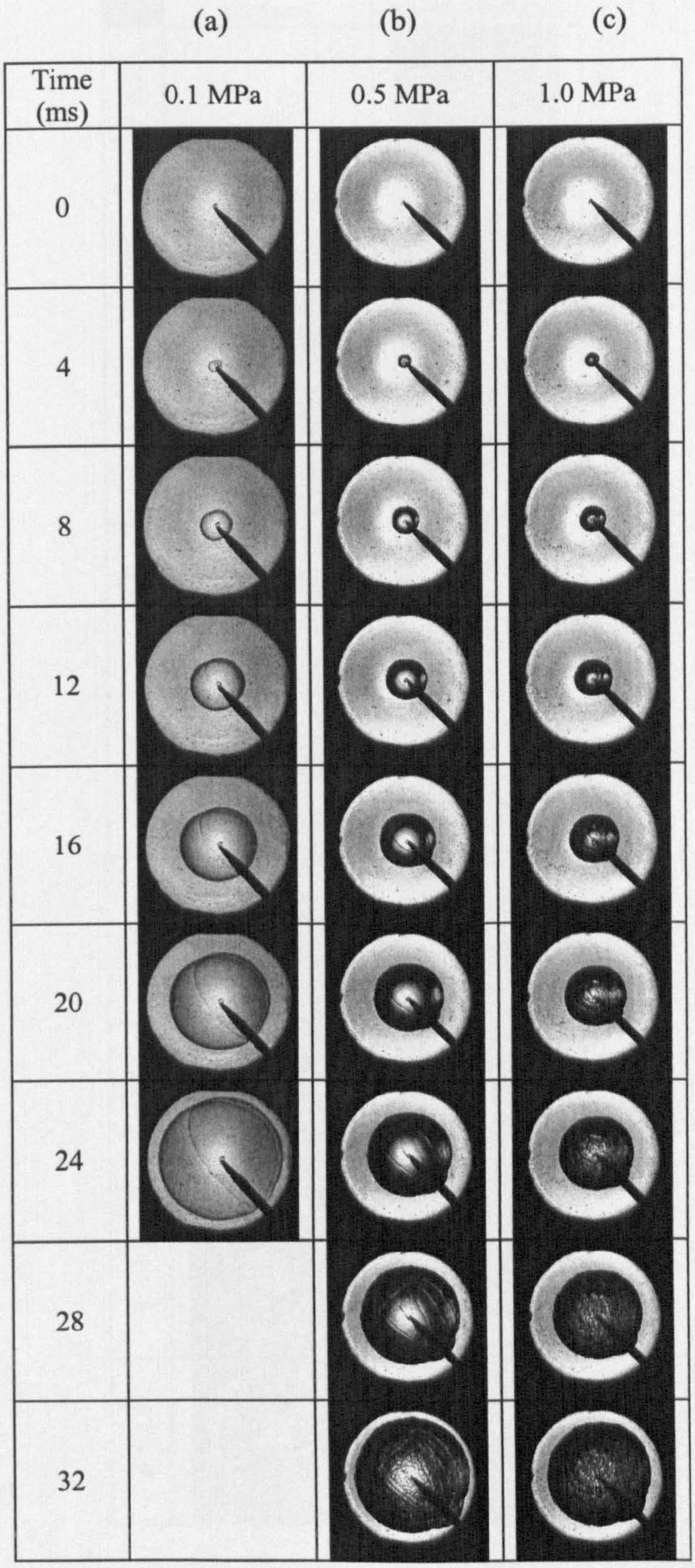

Figure 4.2 Laminar schlieren images of $\phi = 1$, iso-octane-air flames at initial pressure of (a) 0.1 MPa, (b) 0.5 MPa and (c) 1.0 MPa at 360 K in all cases. Time interval of 4ms.

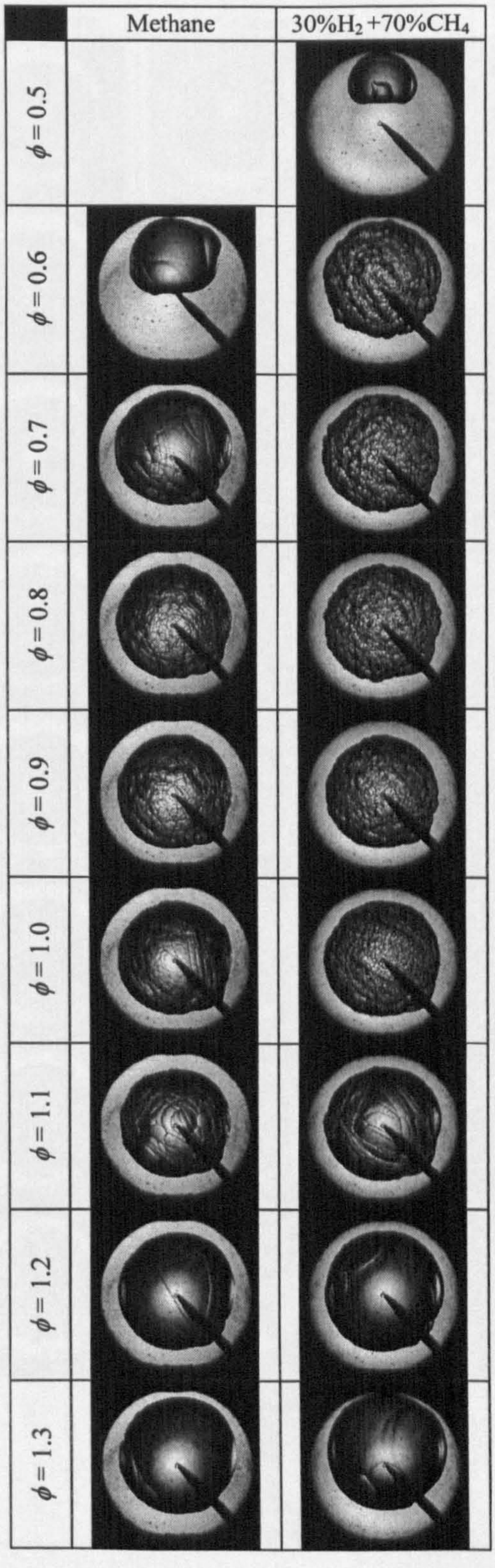

Figure 4.3 Laminar schlieren images of methane and 30%H_2+70%CH_4 with air at a radius of circa 50mm, with the exception of the buoyant cases. Initial pressure of 0.5 MPa and temperature of 360 K in all cases.

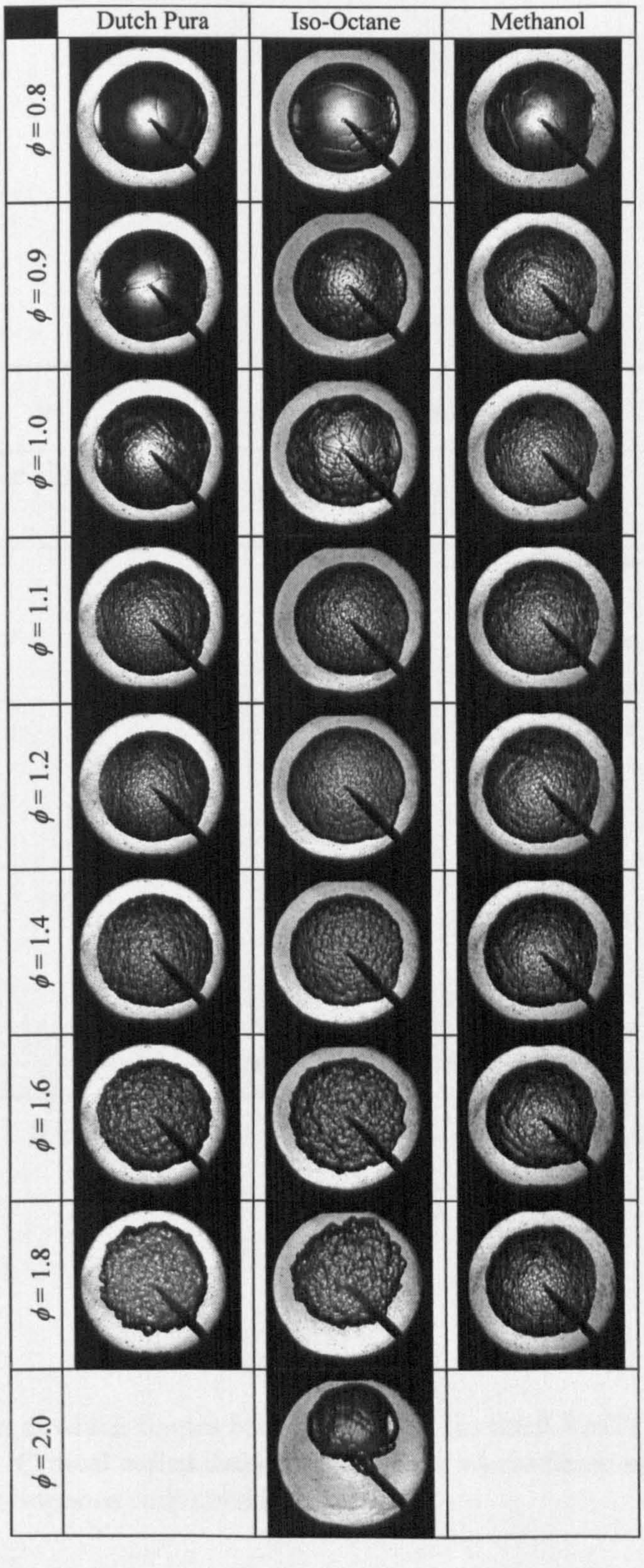

Figure 4.4 Laminar schlieren images of dutch-pura (a), iso-octane (b) and (c) methanol with air at a fixed radius of circa 50mm, with the exception of the buoyant case. Initial pressure of 0.5 MPa and temperature of 360 K in all cases.

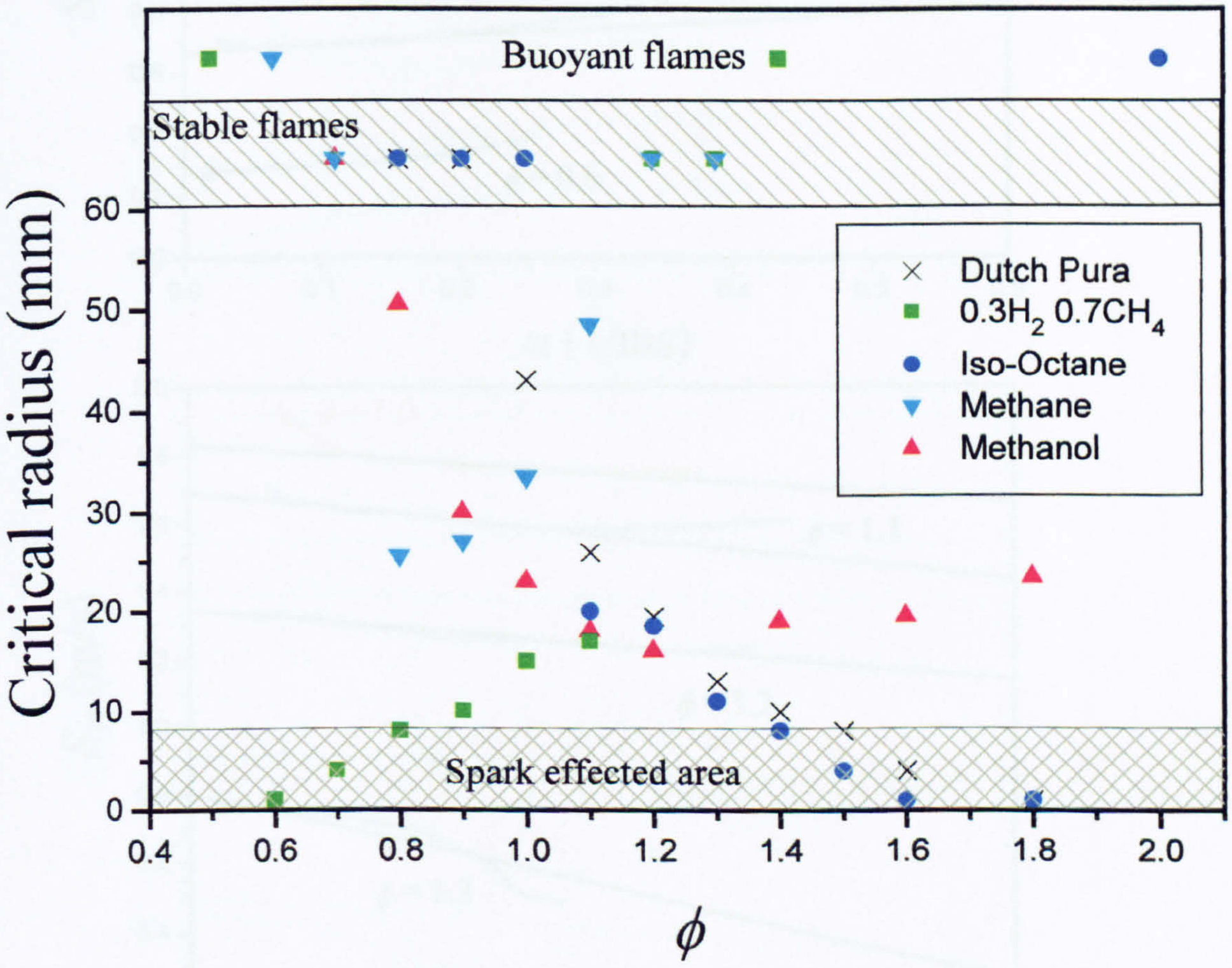

Figure 4.5 Radius at which flames become cellular, for the 0.5 MPa 360 K laminar conditions. Critical radius determined at point where flame-speed deviates from linear response with stretch.

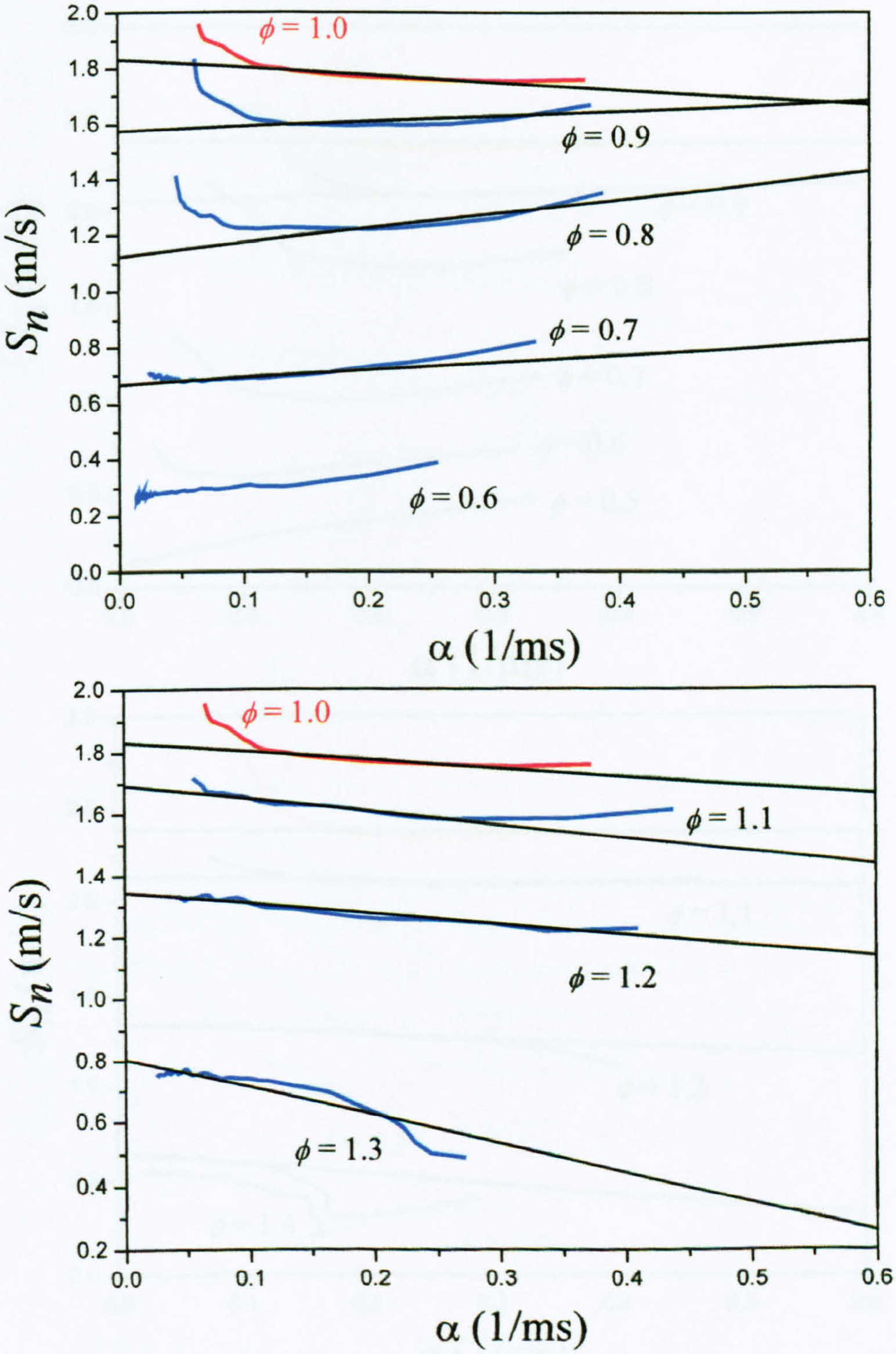

Figure 4.6 Measured flame speeds at different stretch rates and equivalence ratios for methane – air mixtures at 0.5 MPa and 360 K. Upper graph shows the lean flame-speeds, lower graph shows the rich results. The fastest condition is shown on both graphs.

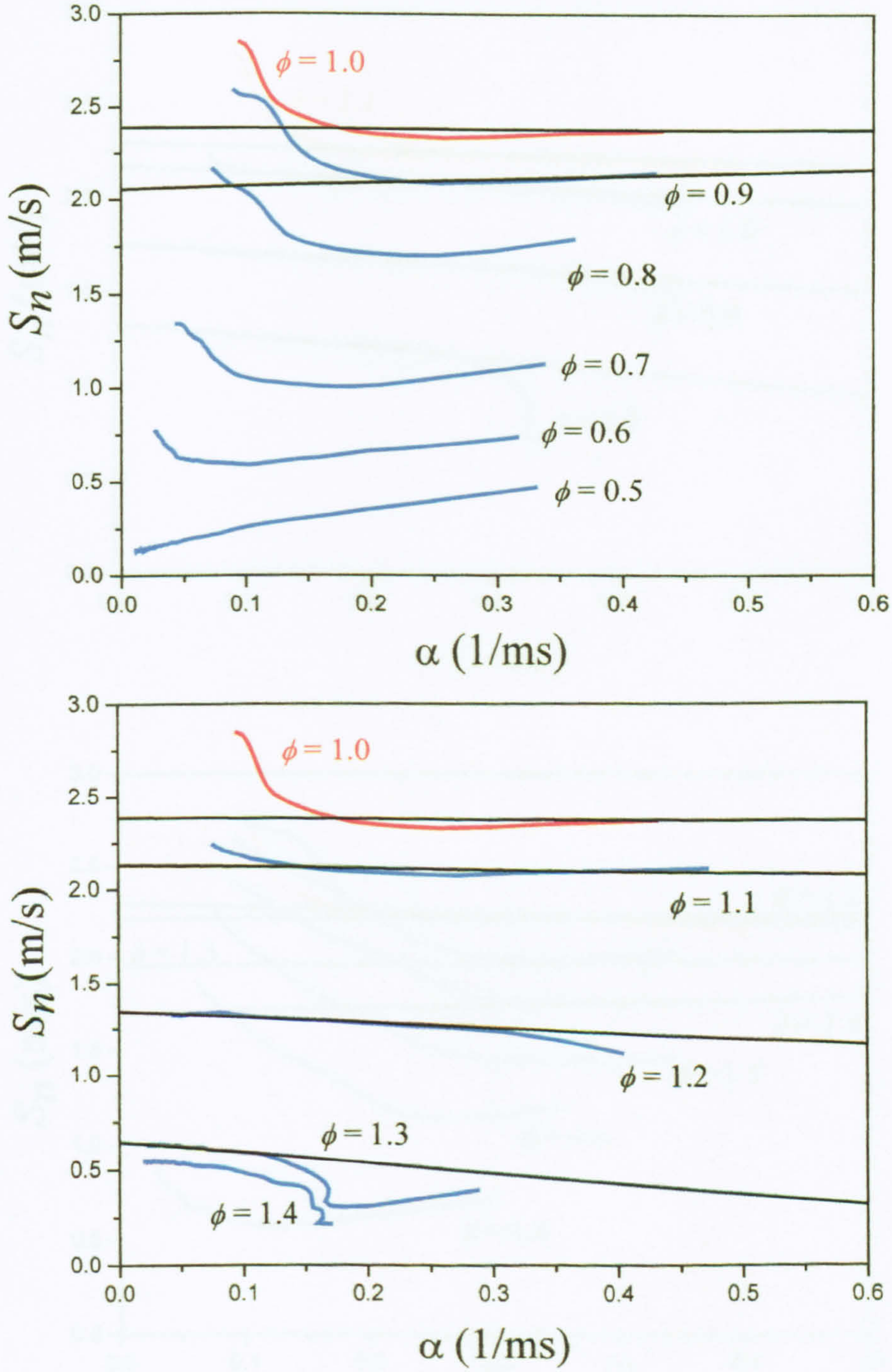

Figure 4.7 Measured flame speeds at different stretch rates and equivalence ratios for binary mixtures of 30%H_2+70%CH_4 with air mixtures at 0.5 MPa and 360 K. Upper graph shows the lean flame-speeds, lower graph shows the rich results. The fastest condition is shown on both graphs.

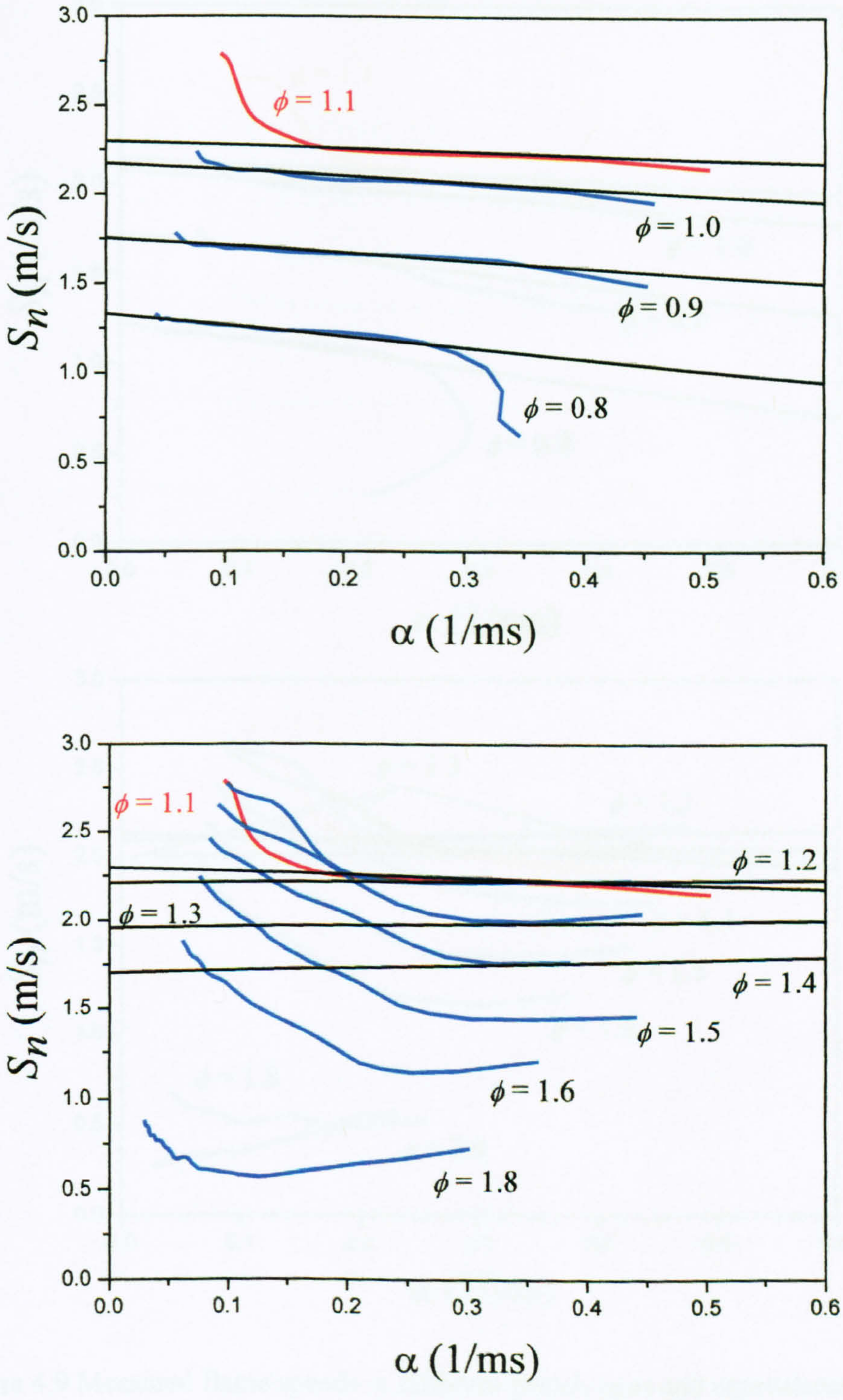

Figure 4.8 Measured flame speeds at different stretch rates and equivalence ratios for dutch-pura – air mixtures at 0.5 MPa and 360 K. Upper graph shows the lean flame-speeds, lower graph shows the rich results. The fastest condition is shown on both graphs.

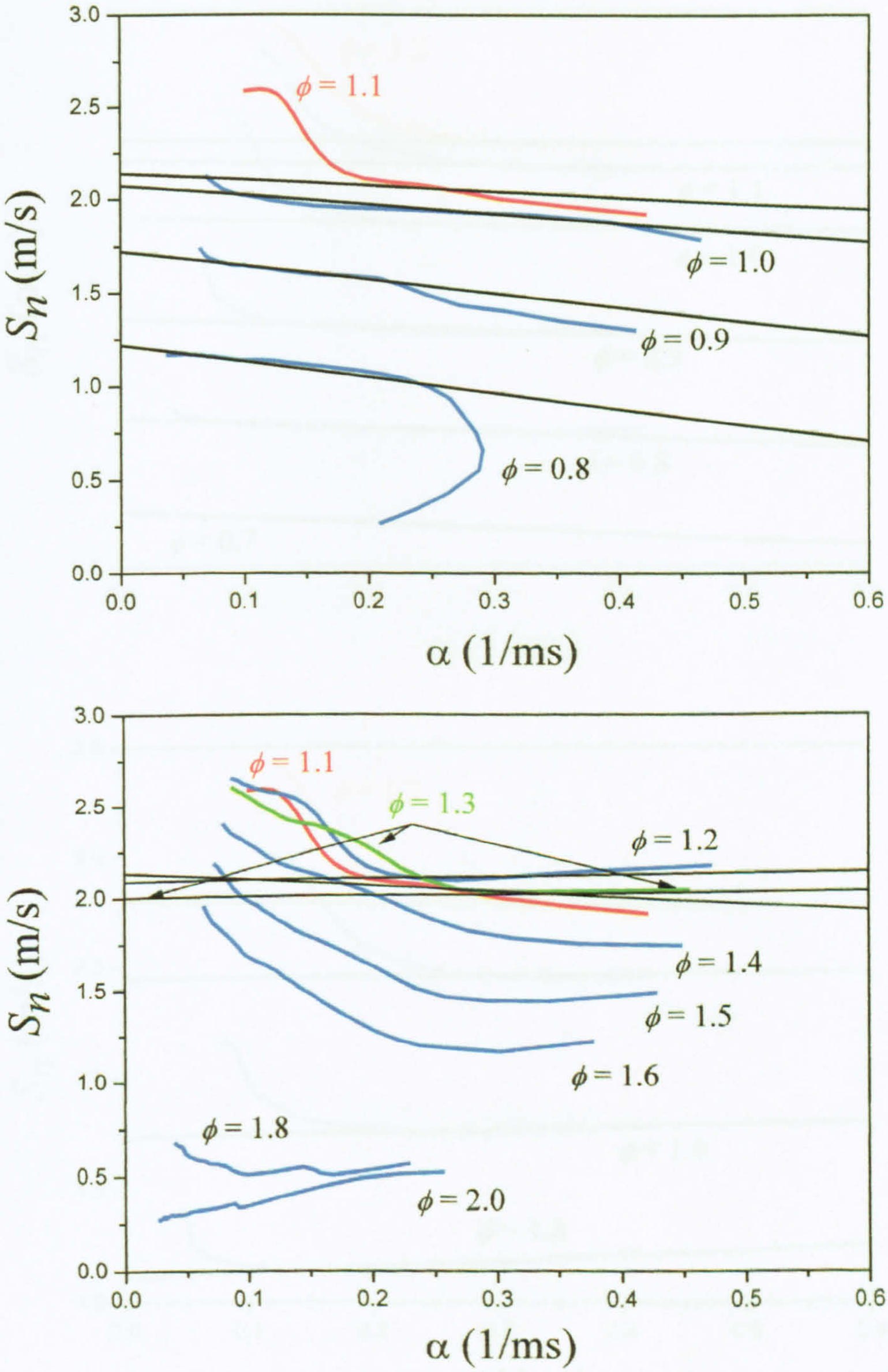

Figure 4.9 Measured flame speeds at different stretch rates and equivalence ratios for iso-octane – air mixtures at 0.5 MPa and 360 K. Upper graph shows the lean flame-speeds, lower graph shows the rich results. The fastest condition is shown on both graphs

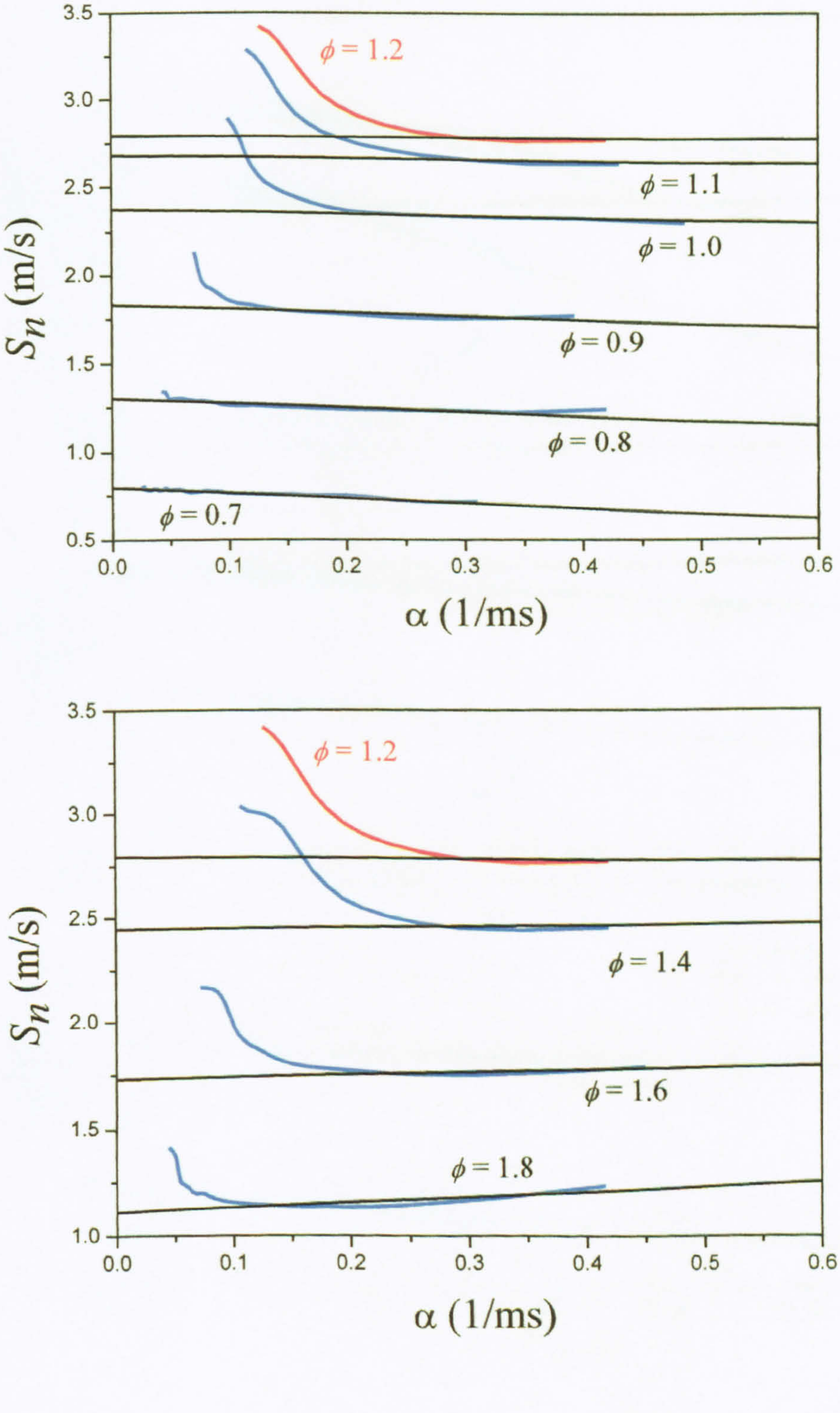

Figure 4.10 Measured flame speeds at different stretch rates and equivalence ratios for methanol – air mixtures at 0.5 MPa and 360 K. Upper graph shows the lean flame-speeds, lower graph shows the rich results. The fastest condition is shown on both graphs.

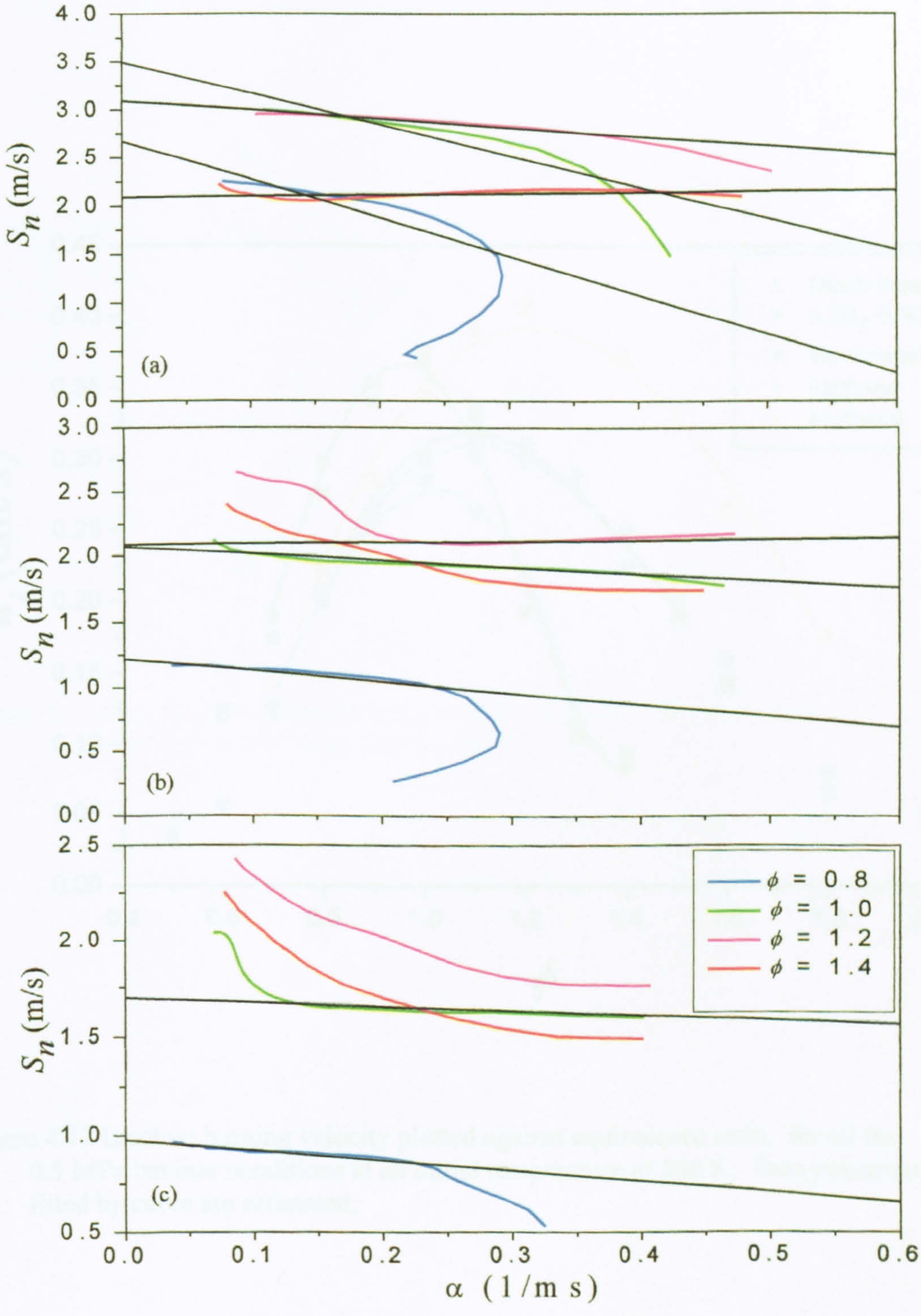

Figure 4.11 Measured flame speeds for iso-octane-air flames at different stretch rates, equivalence ratios and pressures of (a) 0.1 MPa, (b) 0.5 MPa and (c) 1.0MPa and 360 K.

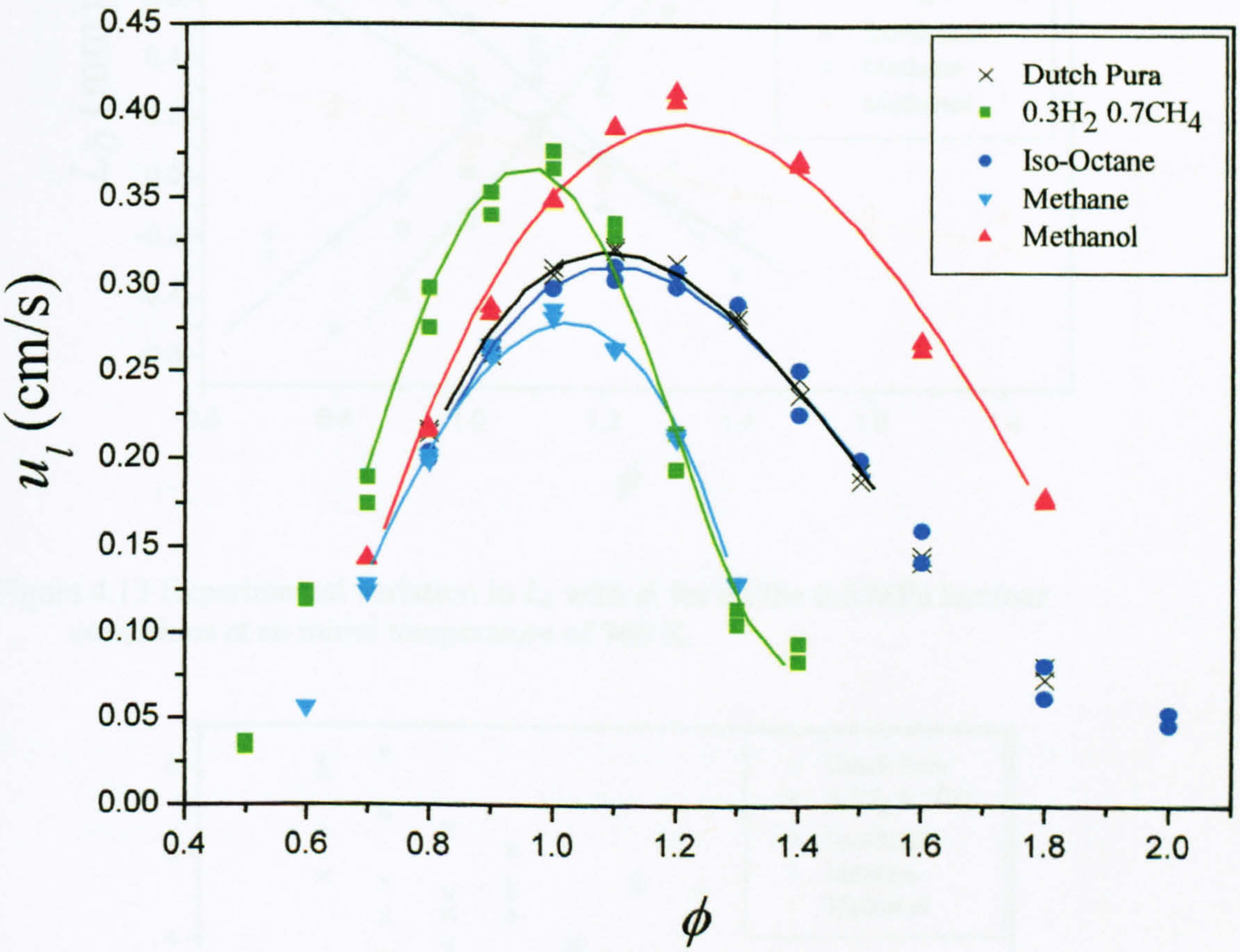

Figure 4.12 Laminar burning velocity plotted against equivalence ratio, for all the 0.5 MPa laminar conditions at an initial temperature of 360 K. Data points not fitted by curve are estimated.

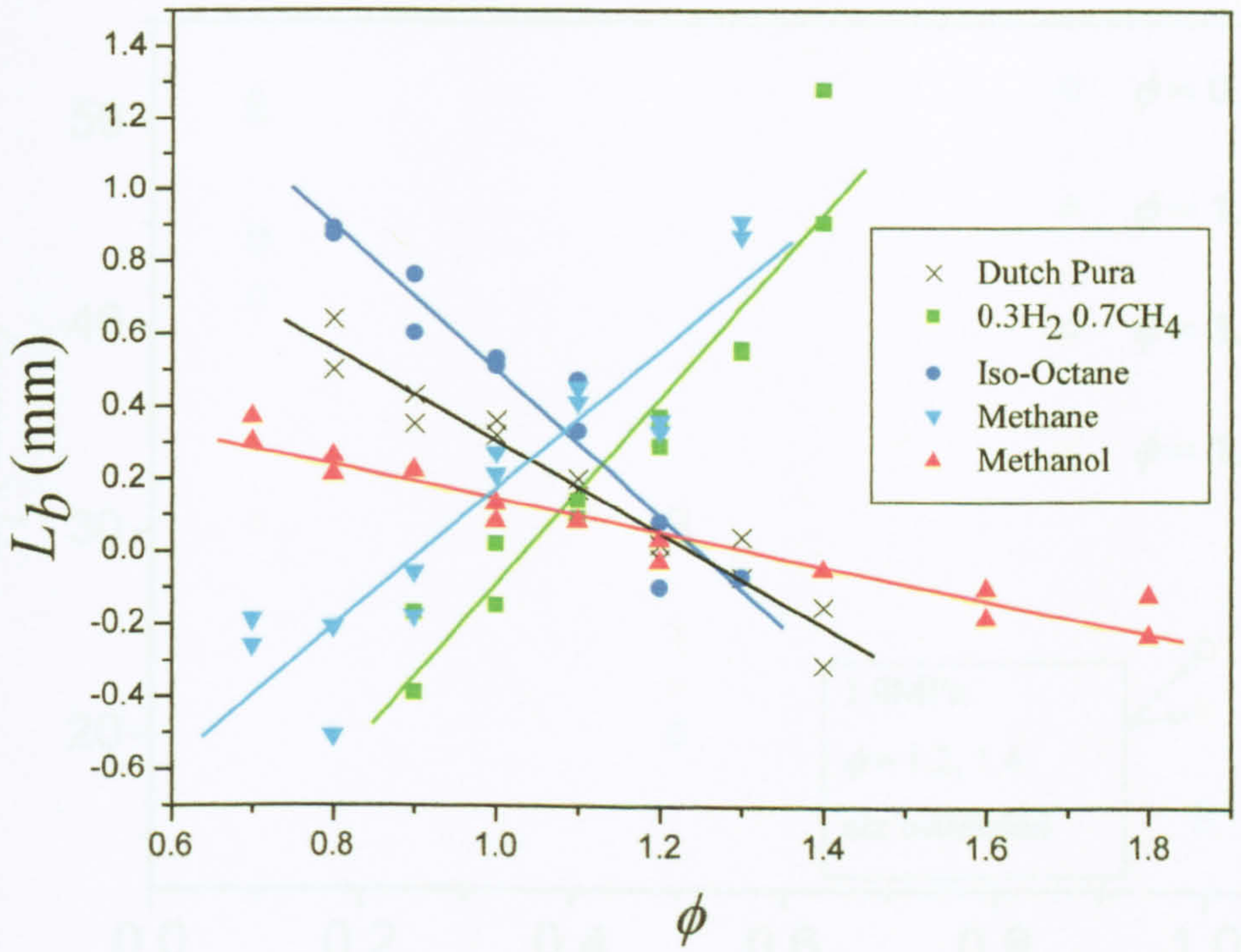

Figure 4.13 Experimental variation in L_b with ϕ, for all the 0.5 MPa laminar conditions at an initial temperature of 360 K.

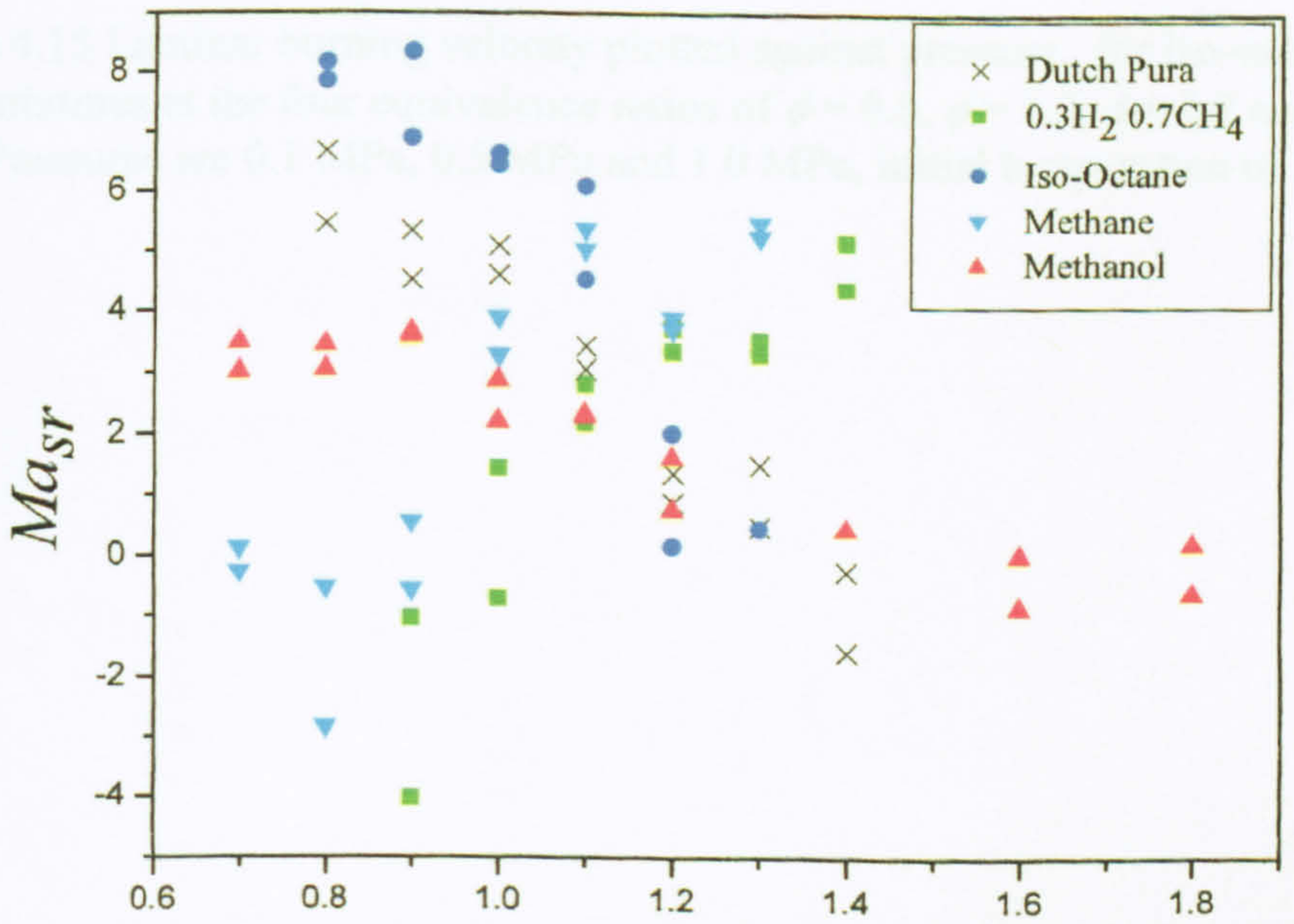

Figure 4.14 Experimental variation in Ma_{sr} with ϕ, for all the 0.5 MPa laminar conditions at an initial temperature of 360 K.

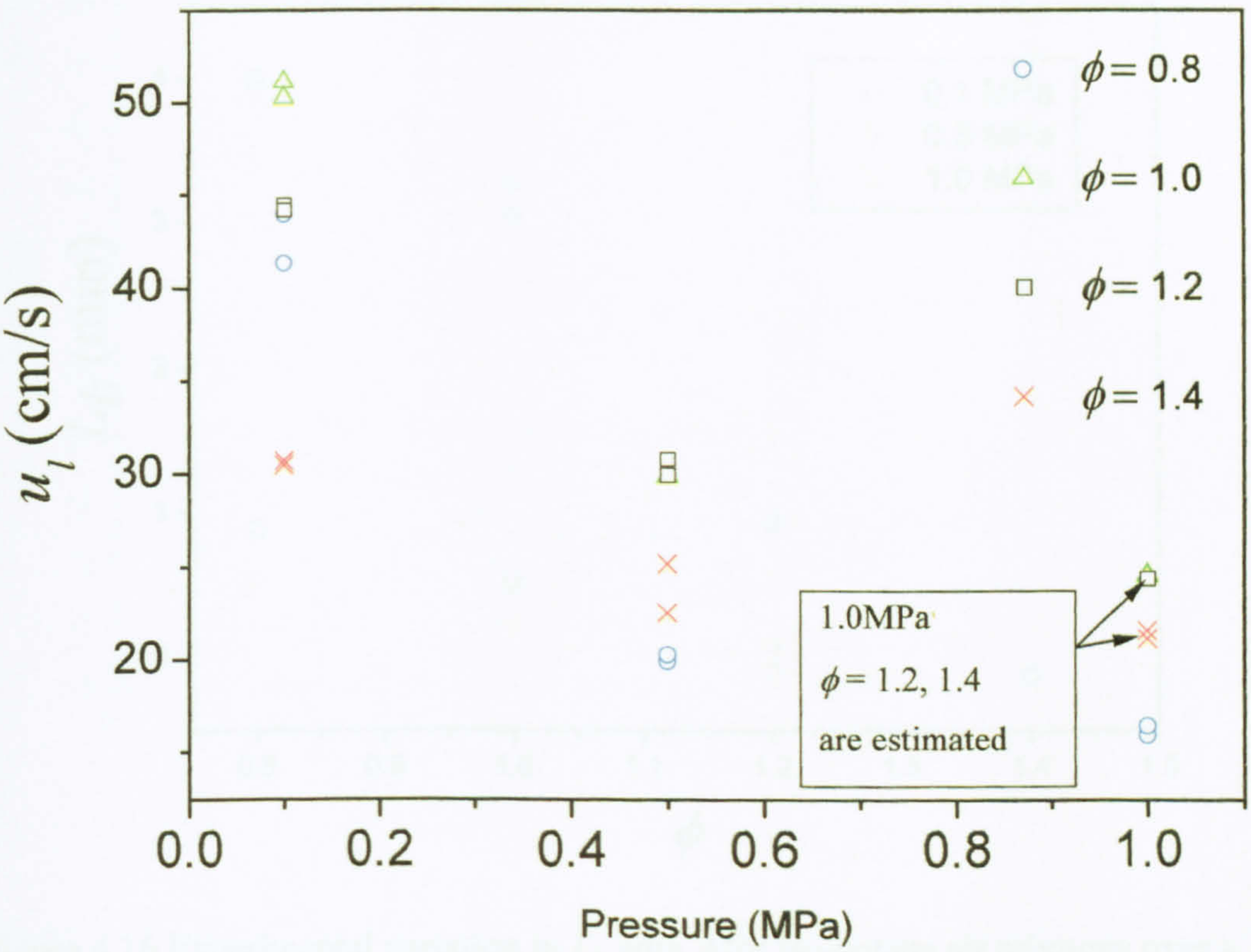

Figure 4.15 Laminar burning velocity plotted against pressure, for iso-octane-air mixtures at the four equivalence ratios of ϕ= 0.8, ϕ= 1.0, ϕ= 1.2 and ϕ= 1.4. Pressures are 0.1 MPa, 0.5 MPa and 1.0 MPa, initial temperature of 360 K.

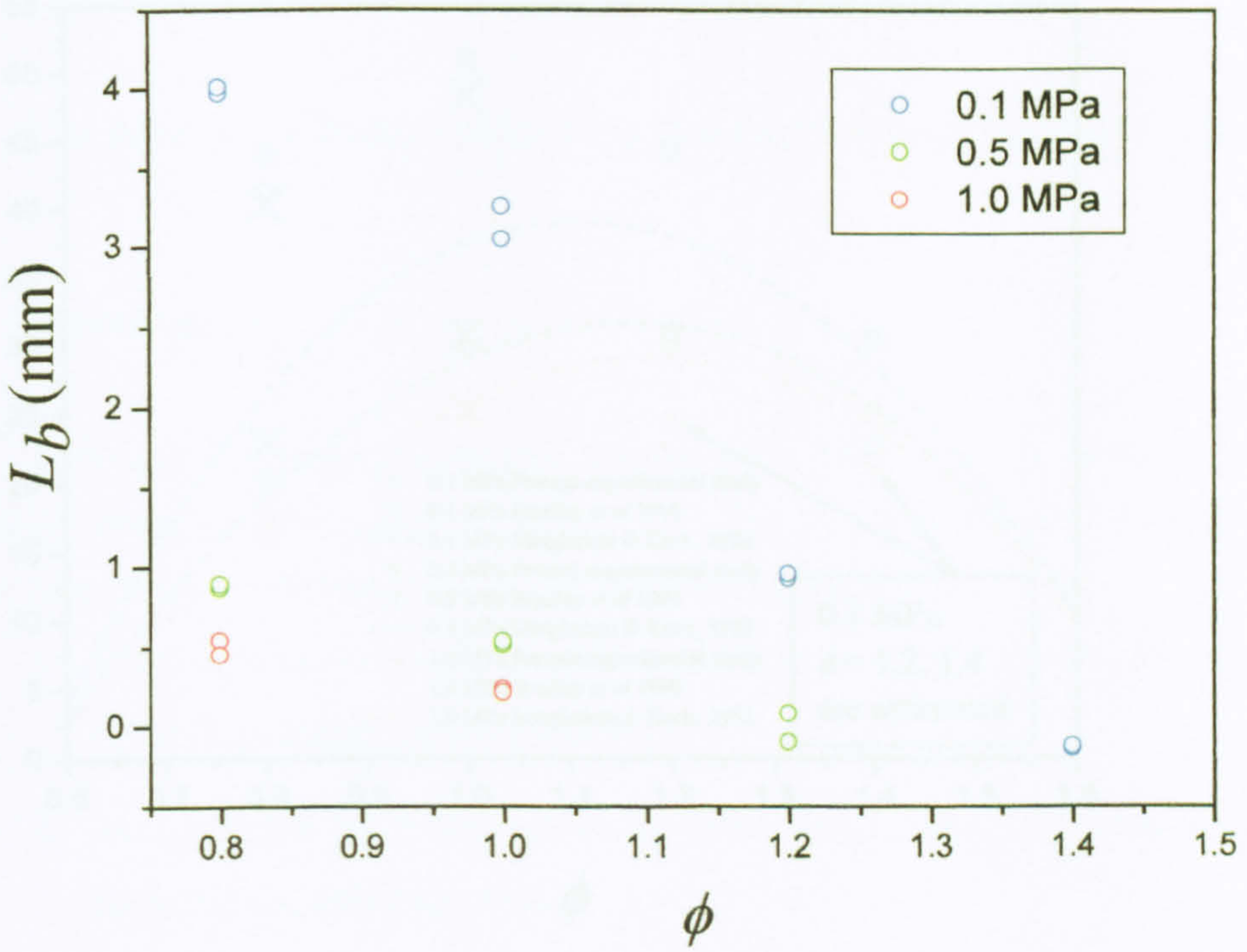

Figure 4.16 Experimental variation in L_b with ϕ for iso-octane air mixtures over a range of initial pressures at 360 K.

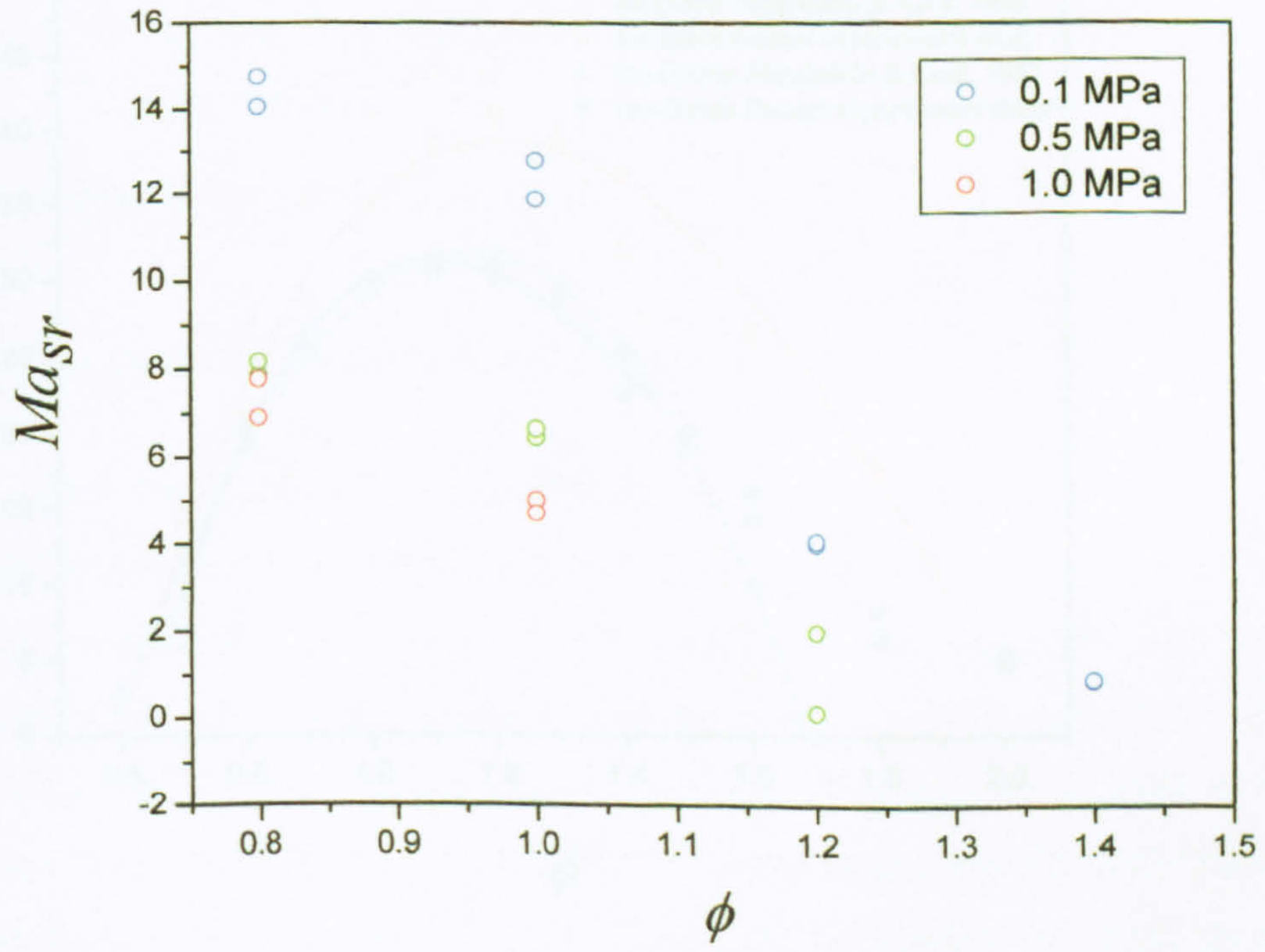

Figure 4.17 Experimental variation in Ma_{sr} with ϕ for iso-octane air mixtures over a range of initial pressures at 360 K

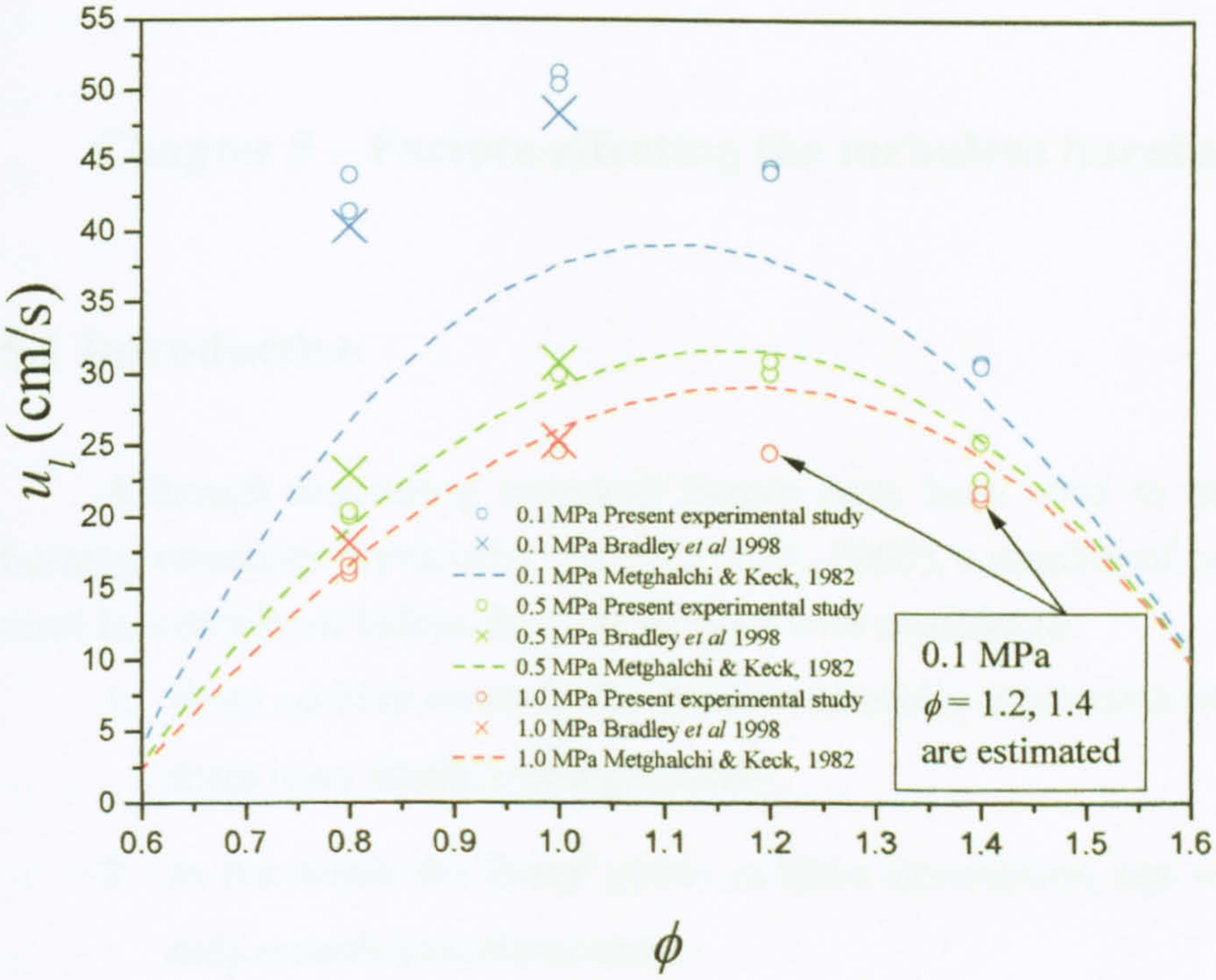

Figure 4.18 Laminar burning velocity plotted against equivalence ratio for iso-octane air mixtures over a range of pressures at 360 K, showing comparisons with other workers.

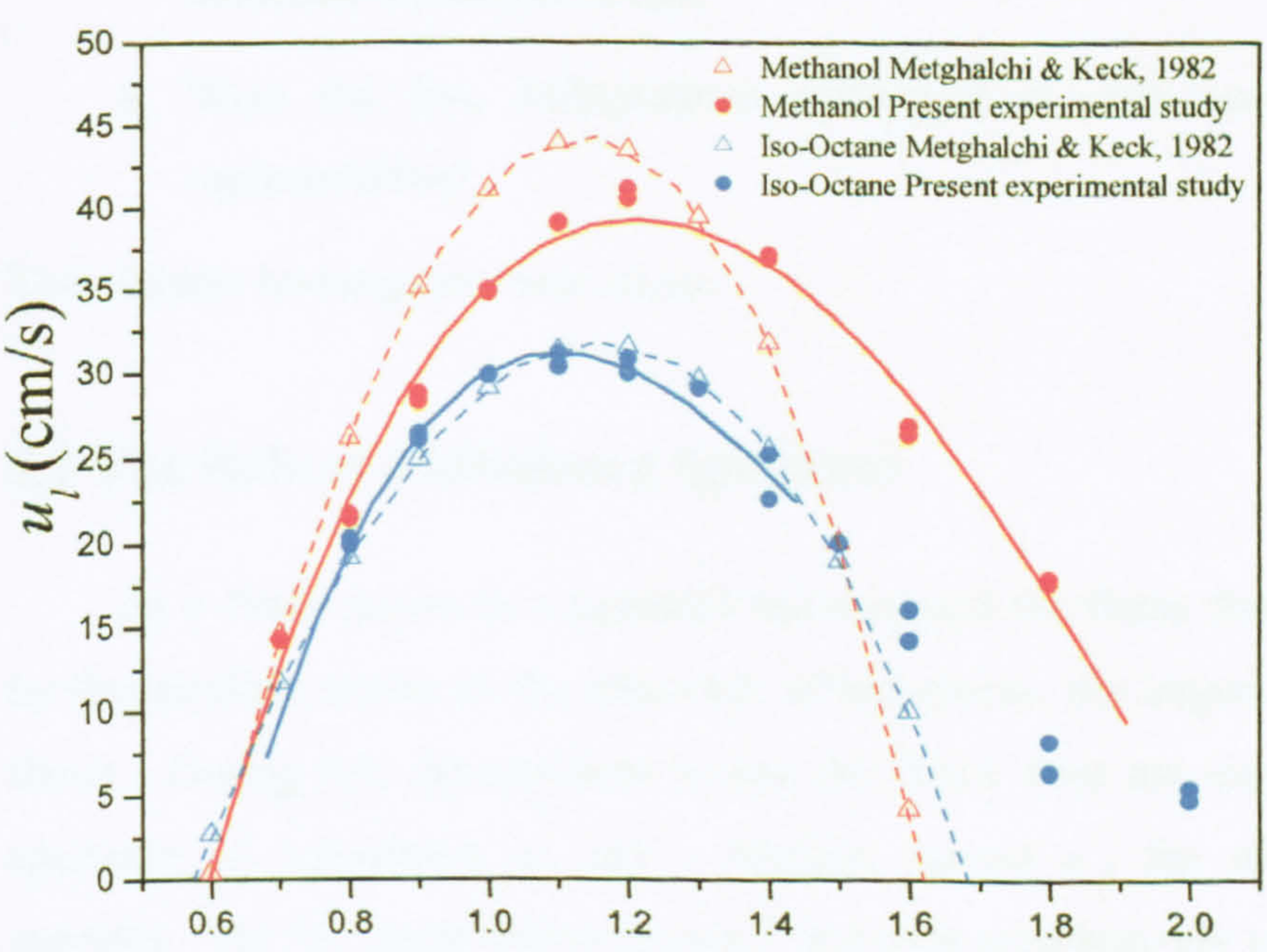

Figure 4.19 Laminar burning velocity plotted against equivalence ratio for iso-octane and methanol air mixtures at 0.5 MPa 360 K, showing comparisons with other workers.

Chapter 5 – Factors effecting the turbulent burning velocity

5.1 Introduction

Although expanding turbulent flames have been used to measure turbulent burning velocities previously, (Bradley *et al.*, 2003), a number of outstanding issues must be considered before they can be used with confidence.

1. From ignition onwards the flame continually accelerates (or develops), thus there is no single burning velocity.
2. In the bomb the flame grows in three dimensions, but schlieren imaging only records two dimensions.
3. The relationship used to convert the schlieren radii to u_{tr}, the burning velocity based on production (Eq. 3.17) has only been validated up to moderate turbulence levels.
4. Were the five deflagrations performed at each condition sufficiently representative?

This chapter investigates these issues.

5.2 The Role of Turbulence Spectrum

As a flame grows in a turbulent environment the flame front is first wrinkled by the smallest scales of the spectrum of turbulence, the larger scales convect the flame. During this development period the flame does not experience the whole spectrum of turbulence u', but a fraction termed u'_k the effective turbulence intensity. As the flame kernel grows it becomes progressively exposed to more of the spectrum until the flame is of sufficient size to experience the whole spectrum of turbulence, where it is said to be fully developed, wrinkled by all of the spectrum of turbulence and u'_k is equal to u'. Abdel-Gayed *et al.* (1987) derived a non-dimensional turbulence power spectrum in terms of dimensionless frequency using

laser-doppler measurements of isotropic turbulence in a fan stirred bomb. They assumed the frequency band affecting flame development extended from the highest frequency to a threshold frequency given by the reciprocal of the time elapsed from ignition.

The non-dimensional power spectrum was improved by Scott (1992) who replaced the dimensionless frequency with a dimensionless wave number, $\bar{k}_\eta$, defined as:

$$\bar{k}_\eta = k\eta \qquad 5.1$$

Here k is the wave number, η is the Kolmogorov length scale. The wave number provides a link to either the time from ignition or flame size. At an elapsed time from ignition, t, the corresponding value of k, is given by:

$$k = \frac{2\pi}{s\ t} \qquad 5.2$$

Where s is the mean cold gas speed. In the fan-stirred vessel there is no mean velocity, Abdel-Gayed *et al.* (1987) related s to u' by:

$$s = u'(8/\pi)^{0.5} \qquad 5.3$$

Alternatively the effective wrinkling could be controlled by the flame radius in which case:

$$k = \frac{2\pi}{d} \qquad 5.4$$

Where d is the flame diameter.

The turbulent Reynolds number used in this study was based on the Taylor scale (Scott, 1992):

$$R_\lambda = \frac{u'\ \lambda}{\nu} \qquad 5.5$$

λ is the Taylor microscale and ν is the kinematic viscosity of the mixture. It can be shown that the Kolmogorov scale is given by;

$$\eta = \frac{\lambda}{15^{0.25} R_\lambda^{\ 0.5}} \qquad 5.6$$

The integral length scale L relates λ and R_λ by;

$$\frac{\lambda}{L} = \frac{A}{R_\lambda} \qquad 5.7$$

Scott (1992) suggested that A = 16 ± 1.5, gives the best fit to the spectral experimental measurements reported by McComb (1990). Values of $S(k_\eta)$, determined over a wide range of conditions, reveal that spectra at higher wavenumbers collapse to a universal form of $k_\eta^{-5/3}$ (McComb, 1990) and for reducing Reynolds numbers, the spectra show shorter ranges of universal behaviour. Scott (1992) compared measured spectra for a wide range of Reynolds numbers and produced a universal best-fit correlation to:

$$\bar{S}(\bar{k}_\eta) = \frac{0.1668 R_\lambda^{\ 2.5} + 3.74 R_\lambda^{\ 0.9} - 70 R_\lambda^{\ -0.1}}{1 + (0.127 R_\lambda^{\ 1.5} \bar{k}_\eta)^{\frac{5}{3}} + (1.15 R_\lambda^{\ 0.622} \bar{k}_\eta)^4 + (1.27 R_\lambda^{\ 0.357} \bar{k}_\eta)^7} \qquad 5.8$$

Shown in Fig. 5.1 are the correlation (Eq. 5.8) (solid lines) and a wide range of experimental data shown (symbols) reported by McComb (1990). The agreement is excellent.

Haq (1998) using the approach of Abdel-Gayed *et al.* (1987) shows that at a point after ignition the r.m.s. turbulent velocity influencing the flame propagation u'_k is given by;

$$u'_k = u' \left[\frac{15^{0.5}}{R_\lambda} \int_{\bar{k}_\eta}^{\infty} \bar{S}(\bar{k}_\eta) d\bar{k}_\eta \right]^{\frac{1}{2}} \qquad 5.9$$

The elapsed time from ignition, t, or flame size is now embodied in the wave number $\bar{k}_\eta$. Values of u'_k can now be obtained by integrating over the power spectrum between infinity and the value of the wave number relating to the time from ignition (temporal) or flame size (spatial).

Figure 5.2 shows the generalised psd (power spectral density) function of the spectrum of turbulent energy for 0.5 MPa for u' = 0. 5 to 6 m/s. At high values of wave number (small scale) the curves for the different values of u' are indistinguishable, at low wave numbers the curves separate depending on the Reynolds number.

In Fig.5.3 u'_k/u' against time from ignition normalised by the integral time scale, τ, is plotted at 0.5 MPa for the values of u' used experimentally. Here the development of the effective turbulence intensity has been calculated using the temporal assumption, Eq. 5.2. Calculating u'_k/u' using the spatial assumption shows similar trends, see Fig.5.4. Using either assumption for the flames in the combustion bomb results in almost the same values of u'_k/u'

The effect of differing pressures on the development of the effective r.m.s is shown in Figs. 5.5 (temporal) and 5.6 (spatial). The rate of development at 0.1 MPa is the slowest when calculated using both assumptions, as at 0.1 MPa the kinematic viscosity is an order of magnitude larger (compared to 0.5 MPa) and therefore the Kolmogorov scale is larger. The differences between 0.5 and 1.0 MPa are not significant, u'_k is mainly a function of L or τ (the length and time scale) which does not change greatly with pressure within the experimental vessel, Abdel-Gayed *et al.* (1987).

Experimentally derived values of the turbulent burning velocity from schlieren images are shown against time in Fig. 5.7 for (representative case) stoichiometric methane-air flames at 0.5 MPa, 360 K and u' = 2 m/s. Also plotted are the derived values of u'_k found assuming temporal flame development. Stoichiometric methane has been used for this comparison as its Lewis number is close to 1 so thermal diffusive effects are limited. After a slight dip just after ignition the turbulent burning velocity continually accelerated with time. However, the calculated effective turbulence intensity, u'_k, bent over from 2 ms onwards. The experimental u_{tr} continued to accelerate as u'_k tailed off.

Figure 5.8 shows the same experimental data but here u'_k was calculated spatially. After the initial dip at ignition the u_{tr} rapidly increased from ignition but bent over at around 15 mm after which the turbulent burning velocity continued to

increase but at a slower rate. Values of u'_k calculated assuming spatial development developed in a similar manner and coincidentally with a similar magnitude. The turbulent flame brush thickness may be controlled by the flame diameter leading to the better fit to experimental data seen in Fig. 5.8 compared with Fig 5.7. Previous turbulent burning velocity measurements by other workers have been presented with respect to the turbulent flame brush thickness (Lipatnikov and Chomiak, 2005). However, there is no evidence to confirm this and further laser sheet measurements are required. It has been suggested that the time and radius may influence u'_k simultaneously (Drake 2000). For example a flame in low turbulence might 'see' 3 integral length scales (in space) by the time the flame edge reaches the window diameter, but the time taken may be only half an integral time scale. In this case the correct choice of u'_k would be that calculated using temporal flame development, as the flame although it had encountered a number of length scales has insufficient time to be wrinkled by them.

From comparison of Figs. 5.8 and 5.7 it was decided to use the diameter for the calculation of u'_k. Previous studies have used time (Haq 1998, Bradley 2002). Turbulent results have been compared to each other at a fixed radius of 30mm, L is constant in the vessel for all experimental conditions so using this assumption meant all flames were equally developed. There was significantly less variation in values of u_{tr} (for flames at the same condition) when comparing at fixed radii rather than at fixed times. Conditions at ignition can cause significant cause delays in flame propagation (Nwagwe, 2000) which can result in delays in the flame propagation unrelated to flame development.

5.3 Schlieren and pressure derived turbulent burning velocities.

Burning velocities derived from spherically expanding laminar flames in the current experimental vessel were found to be the same when measured by schlieren imaging and pressure measurement (Al-Shahrany, 2002). In this study, pressure records were simultaneously recorded along with schlieren imaging. Pressure records were then processed to obtain a burning velocity. These were used to check the validity of Eq. 3.17;

$$u_{tr}(R_v) = \left(\frac{1}{1.11}\frac{\rho_b}{\rho_u}\right)\frac{dR_{sch}}{dt} \qquad 3.17$$

This empirical equation converts the turbulent flame speed obtained from the schlieren images to a burning velocity based on the production of mass, similar in definition to that derived from pressure measurements. Pressure measurements were also used to 'validate' the schlieren results. The schlieren velocities are only a 2D representation of a 3D event, whilst the pressure rise in the vessel increases as a result of burning across the whole flame front.

Shown in Fig. 5.9 (a) are typical schlieren image derived mean flame radii and pressure histories, plotted against time from ignition for three selected equivalence ratios for methane flames. Corresponding values of $u_{tr,}$ derived from successive schlieren images and application of Eq. 3.17, are displayed in Fig.5.9 (b). It was only possible to process turbulent flame image data to a mean (equivalent spherical) radius of 50-60 mm. Beyond this, as a result of flame kernel centroid migration and flame shape distortion some part of the flame circumference would extend beyond the viewing area (window radius = 75 mm). In Fig.5.9 (a) as the flame radii reach their maximum recorded size the pressure rise was still relatively small less than 0.01 MPa. At earlier flame times the pressure rise was too low (relative to signal noise) for accurate determination of $u_{tr,p}$. At greater times the flame grew beyond the central region where the turbulence has been measured and is well characterised, eventually reaching the fans (100 mm from spark gap). As the unburned gas pressure was compression there was an increased in unburned gas temperature. Hence it was only possible to derive useful values of pressure derived $u_{tr,p}$ for a relatively narrow range of times from ignition, Fig. 5.9 (b), and the region of overlap between u_{tr} and $u_{tr,p}$ was even smaller. Nevertheless, the agreement seen in Fig. 5.9 (b) (typical for the range of fuels and conditions examined) was considered to be confirmation of Eq. 3.17. This agreement is also repeated for methanol-air and iso-octane air flames, shown in Figs. 5.10 and 5.11. In each of Figs. 5.9 to 5.11 the stoichiometric and the outermost rich and lean cases have been shown for each fuel.

In processing the pressure measurements it was necessary to assume the flames grew spherically. If the schlieren and pressure derived flame radii were very

different it would indicate that the schlieren image was unrepresentative of the total flame growth or the constant in Eq. 3.17 was incorrect. Burning velocities were determined using the two methods and were then compared and ranked. It was found that the fastest schlieren burning velocity was also usually the fastest pressure derived burning velocity, and that second fastest were also the same and so on for all five turbulent tests at each condition. The schlieren and pressure burning velocities ranked in the majority of cases in this study. Further comparisons of the two methods at increasing values of r.m.s turbulence velocity are shown in Figs. 5.12 to 5.15 for stoichiometric iso-octane air mixtures, (Prepared by C. Mandilas).

In this study the ratio u'/u_l reached 36 which is greater than the flames studied by Bradley *et al.* (2003) where $u'/u_l < 15$. The excellent agreement between the schlieren and pressure determined burning velocities supports the use of the empirical Eq. 3.17 over a larger range of u'/u_l than it was originally derived.

5.4 Variation in measured turbulent burning velocities.

Generally five turbulent explosions were performed at each condition. In an effort to determine if this was statistically adequate twenty further experiments were performed at four cases for iso-octane at 0.5 MPa, 360 K at equivalence ratios and r.m.s turbulence velocities of $\phi = 0.8$, 1.0, 1.4 at $u' = 2$ m/s, and $\phi = 1.0$ at $u' = 4$ m/s. Shown in Figs. 5.16 to 5.19 are the initial five explosions (shown in red) plotted with the later twenty. The schlieren system was changed from a laser to lamp based system between the two sets of measurements. The two data sets show similar results. However, at $\phi = 1$, $u' = 2$ m/s (shown in Fig.5.17) the initial five measurements lie towards the bottom of the experimental scatter. It is uncertain whether this difference is a consequence of random "cycle-to-cycle" variation or due experimental differences. The other conditions shown on Figs. 5.16, 5.18 and 5.19 are in better agreement.

Shown in Fig. 5.20 is the coefficient of variance (the standard deviation normalised by the mean) in u_{tr} against radius. The covariance of u_{tr} decreased as the flames grew. This is due to flame development, as the larger flames yield better

spatial averaging seeing a greater proportion of the spectrum and therefore the extreme velocity fluctuations become less influential.

A radius of 30 mm was chosen for use through out this study to represent and compare the turbulent burning velocities. A radius as large as possible was desirable to get the most developed flame and large enough to average out extreme flow velocities. At 30 mm u'_k/u' was 0.62 calculated using the spatial assumption. This radius was deemed suitable as its well away for the influences of ignition, if a larger radius was selected then a significant number of flames never reached the radius due to flame distortion and convection.

Shown in Table 5.1 are mean, standard deviation and covariance values for flames at 30 mm for the one hundred experiments performed in this investigation of variation. The mean of the initial five experiments was slightly lower than those of the larger data set (typically 10 %). This is the uncertainty applied to measurements within the present study.

0.5 MPa 360 °K Iso-octane Air	Mean u_{tr} (m/s)		Standard Deviation (m/s)		Covariance	
	20 expts	5 expts	20 expts	5 expts	20 expts	5 expts
$\phi = 0.8, u' = 2$	0.63	0.55	0.06	0.04	0.10	0.08
$\phi = 1.0, u' = 2$	0.97	0.86	0.09	0.08	0.09	0.09
$\phi = 1.4, u' = 2$	1.27	1.20	0.17	0.14	0.13	0.12
$\phi = 1.0, u' = 4$	1.41	1.29	0.16	0.16	0.11	0.12

Table 5.1 Mean, standard deviation and covariance values of u_{tr}. Found at a radius of 30 mm for twenty-five experiments at 0.5 MPa 360 K using Iso-octane - Air.

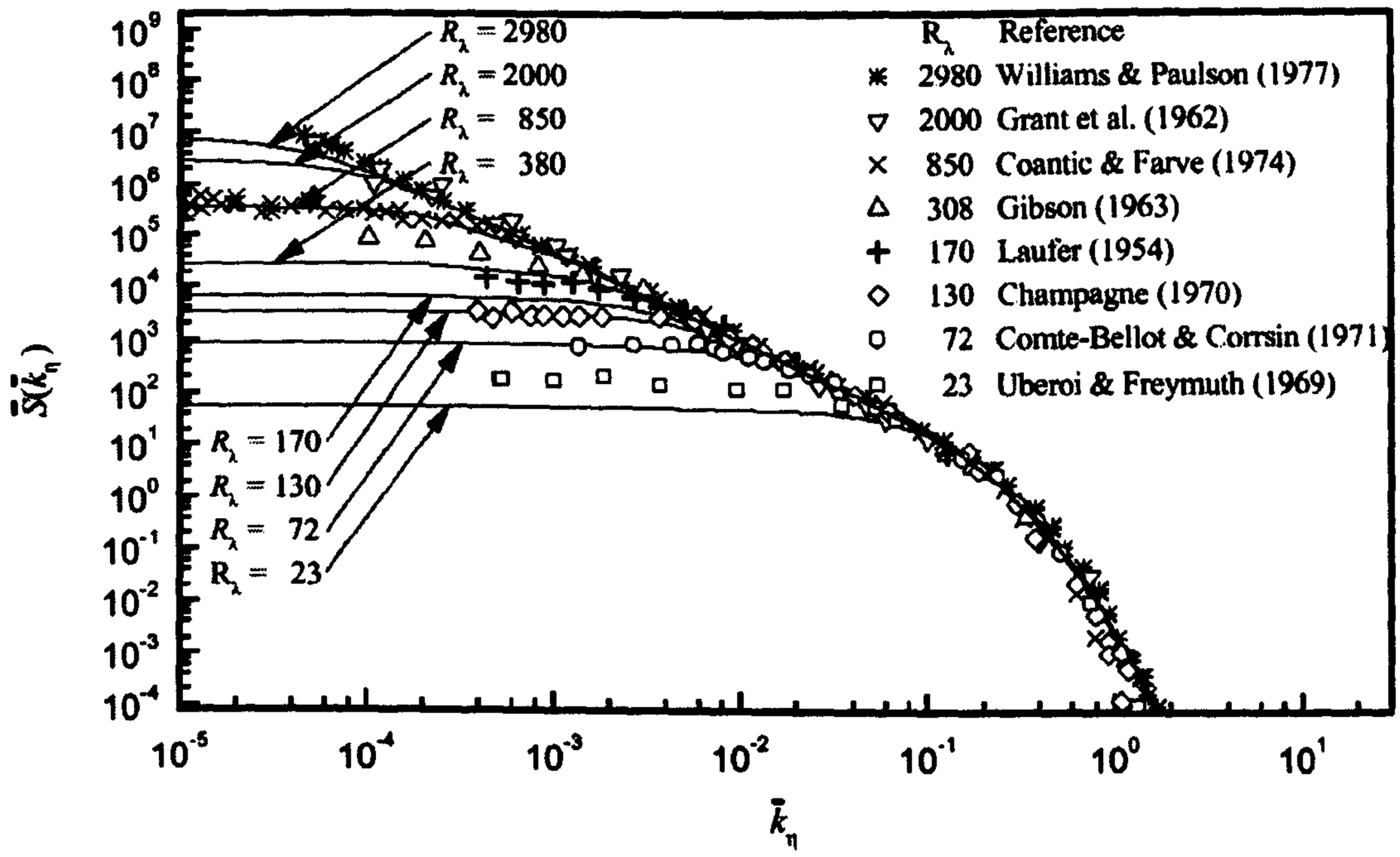

Figure 5.1 Generalised psd function showing the spectrum of turbulent energy. Solid lines were calculated using Eq. 5.8 and 5.9, the symbols are experimental values reported my McComb (1990). *Reproduced from Haq (1998).*

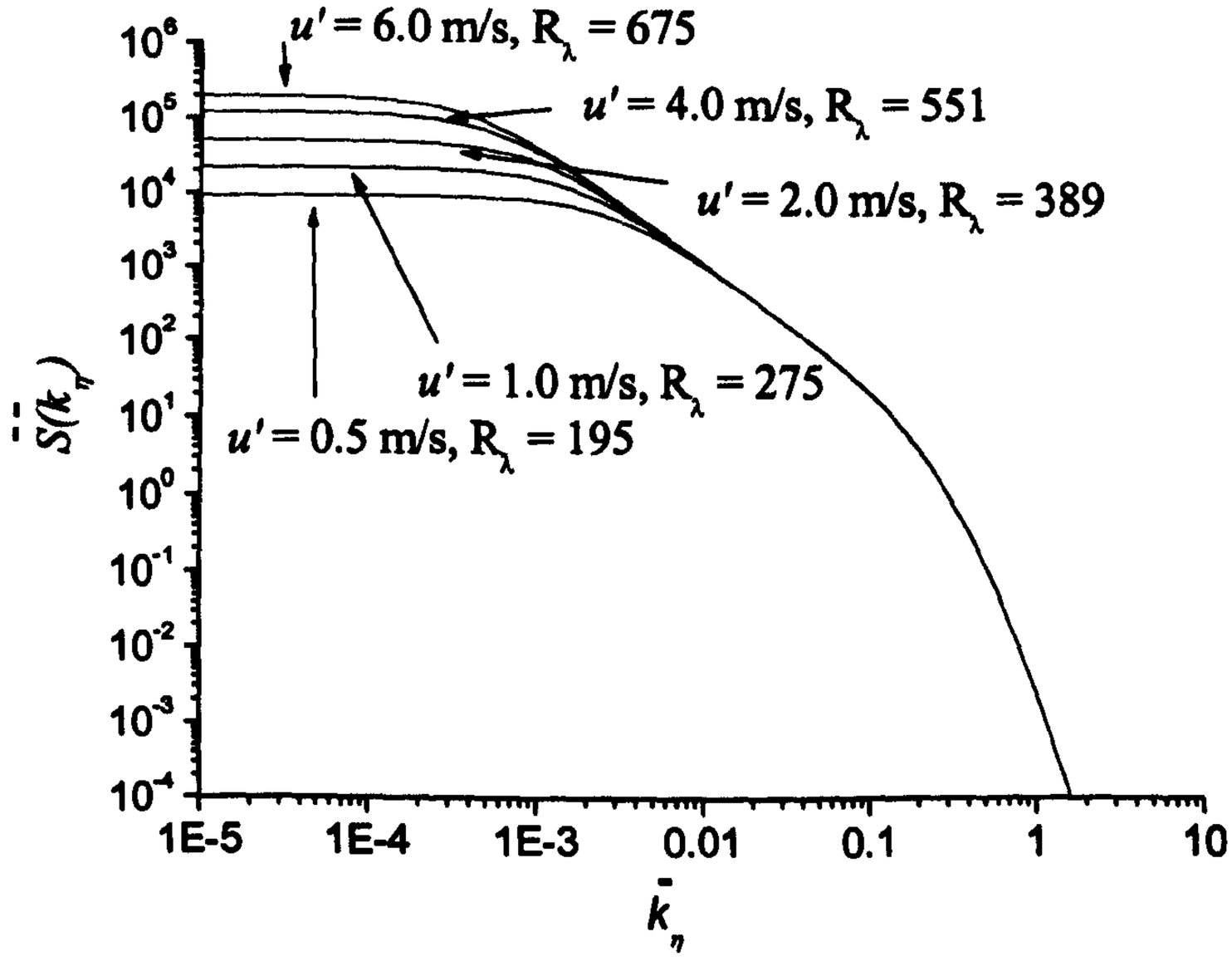

Figure 5.2 Generalised psd function showing the spectrum of turbulent energy for the turbulent intensities studied at 0.5 MPa. Calculated using Eq. 5.8 and 5.9.

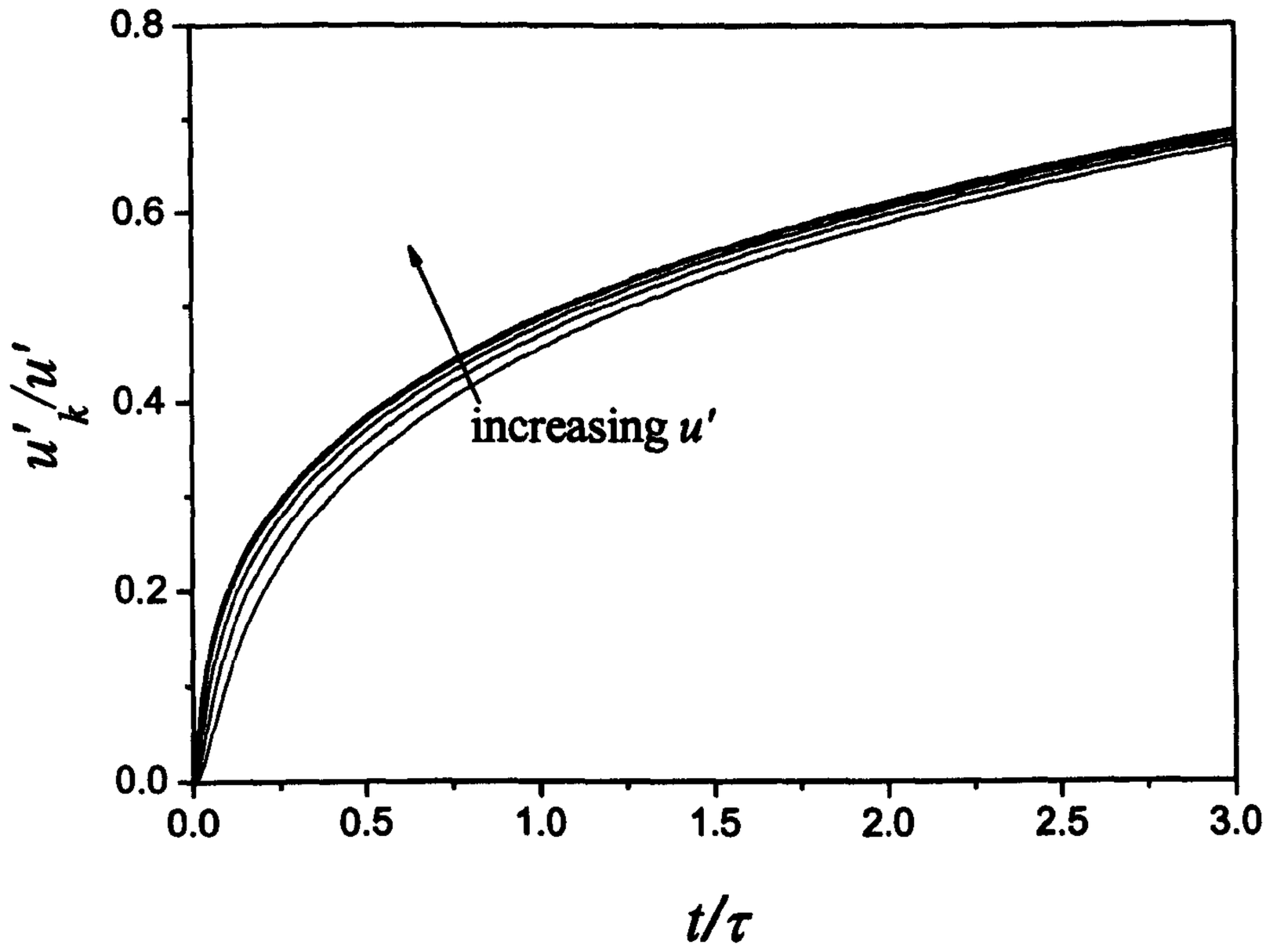

Figure 5.3 Temporal development of the effective r.m.s. turbulent velocity for the values of u' used at 0.5 MPa, 360 K.

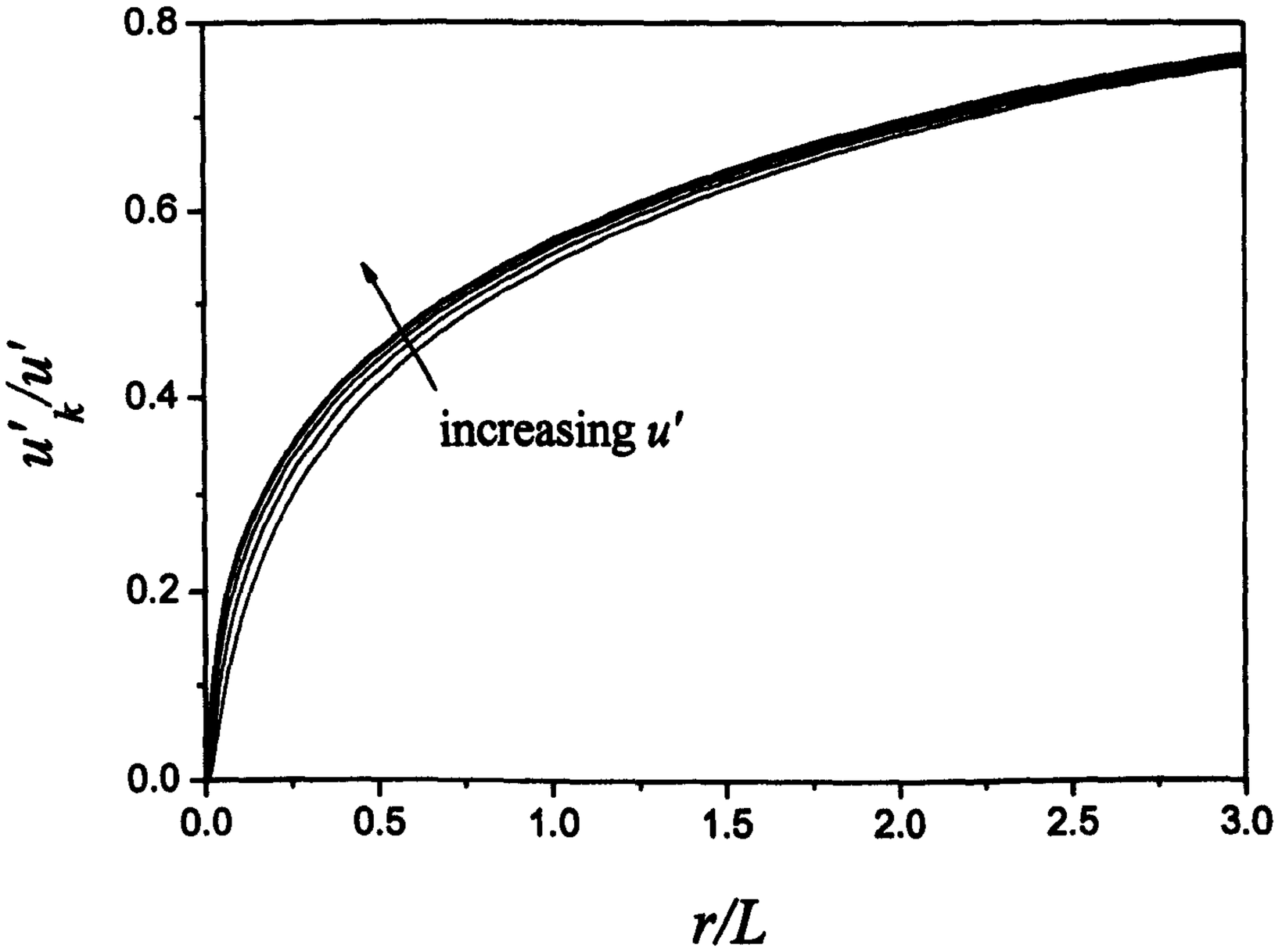

Figure 5.4 Spatial development of the effective r.m.s. turbulent velocity for the values of u' used at 0.5 MPa, 360 K.

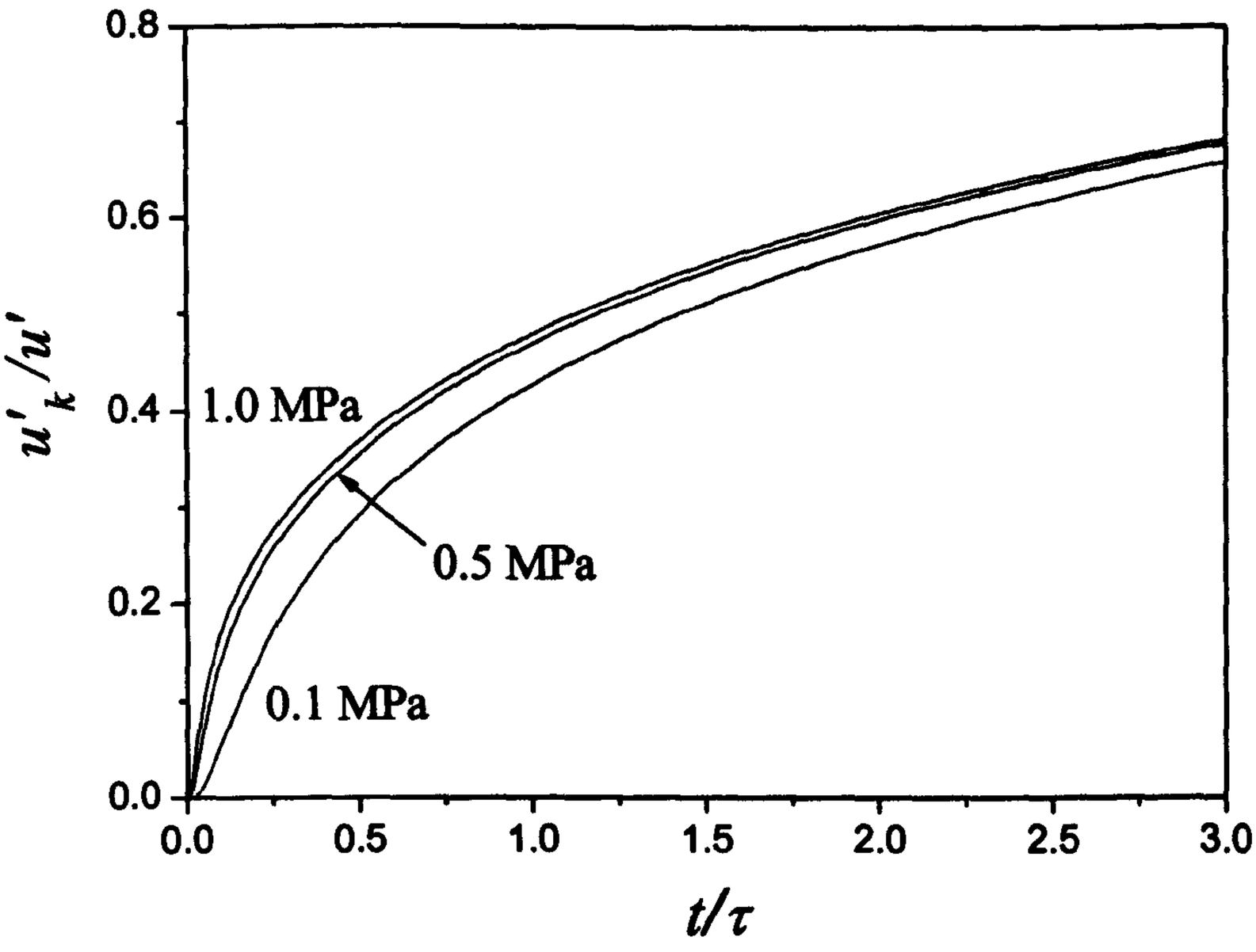

Figure 5.5 Temporal development of the effective r.m.s. turbulent velocity for pressures used, 360 K, at $u' = 1$ m/s.

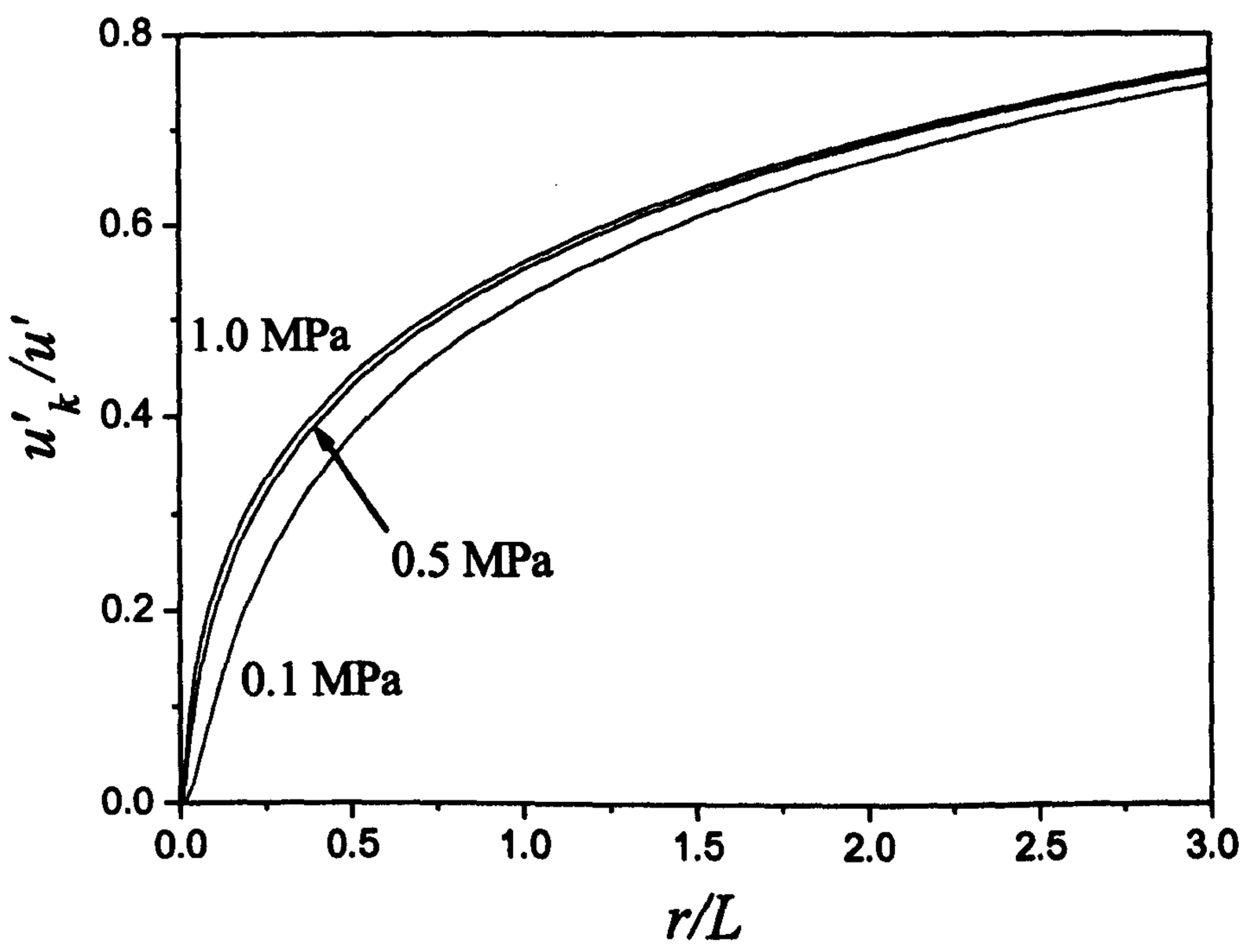

Figure 5.6 Spatial development of the effective r.m.s. turbulent velocity for pressures used, 360 K, at $u' = 1$ m/s.

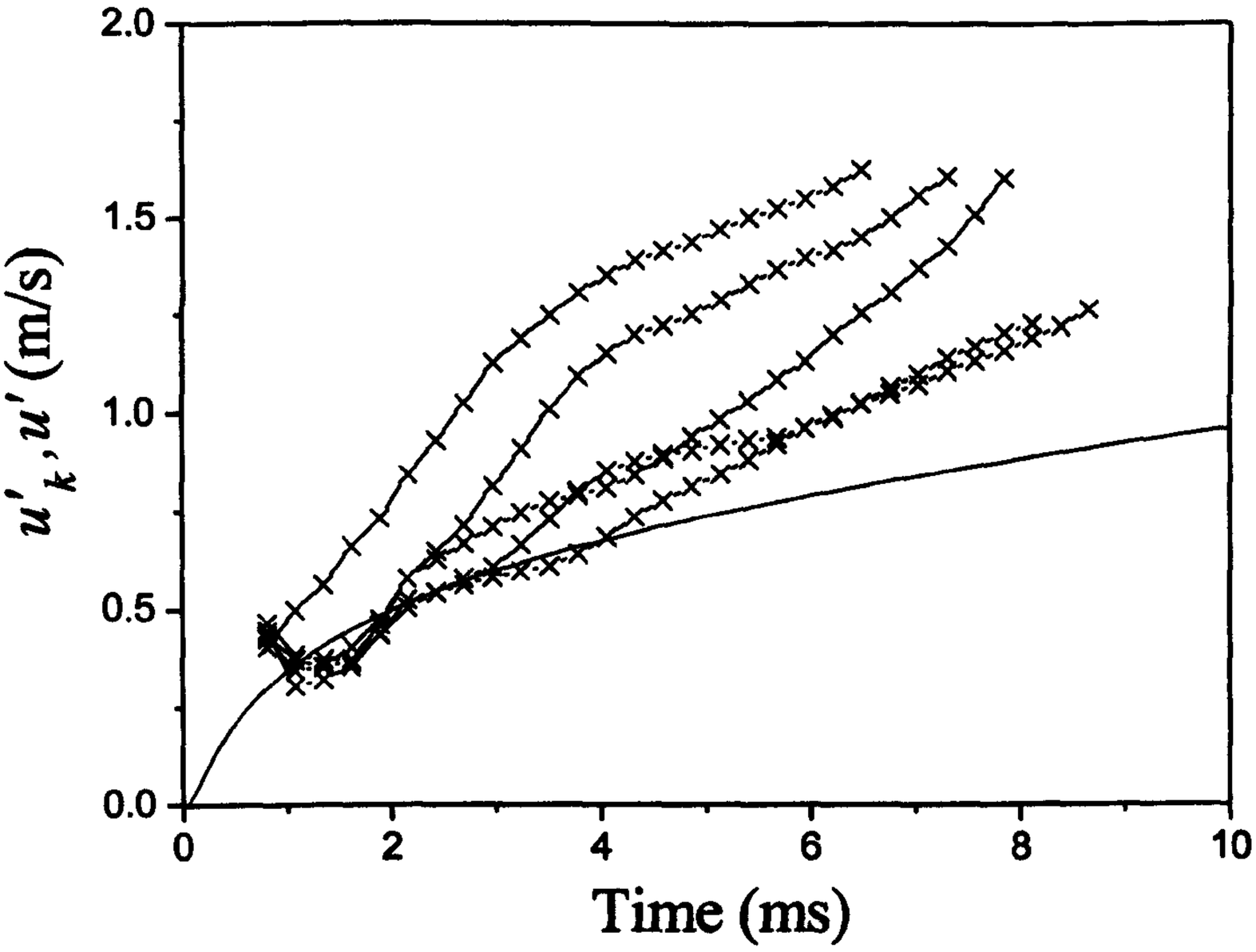

Figure 5.7 Effective turbulence intensity (line) and turbulent burning velocity (symbol) development against time. Methane – air at 0.5 MPa, 360 K, $\phi = 1$ and $u' = 2$ m/s.

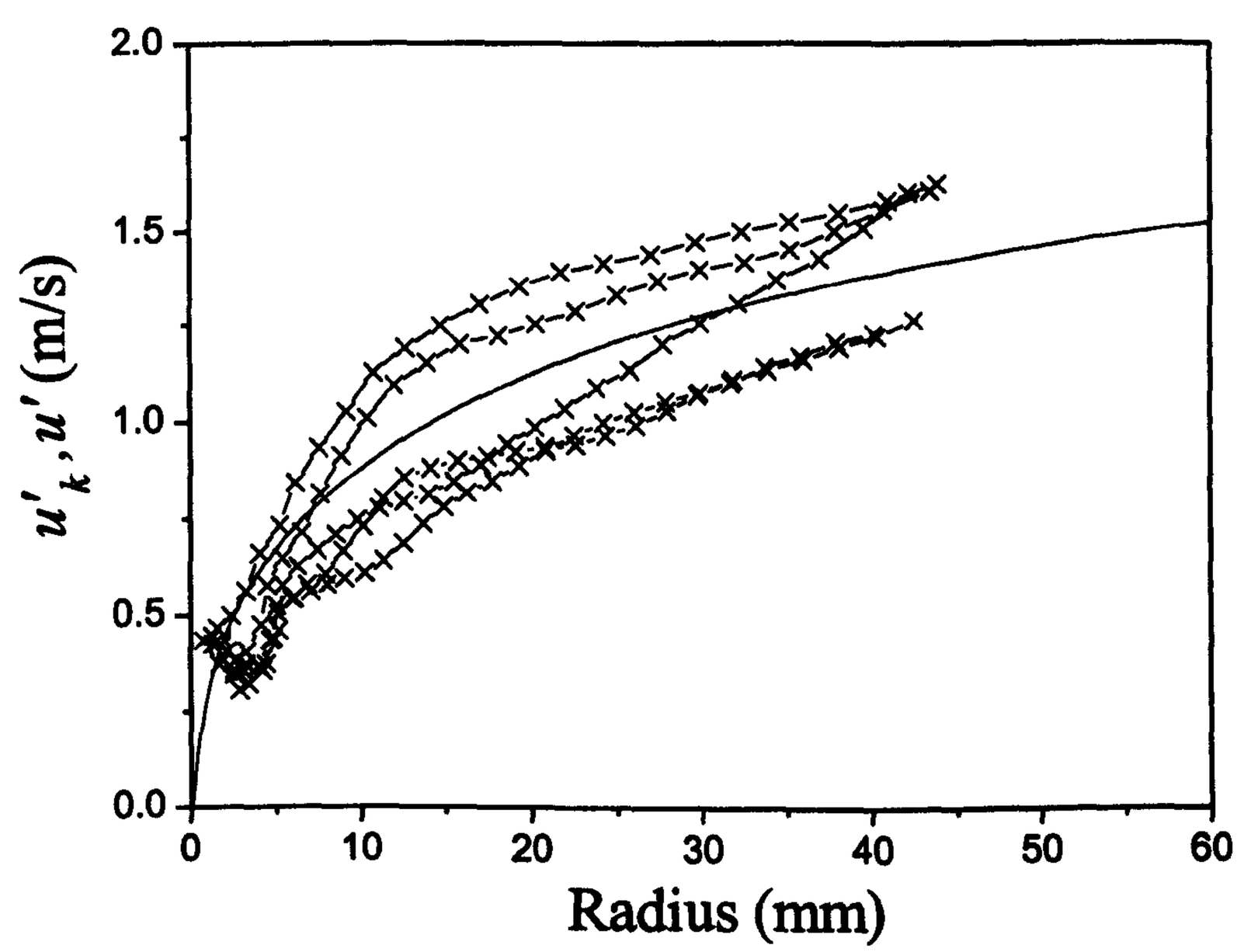

Figure 5.8 Effective turbulence intensity (line) and turbulent burning velocity (symbol) development against radius. Methane – air at 0.5 MPa, 360 K $\phi = 1$ and $u' = 2$ m/s.

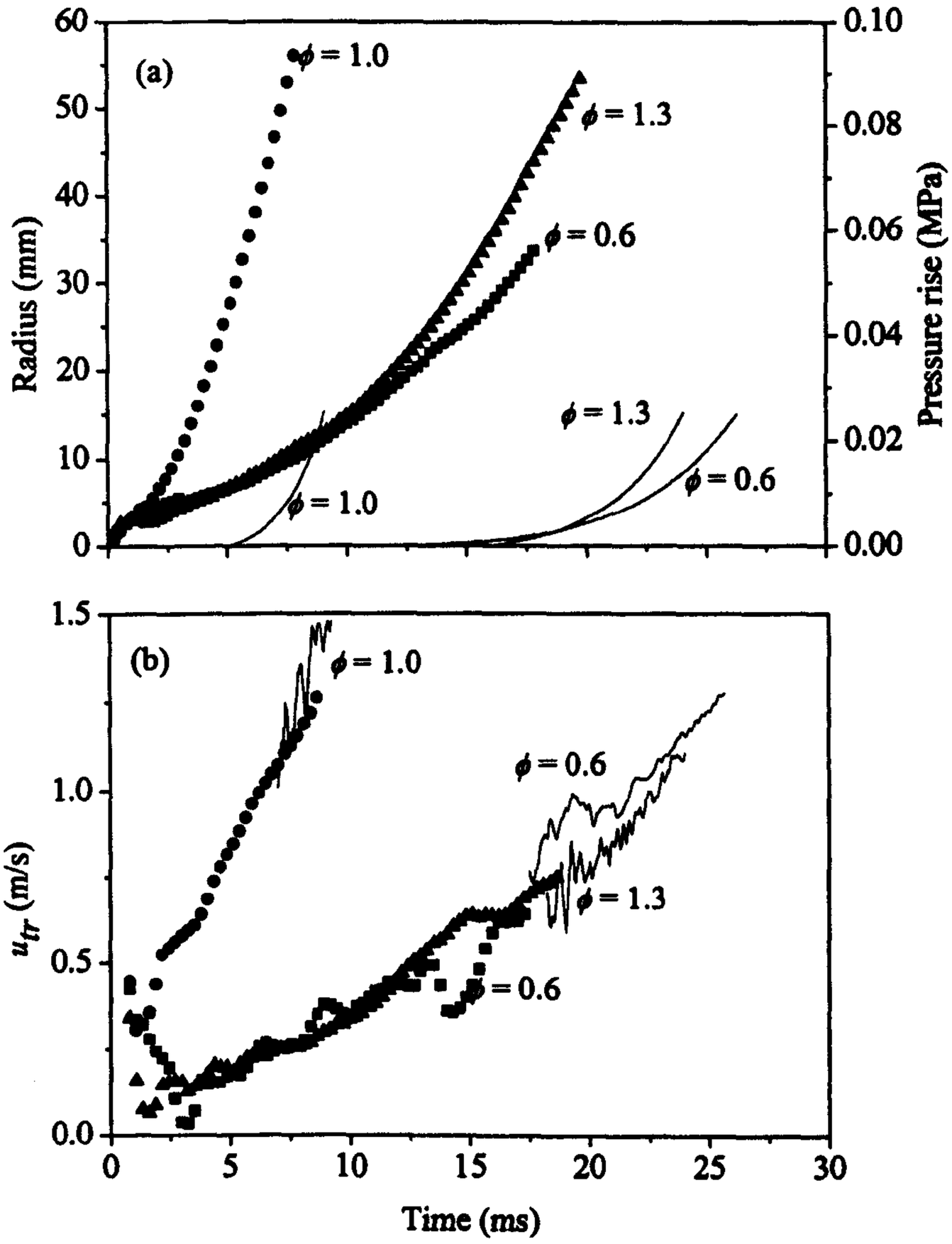

Figure 5.9 (a) Schlieren flame radius, pressure rise and (b) turbulent burning velocity, u_{tr}, against time from ignition for three methane-air flames at $\phi = 0.6$, 1.0 and 1.3. At 0.5 MPa, 360 K, $u' = 2$. Symbols derived from schlieren and solid lines from pressure measurements.

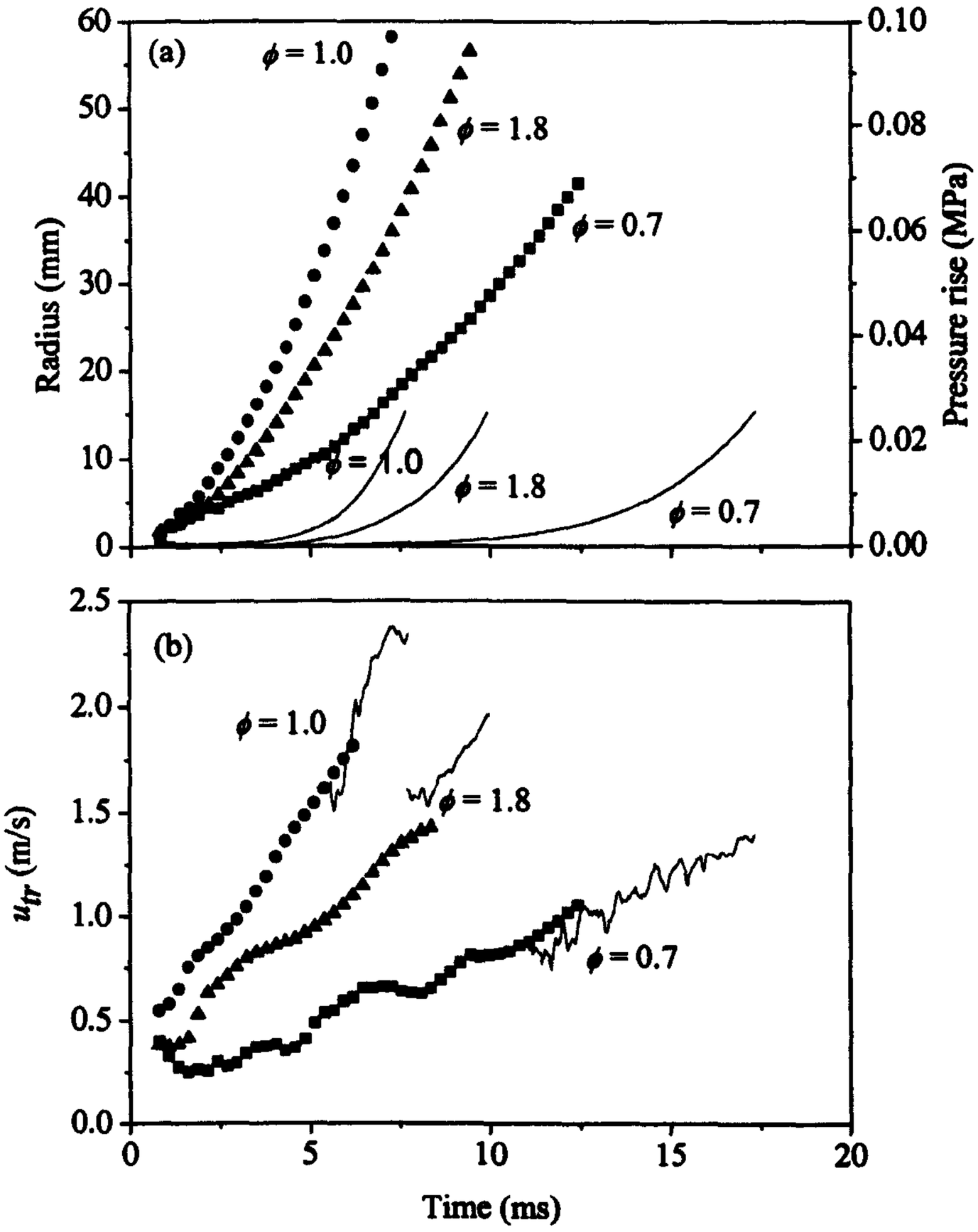

Figure 5.10 (a) Schlieren flame radius, pressure rise and (b) turbulent burning velocity, u_{tr}, against time from ignition for three methanol-air flames at $\phi = 0.7$, 1.0 and 1.8. At 0.5 MPa, 360 K, $u' = 2$. Symbols derived from schlieren and solid lines from pressure measurements.

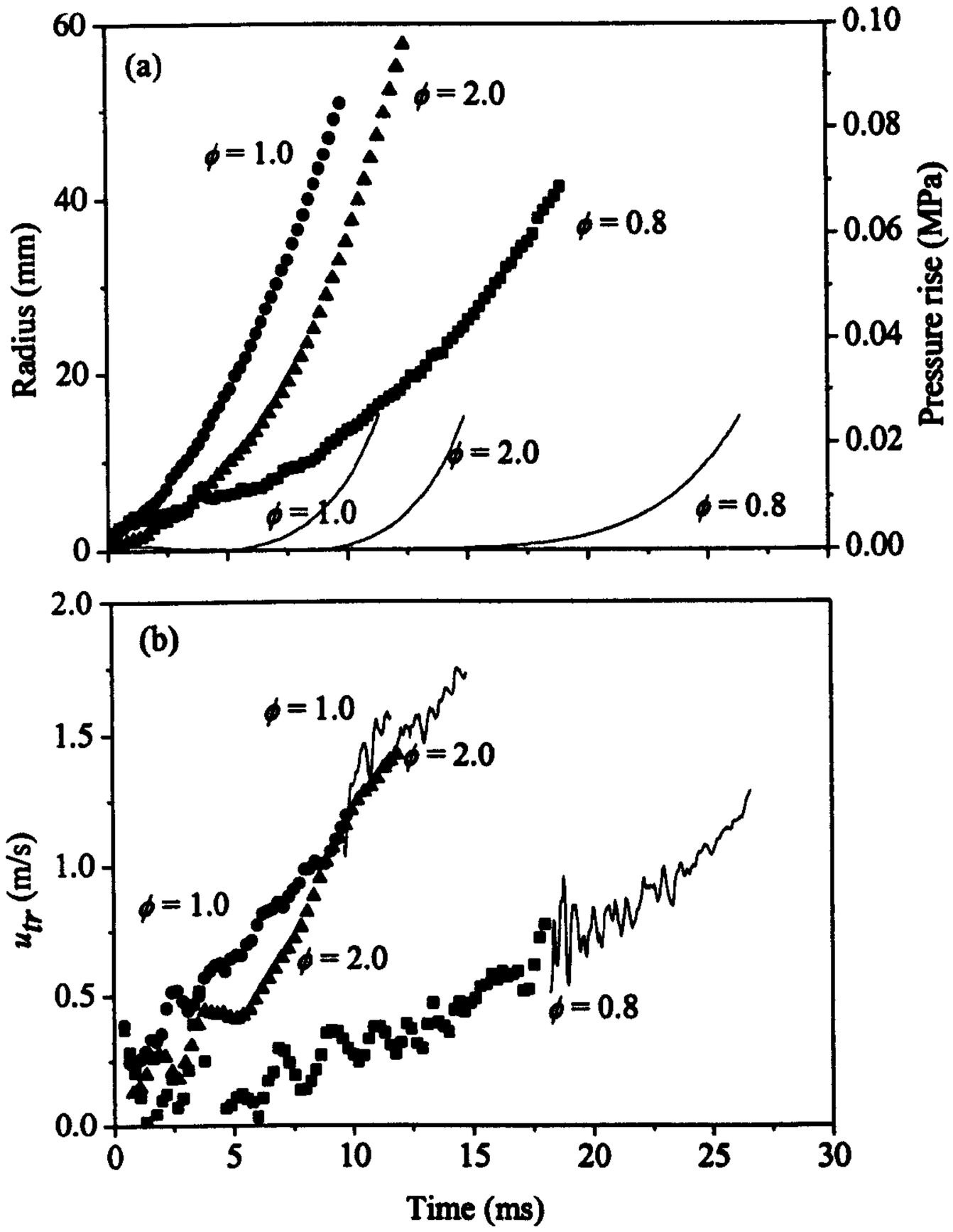

Figure 5.11 (a) Schlieren flame radius, pressure rise and (b) turbulent burning velocity, u_{tr}, against time from ignition for three iso-octane-air flames at $\phi = 0.8$, 1.0 and 2.0. At 0.5 MPa, 360 K, $u' = 2$. Symbols derived from schlieren and solid lines from pressure measurements.

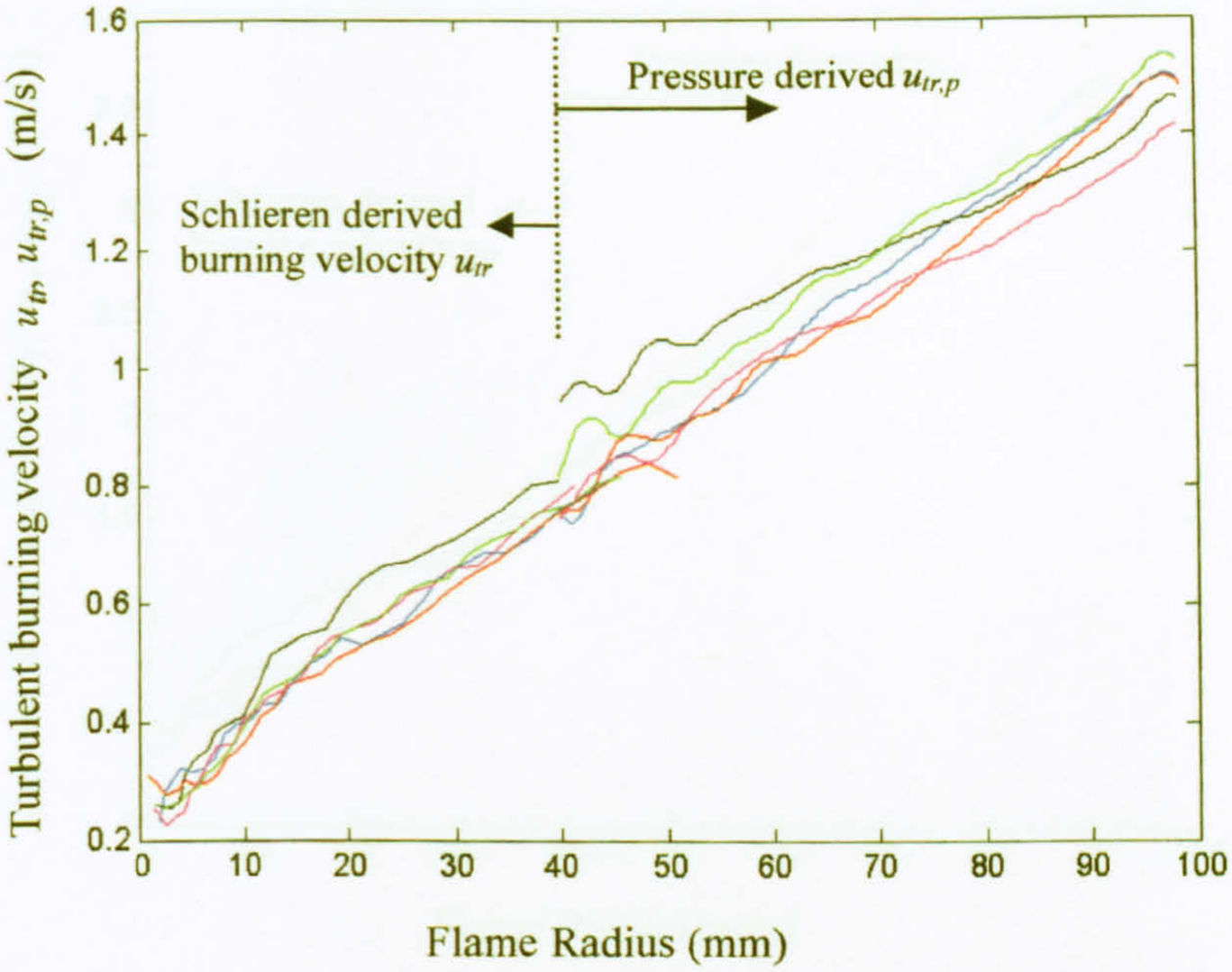

Figure 5.12 Turbulent Burning Velocities u_{tr} from schlieren and $u_{tr,p}$ found from pressure rise for iso-octane air $\phi = 1$, 0.5 MPa, 360 K, $u' = 1$ m/s

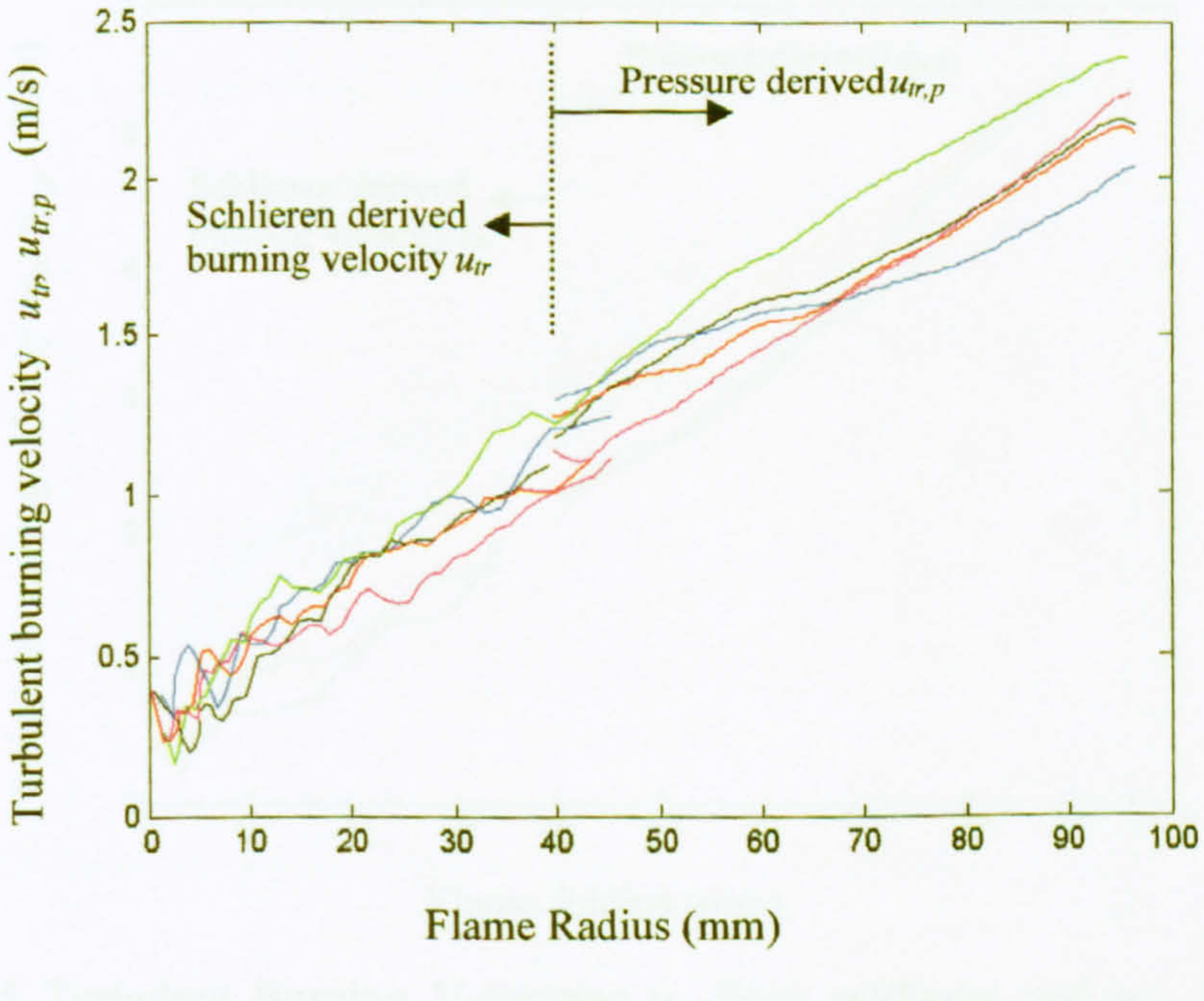

Figure 5.13 Turbulent Burning Velocities u_{tr} from schlieren and $u_{tr,p}$ found from pressure rise for iso-octane air $\phi = 1$, 0.5 MPa, 360 K, $u' = 2$ m/s

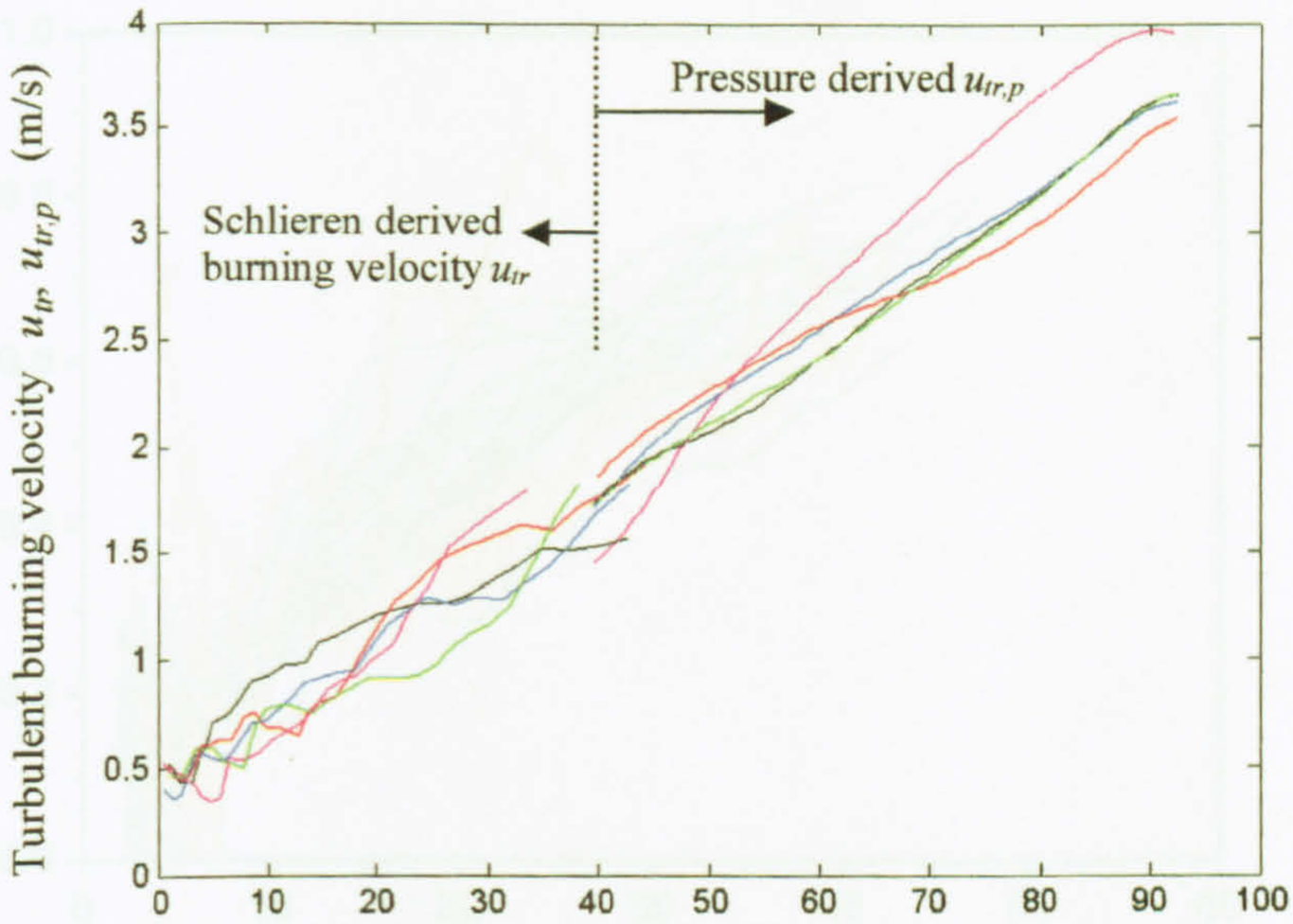

Figure 5.14 Turbulent Burning Velocities u_{tr} from schlieren and $u_{tr,p}$ found from pressure rise for iso-octane air $\phi = 1$, 0.5 MPa, 360 K, $u' = 4$ m/s

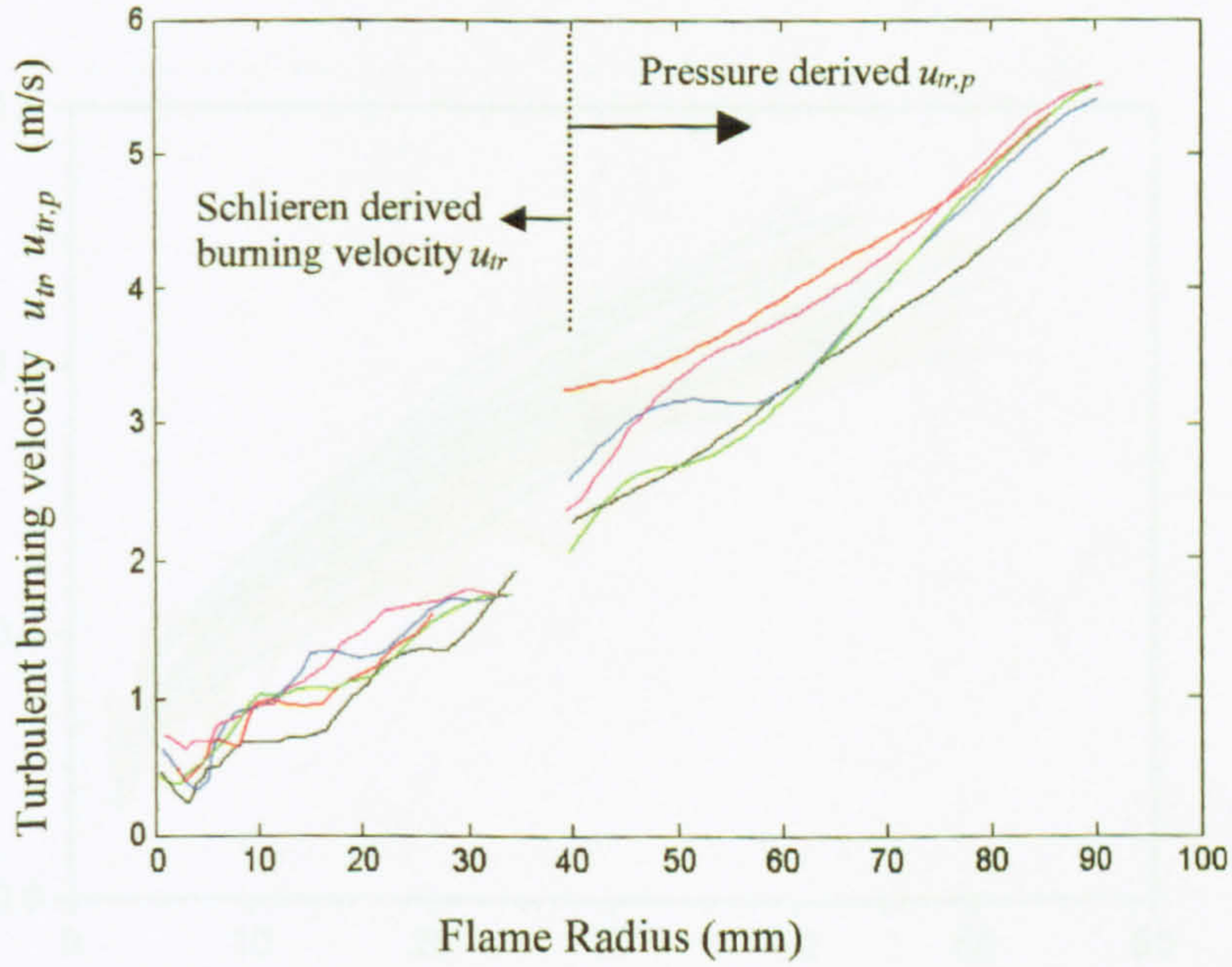

Figure 5.15 Turbulent Burning Velocities u_{tr} from schlieren and $u_{tr,p}$ found from pressure rise for iso-octane air $\phi = 1$, 0.5 MPa, 360 K, $u' = 6$ m/s

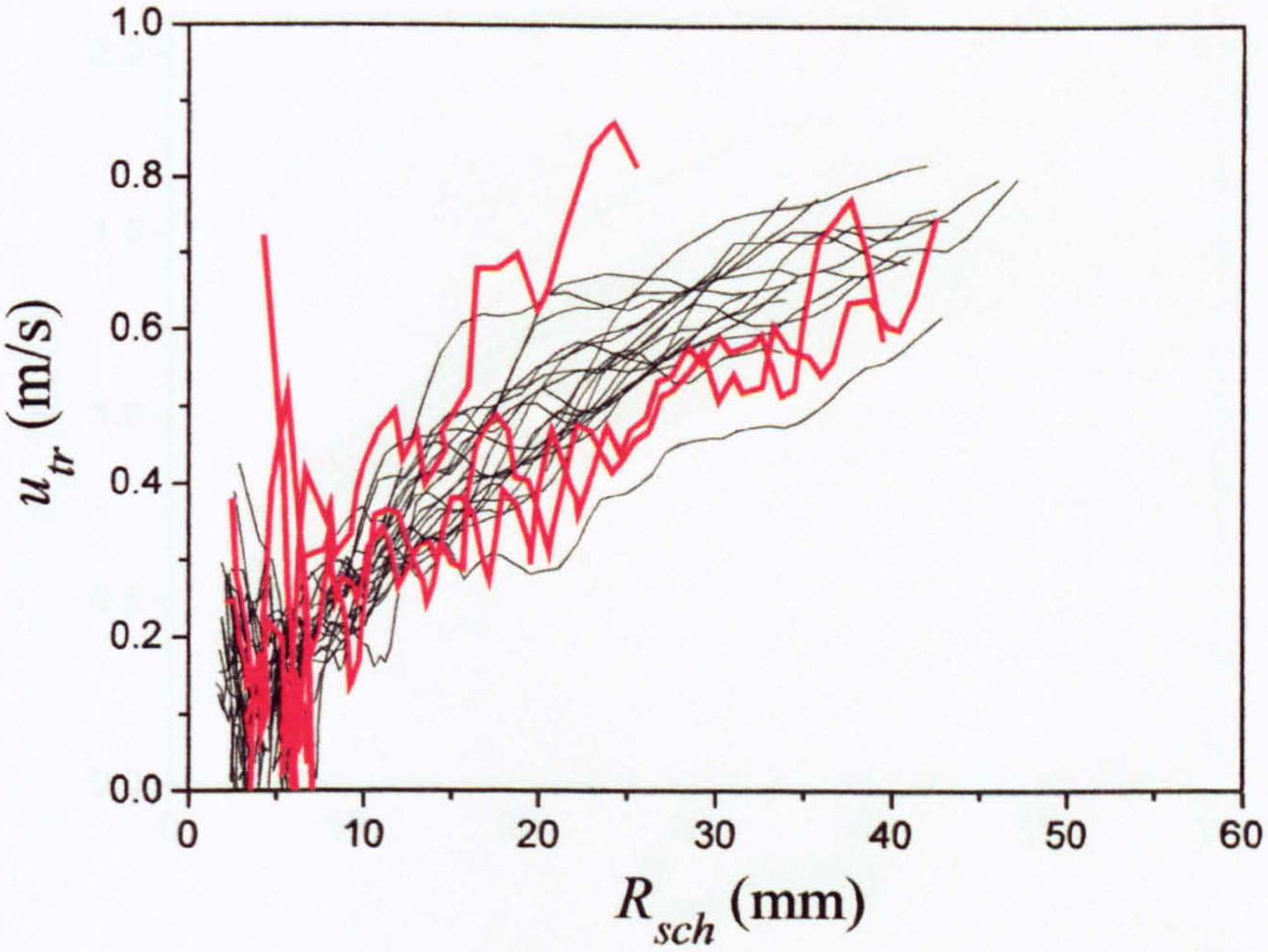

Figure 5.16 Turbulent burning velocity plotted against schlieren radius for 5 initial experiments (red lines) and 20 further experiments (black lines) for iso-octane air flames at 0.5 MPa, 360 K, $u' = 2$, at an equivalence ratio of $\phi = 0.8$.

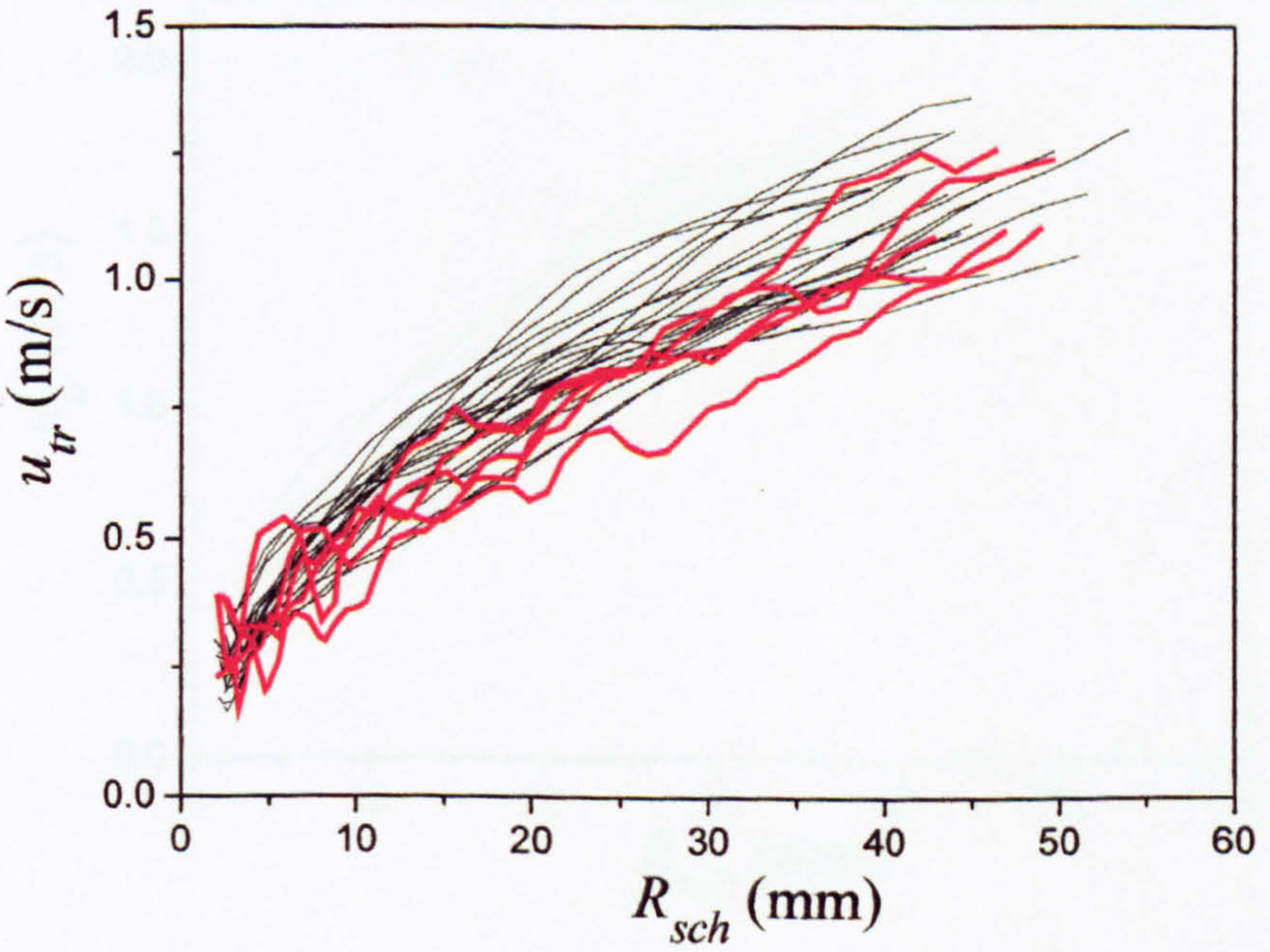

Figure 5.17 Turbulent burning velocity plotted against schlieren radius for 5 initial experiments (red lines) and 20 further experiments (black lines) for iso-octane air flames at 0.5 MPa, 360 K, $u' = 2$, at an equivalence ratio of $\phi = 1.0$.

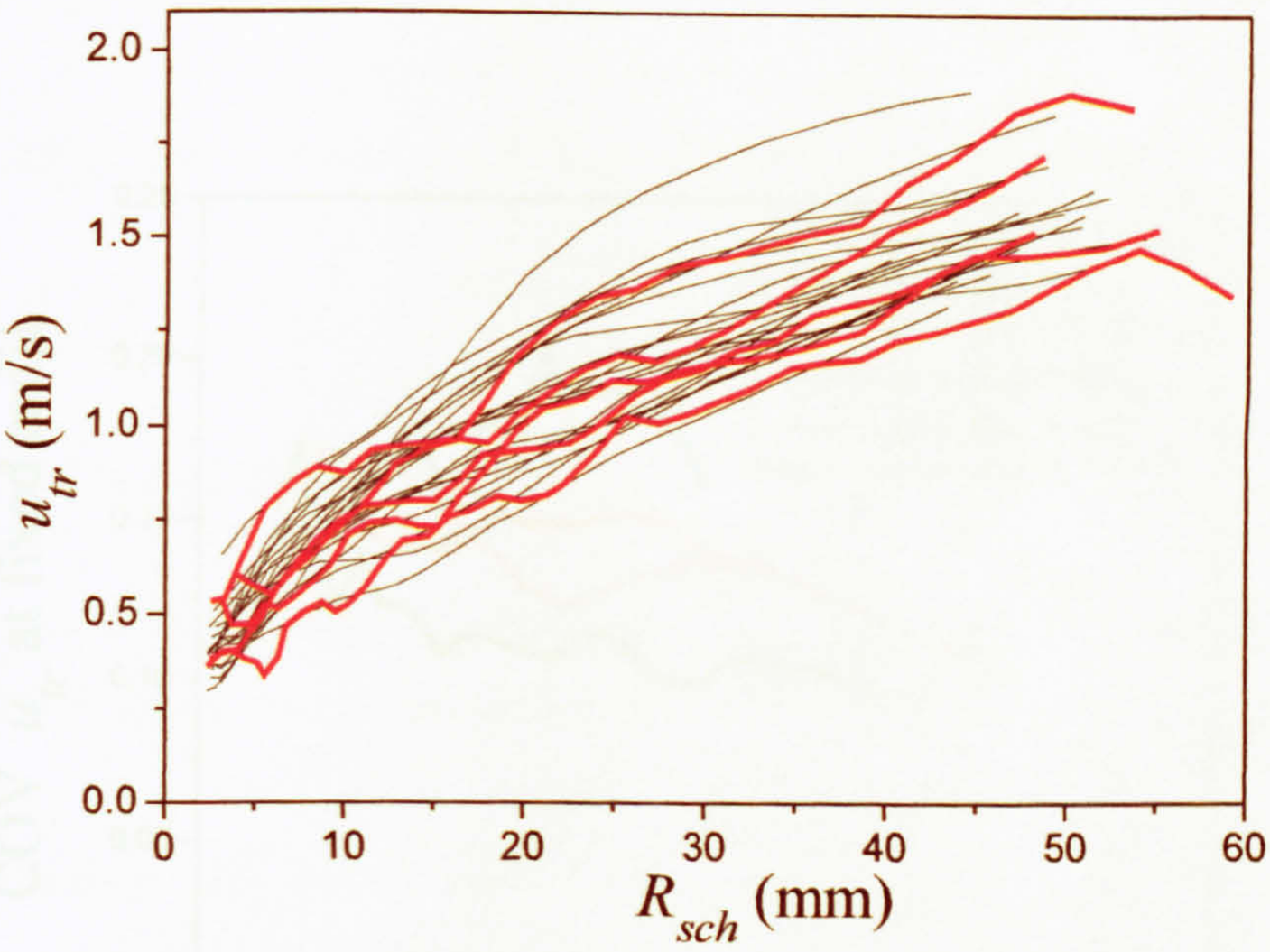

Figure 5.18 Turbulent burning velocity plotted against schlieren radius for 5 initial experiments (red lines) and 20 further experiments (black lines) for iso-octane air flames at 0.5 MPa, 360 K, $u' = 2$, at an equivalence ratio of $\phi = 1.4$.

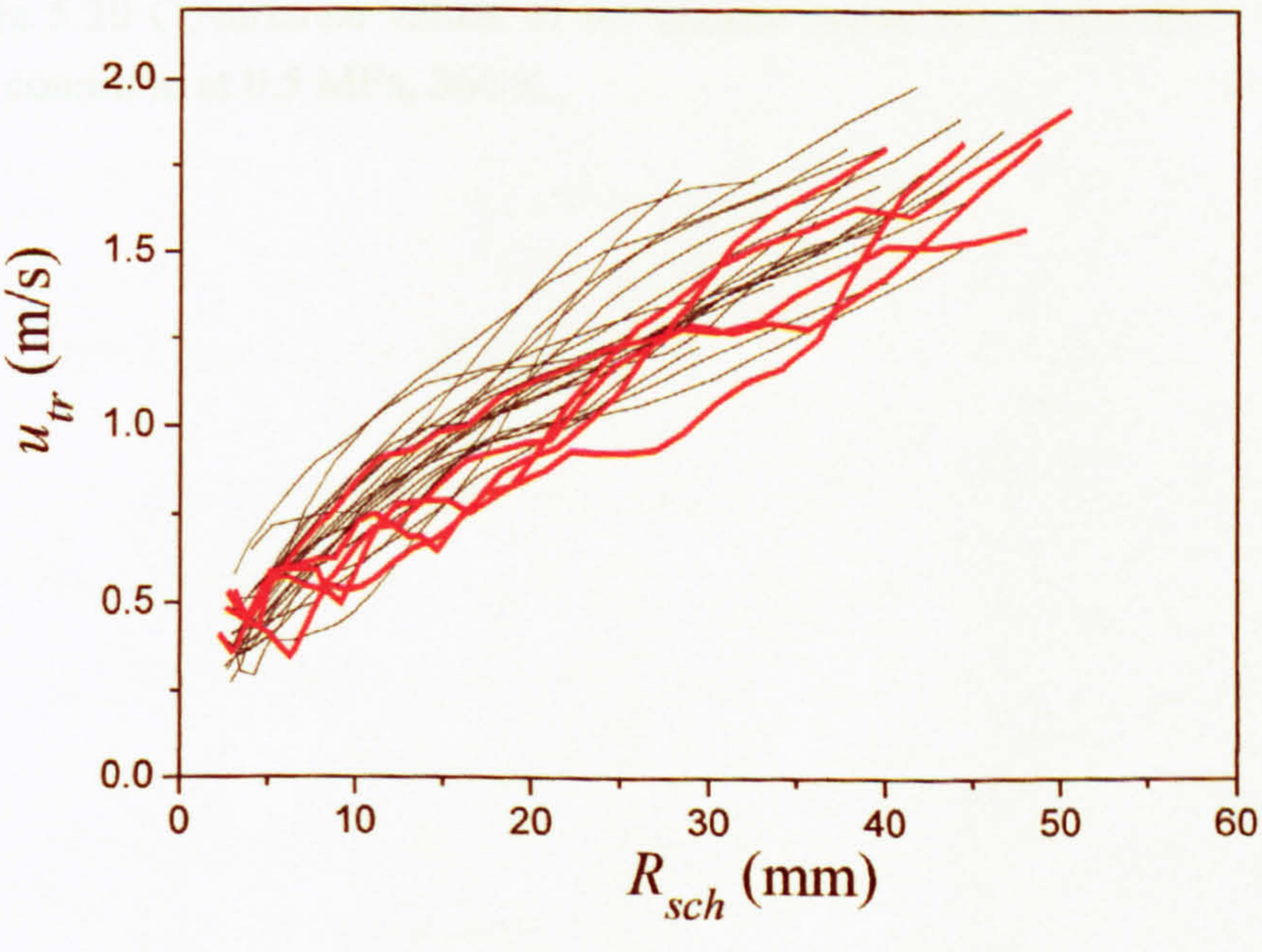

Figure 5.19 Turbulent burning velocity plotted against schlieren radius for 5 initial experiments (red lines) and 20 further experiments (black lines) for iso-octane air flames at 0.5 MPa, 360 K, $u' = 4$, at an equivalence ratio of $\phi = 1.4$.

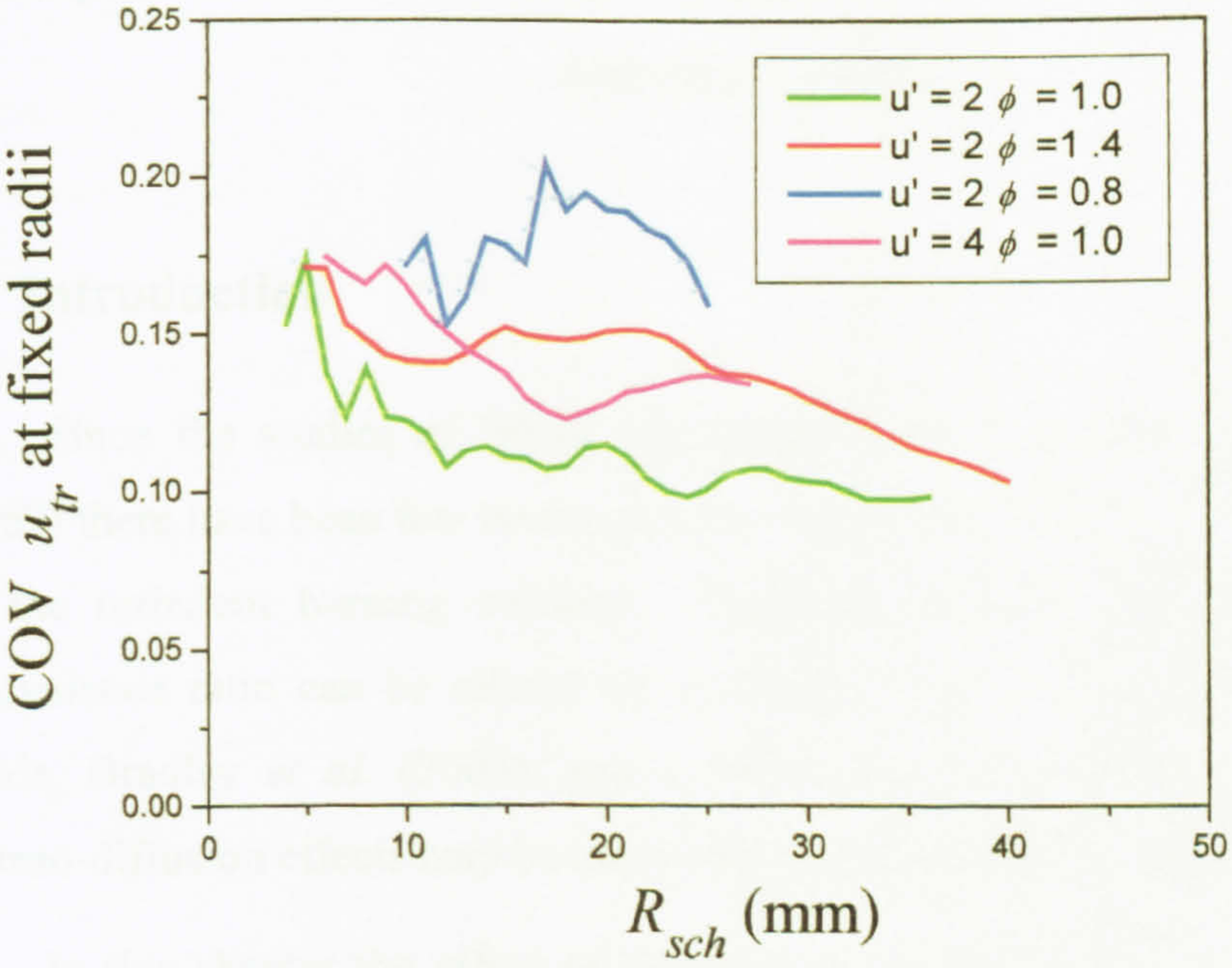

Figure 5.20 Covariance values of u_{tr} against radius for twenty-five experiments at each condition at 0.5 MPa, 360 K.

Chapter 6 – Results - Effect of equivalence ratio on the turbulent burning velocity

6.1 Introduction

Since the studies of Wohl and Shore (1955) and Palm-Leis and Strehlow (1969) there have been few investigations studying the influence of equivalence ratio on the turbulent burning velocity. Typically the effect on u_t of changing the equivalence ratio can be related by u_l (Peters, 2000). However measurements at Leeds, Bradley *et al.* (2003), and Lipatnikov and Chomiak (2005) suggest that thermo-diffusion effects may be important as the equivalence ratio is changed.

In this chapter the effect of changing the equivalence ratio on five fuels has been investigated. The pressure (0.5 MPa), temperature (360 K) and r.m.s. turbulence velocity (2 m/s) were kept constant for all the experiments. Values of u_{tr} are compared with corresponding values of u_l and Markstein number (laminar data from Chapter 4).

6.2 Turbulent flame shape

Shown in Fig. 6.1 are experimental images for methane-air flames for all tested equivalence ratios. At each condition five experiments were undertaken, one example image from each experiment is shown at a schlieren radius of 30 mm (± 2 mm). For highly convoluted or convected flames, which did not reach 30 mm within the field of view, the final image has been shown and the radii noted on the figure. The $\phi = 0.6$ equivalence ratio is an example of a condition where the flame centroid was often convected away from the point of ignition. In the second example at $\phi = 0.6$ it is possible there are two kernels which may or may not be connected as they seam on the image. Representing these flames as expanding spherically from the spark would seam questionable. Moving richer towards

stoichiometric the flames become more spherical in appearance, richer still they return to more convoluted flame shapes

Shown in Fig. 6.2 are turbulent flame kernels of hydrogen-methane mixtures. Some intermediate equivalence ratios have not been shown. It was possible to ignite the (30%) hydrogen (70%) methane air ($\pm\ \phi = 0.1$) richer and leaner than pure methane. The kernel shapes changed with equivalence ratio similarly to those of methane, the $\phi = 0.8$, $\phi = 0.9$, $\phi = 1.0$ flames are the most spherical, flame distortion and convection increased at lean and rich extremes.

The flame kernels of dutch-pura (Fig. 6.3) and iso-octane (Fig. 6.4) are distorted when lean ($\phi = 0.8$) but show an increasingly spherical shape at stoichiometry and far into the rich. Methanol flame kernels shown in Fig. 6.5 (with the exception of $\phi = 0.7$) were very similarly spherical across the tested equivalence ratio range. It is likely the amount of flame distortion relates to the flame-speed, slower flames exist for longer and so consequently are more distorted.

6.3 Experimental development of turbulent flames

The turbulent burning velocity is plotted against flame radius for all tested fuels and equivalence ratios in Figs. 6.6 to 6.10. For each equivalence ratio five explosions were repeated, the experiment with the median value of u_{tr} at 30 mm has been plotted. Figure 6.6 shows the derived turbulent burning velocities against schlieren radius for the methane-air flames. All of the flames accelerated throughout the period they were filmed due to flame development.

Initially the flame kernels are subjected to ignition effects. After this ignition period there is a bend over followed by an almost linear increase in the turbulent burning velocity with flame radius. Throughout the optically viewed period the fastest equivalence ratio was $\phi = 0.9$. The $\phi = 0.7$ and $\phi = 1.2$ flames are very similar initially but at a radius of around 10 mm the two flames diverge with the burning velocity of the lean flame increasing with radius at a greater rate than the rich flame. The same thing occurs with the $\phi = 0.6$ and $\phi = 1.3$ flame which had identical

burning velocities between 5 and 13 mm but then the $\phi = 0.6$ becomes faster than $\phi =$ 1.3 with the difference between them increasing with radius.

The occurrence of 'turndown', a slow down in the rate of increase in the burning velocity which was associated with flame development in Chapter 5 is clearly evident at most equivalence ratios around 5-10 mm. However no turndown was observed at the slowest equivalence ratios $\phi = 0.6$ and $\phi = 1.3$.

Turbulent deflagrations of binary mixtures of (30%) hydrogen and (70%) methane with air are potted in Fig. 6.7. Here the $\phi = 0.7$ $\phi = 0.8$ and $\phi = 0.9$ flames are the fastest conditions of all, and are faster than the stoichiometric. The lean conditions at $\phi = 0.6$ and $\phi = 0.5$ are fast when compared to their laminar burning velocities. The rich flames $\phi = 1.2$, $\phi = 1,3$ and $\phi = 1.4$ are slower, more so than the extremely lean ($\phi = 0.5$) condition.

The developing dutch-pura air flames are shown in Fig. 6.8. Here the equivalence ratios of $\phi = 1.1$ to $\phi = 1.8$ are grouped as the fastest conditions. At a schlieren radius of 30 mm the fastest condition shown is for $\phi = 1.2$. The stoichiometric and lean conditions are slower $\phi = 0.8$ to $\phi = 1.0$ respectively. The $\phi = 0.8$ flame initially struggles to develop, its turbulent burning velocity falls to near zero at a radius of 4mm, after this the flame recovers and grows. The gasoline flames contrasts with the methane deflagrations in that the rich gasoline flames have an enhanced turbulent burning velocity, unlike the methane deflagrations where the lean flames were relatively faster considering their values of u_l.

Iso-octane, which is used to represent gasoline in engine studies also demonstrates a rich shift in the peak turbulent burning velocity. In Fig. 6.9 the fastest condition at 30 mm is at the equivalence ratio of $\phi = 1.4$. The rich flames all have very similar burning rates. The $\phi = 2.0$ which was the greatest equivalence ratio in this current study is equally as fast as the stoichiometric case. The laminar ϕ = 2.0 flame was so slow that the flame was buoyant. The stoichiometric and $\phi = 0.9$ cases have similar burning velocities. The leanest flame shows a drop just after ignition, this case nearly quenched reaching a zero at 6 mm, then it does recover and develop, this was the slowest of all turbulent conditions.

Methanol deflagrations are shown in Fig. 6.10. Here the fastest flame at 30mm radius is for $\phi = 1.2$. There is no marked shift in the ratio of turbulent to laminar burning velocity.

6.4 Influence of equivalence ratio in developing turbulent deflagrations

The experiments discussed in this chapter have been completed at a fixed turbulence of $u' = 2$ m/s, a constant pressure (0.5 MPa) and temperature (360 K). Five fuels have been tested over their experimental ignition range. A radius of 30 mm has been chosen to make a comparison of the turbulent burning velocities. Figure 6.11 shows the turbulent burning velocities at this radius. Considerable scatter in the results for the five individual deflagrations at each condition is evident, this shot to shot 'cyclic variation' is to be expected for a stochastic turbulent environment. A third order least squares fit was used to generate the curves through each set of experimental data. The standard deviation from the fits was found to be circa 0.13 m/s, fuel type had no influence. For all five fuels, the curve fits to the data can be seen to be 'bell-shaped', with u_{tr} values peaking at some equivalence ratio and falling away as the mixtures became richer and leaner. For methane the turbulenct burning velocity peaked around $\phi = 0.9$ and then fell away symmetrically as the equivalence ratio increased and decreased. The methane and hydrogen mixtures had a peak burning velocity further in to the lean circa $\phi = 0.8$, the burning velocity then fell away either side reducing at a slightly slower rate moving rich. The turbulent burning velocities for the binary mixture were higher than those of pure methane over the whole range, this was more pronounced on the lean side.

For methanol, the peak occurred at $\phi = 1.3$, as the mixtures became leaner u_{tr} decreased slightly more than for the rich mixtures. However at lean equivalence ratios the burning velocity dropped sharply so that at $\phi = 0.7$ both pure methane and hydrogen enriched methane are faster than methanol. Dutch-pura and iso-octane have similar trends of burning velocity with equivalence ratio although the gasoline was consistently higher than iso-octane, these fuels peaked around $\phi = 1.35$. The u_{tr}'s decreased little as the mixtures became richer. However as the mixtures were

leaned off the u_{tr} fell relatively rapidly below $\phi = 1.1$. At $\phi = 0.8$, which was the most lean common equivalence ratio that all five fuels could be ignited, iso-octane was the slowest with $u_{tr} = 0.5$ m/s, the fastest was $\phi = 0.8$ for hydrogen enriched methane with $u_{tr} = 1.5$. Interestingly at $\phi = 1.3$ the richest equivalence ratio at which all fuels could be ignited the minimum u_{tr} was again approximately 0.5 m/s and in this case it was methane. At $\phi = 1.3$ methanol was the fastest with a u_{tr} of 1.8 m/s.

6.5 The ratio of turbulent to laminar burning velocities

For the conditions discussed here corresponding laminar flames have been studied to yield unstretched laminar burning velocities and Markstein lengths in Chapter 4. In some cases the flames become unstable, developing a cellular structure and enhanced flame speed, which made accurate determination of such criteria impossible. In such cases flame speed was fitted with linear flame stretch to flame-speed within the spark effected zone. For these "best guess" values there was an estimated over prediction of 10% in the determination of u_l; over and above other experimental and processing errors. The slowest burning mixtures (methane-air $\phi =$ 0.6, $0.3H_2+0.7CH_4$ $\phi = 0.5$ and $\phi = 1.4$ and iso-octane-air at $\phi = 2.0$) were significantly affected by buoyancy; resulting in non-spherical flames (albeit still expanding with a smooth surface).

For each fuel, the turbulent burning velocity at 30 mm was normalised by the corresponding unstretched laminar burning velocity (or "best guess"), the results are shown in Fig. 6.12. A third order least squares fitting routine was used to generate the curves, with the exception of binary hydrogen-methane mixtures where a fourth order fit was required, the standard deviation from the fits was found to be 0.1–0.15.

Over the range $\phi = 1.1$ to 1.2, the magnitude of u_{tr} was approximately 4 times u_l for all of the fuels. Away from these equivalence ratios, considerable differences in the behaviour of the fuels can be seen. For methane, the ratio of u_{tr}/u_l was observed to be above 10 at $\phi = 0.6$, thereafter falling with increasing equivalence ratio, before becoming essentially constant above $\phi = 1.0$. The hydrogen-methane deflagrations had a similar overall trend, the greatest ratio of u_{tr}/u_l was observed

exceeding 25 at $\phi = 0.5$. The rich flames of this fuel have greater values of u_{tr}/u_l than found at stoichiometry.

In the case of methanol, the magnitude of u_{tr}/u_l can be seen to remain comparatively constant with equivalence ratio (compared with the other fuels); with $u_{tr}/u_l = 4$ for a stoichiometric mixture rising to about 6 at the extreme fuel rich and lean equivalence ratios. Lean iso-octane and dutch-pura exhibit the lowest value of u_{tr}/u_l, of roughly 2.5 at $\phi = 0.8$. However, for these fuels the ratio of u_{tr}/u_l rose continuously with equivalence ratio, which for iso-octane exceeded 20 at $\phi = 2.0$.

The stretched spherically expanding flames were also processed to give Markstein Numbers indicting the effect of stretch in the flame surface. The accurate determination of Markstein values was complicated by laminar instability. In Fig. 6.13 values of Markstein length (L_b) (quoted in Chapter 4) have been plotted against the ratio of u_{tr}/u_l. The Markstein length, L_b, is used here as it is a direct measurement obtained from the flame-speed against stretch curve. Whilst the values of L_b obtained were generally very repeatable, they were difficult to determine for cases where the onset of instabilities occurred soon after the cessation of ignition effects. This could result in potentially large errors (± 2 or more) in derived L_b. Nevertheless a consistent trend is observed in this figure with equivalence ratios with negative values of L_b exhibiting an enhancement it the turbulent burning velocity. In contrasts positive values of L_b all have similar values of u_{tr}/u_l.

For a flame front comprising a series of flamelets strained by the flow field of unburned mixture, it has been suggested that Markstein Number, Ma_{sr}, strongly influences u_{tr} (Bradley 2002); with local laminar burning velocity reduced, increased and unaffected for positive, negative and zero $Ma_{sr,}$, respectively. The trends in the values of u_{tr}/u_l and L_b, in Fig. 6.14, are consistent with this. For methane and hydrogen-methane the highest values of u_{tr}/u_l (at the leanest equivalence ratios) corresponded with the lowest values of Markstein Number. Similarly, for iso-octane and dutch-pura, the largest values of u_{tr}/u_l (in this case at rich conditions) corresponded to the lowest (and negative) values of Ma_{sr}. Methanol, with relatively

little variation of Ma_{sr} with equivalence ratio, exhibited approximately constant behaviour in $u_{tr}/u_{l,}$ with equivalence ratio.

ϕ	1	2	3	4	5
0.6					
0.7	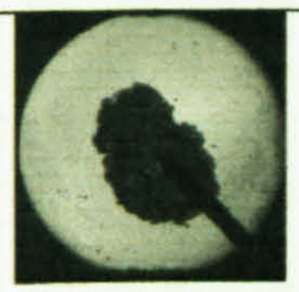	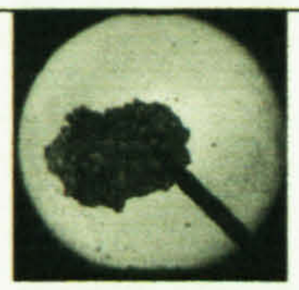			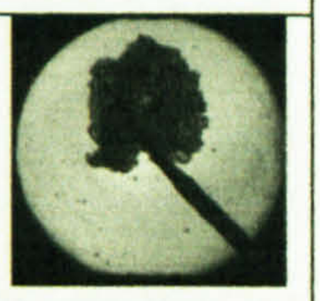
0.8					
0.9					
1.0					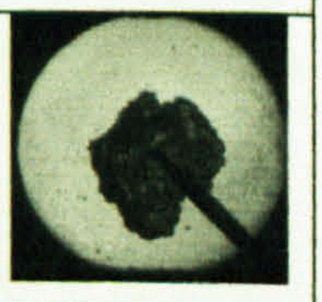
1.1			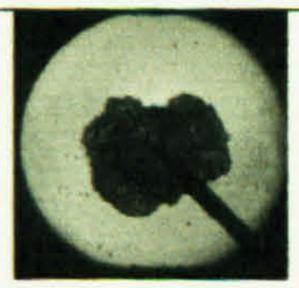		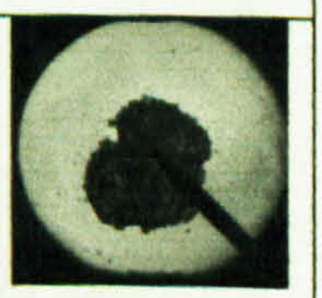
1.2					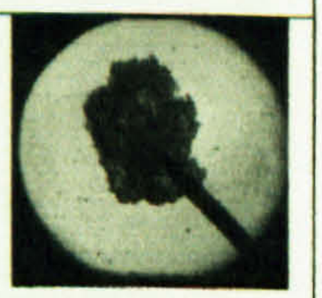
1.3			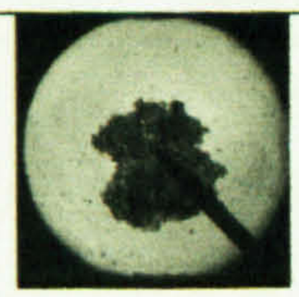		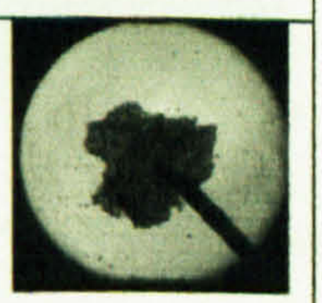

Figure 6.1 Turbulent flame kernels at a R_{sch} of 30 mm (± 2 mm) of methane-air flames over a range of equivalence ratios. At u' = 2 m/s, initial pressure of 0.5 MPa and 360 K.

ϕ	1	2	3	4	5
0.5				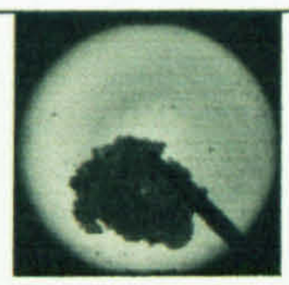	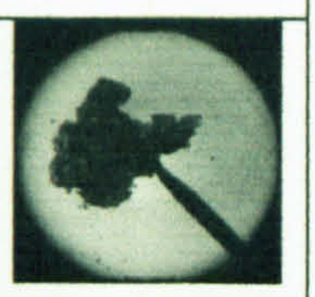
0.6	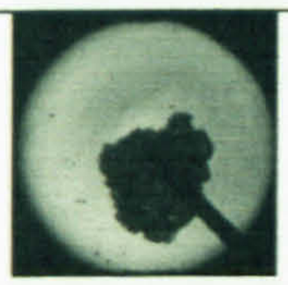				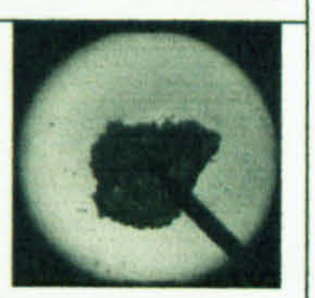
0.8					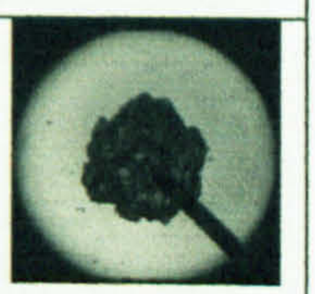
0.9					
1.0					
1.2					
1.3					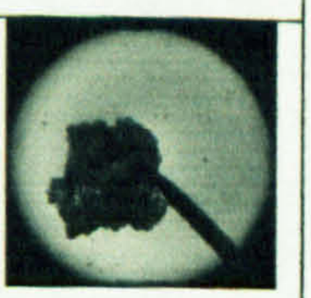
1.4					

Figure 6.2 Turbulent flame kernels at a R_{sch} of 30 mm (± 2 mm) of hydrogen (30%) and methane (70%) with air flames over a range of equivalence ratios. At u' = 2 m/s, initial pressure of 0.5 MPa and 360 K.

ϕ	1	2	3	4	5
0.8					
0.9					
1.0		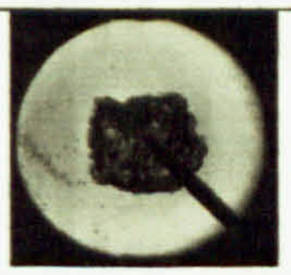			
1.1					
1.2					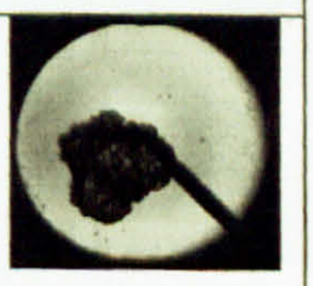
1.4			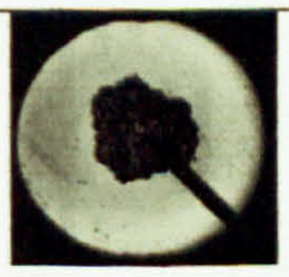		
1.6				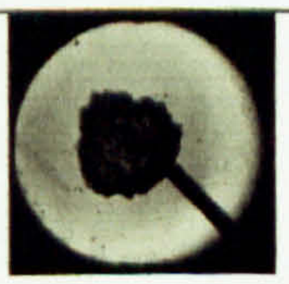	
1.8					

Figure 6.3 Turbulent flame kernels at a R_{sch} of 30 mm (± 2mm) of dutch-pura with air flames over a range of equivalence ratios. At u' = 2 m/s, initial pressure of 0.5 MPa and 360 K.

ϕ	1	2	3	4	5
0.8					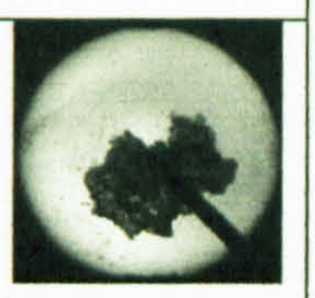
0.9					
1.0					
1.1					
1.4				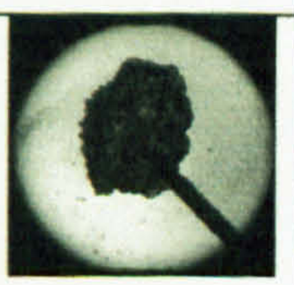	
1.6					
1.8					
2.0					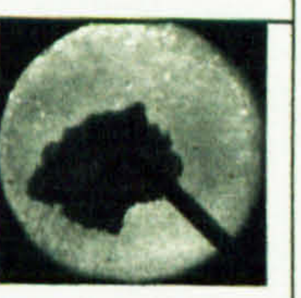

Figure 6.4 Turbulent flame kernels at a R_{sch} of 30 mm (± 2 mm) of iso-octane-air flames over a range of equivalence ratios. At u' = 2 m/s, initial pressure of 0.5 MPa and 360 K.

ϕ	1	2	3	4	5
0.7				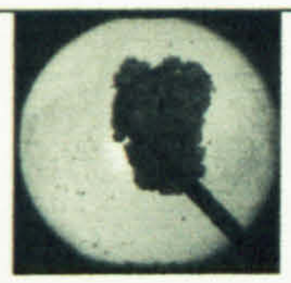	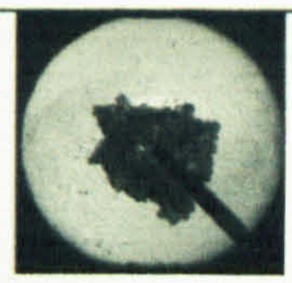
0.9		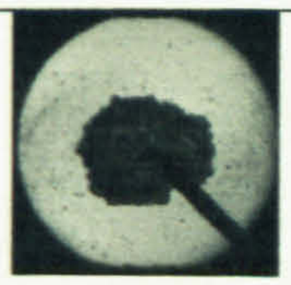			
1.0					
1.1					
1.2	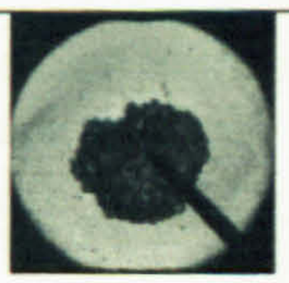				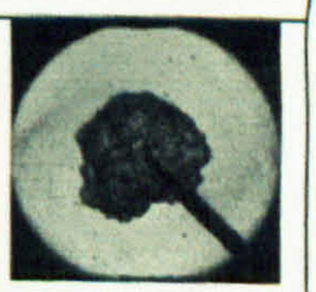
1.4				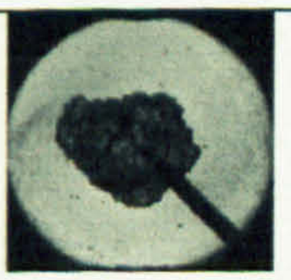	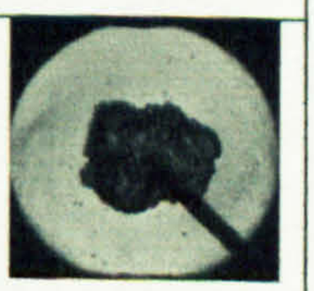
1.6					
1.8	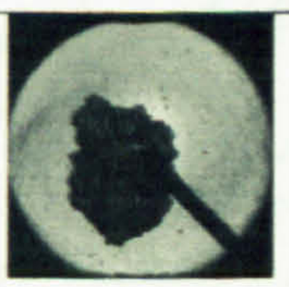				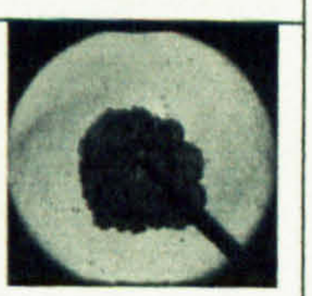

Figure 6.5 Turbulent flame kernels at a R_{sch} of 30 mm (± 2 mm) of methanol-air flames over a range of equivalence ratios. At u' = 2 m/s, initial pressure of 0.5 MPa and 360 K.

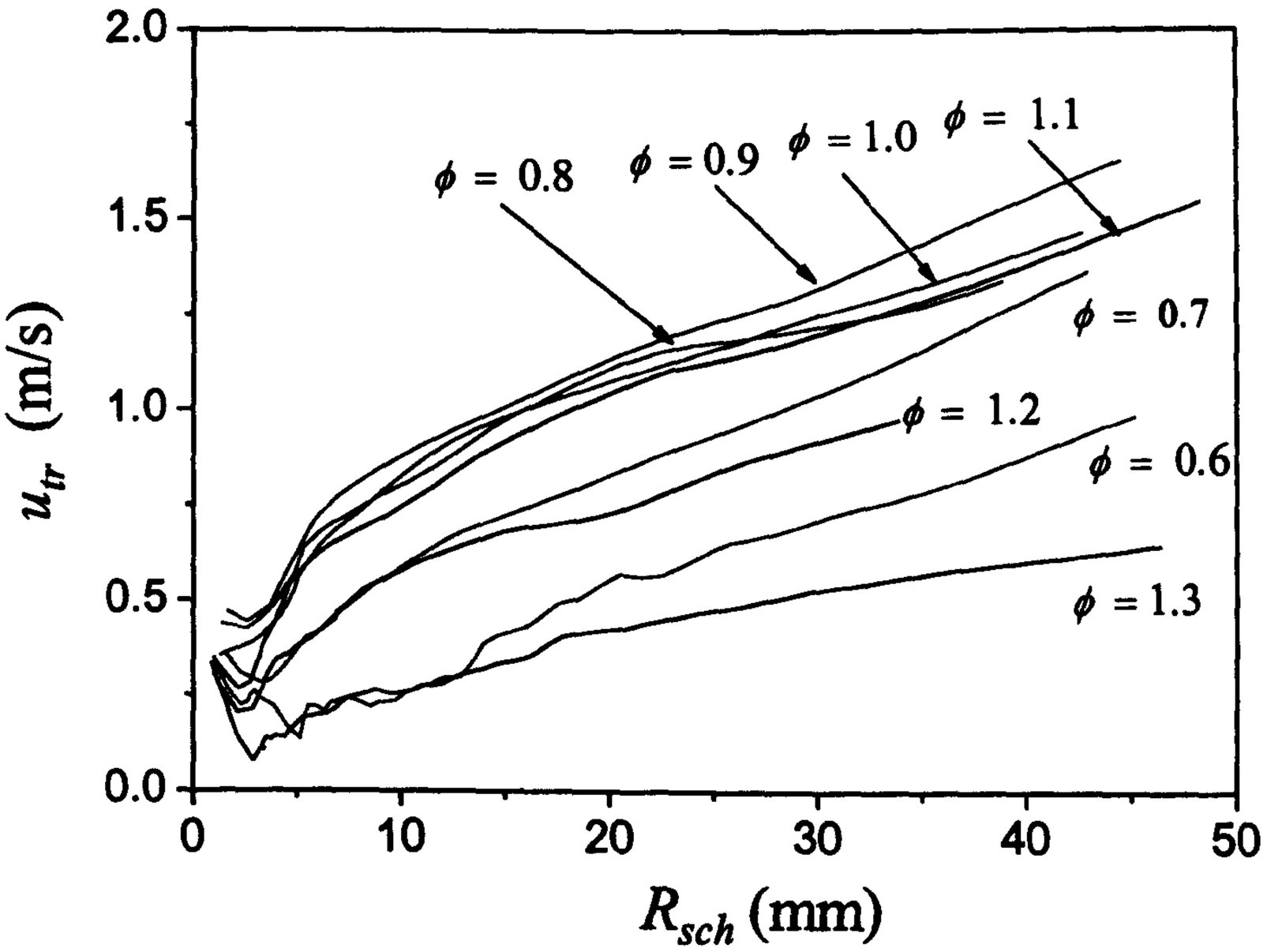

Figure 6.6 Derived turbulent burning velocities against schlieren radius for methane air flames. At u' = 2 m/s, initial pressure of 0.5 MPa and 360 K.

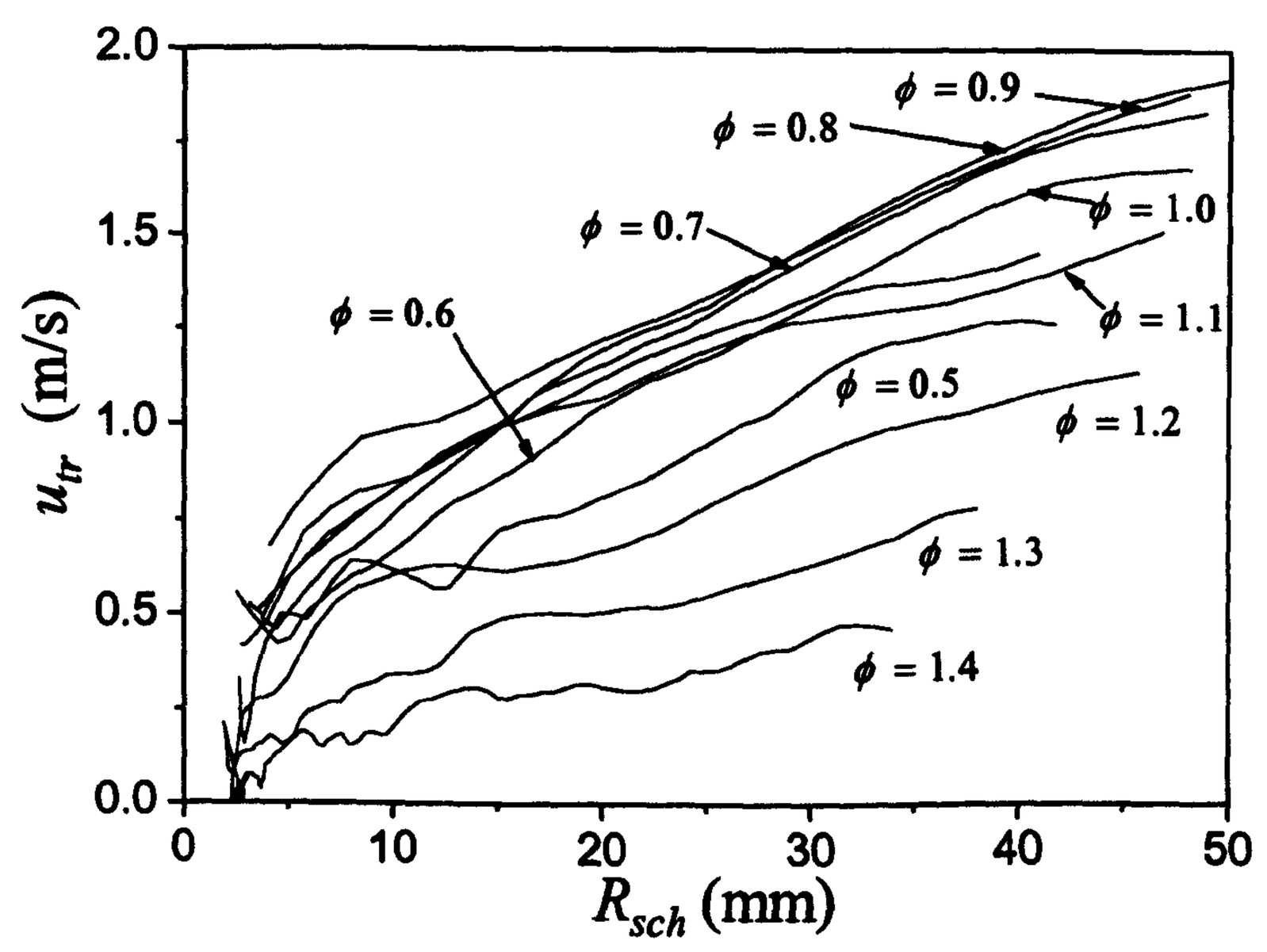

Figure 6.7 Derived turbulent burning velocities against schlieren radius for hydrogen (30%) and methane (70%) with air flames. At u' = 2 m/s, initial pressure of 0.5 MPa and 360 K.

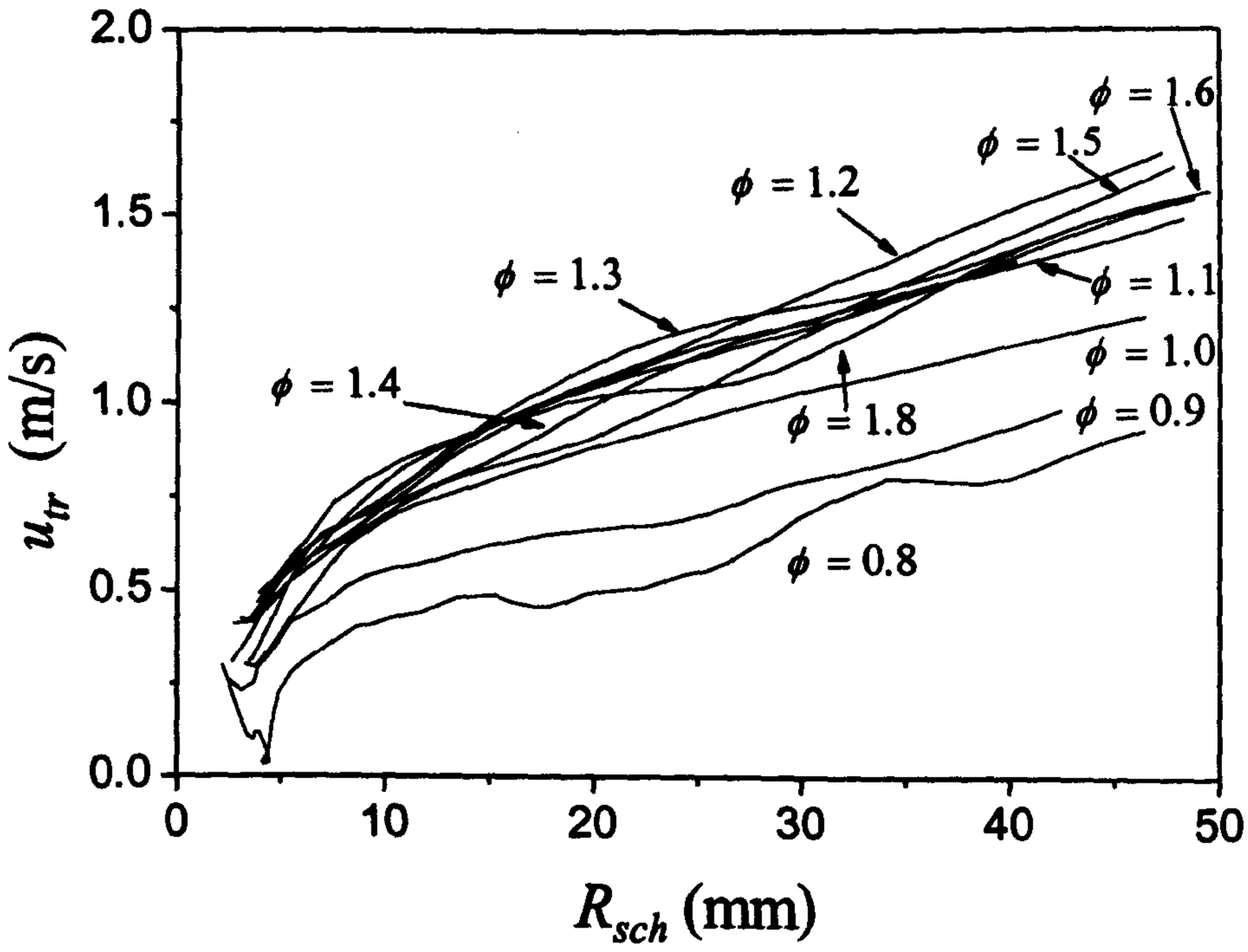

Figure 6.8 Derived turbulent burning velocities against schlieren radius for dutch-pura with air flames. At u' = 2 m/s, initial pressure of 0.5 MPa and 360 K.

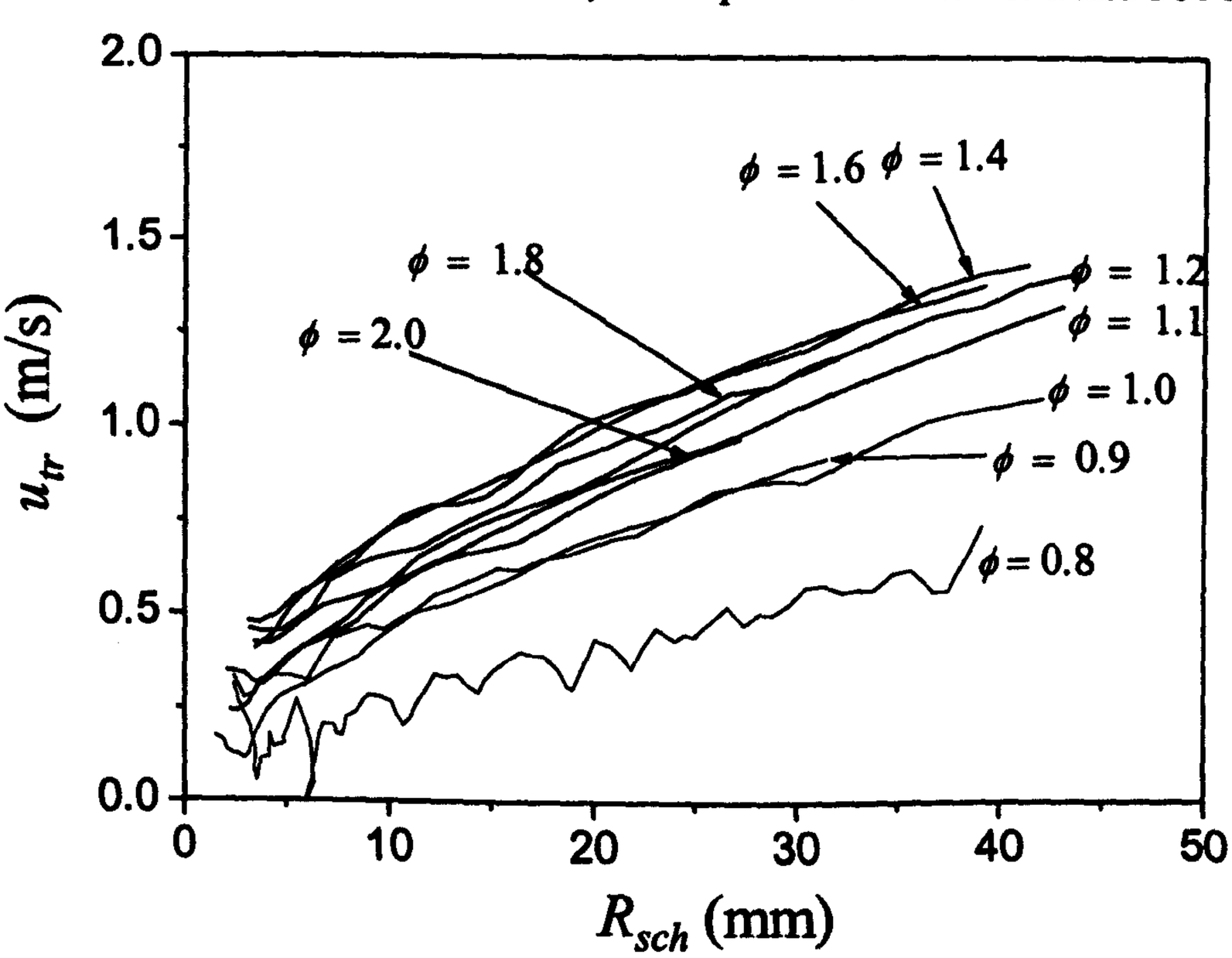

Figure 6.9 Derived turbulent burning velocities against schlieren radius for iso-octane - air flames. At u' = 2 m/s, initial pressure of 0.5 MPa and 360 K.

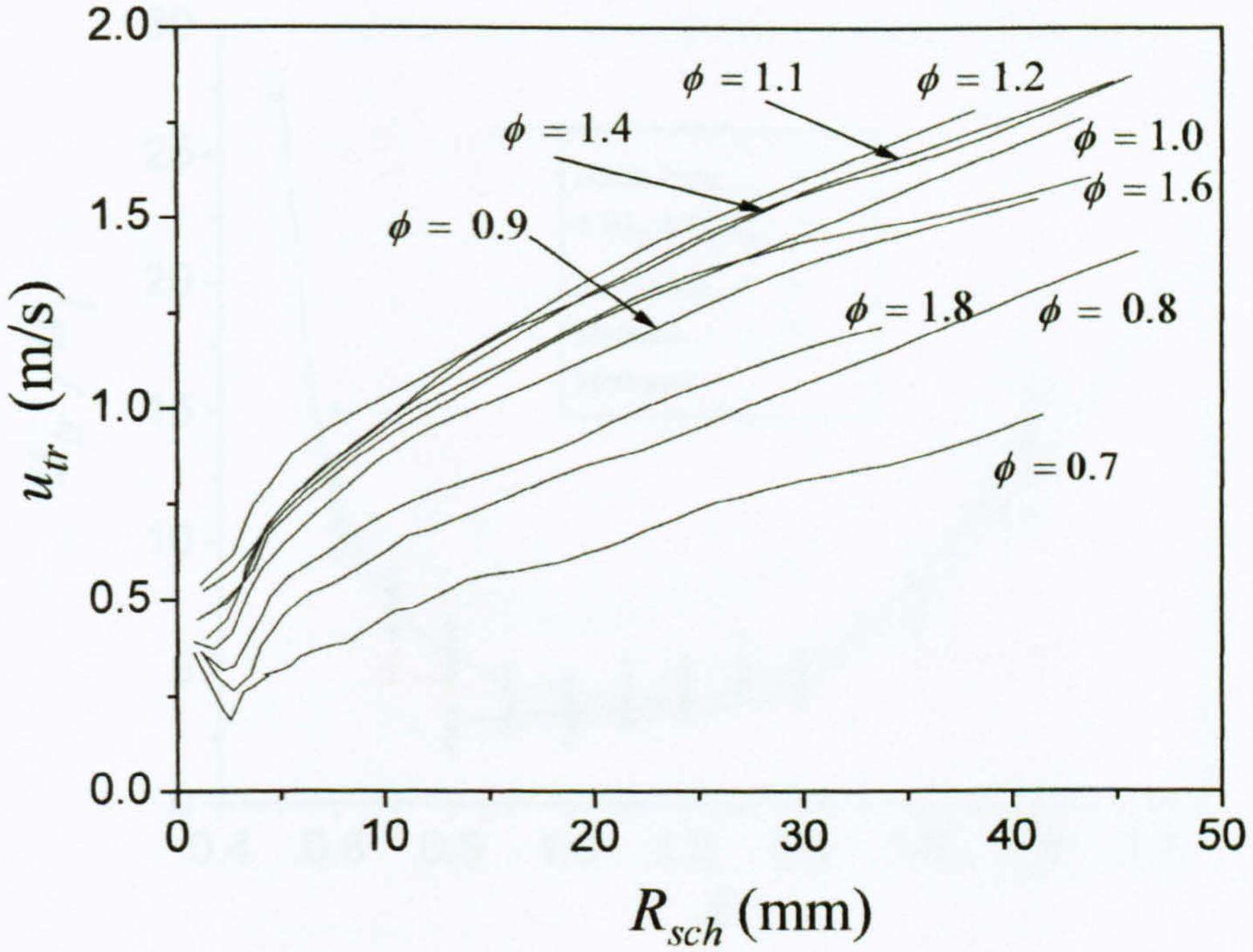

Figure 6.10 Derived turbulent burning velocities against schlieren radius for methanol - air flames. At u' = 2 m/s, initial pressure of 0.5 MPa and 360 K.

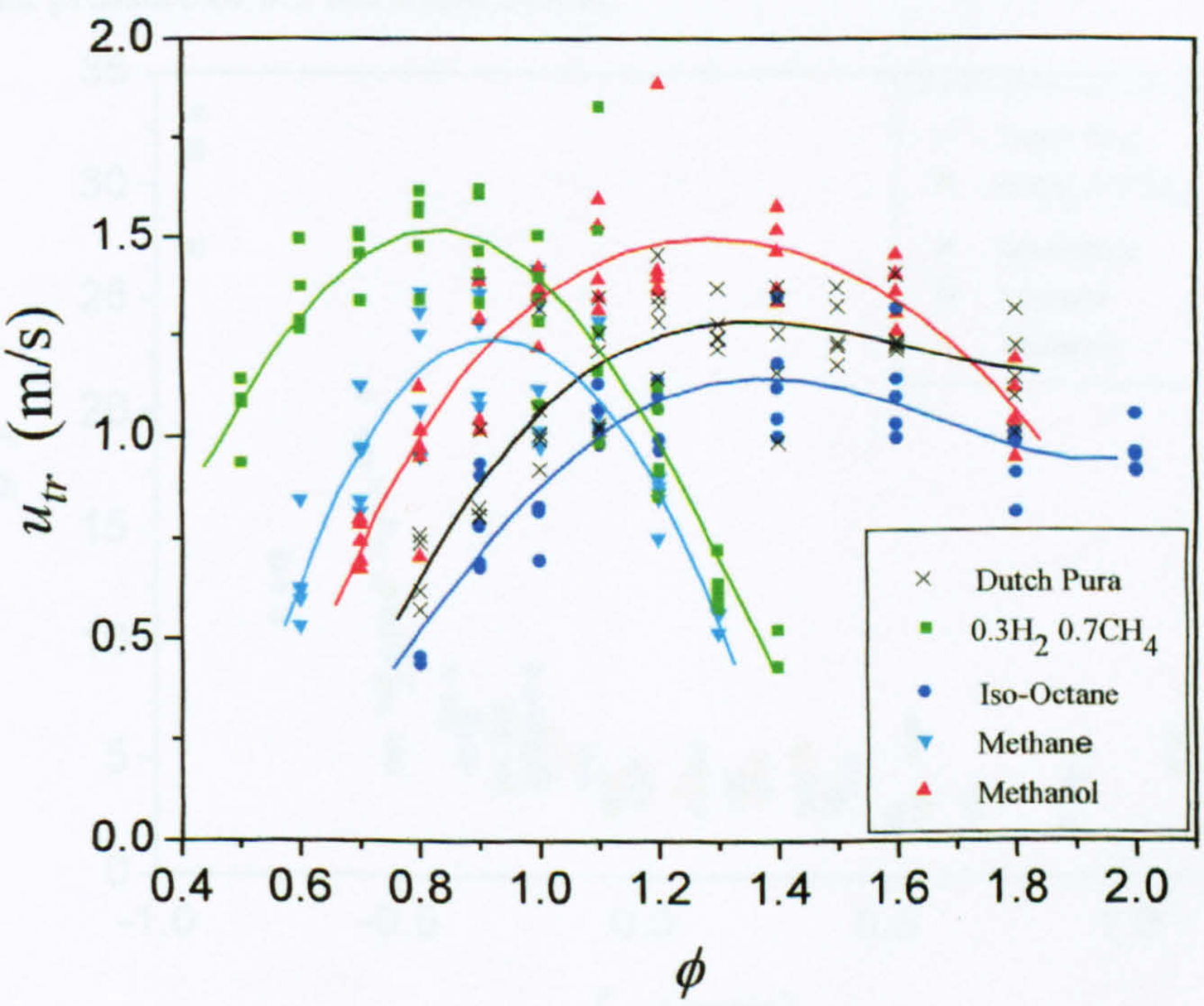

Figure 6.11 Derived turbulent burning velocities for all tested fuels at a R_{sch} of 30 mm plotted against equivalence ratio. At u' = 2 m/s, initial pressure of 0.5 MPa and 360 K.

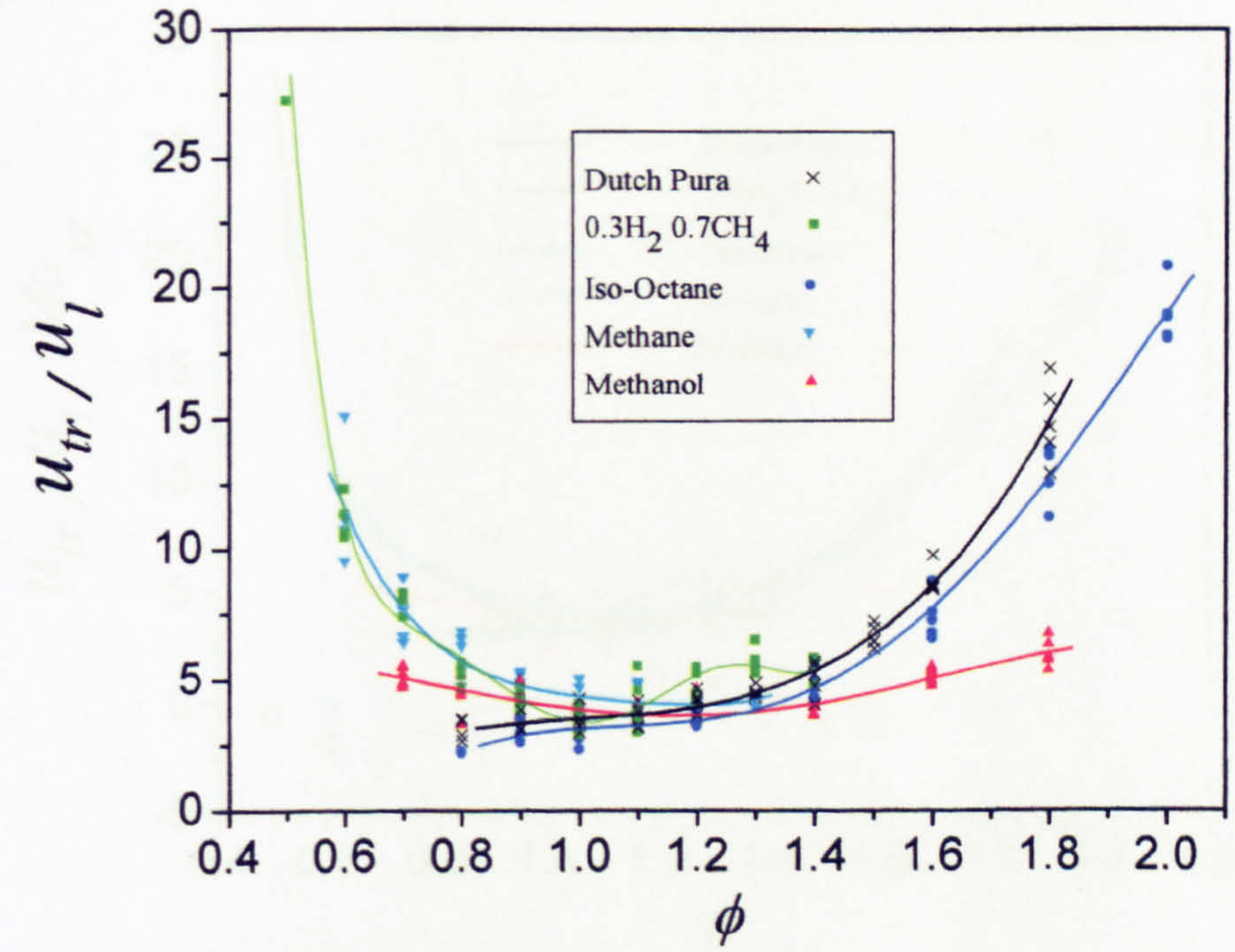

Figure 6.12 Derived turbulent burning velocities (R_{sch} of 30 mm) normalised by the laminar burning velocity plotted against equivalence ratio. At u' = 2 m/s, initial pressure of 0.5 MPa and 360 K.

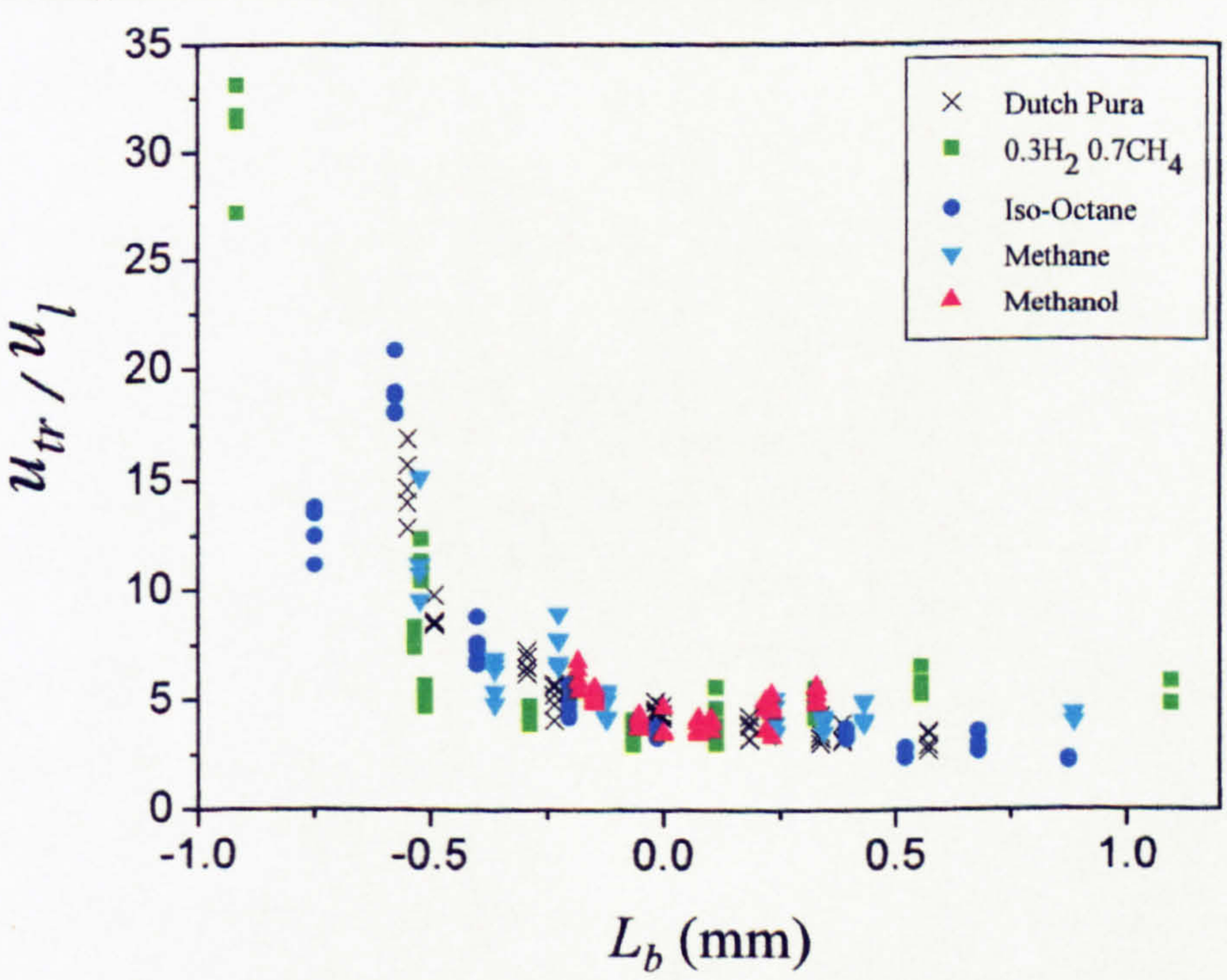

Figure 6.13 Derived turbulent burning velocities (R_{sch} of 30 mm) normalised by the laminar burning velocity plotted against laminar burned gas Markstein length. Turbulent measurements at u' = 2 m/s, initial pressure of 0.5 MPa and 360 K.

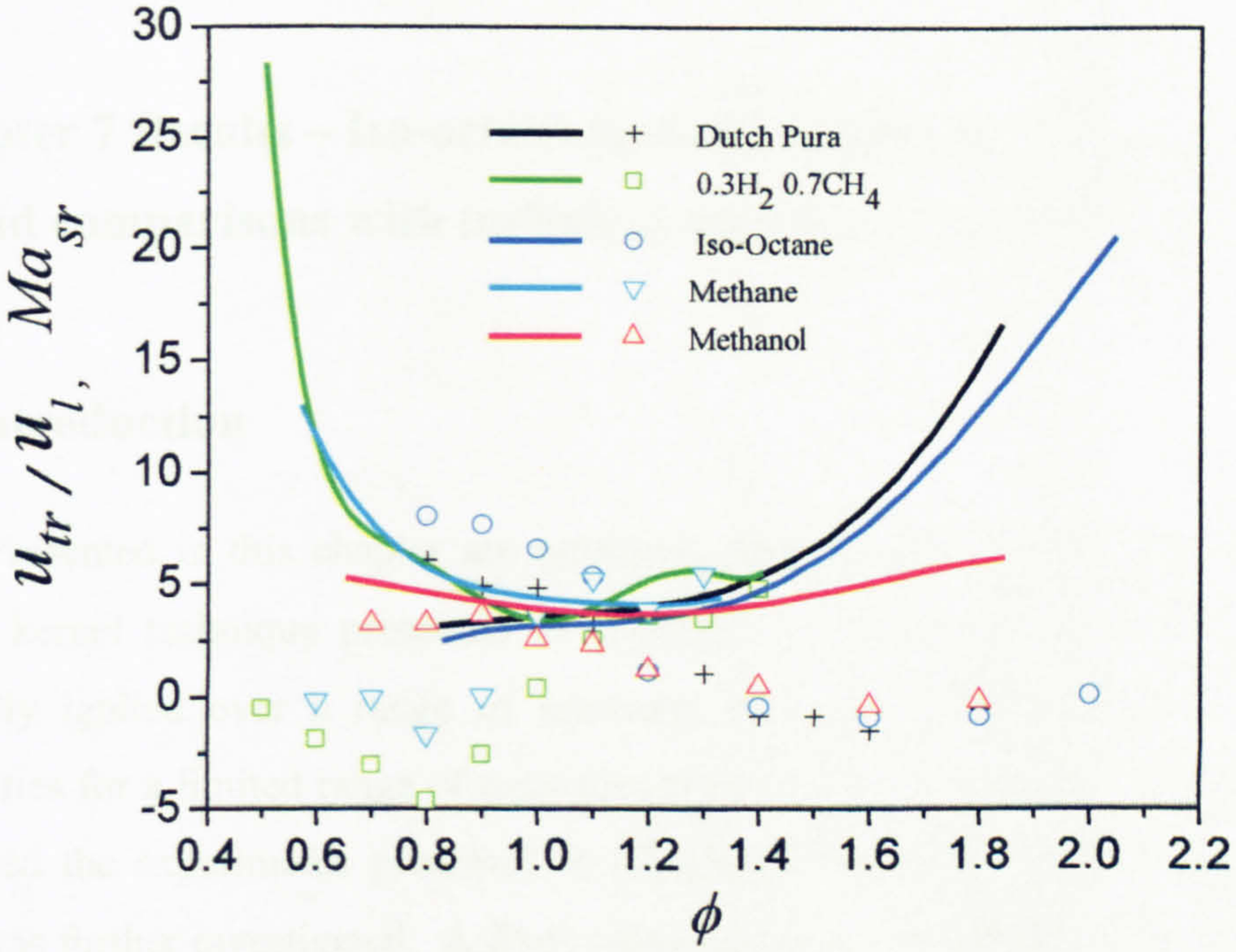

Figure 6.14 Polynomial fits of u_{tr}/u_l (R_{sch} of 30 mm) and measured Markstein length (M_{asr}) plotted against plotted against equivalence ratio. Turbulent measurements at u' = 2 m/s, initial pressure of 0.5 MPa and 360 K.

Chapter 7 Results – Iso-octane turbulent burning velocity database and comparisons with turbulent burning velocity correlations

7.1 Introduction

Presented in this chapter are turbulent burning velocities obtained using the single kernel technique presented in Chapter 3. Flames of iso-octane air were centrally ignited over a range of pressures (0.1, 0.5, 1.0 MPa) and turbulence intensities for a limited range of equivalence ratios (0.8, 1, 1.2 and 1.4). This work preceded the experiments presented in Chapter 6 where the effect of equivalence ratio was further investigated. A fixed temperature was used throughout this current study of 360 K. At 0.5 MPa the turbulence intensities used were u'= 0.5, 1, 2, 4 and 6 m/s, at 0.1 and 1.0 MPa u' = 1 and 4 m/s were studied. The purpose of this area of the study was to generate a new database of turbulent burning data using iso-octane as the reference fuel.

At each of the forty conditions five experiments were performed, later in this chapter values of u_{tr} have been presented at a schlieren radius of 30 mm. These values and the turbulent burning velocities given in Chapter 6 have been compared to existing turbulent burning velocity correlation's.

7.2 Effect of the r.m.s turbulent velocity on developing flames

Shown in Fig. 7.1 are turbulent burning velocities plotted against flame radius for developing stoichiometric iso-octane air flames at 0.5 MPa for a number of r.m.s turbulent velocities. The laminar burning velocity, u_l, was 0.3 m/s at this condition. Initially after ignition the flames should burn at u_l until the kernel becomes wrinkled by turbulent eddies. At lower values of u' the flame took a few millimetres to attain the laminar burning velocity as stretch effects resulted in a reduced burn rate. However, at higher r.m.s. turbulence velocities u_l was achieved almost immediately as the smaller turbulent scales had more energy and wrinkled the surface quicker.

There was shot to shot variation between the experiments but the data at u' 0.5, 1, and 2 m/s formed discrete bands. The higher u' of 4 and 6 m/s overlapped each another, here the increase in u' from 4 to 6 did not result in a clear increase in u_{tr}. These faster flames were convected and became increasingly non-spherical, they consequently tended not to reach as large a radius within the field of view than experiments performed at lower values of u'.

Figure 7.2 shows iso-octane deflagrations for a lean equivalence ratio of ϕ = 0.8, at 0.5 MPa for all tested values of u'. At ϕ = 0.8 the u' = 0.5 and 1 m/s data are very close together whereas at ϕ = 1.0 the u' = 1 m/s was significantly faster. The ϕ = 0.8 flames had very low burning velocities, often collapsing to zero just after ignition. This was also true for the laminar case at this condition where a fall in the flame speed was the result of flame stretch. Above u' = 1 m/s the observed flames were highly convected, non-spherical and contained evidence of flame quench with areas of the schlieren edge disappearing over a few milliseconds and sometimes reappearing after. Five experiments were always performed, flames did not grow to sensible radii before being either convected from view or flames were quenched the data has not been plotted (this only effected a few conditions notably ϕ =0.8 iso-octane).

The equivalence ratio of 1.4 is shown for the same pressure and range in u' in Fig. 7.3. Here there was no observable evidence of flame quench, the flames were generally more spherical than at ϕ = 1. The data from each u' formed in to discrete bands. Experiments performed at ϕ = 1.2 were similar to those at ϕ = 1.4.

To summarise the effect of changing the r.m.s turbulent flow field velocity the u_{tr} at a radius of 30 mm have been plotted against u' in Fig. 7.4. All equivalence ratios showed evidence of 'turndown'; that is the turbulent burning velocity increased with u' at a slower rate as u' increases, thus u_t did not increase linearly with u' over the range of u' investigated here.

7.3 Effect of the equivalence ratio on the turbulent burning velocity

The effect of equivalence ratio has been investigated in Chapter 6 at a u' = 2 m/s and 0.5 MPa, however, shown in Fig. 7.5 is the effect of equivalence ratio at u'=0.55 m/s at 0.5 MPa and 360 K. The lean condition (ϕ = 0.8) is very slow beginning at a value of u_{tr} of around 0.05 m/s, compared to u_l at this condition was 0.2 m/s. These lean flames remained slow throughout the filmed period taking until a radius of around 20 mm to achieve the laminar burning velocity. The other equivalence ratios banded together as at u' = 2 discussed in Chapter 6. Figure 7.6 shows these equivalence ratios at a u' of 6 m/s. Here the lean flame shows oscillatory behaviour, which was a consequence of parts of the flame edge quenching. The stoichiometric flames at this high u' were non-spherical and convected possibly suffering from flame quench and are clearly separated from the richer equivalence ratios.

Figure 7.7 shows the values of u_{tr} again at the radius of 30 mm against equivalence ratio for all of the tested r.m.s turbulent velocities. The turbulent burning velocity increased with u' also u_{tr} generally increased with equivalence ratio. At low u' = 0.5 the ϕ= 1.4 flames are slower than those at ϕ = 1.2, as u' increased the peak value of u_{tr} shifts, with the richer flame becoming relatively faster. At u' = 1, 2 and 4 the equivalence ratios ϕ= 1.2 and ϕ= 1.4 had similar value of u_{tr}, at u' = 6 m/s however the u_{tr} increased linearly with equivalence ratio.

Shown in Fig. 7.8 is the effect of equivalence ratio at 0.1 MPa for a u' = 1 m/s and at 0.1 MPa where u'= 4 m/s in Fig. 7.9. At u'= 4 the ϕ = 0.8 flames were quenched at the spark plug. Figure 7.10 shows the summary of this data at a schlieren radius of 30 mm. At the lower u' the u_{tr} increased with equivalence ratio and the ϕ = 1.2 and ϕ = 1.4 values were similar. At the greater level of turbulence the ϕ = 1.4 were measurably higher than those at ϕ = 1.2. The same conditions were completed at 1.0 MPa, the results are shown in Fig. 7.11. The trend with respect to equivalence ratio is similar to at 0.1 MPa, however, at the higher u' ϕ = 1.4 flames were closer to those at ϕ = 1.2, the scatter however makes is difficult to make definitive conclusions.

7.4 Effect of pressure on the turbulent burning velocity

The effect of pressure was explored at values of u' = 1 and 4 m/s for the four equivalence ratios. Figure 7.12 shows the effect of pressure on the turbulent burning velocity for stoichiometric deflagrations at u' = 1. The values of u_{tr} at 30 mm radius are shown for all equivalence ratios at u' = 1 in Fig. 7.13. The linear fits added here poorly represent the data and there is considerable scatter in u_{tr}. In some cases u_{tr} increases between 0.1 and 0.5 MPa and sometimes decreases. For stoichiometric and lean flames there was a small increase of u_{tr} with increasing pressure, the richer flames show a larger increase however the scatter is large.

Overall at u' = 1 m/s there was a small increase of the turbulent burning velocity with pressure. This is surprising, considering the marked fall in u_l with increasing pressure (measured in Chapter 4).

At the higher level of turbulence where u' = 4 m/s the effect of pressure is more pronounced. Figure 7.14 shows the experimental development of stoichiometric iso-octane air flames for the pressure range. The results for the other equivalence ratios at this r.m.s turbulent velocity are shown in Fig. 7.15. It was not always possible to ignite at ϕ = 0.8, for the other equivalence ratios u_{tr} increases with pressure but the scatter is very high with this level of turbulence.

7.5 Comparisons with other workers and turbulent burning velocity correlations

Difficulty arises when attempting to qualify experimental turbulent burning velocity measurements with those from other workers who have used differing methods and apparatus. Even with the same fuel, temperature, pressure, r.m.s turbulence velocity and length scale the available results in the literature have a large variation. The major cause of this variation is the definition of the turbulent burning velocity. In this study u_{tr} has been used which is based on the rate of mass production. Many other workers based there experimental values on u_{te}, the rate of mass entrainment into the flame front, in much of the early work the turbulent burning velocity was not defined.

To compare the current work with that of others four turbulent burning velocity expressions have been used. The theoretical correlation by Damköhler (1940) (Turns, 1996);

$$u_t = u_l + u' \qquad 7.1$$

The experimental correlation Gülder (1991);

$$u_t = u_l + 0.62 u_l^{0.5} u'^{0.5} R_l^{0.25} \qquad 7.1$$

where R_l is the turbulent Reynolds number. The experimental correlation of Bradley *et al.* (1992);

$$u_t = 0.88(K\,Le)^{-0.3} u' \qquad 7.2$$

where K is the Karlovitz stretch factor $K = u'\delta_l / u_l \lambda$ and λ is the Taylor scale. The theoretical expression of Peters (2000):

$$u_t = u_l + \frac{0.39 u' Da}{b_1}\left[\left(1 + \frac{5.13 b_1^2}{Da}\right)^{1/2} - 1\right] \qquad 7.3$$

where Da is the Damköhler number, $Da = u_l L / u' \delta_l$ and the constant $b_1 = 2$.

The equations of Damköhler, Gülder and Peters contain no Lewis or Markstein number effects. The correlation of Bradley *et al.* incorporates a Lewis number to account for stretch effects. It should be noted that there is a dearth of experimental data at elevated pressures or fuel rich equivalence ratios, which workers could use in developing their correlations at such conditions.

For the purposes of comparison experimental values of u_{tr} at 30 mm are being used, in Chapter 5 flames at this radii were found to be equally developed, at 0.62 u' when calculating u'_k using the spatial assumption. In the above turbulent burning velocity correlations the r.m.s turbulence velocity used was 0.62 of the experimental u'. The laminar burning velocities used in these expressions were those experimentally determined in Chapter 4, values of Le used are those given in Fig. 4.1.

Figure 7.16 shows results from the current study with those predicted from the correlations. The turbulent burning velocity has been plotted against the effective

r.m.s turbulence velocity. All of the correlations and the current data show an increase in the turbulent burning velocity with increasing u'. The correlations show little agreement with each other. The current experimental values of u_{tr} are significantly lower, than those predicted by the correlations.

Figure 7.17 shows the correlations and current work plotted using an alternative method recently adopted by Bradley (2000) and Peters (2000), where U is u_t/u' although for the developing flames used here the 30 mm radius data was used so $U = u_{tr}/u'_k$ for all comparisons. Again the current data is lower than all of the predictions.

Drake (1997) has investigated the effect of the definition of the turbulent burning velocity. The correlation was separated into entrainment burning velocities u_{te} and mass production based burning velocities, u_{tr}, used in the current work. Drake found the entrainment velocities to be significantly higher than mass production u_{tr}. Shown in Figs. 7.18 and 7.19 are the present experimental results with the u_{tr}'s available in the literature (identified by Drake). All methods used a pressure rise to measure u_t. The agreement between the current study and the other workers is much better (than in Fig. 7.17) although the current values are still slightly lower. This clearly shows the importance of the definition of the turbulent burning velocity. The Bradley *et al.* (1992) correlation was based on experimental measurements of u_{te}, although the notation u_t was used (Gillespie *et al.* 2000). This fact explains to some degree why the current experimental values are lower as the rate of entrainment u_{te} were found to be greater than those of u_{tr} by Bradley *et al.* (2003). The current measurements have significantly extended the range of measured conditions in terms of u'_k/u_l. However from Fig. 7.19 it can be seen that the maximum K measured has not been furthered.

The correlations have been tested for the effect of changing equivalence ratio and compared with the measurements of Chapter 6 in Figs 7.20 to 7.23. In theses figures the derived values of u_t have been normalised by the maximum value found for the particular correlation. (e.g. at $\phi = 1$, 0.5 MPa and 360 K the Damköhler equation predicted a maximum u_t of 1.29 m/s, this value was used to normalise the other Damköhler predictions for this pressure, temperature and fuel.)

In Fig. 7.20, all of the correlations predict a maximum u_t for methane at 0.5 MPa to occur at $\phi = 1$, the experimental maximum occurred slightly into the lean circa $\phi = 0.92$. The expressions of Bradley *et al.* and Gülder seem to 'best fit' the trend in experimental data showing a dependence of ϕ on the turbulent burning velocity, whilst Peters and Damköhler under predict the change in u_t at lean and rich equivalence ratios.

Figures 7.21 to 7.23 repeat comparisons in the same way where possible for 30% hydrogen and 70% methane, iso-octane and methanol. The correlations have not correctly predicted the peak burning velocity for any fuel, for the 30% hydrogen and 70% methane mixtures the experimental peak was at $\phi = 0.8$ the correlations all predicted it to occur at $\phi = 1$. Iso-octane reached its measured peak burning velocity at $\phi = 1.4$ but all of the correlations gave a peak equivalence ratio of 1.1, the experimental methanol flames had a peak at $\phi = 1.3$ but the predictions were at $\phi = 1.2$. The predicted effect of equivalence ratio on u_t was similar in Figs. 7.21 to 7.23 as it was in Fig 7.20, with the expressions of Bradley *et al.* and Gülder following the trend in experimental data and Peters and Damköhler showing little consideration to equivalence ratio.

In Figs. 7.24 and 7.25 the turbulent burning velocity expressions are used to generate predicted values of u_t for stoichiometric iso-octane air at pressures 0.1, 0.5 and 1.0 MPa with $u' = 1$ and 4 m/s. The calculated values of u_t from the expressions are again quite different from one another, furthermore they disagreed on the effect increasing pressure has. Over the range 0.1 to 1.0 MPa at $u' = 1$ m/s the expressions of Damköhler, Bradley *et al.* and Peters predict a reduction in u_t of 23.2 %, 8.6 % and 14.4 % respectively. The Gülder correlation predicts a rise in u_t of 5.0%, the current study also shows an increase in the mean of the 0.1 and 1.0 MPa experiments of 7.2 % at $u' = 1$ m/s. At the higher r.m.s turbulence velocity of 4 m/s Damköhler (-8.8%), Bradley *et al.* (-8.6%) and Peters (-1.4%) again predict a fall in u_t. Gülder suggests a rise of 15.6 %, the current measurements however show an increase of 44.5% at $u' = 4$ m/s although the experimental scatter is high. Kobayashi *et al.* (1996, 1998 and 2005) have also shown a rise in turbulent burning velocity with pressure for methane, ethylene and propane.

Regime diagrams are shown for the iso-octane database conditions in Fig. 7.26 and of the equivalence ratio study of Chapter 6 in Fig. 7.27. Most of the experimental conditions are within the corrugated flamelet regime. Some conditions however are in the thin reaction zone, these conditions are those at higher values of u' and for those with low values of u_l. Within the thin reaction zone, theory suggests than the turbulence disrupts the flame preheat zone. These diagrams have been used to identify which of the deflagrations fall into the thin reaction zone.

In Figs. 7.28 and 7.29 the current work has been displayed in non-dimensional form. Three types of flames have been identified, (i) corrugated flamelet, (ii) thin reaction flames with a $-L_b$, and (iii) thin reaction flames with a $+L_b$. Plotted in this way the results show three clear zones, the experiments performed in the corrugated flamelet regime behaved as one might have traditionally predicted. Flames in the thin reaction zone and have a $+L_b$ are clearly separated from those with a negative value, deflagrations with positive Markstein lengths suffered from flame quench whereas those with negative values thrive with increasing levels of turbulence. It is these $-L_b$ flames which have displayed the shift in u_t/u_l discussed in Chapter 6.

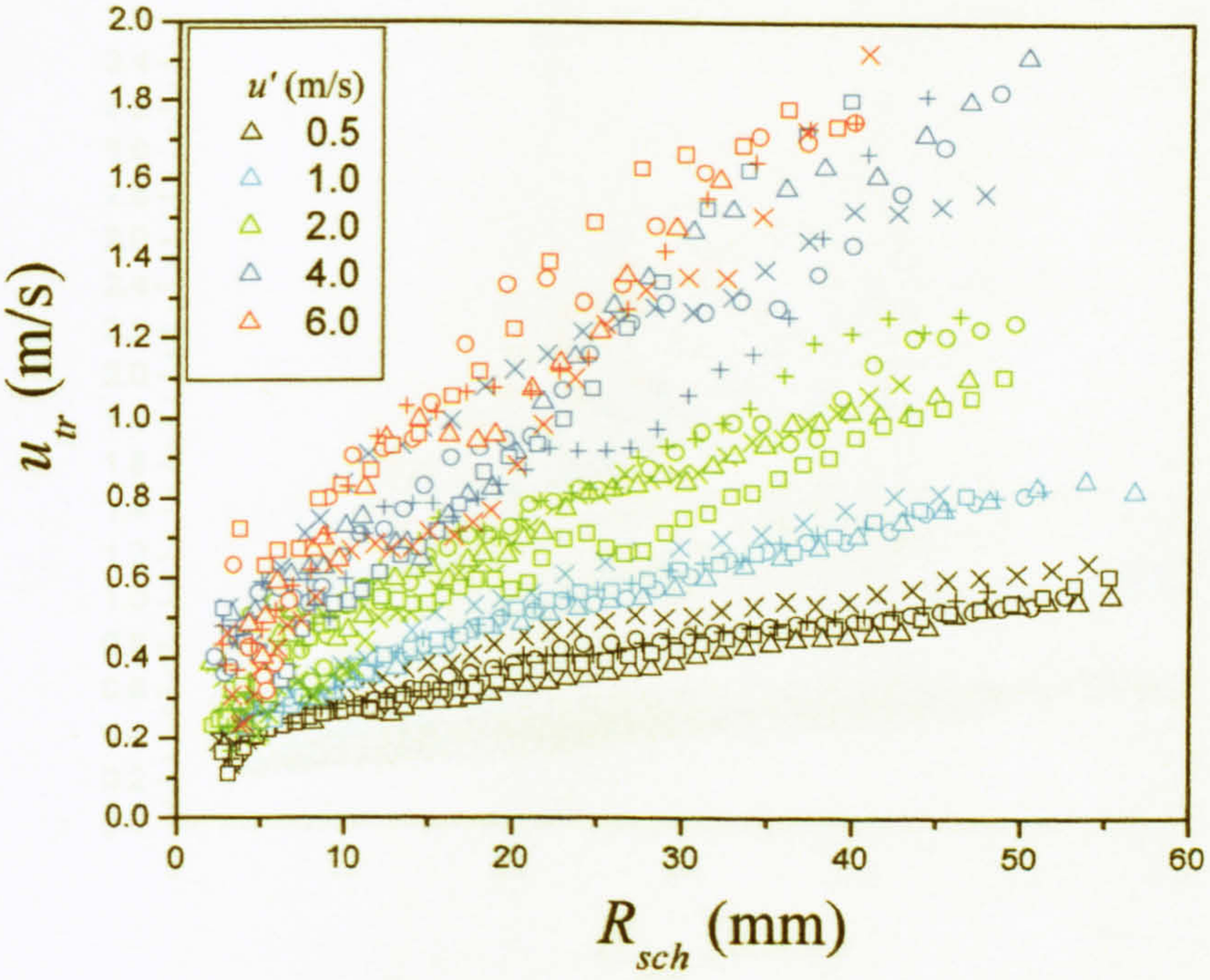

Figure 7.1 Experimental development of stoichiometric iso-octane air flames at 0.5 MPa and 360 K for u' = 0.5, 1, 2, 4 and 6 m/s.

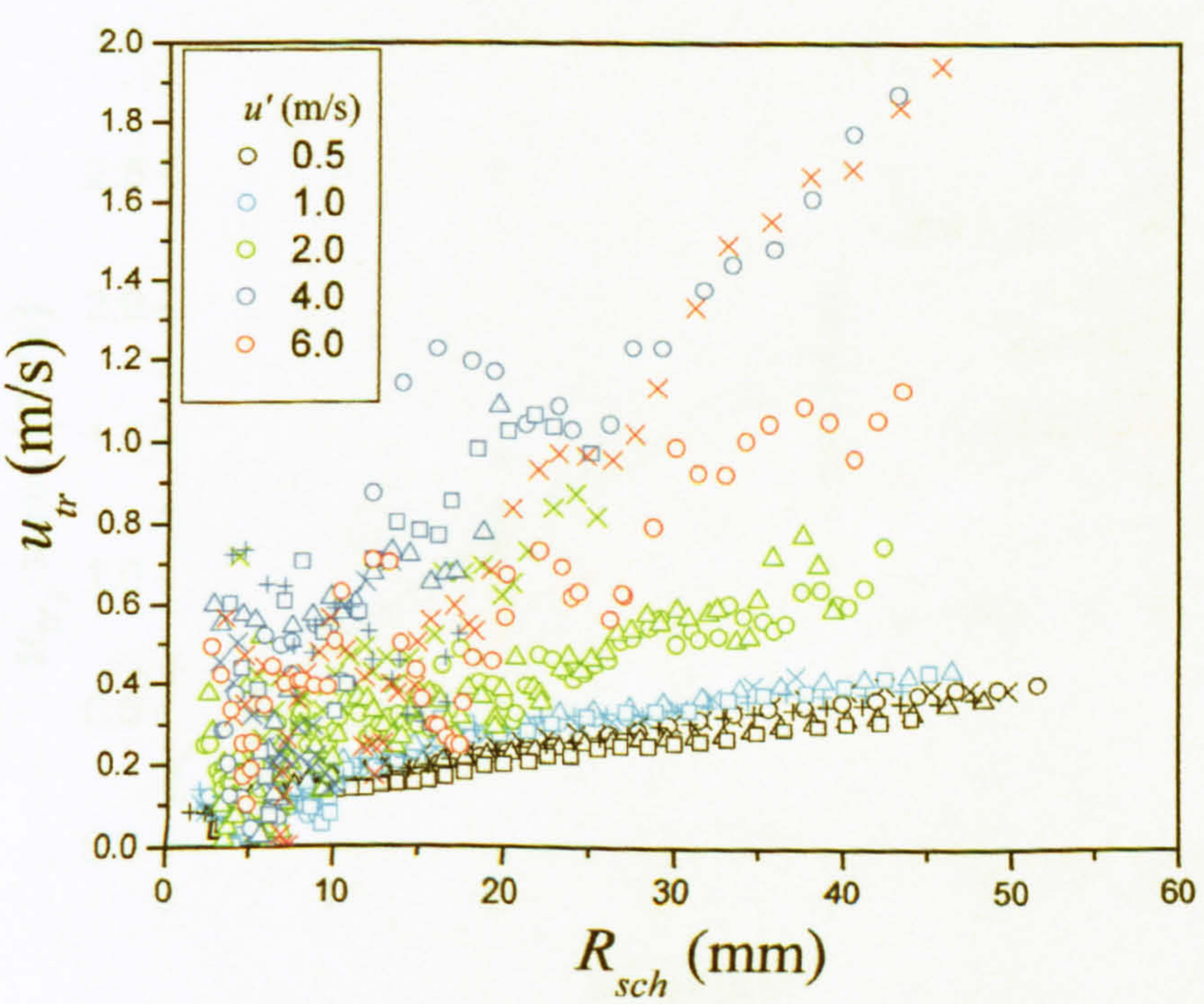

Figure 7.2 Experimental development of ϕ = 0.8 iso-octane air flames at 0.5 MPa and 360 K for u' = 0.5, 1, 2, 4 and 6 m/s.

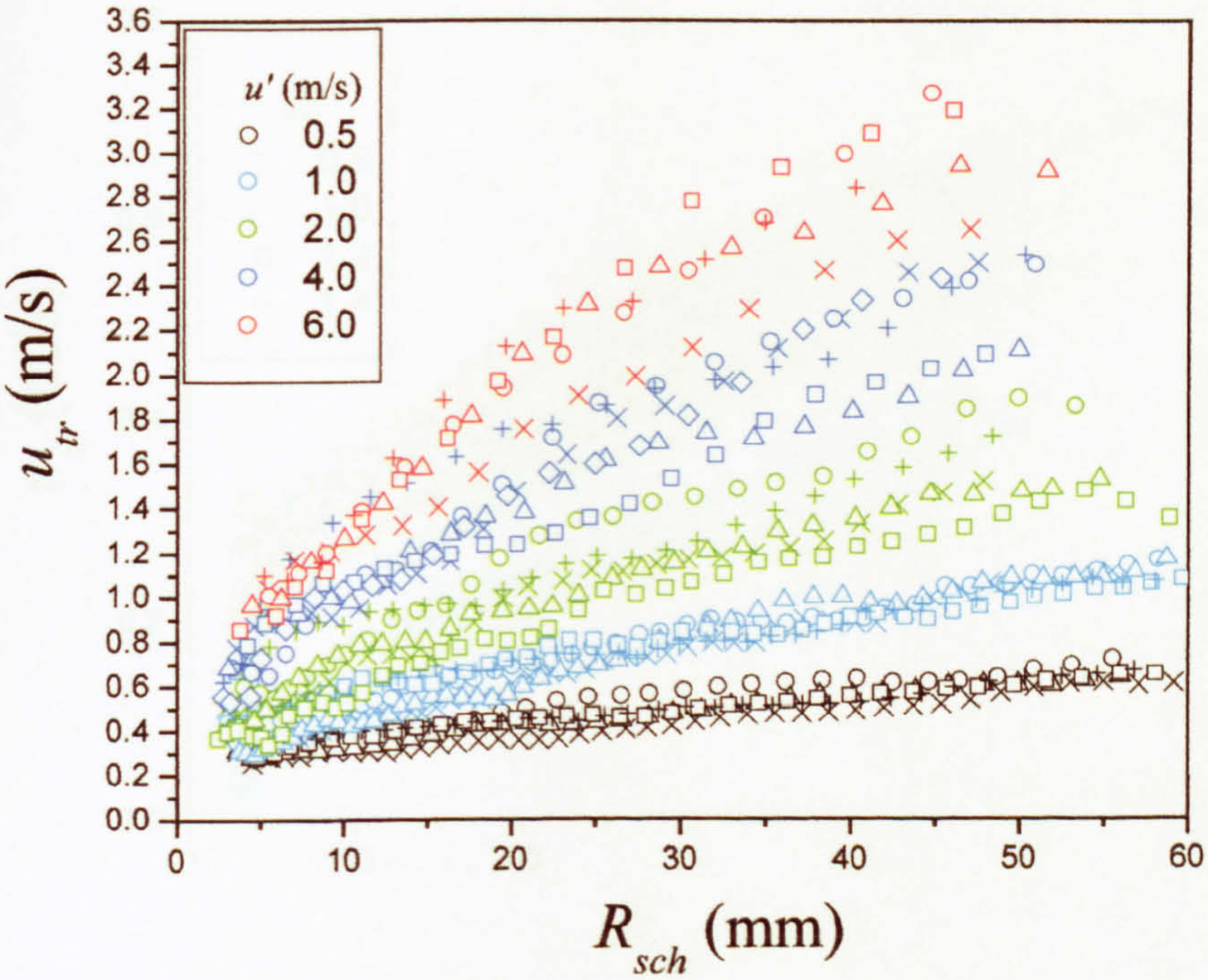

Figure 7.3 Experimental development of $\phi = 1.4$ iso-octane air flames at 0.5 MPa and 360 K for $u' = 0.5$, 1, 2, 4 and 6 m/s.

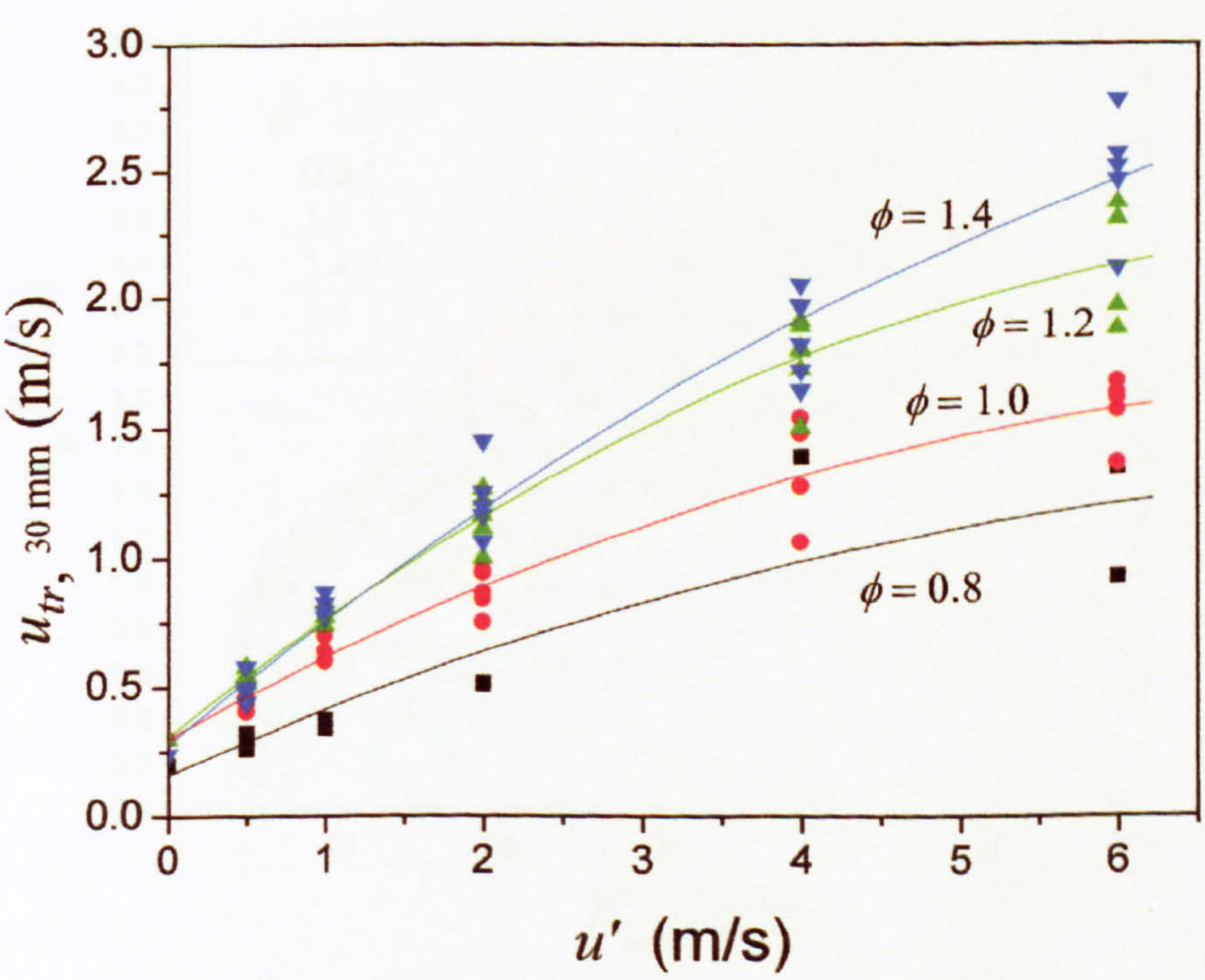

Figure 7.4 Values of the turbulent burning velocity at a schlieren radius of 30 mm, for iso-octane air flames at equivalence ratios of 0.8, 1.0, 1.2, 1.4 at 0.5 MPa and 360 K for $u' = 0.5$, 1, 2, 4 and 6 m/s.

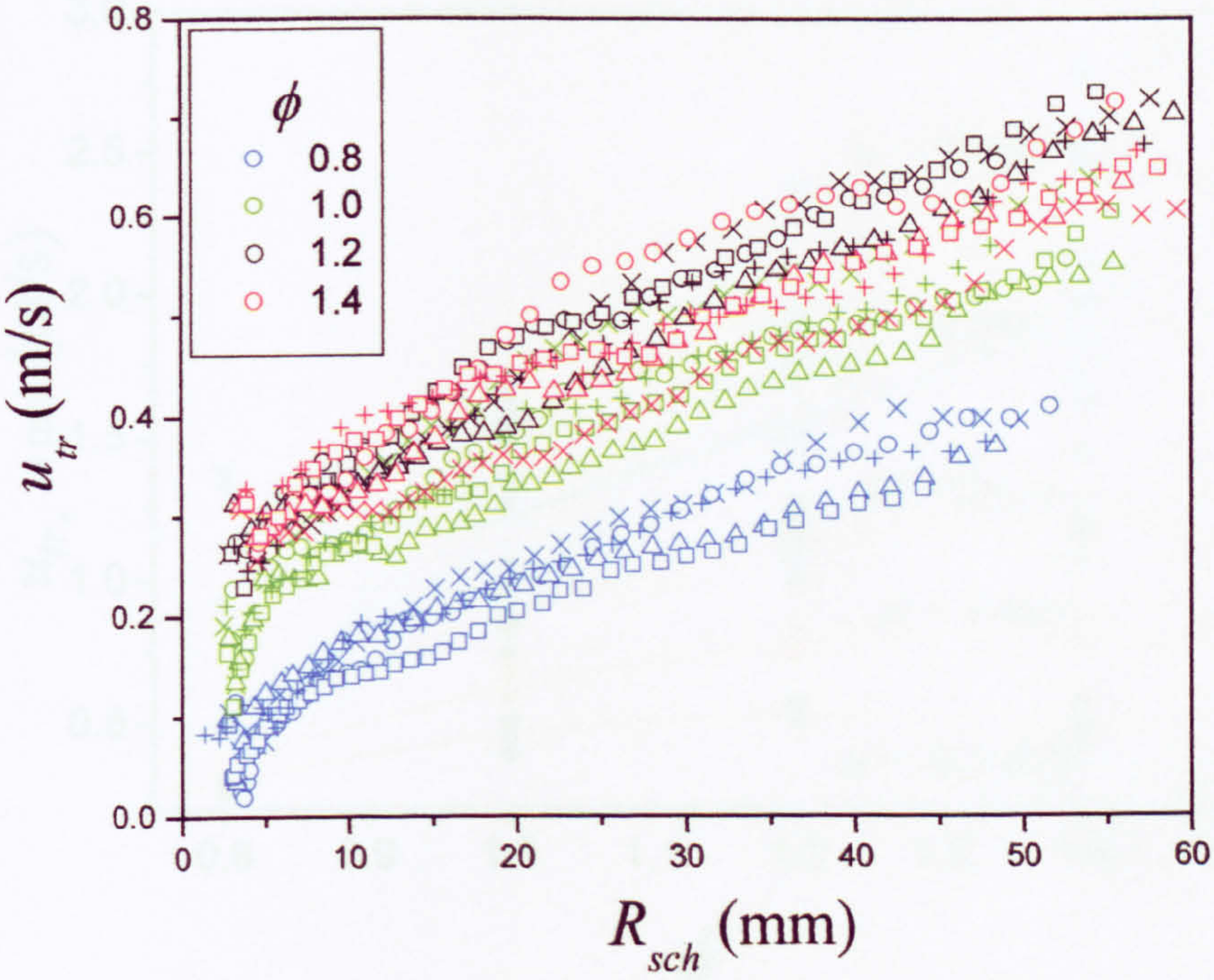

Figure 7.5 Experimental development of iso-octane air flames at 0.5 MPa and 360 K for ϕ 0.8, 1.0, 1.2 and 1.4, where u' = 0.5 m/s.

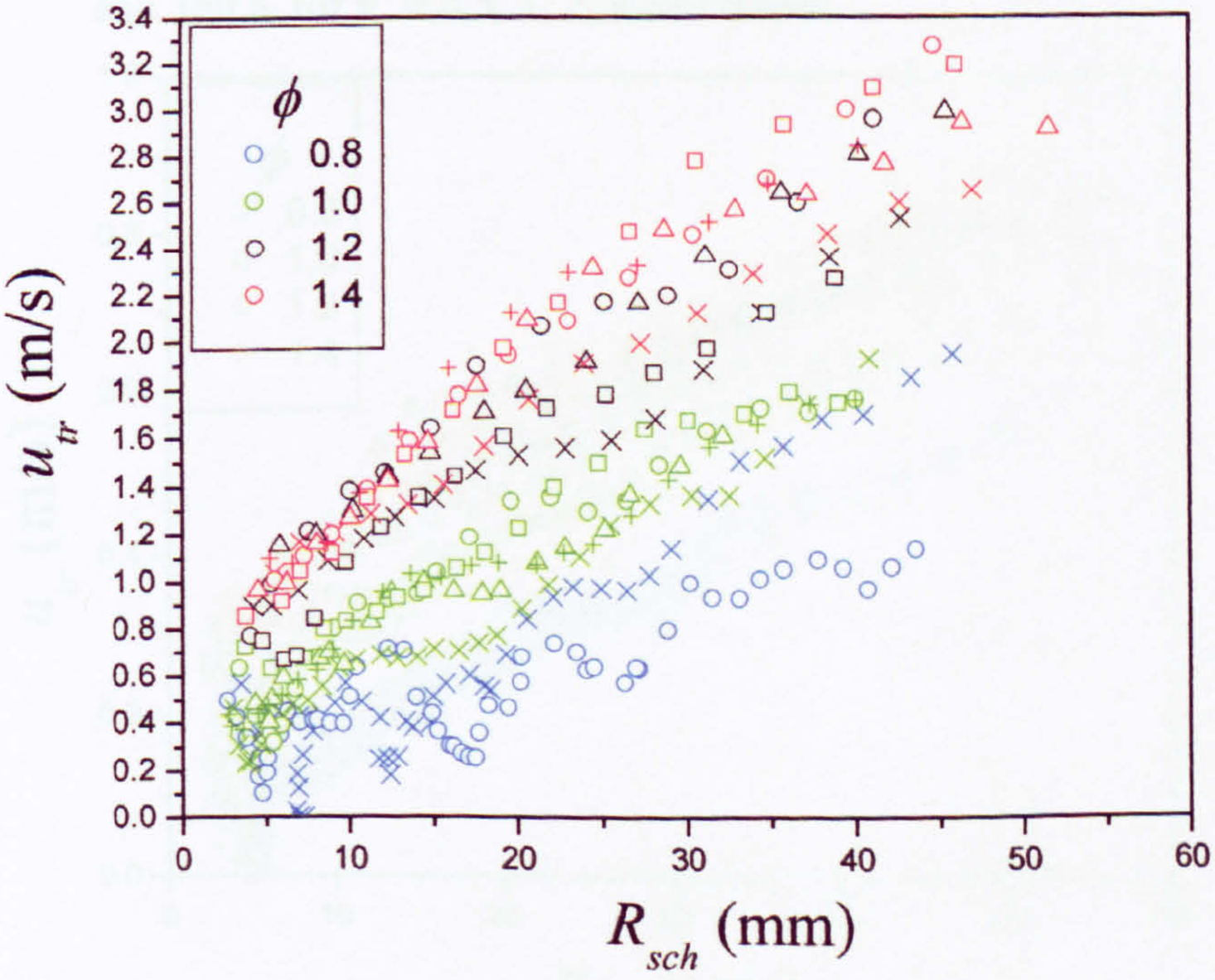

Figure 7.6 Experimental development of iso-octane air flames at 0.5 MPa and 360 K for ϕ 0.8, 1.0, 1.2 and 1.4, where u' = 6 m/s.

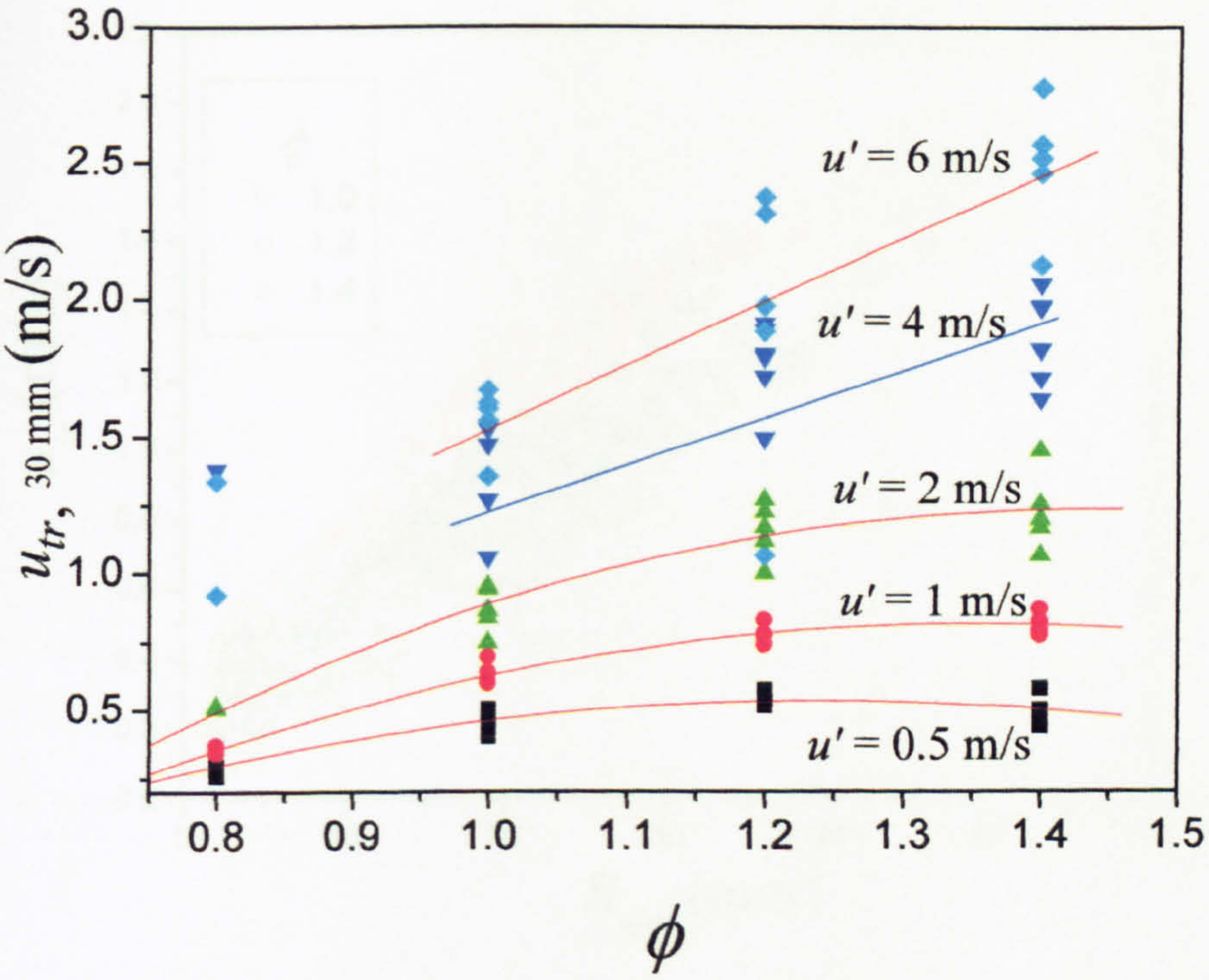

Figure 7.7 Values of the turbulent burning velocity at a schlieren radius of 30 mm, for iso-octane air flames at equivalence ratios of 0.8, 1.0, 1.2, 1.4 at 0.5 MPa and 360 K for u' = 0.5, 1, 2, 4 and 6 m/s.

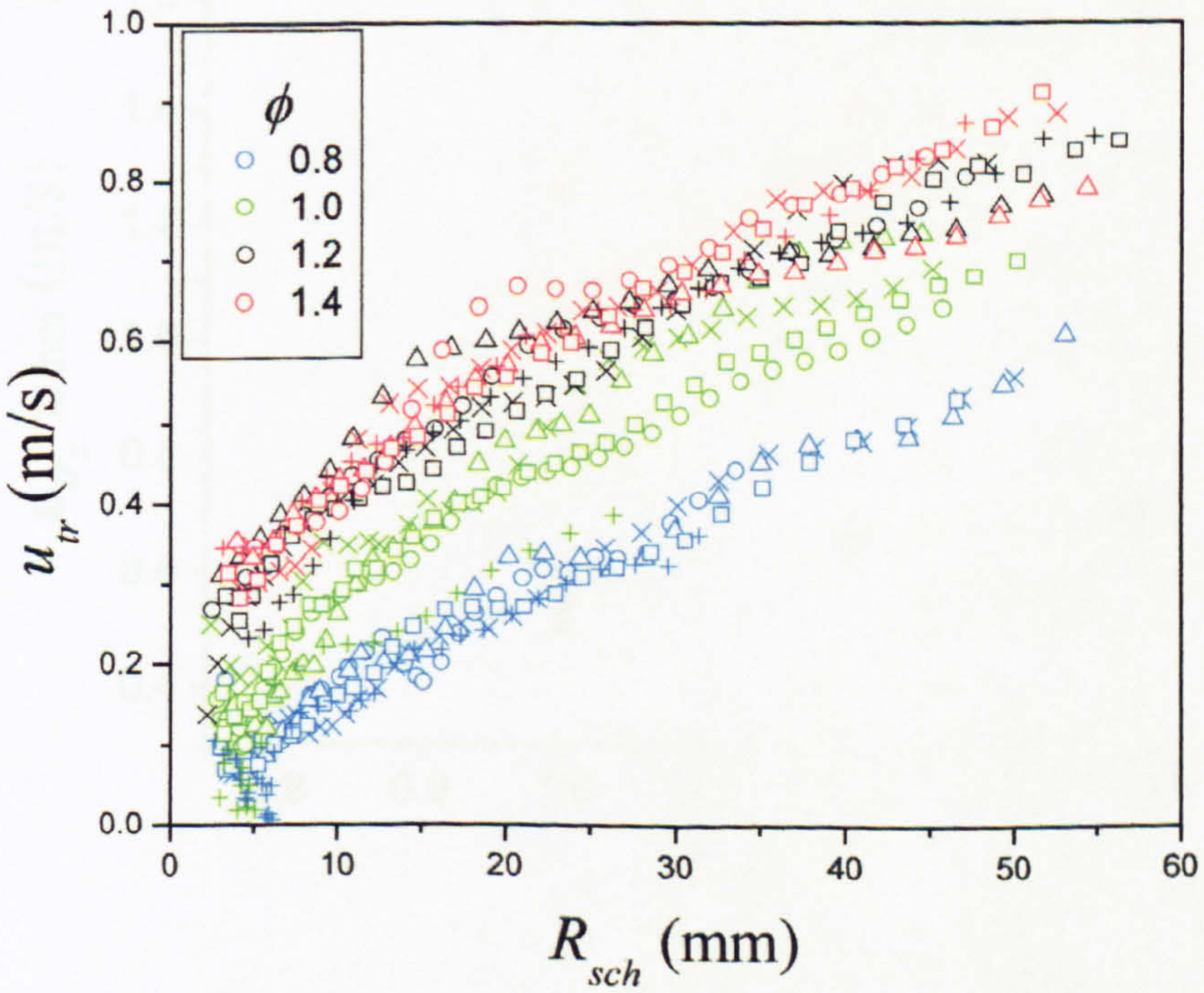

Figure 7.8 Experimental development of iso-octane air flames at 0.1 MPa and 360 K for ϕ 0.8, 1.0, 1.2 and 1.4, where u' = 1 m/s.

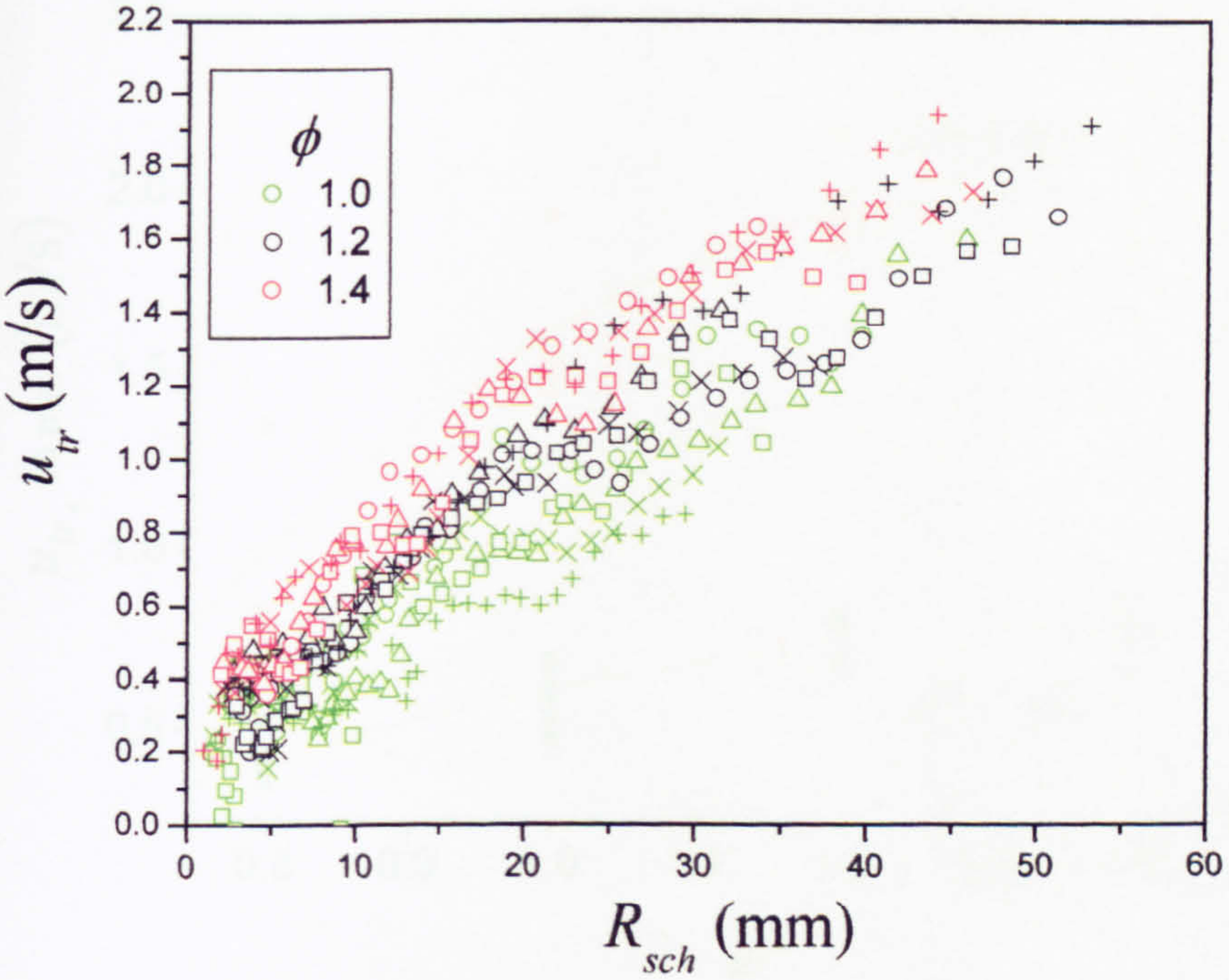

Figure 7.9 Experimental development of iso-octane air flames at 0.1 MPa and 360 K for ϕ 0.8, 1.0, 1.2 and 1.4, where u' = 4 m/s.

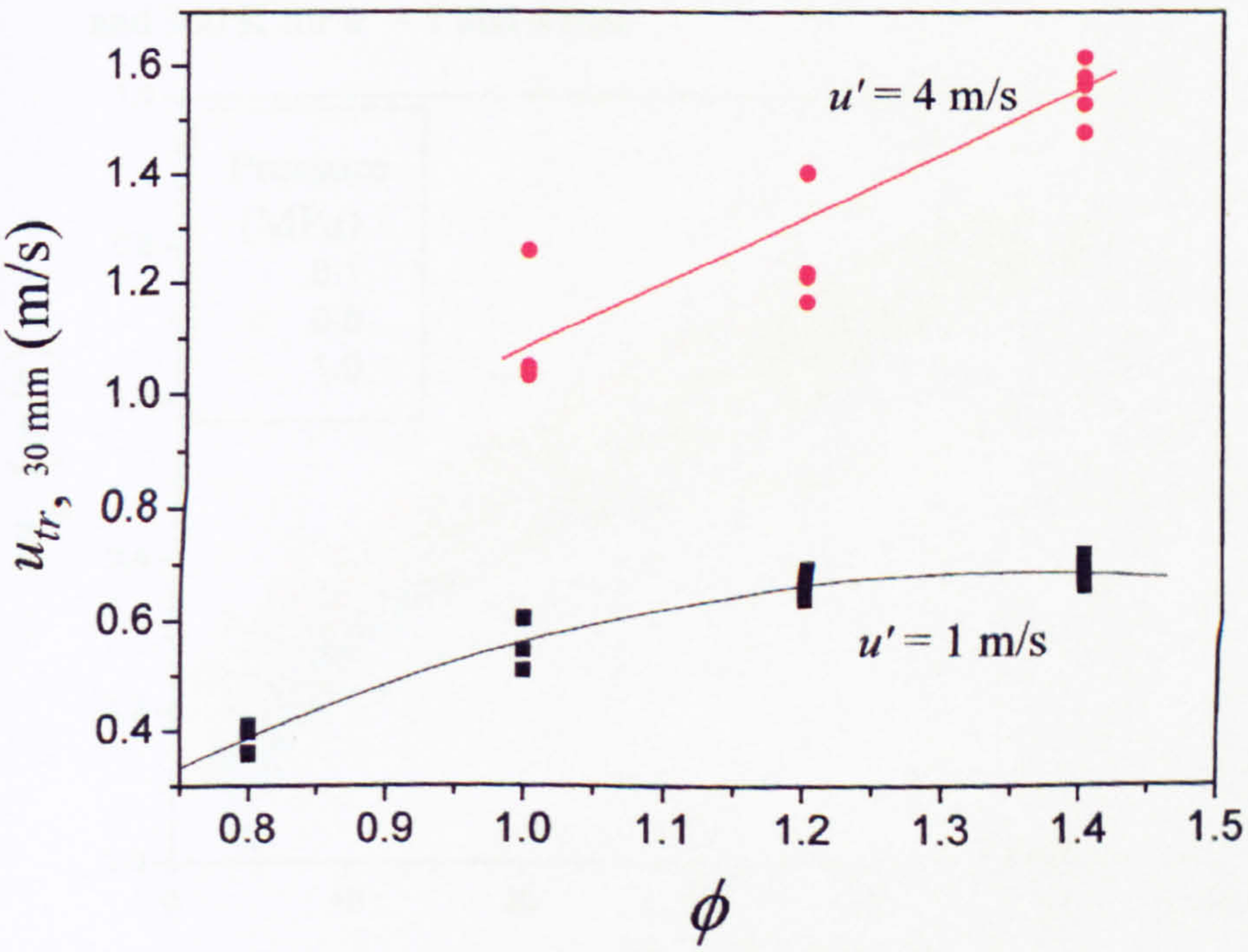

Figure 7.10 Values of the turbulent burning velocity at a schlieren radius of 30 mm, for iso-octane air flames at equivalence ratios of 0.8, 1.0, 1.2, 1.4 at 0.1 MPa and 360 K for u' = 1 and 4 m/s.

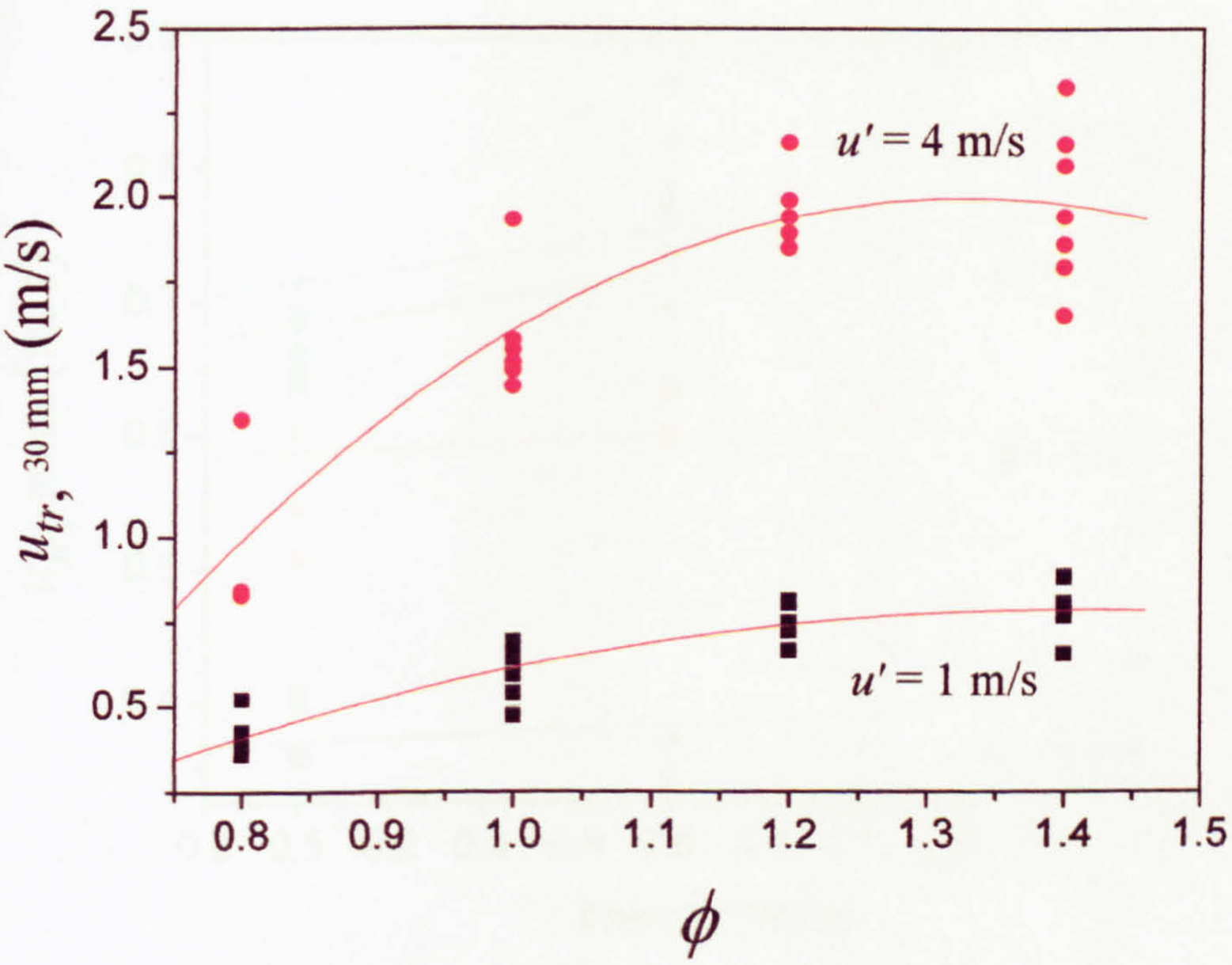

Figure 7.11 Values of the turbulent burning velocity at a schlieren radius of 30 mm, for iso-octane air flames at equivalence ratios of 0.8, 1.0, 1.2, 1.4 at 1.0 MPa and 360 K for u' = 1 and 4 m/s.

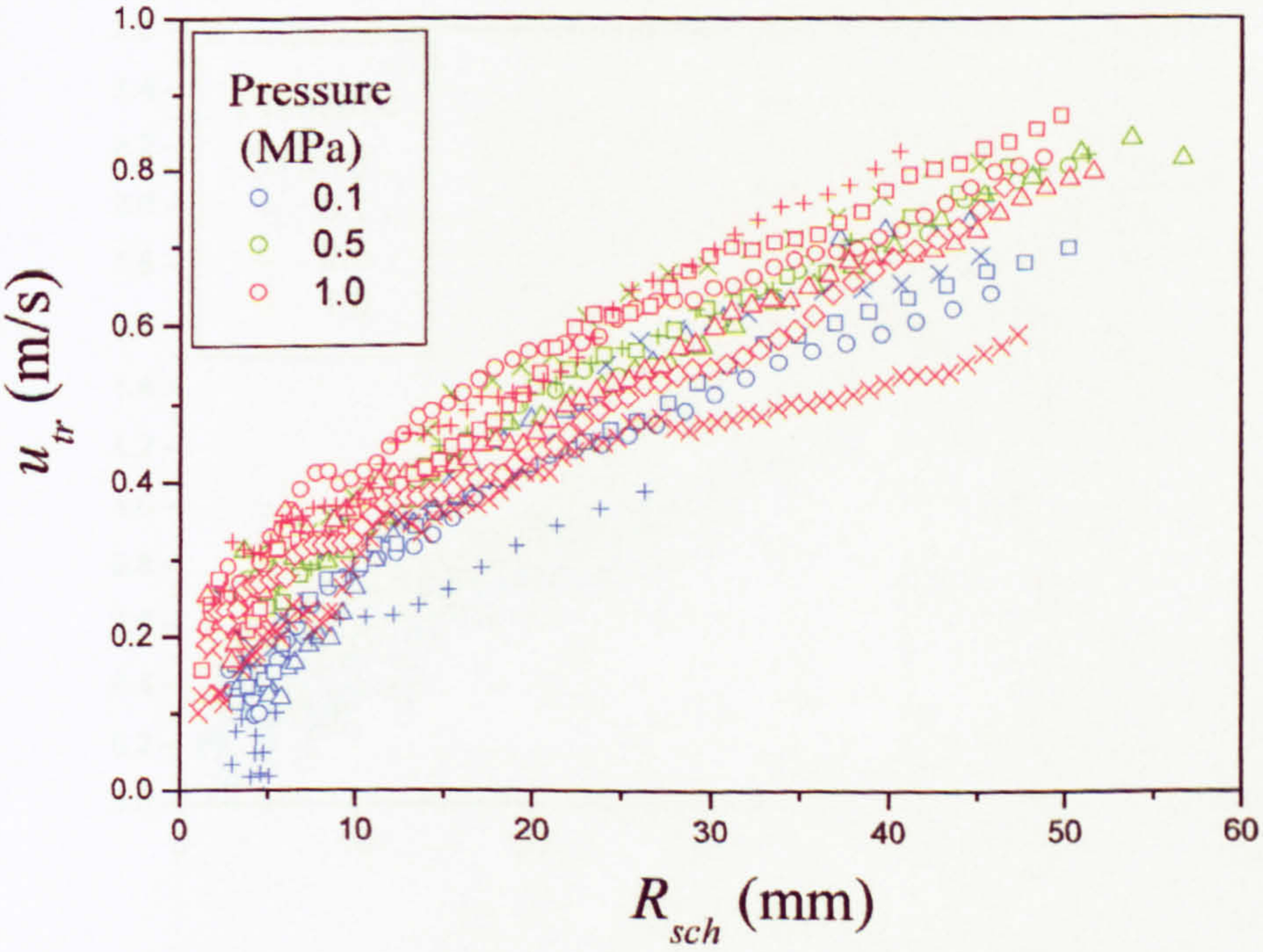

Figure 7.12 Experimental development of iso-octane air flames at ϕ 1.0 and 360 K for pressures 0.1, 0.5, 1.0 MPa, where u' =1 m/s.

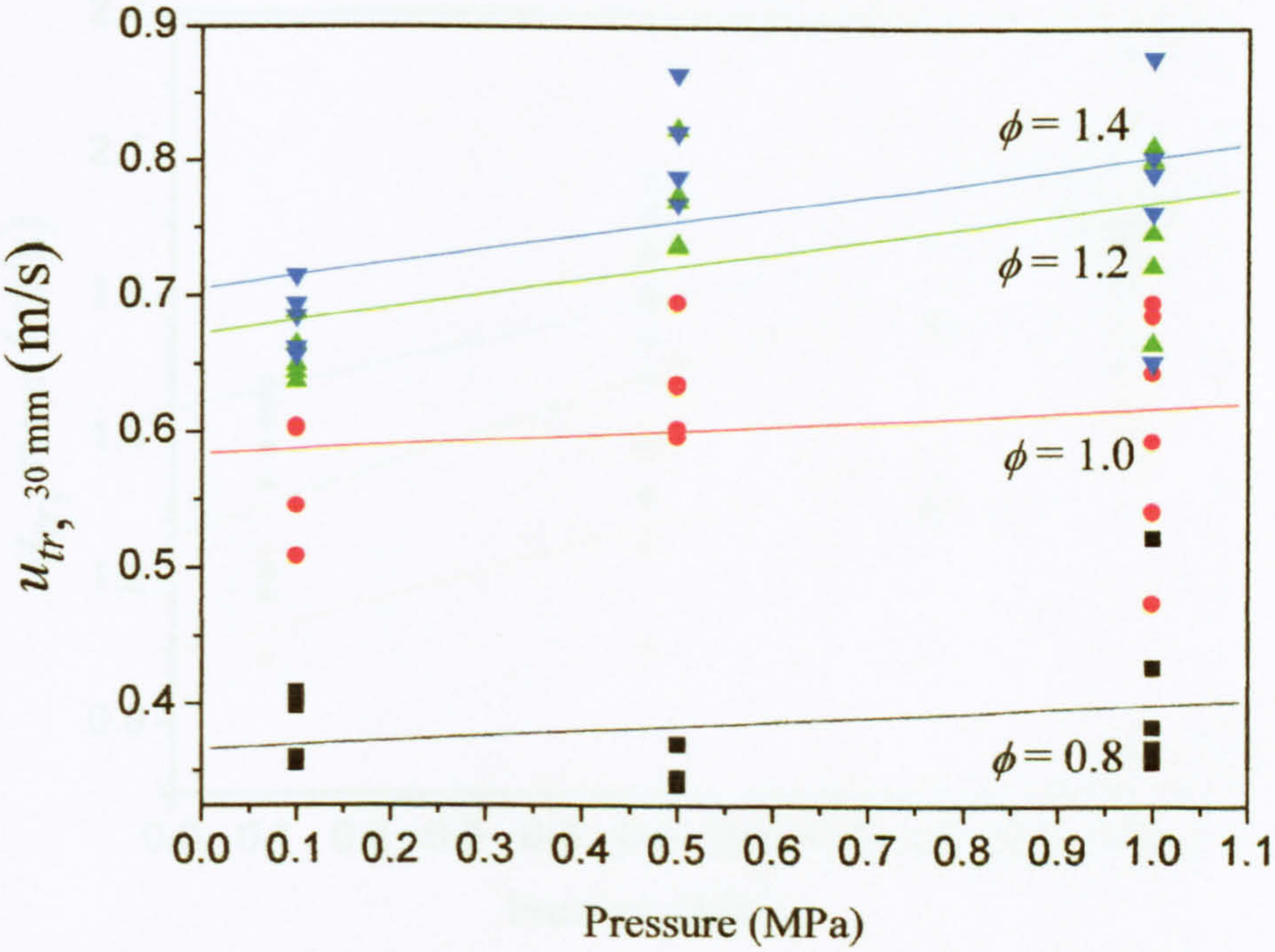

Figure 7.13 Values of the turbulent burning velocity at a schlieren radius of 30 mm, for iso-octane air flames at equivalence ratios of 0.8, 1.0, 1.2, 1.4 at 0.1, 0.5, 1.0 MPa and 360 K for u' = 1 m/s.

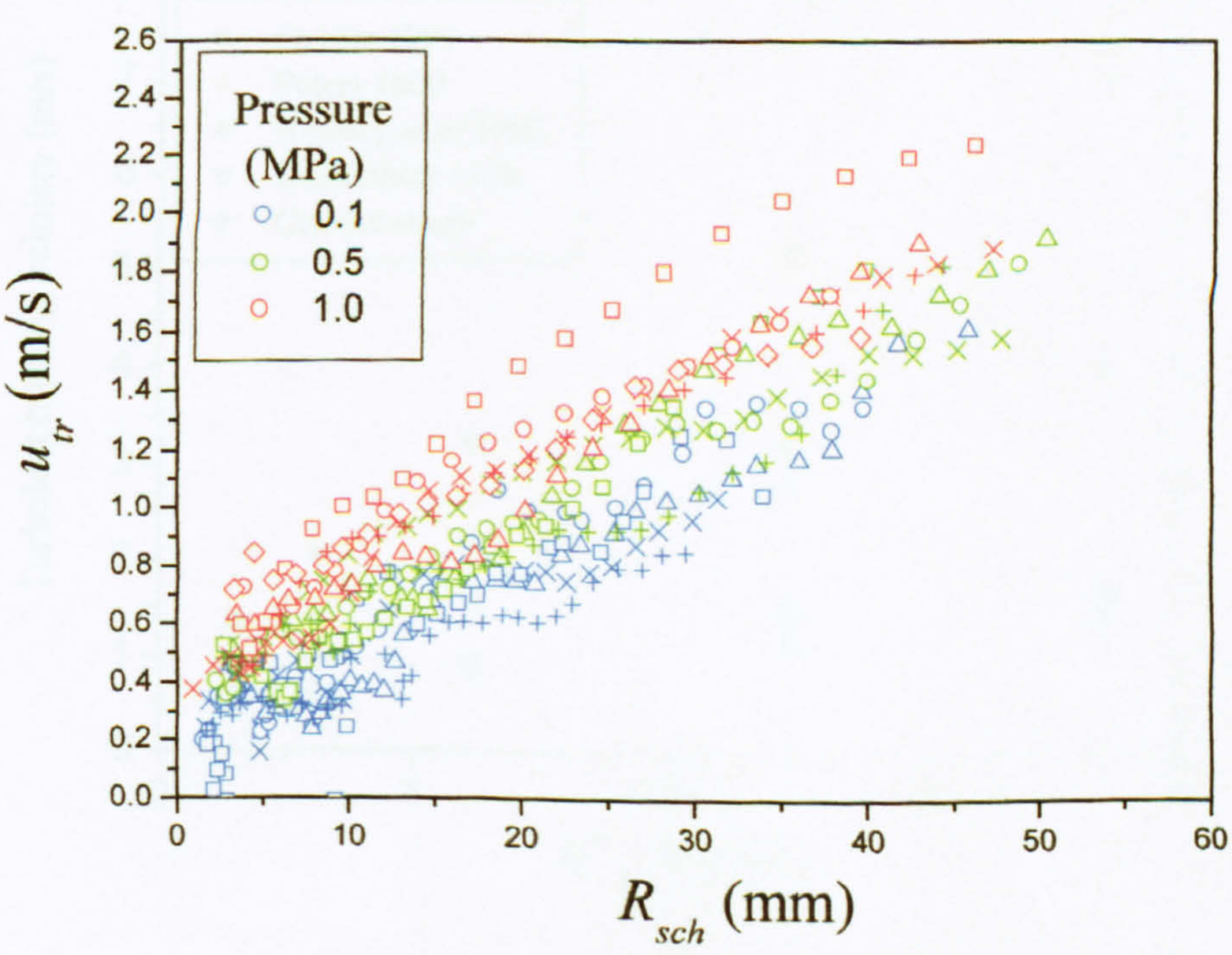

Figure 7.14 Experimental development of iso-octane air flames at ϕ 1.0 and 360 K for pressures 0.1, 0.5, 1.0 MPa, where u' = 4 m/s.

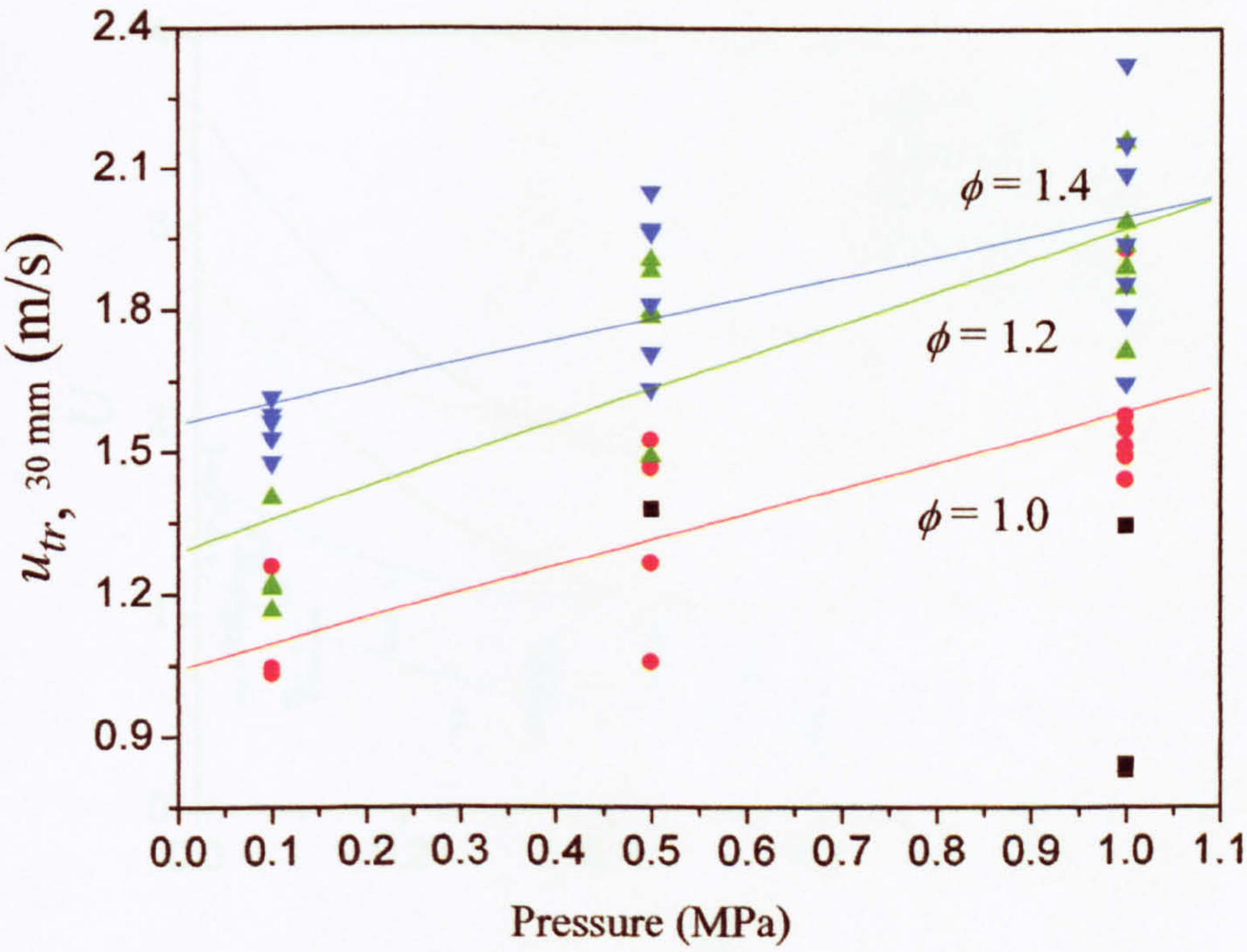

Figure 7.15 Values of the turbulent burning velocity at a schlieren radius of 30 mm, for iso-octane air flames at equivalence ratios of 0.8, 1.0, 1.2, 1.4 at 0.1, 0.5, 1.0 MPa and 360 K for u' = 4 m/s.

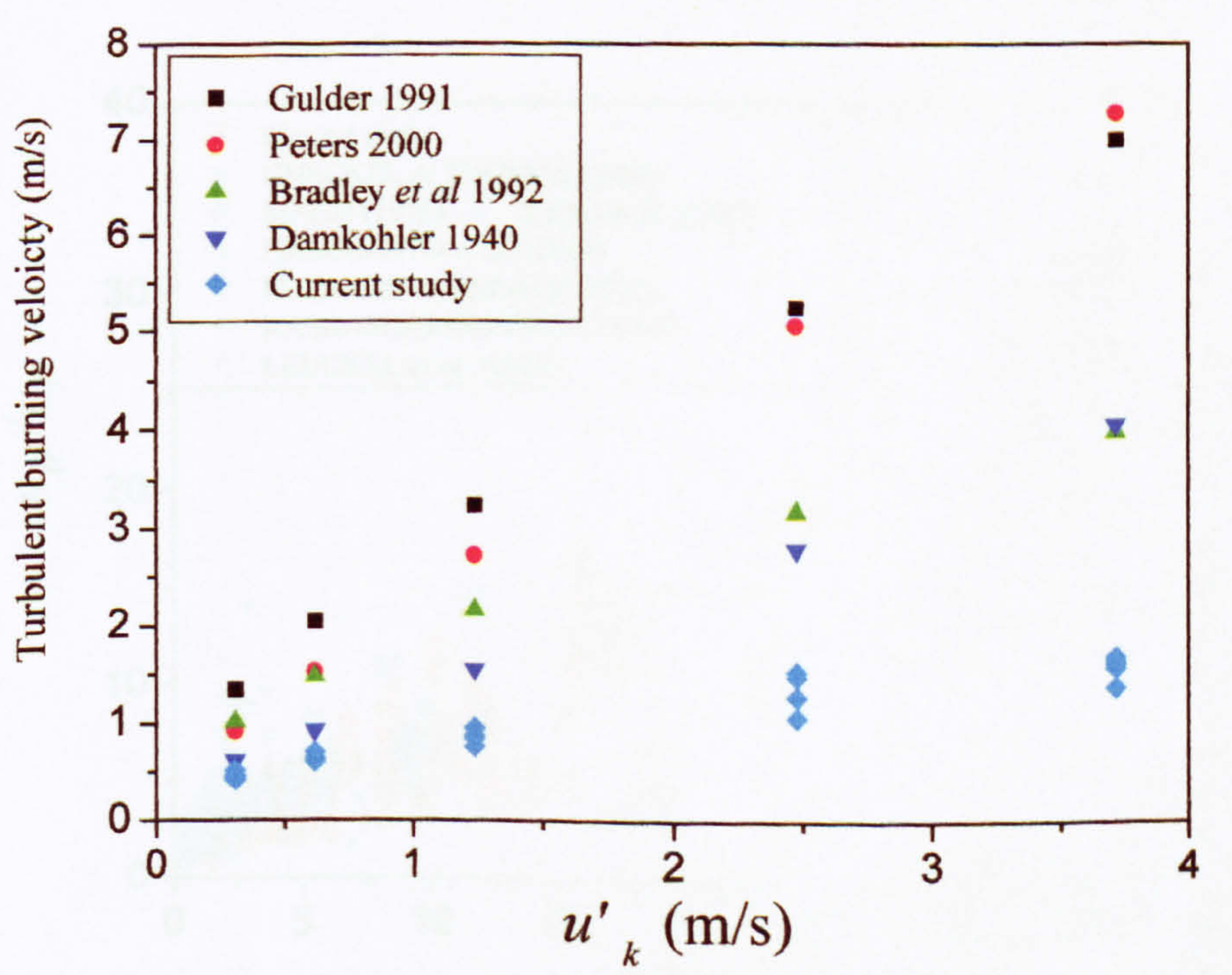

Figure 7.16 Turbulent burning velocity against u'_k comparing theoretical expressions with current study for iso-octane with air at 0.5 MPa and 360 K.

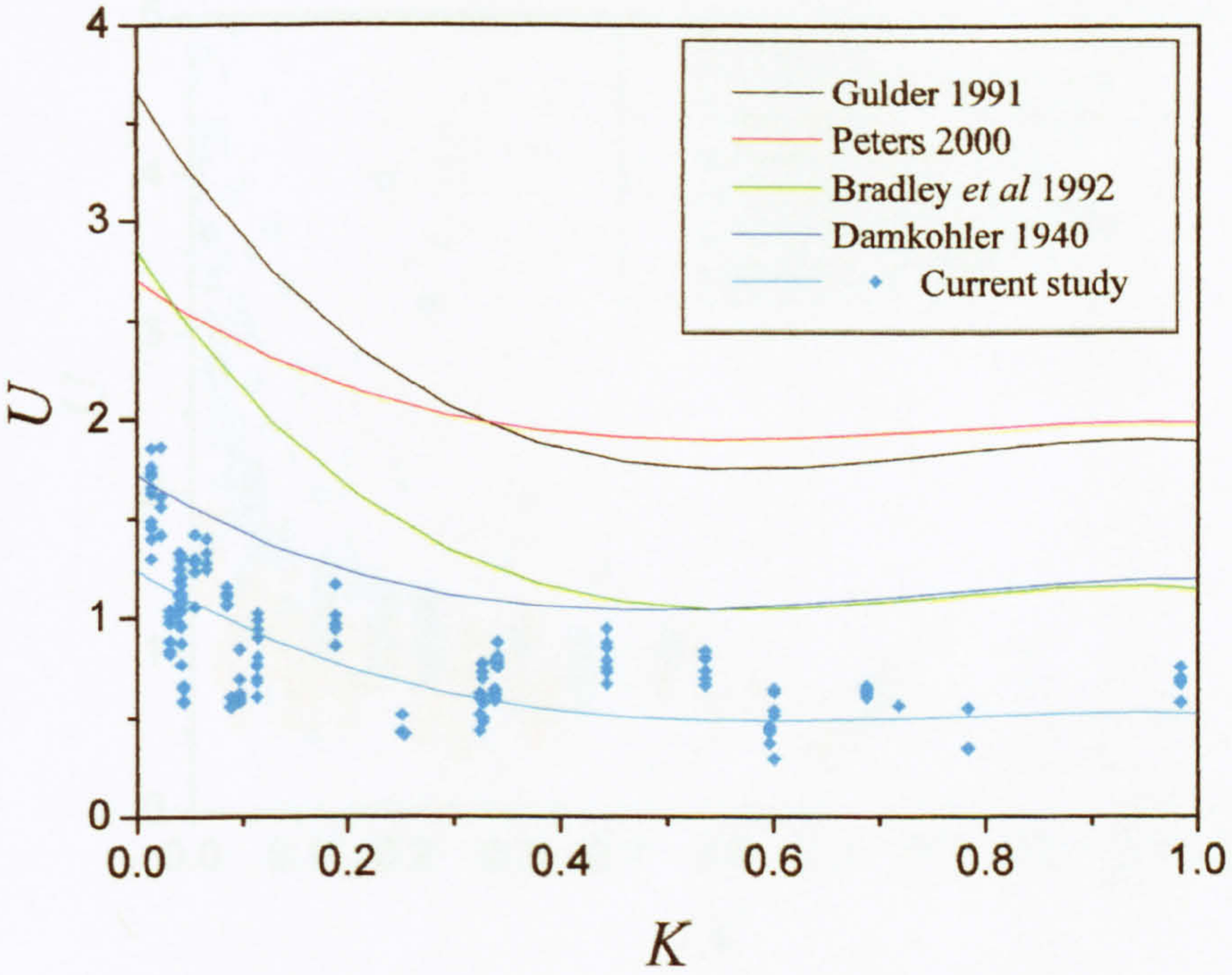

Figure 7.17 Variations in U (u_t/u'_k) against K comparing theoretical expressions with current study; for iso-octane database experiments.

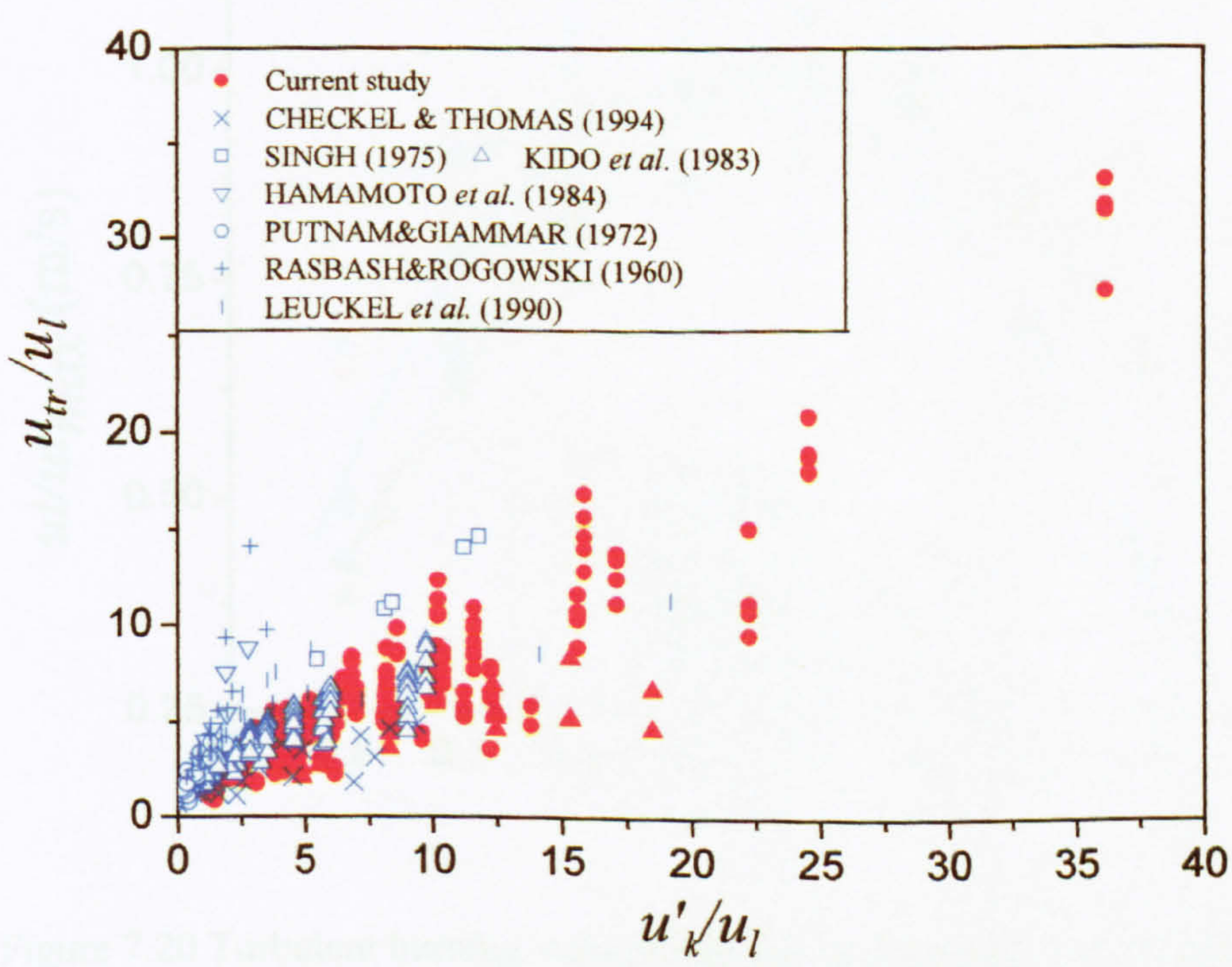

Figure 7.18 All conditions of current study plotted with other workers who have experimentally found u_t based on pressure rise methods.

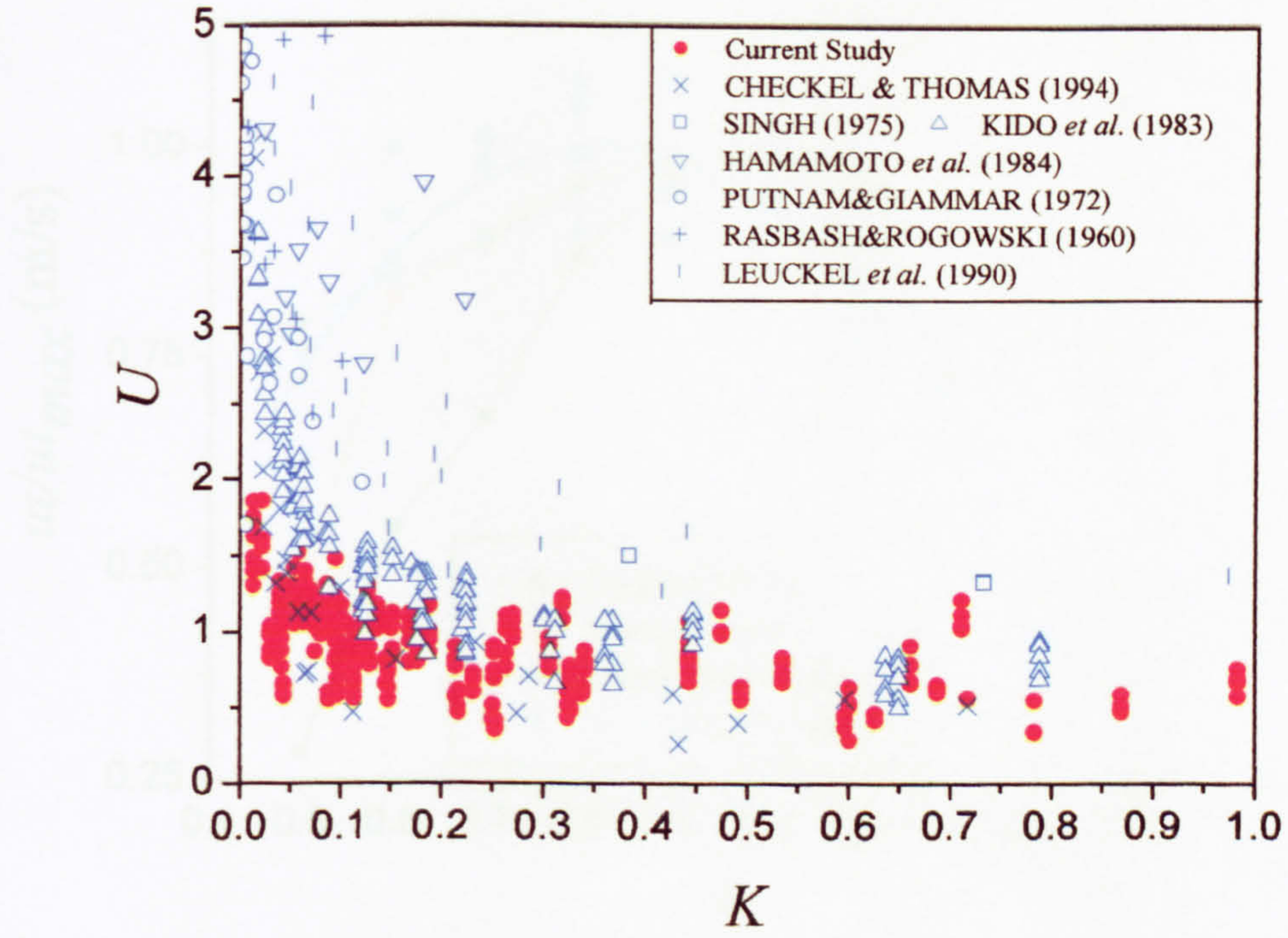

Figure 7.19 All conditions of current study plotted with other workers who have experimentally found u_t based on pressure rise methods.

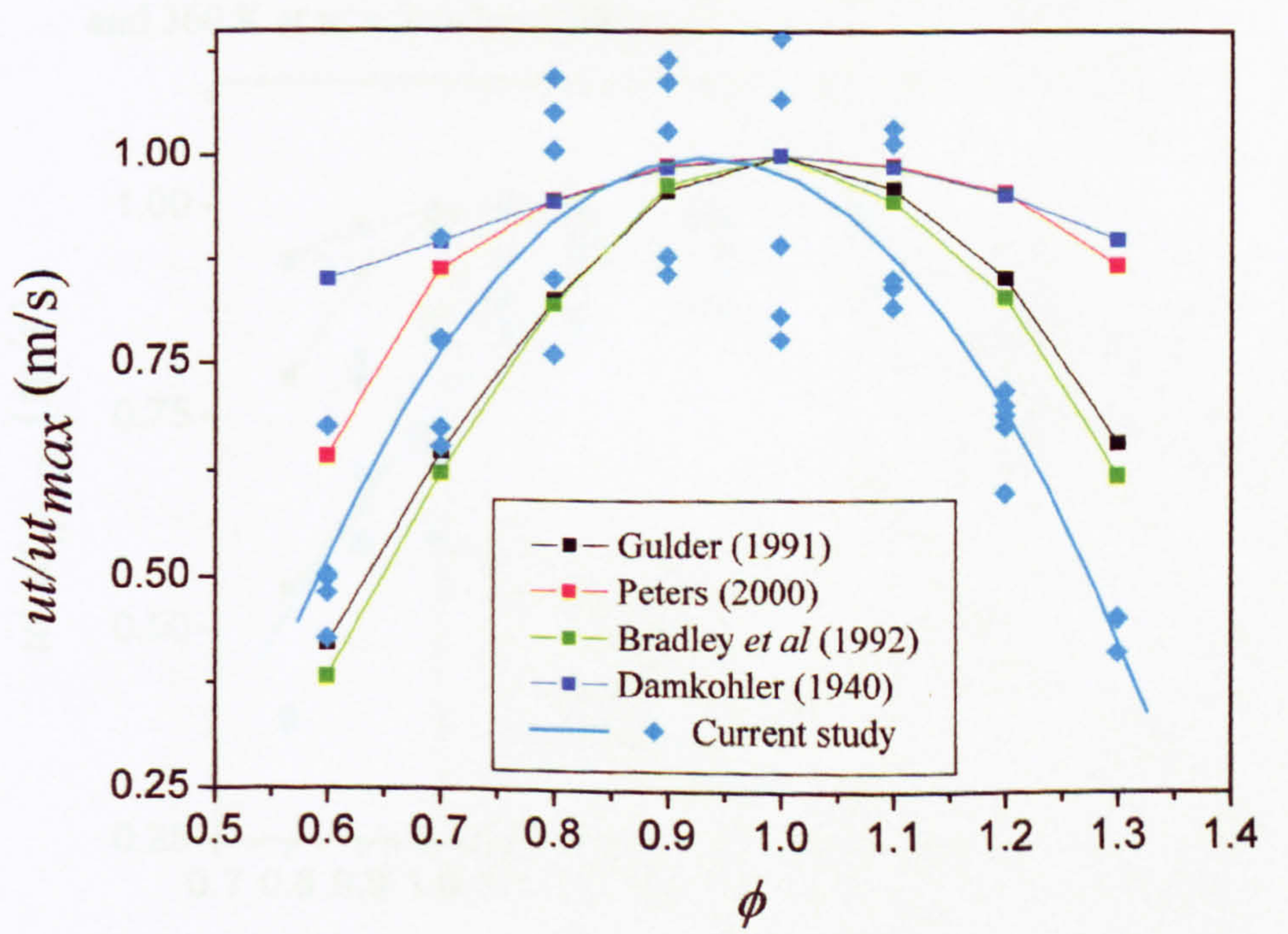

Figure 7.20 Turbulent burning velocity against equivalence ratio comparing theoretical expressions with current study for methane-air at 0.5 MPa and 360 K at $u' = 2$ ($u'_k = 1.24$) m/s.

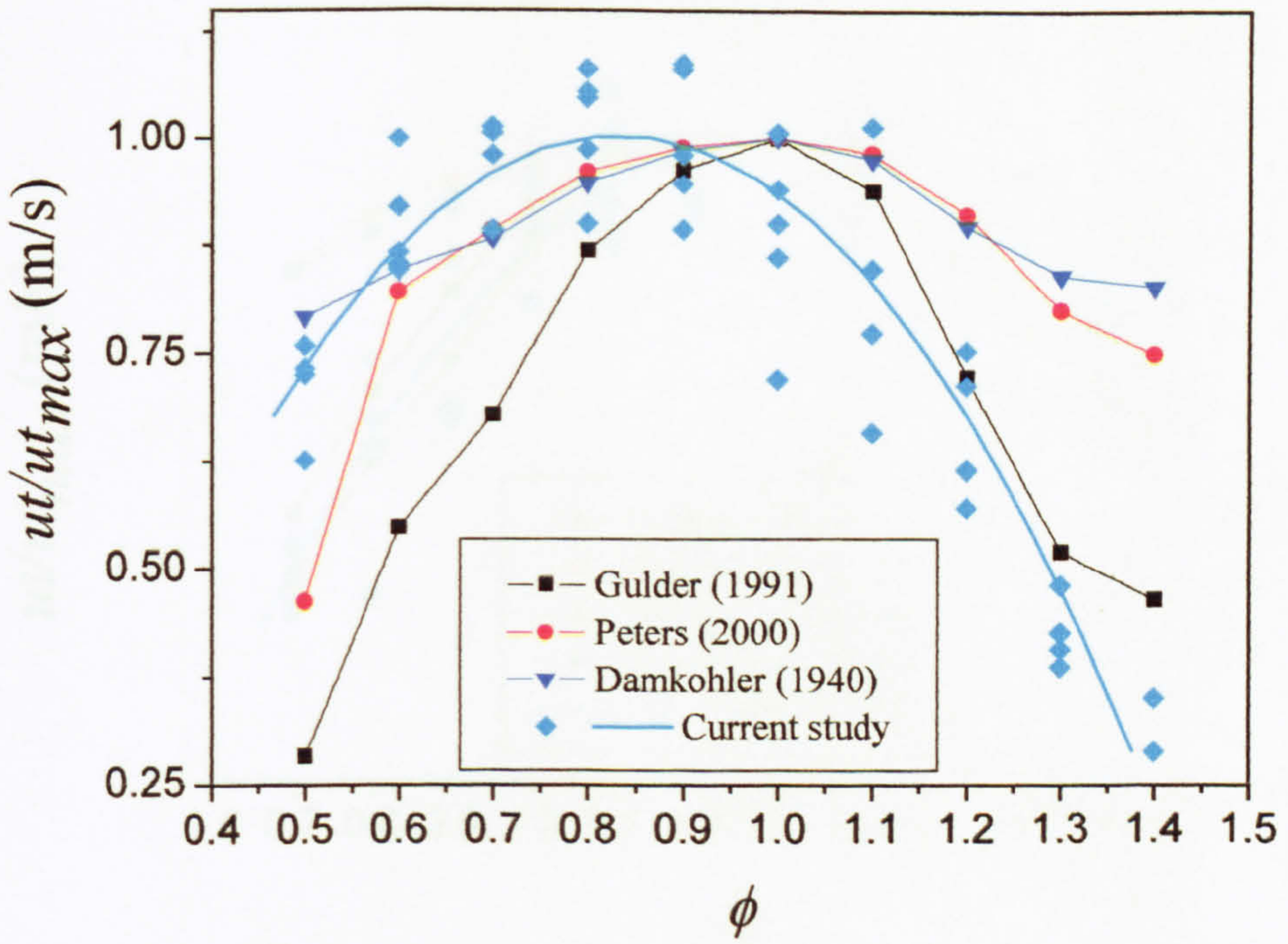

Figure 7.21 Turbulent burning velocity against u'_k comparing theoretical expressions with current study for hydrogen (30%) and methane (70%) with air at 0.5 MPa and 360 K at $u' = 2$ ($u'_k = 1.24$) m/s.

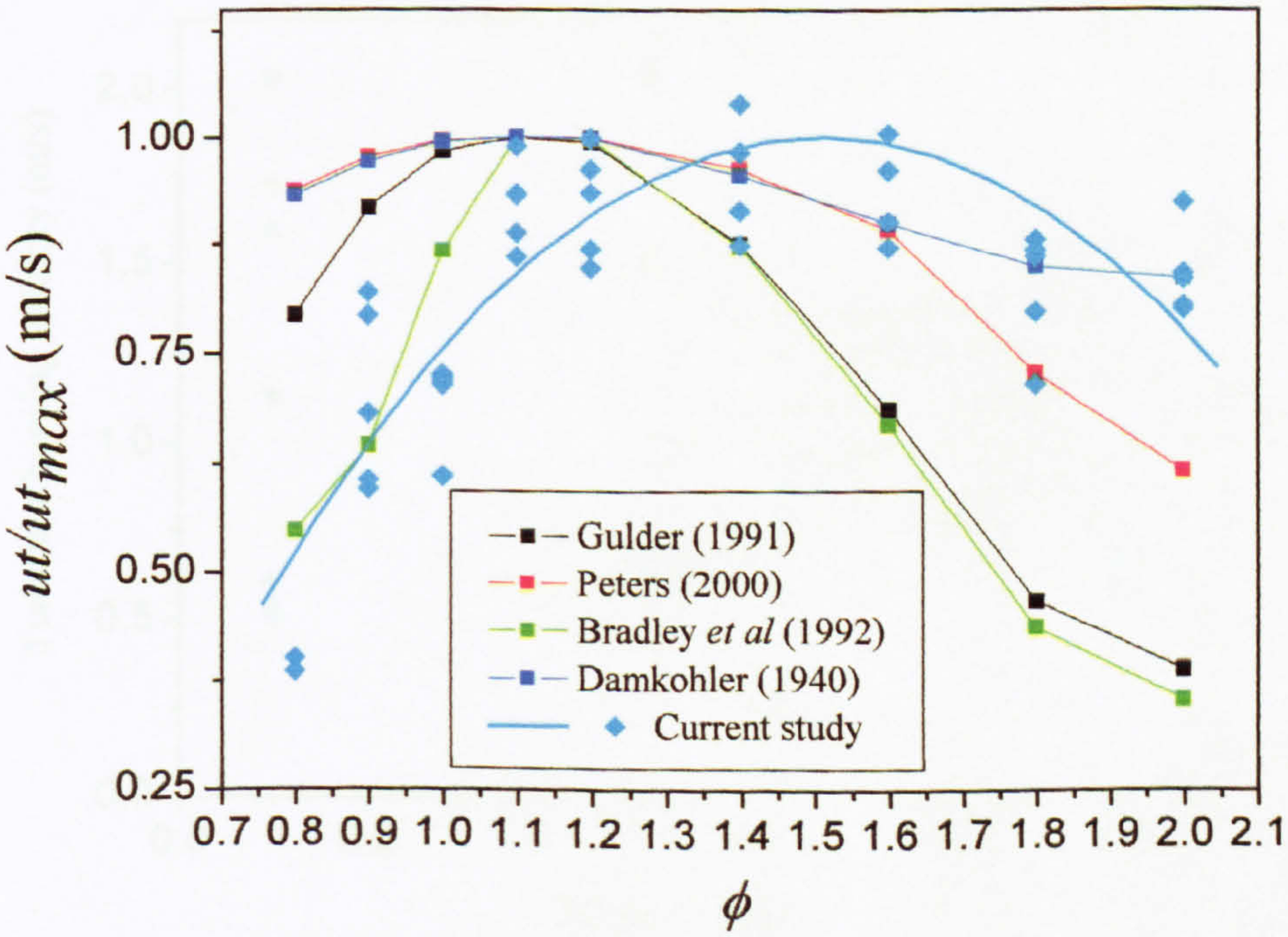

Figure 7.22 Turbulent burning velocity against equivalence ratio comparing theoretical expressions with current study for iso-octane with air at 0.5 MPa and 360 K, at $u' = 2$ ($u'_k = 1.24$) m/s.

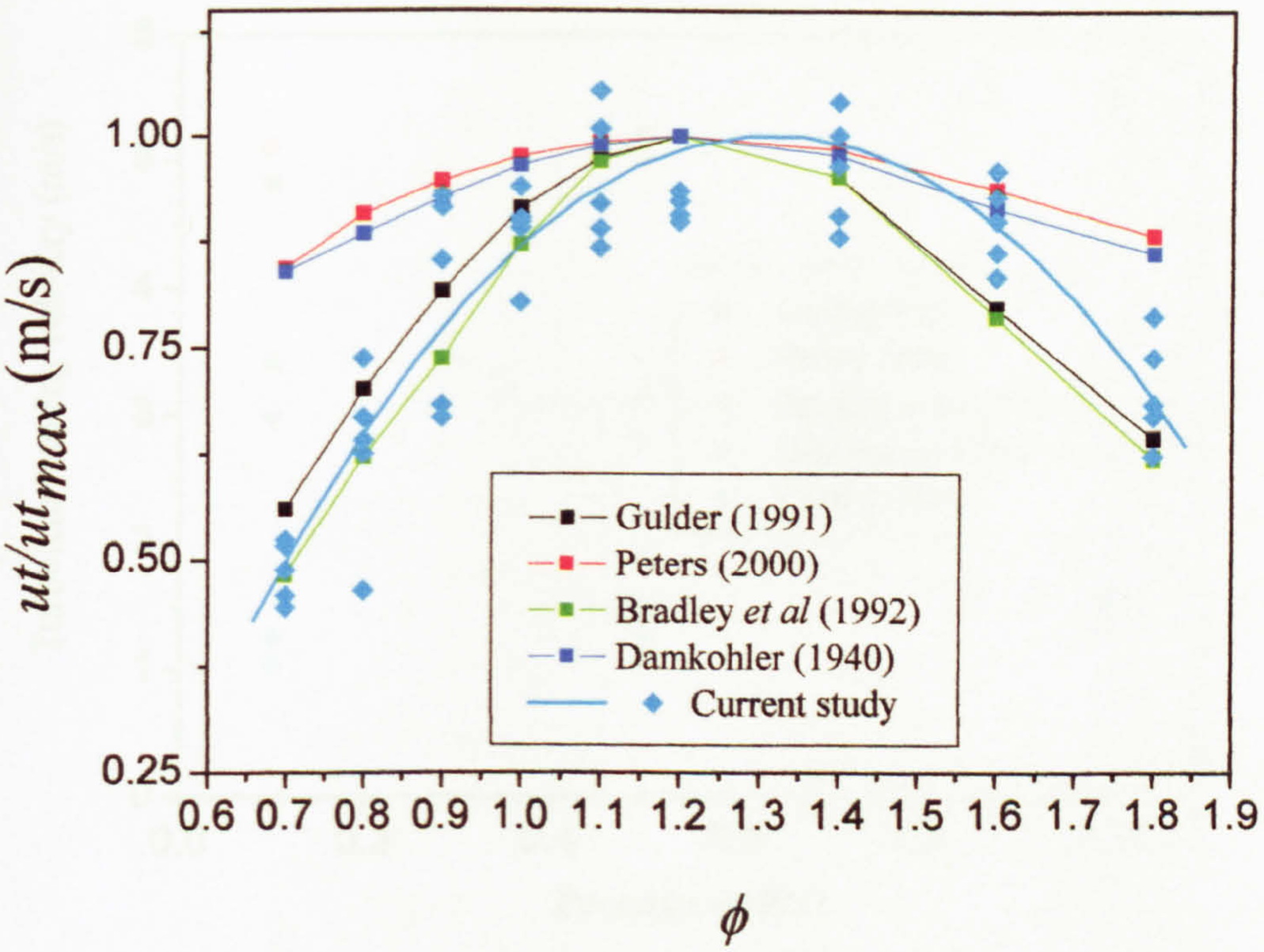

Figure 7.23 Turbulent burning velocity against equivalence ratio comparing theoretical expressions with current study for methanol-air at 0.5 MPa and 360 K at $u' = 2$ ($u'_k = 1.24$) m/s.

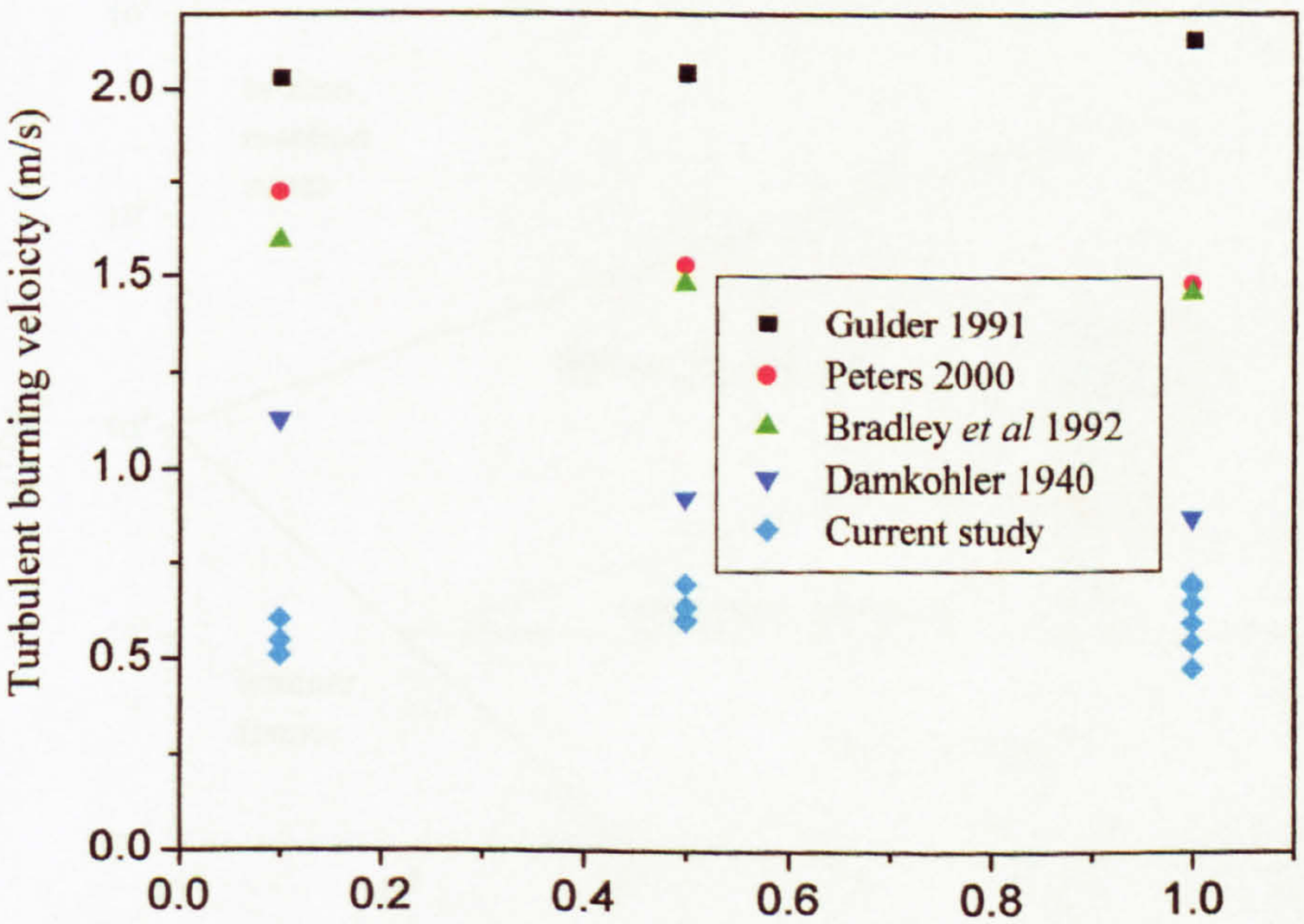

Figure 7.24 The turbulent burning velocity against pressure comparing theoretical expressions with current study for iso-octane air $\phi = 1$, 360 K, $u' = 1$ ($u'_k = 0.62$) m/s.

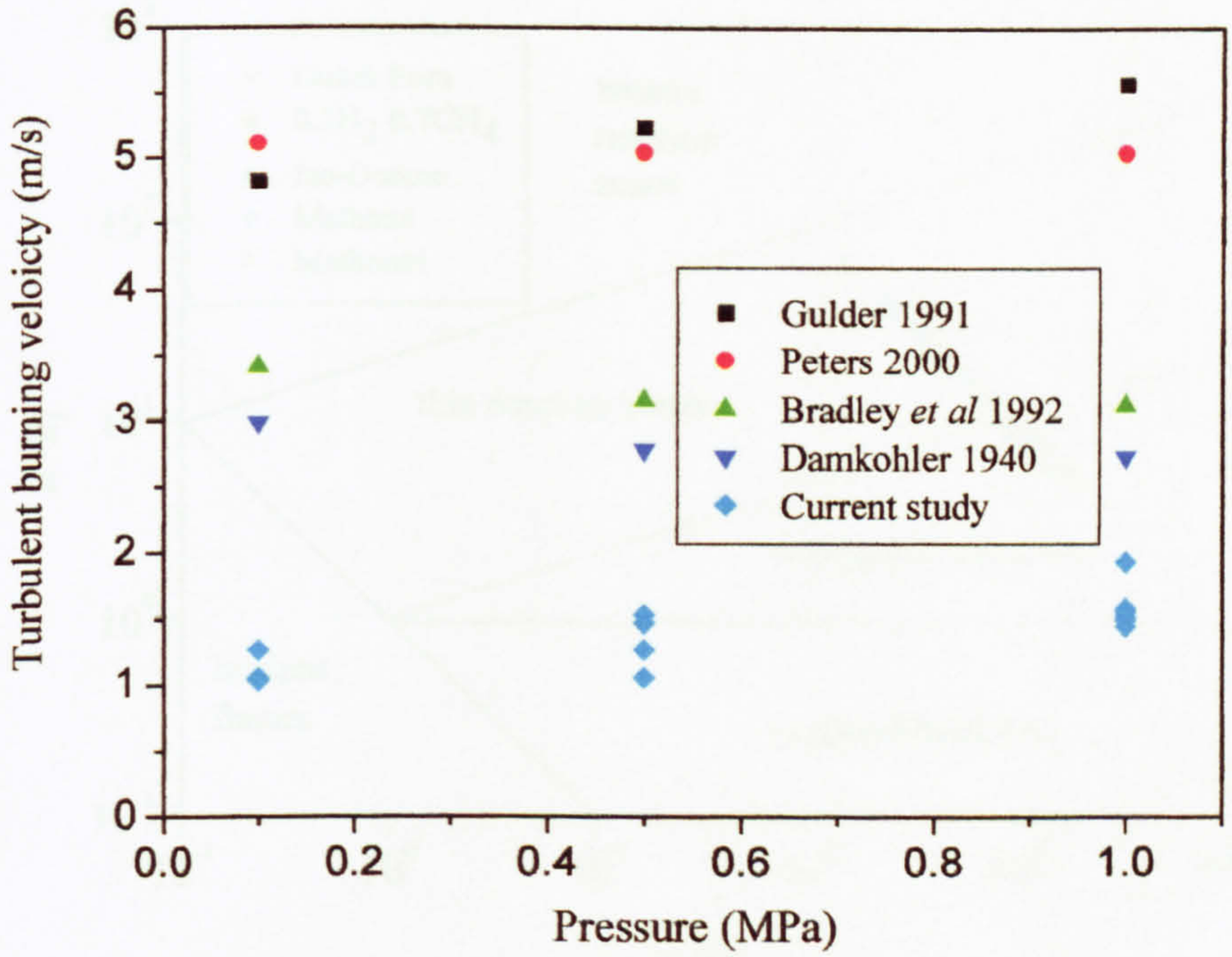

Figure 7.25 The turbulent burning velocity against pressure comparing theoretical expressions with current study for iso-octane air $\phi = 1$, 360 K, $u' = 4$ ($u'_k = 2.48$) m/s.

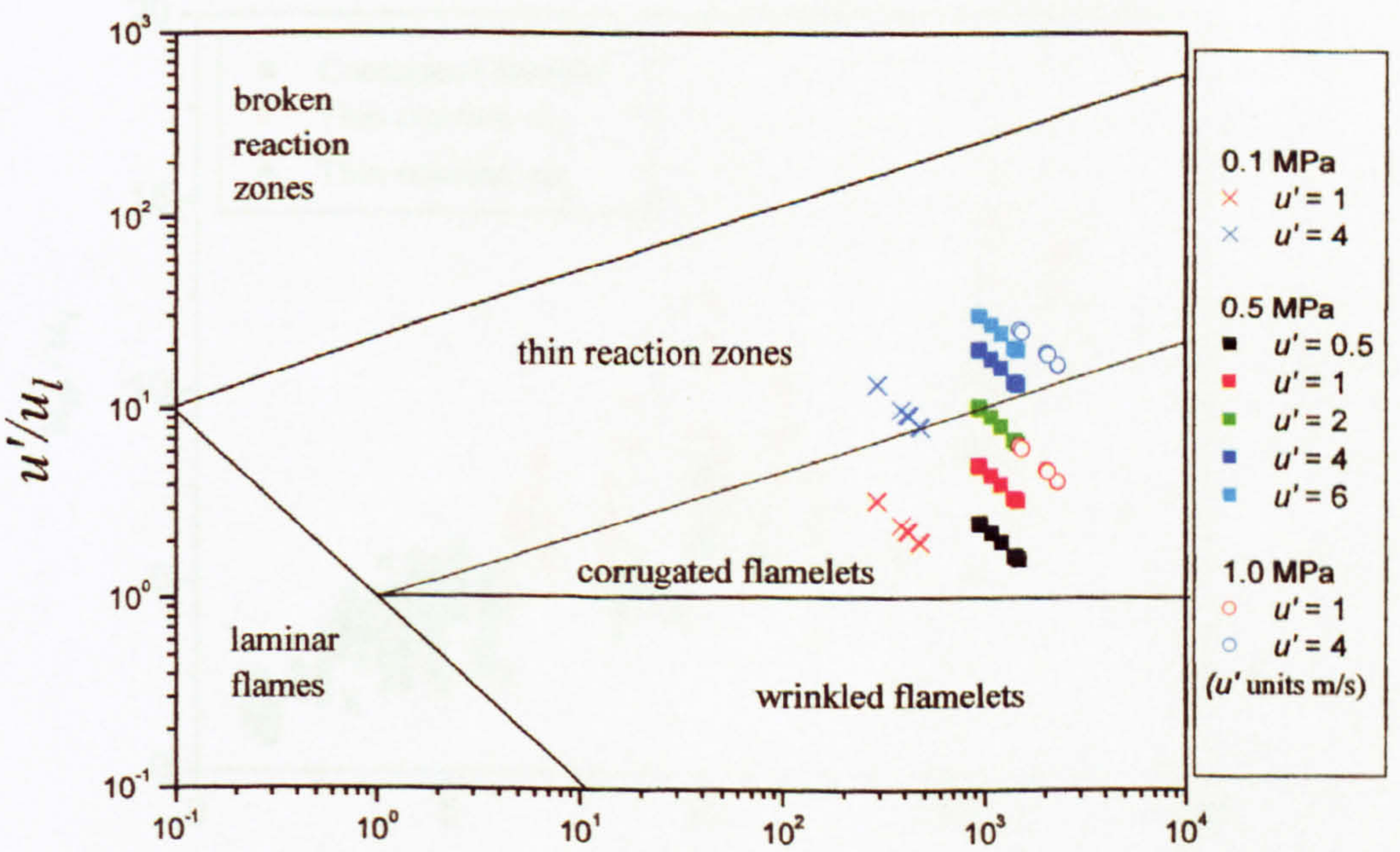

Figure 7.26 Regime diagram for premixed combustion. Iso-octane database conditions shown at 360 K.

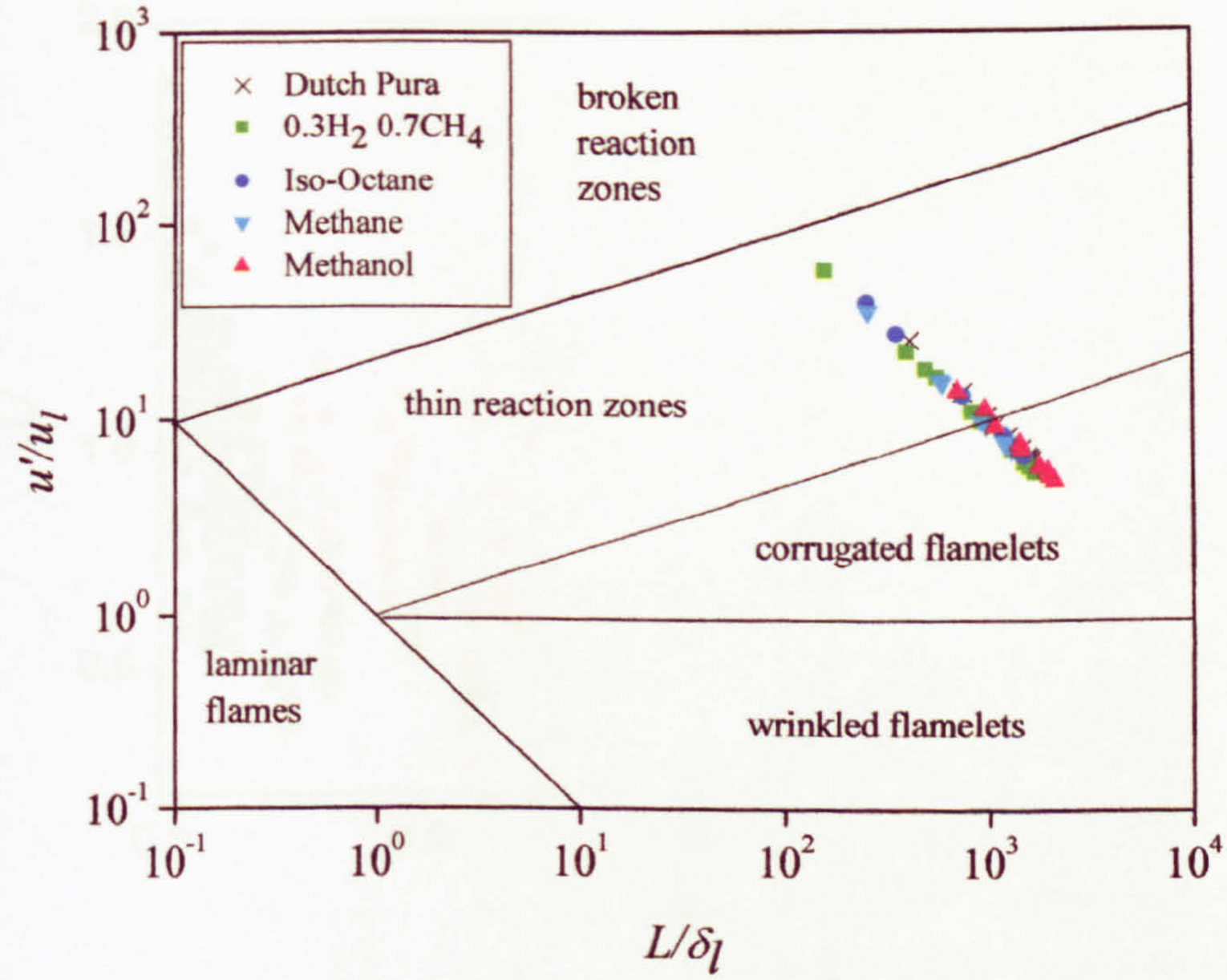

Figure 7.27 Regime diagram for premixed combustion. Five fuels shown (those discussed in chapter 6) at 0.5 MPa 360 K and $u' = 2$ ($u'_k = 1.24$) m/s.

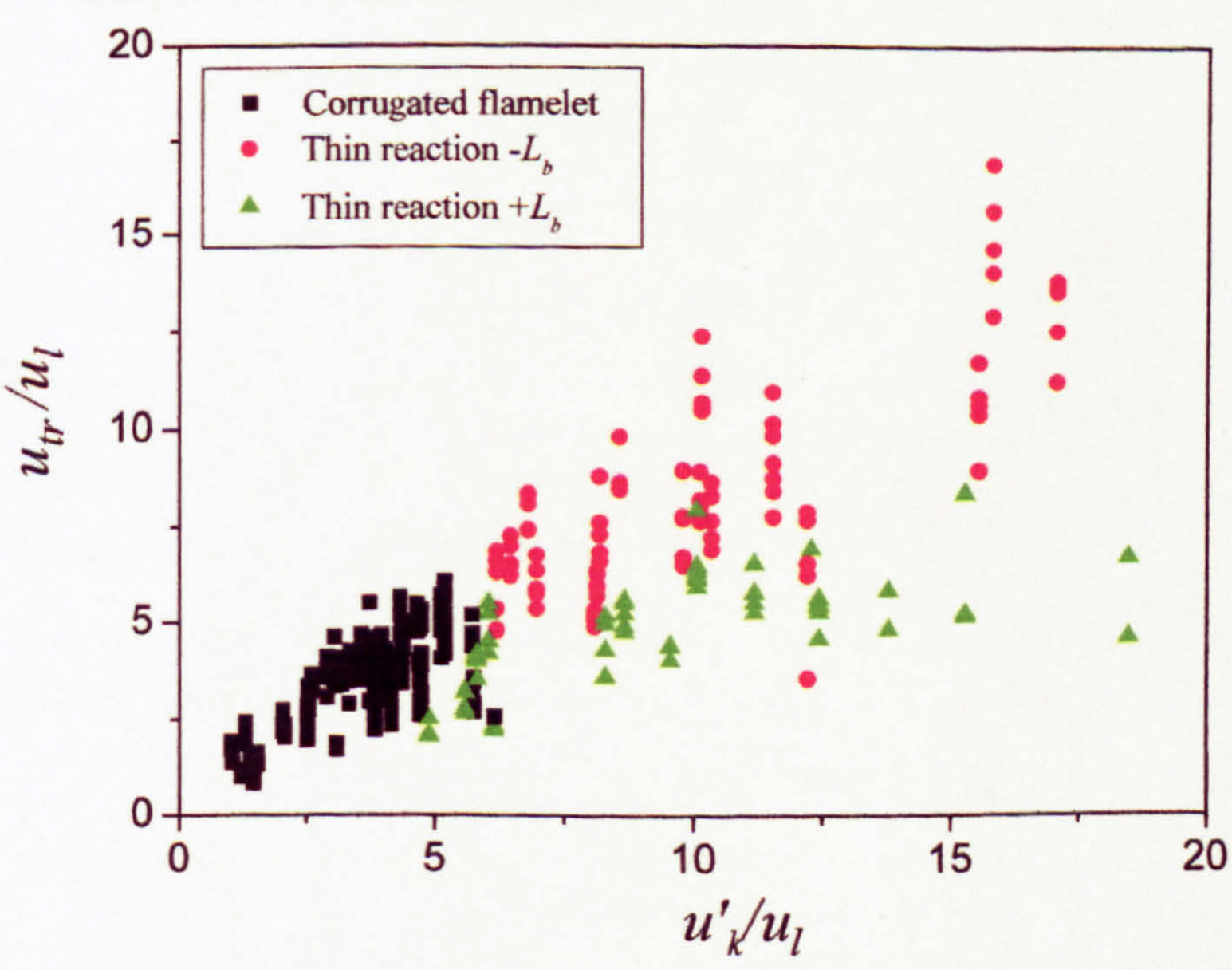

Figure 7.28 The turbulent burning velocity u_{tr} at 30 mm for turbulent conditions of current study plotted against u'_k, both axis have been normalised by u_l. Conditions have been classified using regime diagrams Figs 7.17, 71.8. Flames, which are in the thin reaction zone, have been shown separately for those experiments with negative and positive Markstein Lengths.

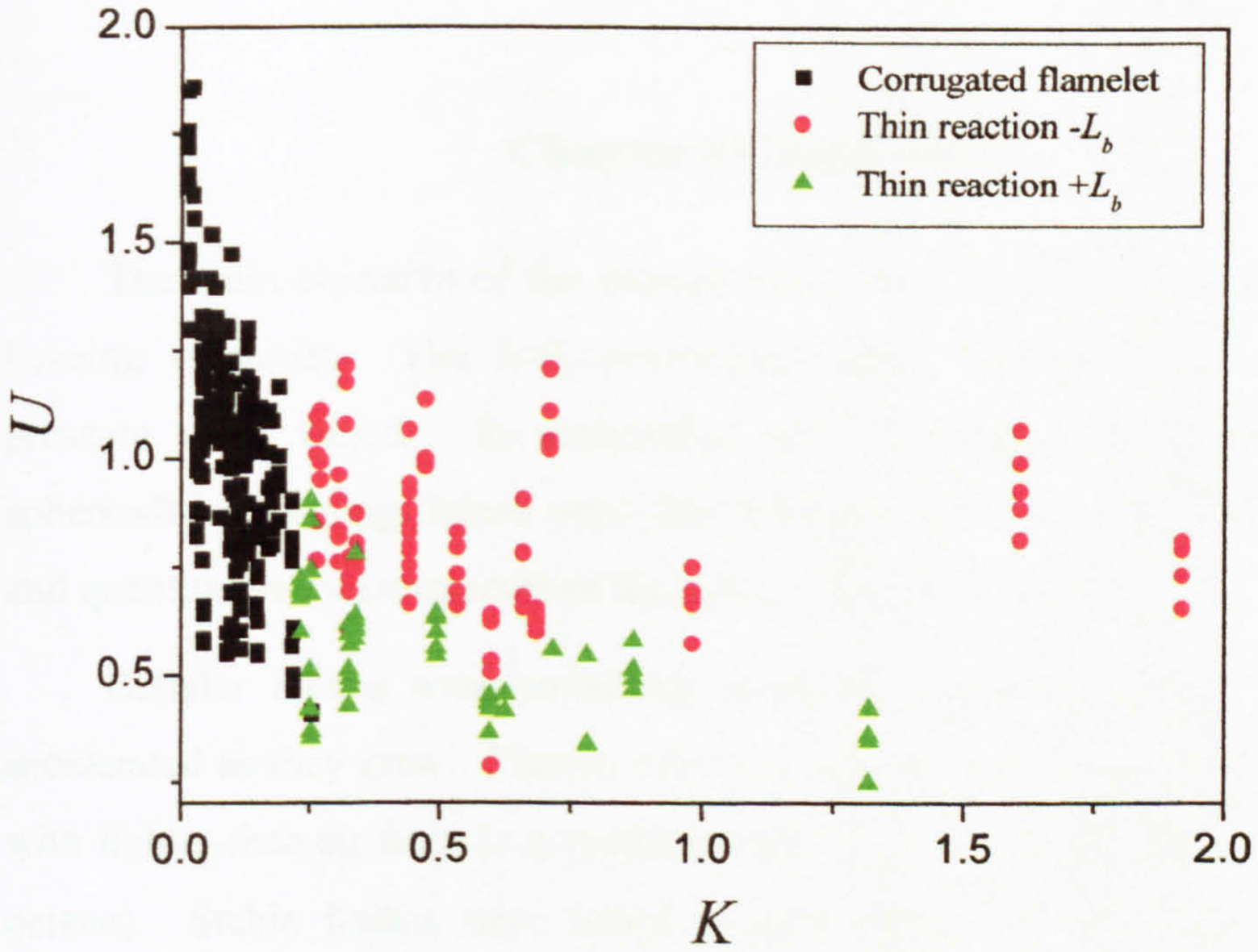

Figure 7.29 Variations in U (u_t/u'_k) against K. Flames, which are in the thin reaction zone, have been shown separately for those experiments with negative and positive Markstein Lengths

Chapter 8 Conclusions

The main objective of the present work was to obtain well defined turbulent burning velocities. The fuel, equivalence ratio, turbulence r.m.s velocity and pressure were varied. In association with each turbulent condition, laminar spherically expanding flames were also filmed to obtain laminar burning velocities and quantitative measurements of the flame response to stretch.

Cellular flames were commonly reported at higher pressures, such flames accelerated as they grew. Flames were found to be increasingly cellular when lean with lighter-than-air fuels (e.g. methane) and when rich with heavier fuels (e.g. iso-octane). Stable flames were found to have positive Markstein lengths, cellular flames consistently had increasingly negative values. The propensity for cellularity was found to be related to the Markstein number. Buoyant flames had a reduction in surface cellularity, possibly as a result of stretch.

A large variation in measured u_l's were found over the range of equivalence ratios tested at 0.5 MPa. The peak burning velocity was found at $\phi = 1$ for methane and 30% hydrogen 70% methane, $\phi = 1.1$ for iso-octane and the gasoline (dutch-pura) and $\phi = 1.2$ for methanol. Either side of the peak for each fuel the burning velocity reduced. Iso-octane and the gasoline had very similar values of u_l, which adds support to the use of iso-octane to represent gasoline in combustion research. The gasoline was slightly faster than iso-octane at the peak by around 1 cm/s, this difference was also measurable moving lean, richer values were indistinguishable with the current experimental limits.

Iso-octane laminar flames were also studied over a range of pressures for a limited number of equivalence ratios. The increase in pressure resulted in a reduction in the value of u_l for all equivalence ratios.

Measurements of the Markstein length L_b were generally very repeatable. Increasing pressure reduced L_b. The effect of equivalence ratio on L_b was found to

be dependent upon the fuel, the lighter than air fuels had increasingly negative values of L_b moving lean, whilst heavy fuels became more negative moving rich.

Where it was possible measured values of u_l were compared to those reported in the literature;

1. The power law presented by Metghalchi and Keck (1982) allowed a comparison for iso-octane and methanol to be made. Atmospheric pressure measurements were far lower than those predicted by Metghalchi and Keck. At higher pressures values of u_l for iso-octane compared remarkably well from at 0.5 MPa $\phi = 0.8$ to 1.4 and 1.0 MPa $\phi = 0.8$ and 1.0.

2. Agreement was found with the iso-octane measurements of Bradley *et al.* (1998) which were performed at identical conditions in the same vessel.

3. The laminar burning velocities of methanol, which is commonly used in automotive engines, were also compared with the Metghalchi and Keck (1982) power law at 0.5 MPa 360 K from $\phi = 0.5$ to 1.8. The peak burning velocity was experimentally found to be 0.1 of an equivalence ratio richer than the prediction. The measured values of u_l were lower than predicted values from $\phi = 0.5$ to 1.3, richer than $\phi = 1.3$ the values from this study were substantially greater.

Spherically centrally ignited expanding flames have been studied in a turbulent flow to gain turbulent burning velocities defined as u_{tr}, which characterises the mass rate of burning. The turbulent flames developed and so had no unique value of burning velocity (i.e. the burning velocity increased whilst being measured). The method developed by Bradley *et al.* (2003) was used in conjunction with an established technique based on experimental pressure rise presented by Lewis and Von Elbe. The consistency between the values derived using the two techniques (schlieren and pressure), for all fuels and pressures for both fuel lean and rich mixtures, proved very good. In this study the ratio u'/u_l reached 36 which is greater than the flames studied by Bradley *et al.* (2003) where $u'/u_l < 15$, the agreement between the two methods not only confirmed the technique but extended its experimental range.

The effective turbulence intensity, u'_k, was calculated using the flame diameter, whereas previous workers used time from ignition. At equal radii the flames were found to be equally developed, at a radius of 30 mm (where $u'_k = 0.62$ u') was chosen to make comparisons between experimental results and those of other workers.

A study of cycle to cycle turbulent burning velocity variation was completed. At four experimental conditions twenty tests were repeated. The data was re-interpolated and mean and covariance values were obtained for flame radii. Covariance was found to reduce with flame size. Covariance between the conditions was similar in order despite a doubling of r.m.s turbulence velocity and equivalence ratio variation from 0.8 to 1.4. Typically in the rest of this study five turbulent deflagrations were performed at each condition, the 'cycle to cycle' data set was compared to the five tests repeated at the same conditions. The mean of the five experiments was slightly lower than those of the larger data set (typically 10 %). This uncertainty is applied to turbulent measurements within the present study.

The peak turbulent burning velocity often occurred at different equivalence ratios than the laminar burning velocity. The ratio, u_{tr}/u_l was much higher for lean lighter than air fuels (methane and 30% hydrogen 70% methane), and when rich for heavier fuels (iso-octane and gasoline) than for other turbulent flames. These flames burned much more rapidly than might be expected on the basis of their corresponding values of u_l. Also their measured values of Markstein number were either zero or negative. Flames with a positive Markstein number generally produced values of $u_{tr}/u_l \approx 4$ (all fuels gave this value at $\phi = 1.1$ to 1.2). The ratio, u_{tr}/u_l showed a strong dependency on the laminar response to flame stretch, flames with negative values of L_b exhibited an enhancement in the turbulent burning velocity. Flames with positive Markstein lengths suffered from flame quenching with increasing levels of turbulence as those with negative values thrived.

Generally an increase in u' had a related increase u_{tr}, however, as the level of turbulence was increased further the increase of u_t slowed, hence the turbulent burning velocity is not linearly related to u'. There was also evidence that increasing levels of turbulence also effected the equivalence ratio where the peak u_{tr} was found.

The effect of pressure on the turbulent burning velocity was also probed with experiments performed from atmospheric pressure up to 1.0 MPa. There was considerable scatter in the measured values, at a u'=1 m/s the values of u_{tr} for ϕ = 1.0 and 0.8 across the pressure range were very similar. The rich flames at u' = 1 did show a small rise of around 10 %. However, at u' = 4 m/s the effect of pressure was more pronounced, for ϕ = 1.0 there was a rise in u_{tr} of circa 45 % from 0.1 to 1.0 MPa. Ultimately there was an increase with pressure on the turbulent burning velocity unlike laminar flames where there was a marked reduction. The increase in the turbulent burning velocity however, was not as large as suggested by some other workers.

The current experimental results were compared to existing burning velocity correlations. Large variations between individual correlation's and the results of the current work were found. The present values of u_{tr} are based on the rate of production of burned mass and were found to be much lower than values suggested by the correlations which are based on u_{te}, the rate of entrainment into the flame front. The experimental values compared well with other workers who measured the turbulent burning velocity using the rate pressure rise to derive a burning velocity based on rate of production of burned mass.

None of the correlations properly accounted for equivalence ratio variation. This is not surprising considering the dearth of experimental data at these conditions. The correlations did not give large variations in u_t relative to pressure, this was not echoed for all conditions in the current results.

Finally the current turbulent burning velocities were presented in non-dimensionless terms, it was found that flames which exist in the 'thin reaction zone' behave quite differently dependent upon their laminar response to stretch. The turbulent burning velocity has a strong dependence on Markstein number.

Future work

The original, tentative, aim of this work was to generate a new turbulent burning velocity correlation. Despite 660 experiments (40 % of the Leeds 1992 correlation) it was not felt possible to correlate the present data-set. Further measurements are clearly needed, in the present work the influence of the turbulence length scale (which is a function of the vessel) and temperature were not investigated which should be. To change the length scale it would be necessary to perform equally well characterised measurements on another rig.

More data is also required at the extremes in u'. At very low u', laminar flame 'artefacts' e.g. cellularity, may become influential. At very high values of u', the flames are convected from the spark plug and more repeated experiments than the 5 performed here are required. More data at these extreme u' would also help identify if the peak in the turbulent burning velocity with equivalence ratio is a function of u'. There are indications that this is the case in the present study.

The influence of the Karlovitz stretch factor could be explicitly investigated by selecting different conditions at which it is constant but which have different Markstein (and Lewis) numbers.

Further investigation of the flame structure may help interpret the results. Initially high speed laser sheets images could be used to determine flame brush thickness and other wrinkling parameters. But ultimately laser induced fluorescence would be required to obtain information concerning the structure of the flame front.

References

Abdel-Gayed, R. G., Bradley, D., and Lawes, M. (1987). Turbulent Burning Velocity: A General Correlation in Terms of Straining Rates. *Proc. R. Soc. Lond.* A 414: 389-413.

Ali, Y.B. (1995, May). Fundamentals of Turbulent Combustion Related to Gasoline Engines. *Ph.D. Thesis*, University of Leeds.

Al-Shahrany (2002, March) "Experimental and Theoretical approaches to the measurement of burning velocity in spherical explosions" First year *Ph.D.* progress report, School of Mechanical Engineering, University of Leeds

Atzler (1999). Fundamental Studies of Aerosol combustion. *Ph.D. Thesis*, University of Leeds

Aung, K.T., Tseng, L. K., Ismail, M. A. and Faeth, G. M., (1995). Laminar Burning Velocities and Markstein numbers of Hydrocarbons/air Flames. *Combust. Flame* 102: 526.

Aung, K.T., Tseng, L. K., Ismail, M. A. and Faeth, G. M., (1997). Flame stretch interactions of Laminar Premixed Hydrogen/Air flames at Normal temperature and Pressure. *Combust. Flame* 102: 526.

Bradley, D. (1992). How Fast can we Burn? *Twenty-Fourth Symposium (International) on Combustion*, The Combustion Institute, Pittsburgh, p. 247-262.

Bradley, D., Lau, A. K. C., and Lawes, M. (1992). Flame Stretch Rate as a *Determinant of* Turbulent Burning Velocity. *Phil. Trans. R. Soc.* London, UK. 338:359-387.

Bradley, D., Gaskell, P. H., and Gu, X. J. (1996). Burning Velocities, Markstein Length, and Flame Quenching for Spherical Methane-Air Flames: A Computational Study. *Combust. Flame* 104: 176-198.

Bradley, D., Hicks, R. A., Lawes, M., Sheppard, C. G. W. (1996a). Study of Turbulence and Combustion Interaction: Measurement and Prediction of the Rate of Turbulent Burning. Technical Report, Department of Mechanical Engineering, The University of Leeds, UK.

Bradley, D., Hicks, R. A., Lawes, M., Sheppard, C. G. W., and Woolley, R. (1998). The Measurement of Laminar Burning Velocities and Markstein Numbers for Iso-octane-Air and Iso-octane-n-Heptane-Air Mixtures at Elevated Temperatures and Pressures in an Explosion bomb. *Combust. Flame* 115: 126-144.

Bradley, D., (2000). Flame Propagation in a Tube: The Legacy of Henri Guénoche. *Combust. Sci. and Tech.* 158: 15-33.

Bradley, D., (2002). Problems of predicting turbulent burning rates. *Combust. Theory Modeling* ; 361-382.

Bradley, D., Haq, M. Z., Hicks, R. A., Kitagawa, T., Lawes, M., Sheppard, C. G. W., Woolley, R. (2003). Turbulent Burning Velocity, Burned Gas Distribution, and Associated Flame Surface Definition. *Combust. Flame* 133: 415-430.

Checkel, M.D. & Thomas, A. (1994). Turbulent combustion of premixed flames in closed vessels. *Combust. Flame* 96: 351-370.

Clavin, P. (1985). Dynamic Behavior of Premixed Flame Fronts in Laminar and Turbulent Flows. *Prog. Energy. Combust. Sci.* 11: 1-59.

Clarke, A., Stone, R. and Beckwith, P. (1995). Measuring the Laminar Burning Velocity of Methane/Diluent/Air Mixtures within a Constant-Volume Combustion Bomb in a micro-gravity Experiment. *Journ. Inst. Energy*. 68: 130.

Drake, M., (1997). private communication, University of Leeds.

Gillespie, L., Lawes, M., Sheppard, C. G. W., and Woolley, R. (2000). Aspects of Laminar and Turbulent Burning Velocity Relevant to SI Engines. *SAE Paper* 010192.

Gu, X. J. Private Communication

Gu, X. J., Haq, M. Z., *Lawes, M., and* Woolley, R. (2000). Laminar Burning Velocity and Markstein Length of Methane-Air Mixtures. *Combust. Flame 121: 41-*58.

Gülder, O.L. (1991). *Twenty-third Symposium (International) on Combustion*, The Combustion Institute, Pittsburgh, p. 743.

Haq, Z. (1998). Fundamental Studies of Premixed combustion. *Ph.D. Thesis*, University of Leeds.

Hamamoto, Y., Ohkawa, H., Yamamoto, H & Sugahara, R. (1984). *Bull* JSME 27: 756-762.

Haniff, M. S., Melvin, A., Smith, D. B. and Williams, A. (1998). The Burning Velocities of Methane and SNG Mixtures with Air. *Journ. Inst. Energy* 62: 229.

Hassan, M. I., Aung, K. T. and Feath, G. M. (1998). Measured and Predicted Properties of Laminar Premixed Methane/Air Flames at Various Pressures. *Combust. Flame* 115: 539.

Heywood, J. B. (1988). *Internal Combustion Engine Fundamentals*. McGraw-Hill Book Company.

Hynes, J. (1986). Turbulent effects on combustion in spark ignition engines. *Ph.D. Thesis*, University of Leeds.

Khizer Saeed and C. R. Stone (2004). *Combust. Flame 139*: 152-166.

Kido, H., Wakuri, Y. and Nakashima, K. (1983). ASME/JSME *Thermal Engng Joint Conference* vol. 4: 183-190.

Kobayashi, H., Tamura, T., Maruta, K. and Niioka, T. (1996). Burning Velocity of Turbulent Premixed Flames in a High Pressure Environment. *Twenty-Sixth Symposium (International) on Combustion*, The Combustion Institute, Pittsburgh, p. 389-396.

Kobayashi, H., Kawabata, Y., Maruta, K. (1998). Experimental Study on General Correlation of Turbulent Burning Velocity at High Pressure. *Twenty-Seventh*

Symposium (International) on Combustion, The Combustion Institute, Pittsburgh, p.941-948.

Kobayashi, H., Katsuhiro, S., Hagiwara, H., Ogami, Y. (2005). Burning velocity correlation of methane/air turbulent premixed flames at high pressure and high temperature. *Combust. Flame* 30: 827-834

Kono, M., Niu, K., Tsukamoto, T. and Ujiie,Y., (1989). *Twenty-Second Symposium (International) on Combustion,* The Combustion Institute, Pittsburgh, p.1643.

Leuckel, W., Nastoll, W. & Zarzalis, N. (1990). Experimental Investigation of the influence on the transient premixed flame propagation inside closed vessels. *Twenty-third Symposium (International) on Combustion*, The Combustion Institute, 729-734.

Lewis, B. and Von Elbe, G. (1987). Combustion, Flames and Explosions of Gases. *Academic Press,* London.

Lipatnikov, A.N., and Chomiak, J. (2005). Molecular transport effects on turbulent flame propagation and structure *Progress in Energy and Combustion Science, 31-1: 1-73*

Mandilas, Charalampos (2005) Private communication

Markstein, G. H. (1951). Experimental and Theoretical studies of Flame-Front stability. *J. Aero, Sci.* 18: 199-209.

McComb, W. D. (1990). The Physics of Fluid Turbulence. Oxford University Press.

Metghalchi, M. and Keck, J. C. (1982). Burning Velocities of Mixtures of Air with Methanol, Isooctane and Indolene at High Pressure and Temperature, *Combust. Flame*. 48: 191-210.

Morley, C. (2001). GASEQ Program. (www.gaseq.co.uk).

Nwagwe, K., Weller, H. G., Tabor, G. R., Gosman, A. D., Lawes, M., Sheppard, C. G. W., and Woolley, R. (2000). Measurements and Large Eddy Simulations of Turbulent Premixed Flame Kernel Growth. *Pro. Combust. Inst.* 28: 59-65.

Palm-Leis, A., and Strehlow, R. A. (1969). On the Propagation of Turbulent Flames. *Combust. Flame* 13: 111-129.

Peters, N. (2000). *Turbulent Combustion*, Cambridge University Press. UK.

Putman, A.A. & Giammar, R.D. (1972). *Phase Rep. Research Project*, Battelle Columbus Laboratories, Columbus, Ohio. BR 3-5

Rasbash, D.J. & Rogowski, Z.W. (1960). *Combust Flame* 4:301-312.

Scott, M. J. (1992). Distribution of Strain Rate and Temperature in Turbulent Combustion. *Ph.D. Thesis*, University of Leeds.

Taylor, S. C. (1991). Burning Velocity and the Influence of Flame Stretch. *Ph.D. Thesis*, University of Leeds.

Ting, D. S., Checkel, M. D., (1997) The Importance of Turbulence Intensity, Eddy Size and Flame Size in Spark Ignited, Premixed Flame Growth. *Proc. Instn. Mech. Engrs. Part D* 221: 83-86.

Ting, D. S., Checkel, M. D., and Johnson, B., (1995). The Importance of High Frequency, Small-Eddy Turbulence in Spark Ignited, Premixed Engine Combustion. SAE Paper 952409.

Turns, S. R. (1996). *An Introduction to Combustion: Concepts and Applications.* McGraw-Hill Book Company.

Vagelopoulos, C. M., Egolfopoulos, F. N. and Law, C. K. (1994). Further Considerations on the Determination of Laminar Flame Speeds with Counterflow Twin-Flame Technique. *Twenty-Fifth Symposium (International) on Combustion*, The Combustion Institute, Pittsburgh, p. 1341.

Vagelopoulos, C. M. and Egolfopoulos, F. N. (1998). Direct Experimental Determination of Laminar Flame speed. *Twenty-Seventh Symposium (International) on Combustion*, The Combustion Institute, Pittsburgh, p. 513.

Van Maaren, A., Thung, D. S. and De Goey, L.P.H. (1994). Measurment and Adiabatic Burning Velocity of Methane/Air Mixtures. *Combust. Sci. Tech.* 96:p. 327.

Verhelst, S., Woolley, R., Lawes, M. and Sierens, R. (2004). Laminar and Unstable Burning Velocities and Markstein Lengths of Hydrogen-air Mixtures at Engine-Like Conditions. *Thirtieth Symposium (International) on Combustion*, The Combustion Institute, Chicago, p 209.

Wohl, K., Shore, L. (1955). Experiments with butane-air and methane-air flames. Ind. Eng. Chem. 47:828-34